Modélisation et simulation numérique de la vitesse de propagation d'une piqûre de corrosion

Meriem Bouguezzi

université PARIS-SACLAY

Modélisation et simulation numérique de la vitesse de propagation d'une piqure de corrosion

Modeling and computer simulation of the propagation rate of pit corrosion

Thèse de doctorat de l'université Paris-Saclay

École doctorale n° 574, mathématiques Hadamard (EDMH)

Spécialité de doctorat : Mathématiques appliquées

Unité de recherche : Université Paris-Saclay, CNRS, Laboratoire de mathématiques d'Orsay, 91405, Orsay, France

Référent : Faculté des sciences d'Orsay

Thèse présentée et soutenue à Paris-Saclay, le 13/07/2021, par

Meriem BOUGUEZZI

Composition du Jury

Pascal OMNES Directeur de Recherche au CEA	Président
Philippe LAURENÇOT Directeur de Recherche au CNRS à l'institut de Mathématiques de Toulouse	Rapporteur & Examinateur
Bruno VUILLEMIN Professeur des universités à l'Université de Bourgogne	Rapporteur & Examinateur
Danielle HILHORST Directeur de Recherche Emérite au CNRS, Université Paris-Saclay	Directrice de Thèse
Hiroshi MATANO Professeur à l'Université Meiji, Tokyo	Examinateur
Fabien ROUILLARD Ingénieur-Chercheur au CEA	Examinateur

Direction de la thèse

Danielle HILHORST Directeur de Recherche Emérite au CNRS, Université Paris-Saclay	Directrice de Thèse
Florence LEQUIEN Ingénieur-Chercheur au CEA	Co-Encadrante CEA
Fabien ROUILLARD Ingénieur-Chercheur au CEA	Encadrant CEA
Jean-François SCHEID Maître de Conférence à l'Université de Lorraine	Co-Directeur de Thèse

Thèse de doctorat

NNT : 2021UPASM027

"Travailler c'est prier. On doit travailler et faire ce que l'on peut, et pour le reste, tout prendre avec légèreté et bonne humeur."

À ma famille,

Remerciements

Je suis convaincue que la préparation d'une thèse est loin d'être un travail solitaire. En effet, je n'aurais jamais pu réaliser ce travail doctoral sans le soutien d'un grand nombre de personnes dont la générosité, la bonne humeur et l'intérêt m'ont permis de progresser dans cette phase délicate.

Je voudrais tout d'abord remercier ma directrice de thèse Danielle Hilhorst qui m'a encadrée tout au long de cette thèse et qui m'a fait partager ses brillantes intuitions. J'aimerais également lui dire à quel point j'ai apprécié sa grande disponibilité et son respect sans faille des délais serrés de relecture des documents que je lui ai adressés. Merci de m'avoir partagée votre longue expérience de la recherche. Enfin, j'ai été extrêmement sensible à ses qualités humaines d'écoute et de compréhension tout au long de ce travail doctoral.

Je tiens également à remercier mon co-directeur Jean-François Scheid pour son aide, sa disponibilité permanente et pour les encouragements qu'il m'a prodiguée. C'est grâce à lui que j'ai pu concilier avec bonheur recherche théorique et recherche appliquée pendant la préparation de cette thèse.

Je sais infiniment gré à mon encadrant Fabien Rouillard, Ingénieur-chercheur au CEA, pour sa disponibilité, sa pédagogie et ses judicieux conseils, qui ont contribué à alimenter ma réflexion. C'est un plaisir de pouvoir échanger avec lui. Il était toujours très à l'écoute et m'a beaucoup appris sur le phénomène de corrosion. Il a partagé avec moi ses connaissances et son expérience du milieu de la recherche, tout en m'accordant sa confiance. Je suis ravie d'avoir pu travaillé à ses côtés.

Je souhaite exprimer ma gratitude à ma co-encadrante Florence Lequien, Ingénieure chercheuse au CEA, qui a contribué activement à nos nombreuses réunions et échanges sur mon sujet de thèse. Je voudrais la remercier pour son soutien, son écoute et son esprit critique.

Mes remerciements les plus vifs s'adressent à Monsieur Philippe Laurençot, Directeur de Recherche au CNRS à l'Institut de Mathématiques de Toulouse, et à Monsieur Bruno Vuillemin, Professeur à l'Université de Bourgogne, d'avoir accepté de relire cette thèse et d'en être les rapporteurs. La version finale de cette thèse a bénéficié de leur lecture très attentive et enrichissante et de leurs remarques précieuses.

Je tiens à remercier spécialement les membres de jury pour le grand honneur qu'ils me font en acceptant de juger ce travail. Je vous suis très reconnaissante de l'intérêt que vous portez à cette thèse.

Je voudrais remercier tout particulièrement Monsieur Hiroshi Matano, Professeur à l'Université Meiji, pour son aide, son soutien inestimable et ses judicieux conseils dans la réalisation de cette thèse. Il a été à l'écoute de mes nombreuses questions, et s'est toujours intéressé à l'avancée de mes travaux. Les nombreuses discussions que nous avons eues ensemble ainsi que les conseils qu'il m'a prodigués sont pour beaucoup dans le résultat final de ce travail. Sa gentillesse, ses qualités humaines, sa modestie n'ont d'égal que sa grande compétence. Cette thèse lui doit beaucoup. Je voudrais exprimer mon respect pour ses qualités professionnelles et humaines qui me servent d'exemple.

J'adresse mes sincères remerciements à Monsieur Pascal Omnes, Directeur de recherche au CEA, d'avoir accepté de faire partie de mon jury. J'ai toujours pris un immense plaisir dans nos discussions et nos échanges passionnants sur mon sujet de thèse.

Je tiens à exprimer mes reconnaissance et ma profonde gratitude à Monsieur Christian Bataillon pour son aide et ses conseils qu'il m'a apporté lors des différents suivis.

Je tiens à remercier les enseignants-chercheurs de laboratoire de mathématiques d'Orsay avec qui j'ai partagé mon service d'enseignement pour leur soutien et leur compréhension, notamment Filipa, Astrid, Benjamin, Rémy et Anna. Un grand merci à la secrétaire de l'école doctorale, Madame Séverine Simon, pour son aide dans les démarches administratives pour préparer ma soutenance.

Je tiens également à remercier le CEA pour l'accueil et les conditions de travail privilégiées qui m'ont été offertes. Ce travail n'aurait pu être mené à bien sans leur aide qui, au travers de leur soutien matériel, ont reconnu mon travail et m'ont fait confiance. Je remercie également ORANO et EDF pour leur support financier.

Je voudrais exprimer ma reconnaissance envers tous mes amis et collègues qui m'ont apporté leur soutien moral et intellectuel tout au long de ma démarche. Un grand merci à tout le service SCCME. Véronique, je te remercie pour ta joie de vivre et tes fous rires communicatifs qui nous ont fait passer de bons moments. Nelly, Nadia, Béa, Anais, Stéphanie, Pierre, Benoît, Nathalie, Sophie, Gervaise et Mylène, vous êtes formidables. Clara, Simoney, Sabrina, Émeline, Vinisus, Thalita, Rahma, Rayhana, Anitha, Marie, Élise merci pour les nombreux bons moments passés ensembles. Merci mes chères amies Perla et Marie-Josée, vous étiez toujours présentes.

Mes remerciements vont aussi à ma grande famille et à mes amis qui, avec cette question récurrente, " Quand est-ce que tu la soutiens cette thèse ? ", bien qu'angoissante en période fréquente de doutes, m'ont permis de ne jamais dévier de mon objectif final. Un merci tout particulier à mes chers parents, Neji et Nejma, pour leur soutien quotidien indéfectible et leur enthousiasme contagieux à l'égard de mes travaux comme de la vie en général et pour leur compagnie précieuse pendant la rédaction de cette thèse. Un grand merci à mes chers frère et soeurs, Mohamed, Anouare, Rihab, Imen et Rania et à ma copine Soukaina. Vous êtes ma force.

Finalement, je n'oublie pas non plus ma chère grand-mère qui m'a quittée pendant ma première année de thèse et je n'oublierai jamais ses encouragements et son soutien. Je dédie ce travail à l'âme de ma grand-mère.

Contents

Chapter 1

Introduction

1.1 Contexte physique: Introduction au phénomène de corrosion par piqûre

La corrosion est définie comme une interaction physico-chimique entre un métal et son environnement conduisant à des modifications des propriétés du métal et souvent à une dégradation fonctionnelle du métal lui-même. Dans le cas de la corrosion humide, cette interaction est de nature électrochimique. Elle peut prendre naissance simultanément en différents points d'un même métal ou d'un alliage.

L'importance de la corrosion et de la technologie de surfaces pour notre société n'est plus à démontrer. La corrosion touche toutes les réalisations de l'ingénieur, des plus grandes aux plus petites: production d'énergie, génie civil, transport, machines, matériaux médicaux, composants micro-électroniques, etc...[42].

On estime aujourd'hui que la corrosion détruit un quart de la production annuelle mondiale d'acier, ce qui présente environ 5 tonnes par seconde. La corrosion n'est pas seulement une source de gaspillage de matières premières et d'énergie, elle peut en plus provoquer des accidents aux conséquences graves et, dans certains cas, contribuer à la pollution de l'environnement naturel [42] et avoir des conséquences humaines (crash d'avion).

La prévision du comportement à long terme d'ouvrages métalliques, c'est-à-dire l'évaluation des dommages qu'ils sont susceptibles de subir dans le temps sous l'action de la corrosion représente un challenge important notamment sur le plan économique et scientifique.
Sur le plan économique, toute augmentation de la durabilité des matériaux métalliques entraîne un gain financier important. Connaître la vitesse de corrosion permet par ailleurs un ajustement plus pertinent de la qualité des matériaux utilisés dans la fabrication des ouvrages métalliques en fonction de la durée de vie souhaitée.
Sur le plan scientifique, la prévision du comportement à long terme est un défi car la corrosion est une combinaison de multiples phénomènes d'origine physique, chimique et mécanique. La compréhension de ces phénomènes doit permettre de lutter plus efficacement contre la dégradation des matériaux en choisissant la méthode de protection la plus adaptée.

Le phénomène de corrosion est beaucoup étudié depuis plus d'un siècle. De nombreuses études ont été réalisées et ont permis d'avancer dans la compréhension de ce phénomène qui se présente sous différentes formes. Les recherches sur ce sujet continuent.

Notre étude est centrée sur la corrosion par piqûre en phase aqueuse des aciers inoxydables. Ces aciers sont très utilisés car ils forment de manière naturelle de fins films passifs en surface (à l'échelle nanométrique) ce qui réduit fortement leur vitesse de corrosion dans leur environnement

d'exposition. De tels films passifs, néanmoins, sont souvent susceptibles de se rompre localement ce qui engendre par la suite une dissolution accélérée du métal sous-jacent entrainant la formation en surface de trous de faibles dimensions mais de profondeur importante [12]. Ce phénomène de corrosion est la corrosion par piqûres ("pit corrosion" en anglais). La Figure 1.1.1 présente l'image d'une piqûre par microscopie électronique à balayage.

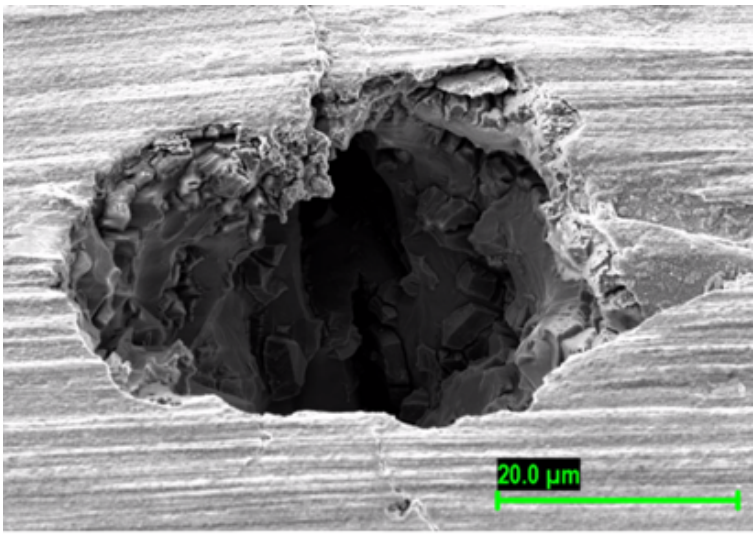

Corrosion par piqûre [1]

[1] National Physical Laboratory | Hampton Road, Teddington, Middlesex, TW11 0LW

Image wase taken with scanning electron microscopy in NPL

Figure 1.1.1: Observation par microscopie électronique à balayage d'une piqûre de corrosion.

Cette attaque localisée peut aboutir à terme à la perforation du matériau ou à la formation d'un site d'initiation de fissures. La durée d'une telle attaque dépend fortement de l'évolution de la chimie locale de la piqûre. Elle peut se produire dans de nombreux milieux. Les milieux oxydants chlorurés sont notamment très favorables au déclenchement de corrosion localisée. En effet, les chlorures revêtent une importance particulière en raison, d'une part, de leur grande distribution dans la nature et, d'autre part, de leur agressivité généralement plus élevée que les autres espèces [11]. Cet environnement aqueux chloré particulièrement agressif pour les aciers inoxydables pourrait notamment être en contact de certaines zones des colis des déchets de l'industrie nucléaire contenant des déchets technologi-
ques (principalement plastiques tels que le PVC) de moyenne activité à vie longue.

Le phénomène de corrosion par piqûre se décompose en trois étapes distinctes:
- l'étape d'amorçage de la piqûre,
- l'étape de propagation de la piqûre,
- l'étape de repassivation de la piqûre.

L'amorçage ("initiation" en anglais) de la piqûre consiste en la rupture locale pour une raison quelconque de la couche passive protectrice. Ceci aboutit à la création d'un embryon de piqûre qui est un défaut de taille nanométrique. Puis en fonction de l'environnement :
- soit la couche passive se reforme et donc une repassivation de la piqûre a lieu,
- soit le métal sous-jacent se corrode ce qui aboutit à la propagation de la piqûre.

Une fois le germe de piqûre initié, certaines piqûres se propagent pendant une durée inférieure à une seconde et parfois même à une milliseconde puis se repassivent car elles ne maintiennent

pas les conditions nécessaires à leur propagation. On parle alors de piqûres "métastables". Si des conditions suffisantes en terme de chimie se développent dans la piqûre pour empêcher la repassivation, alors la piqûre survit à cet état de métastabilité et devient une piqûre dite "stable".

Pour assurer la stabilité de la piqûre, une chimie agressive minimale dans la piqûre est exigée. Ainsi, deux facteurs critiques qui assurent sa stabilité (la continuation de sa propagation) sont identifiés dans la litterature [71–75]. Ils sont décrits en terme de concentration critique en cations métalliques ou en terme de pH (acidité) critique de la solution. Si ces conditions minimales ne sont pas respectées, la chimie dans la piqûre devient défavorable à la poursuite de la dissolution du métal et une repassivation se produit.
Une fois la piqûre repassivée, la couche passive est de nouveau susceptible de se détériorer aboutissant au réamorçage de la piqûre. On parle ainsi d'un cycle de corrosion par piqûre.

La Figure 1.1.2 présente une schématisation d'une piqûre de corrosion en phase de propagation avec une réaction cathodique majoritaire impliquant la réduction de l'oxygène dissous en surface d'un acier inoxydable austénitique tel que l'acier 316 L.

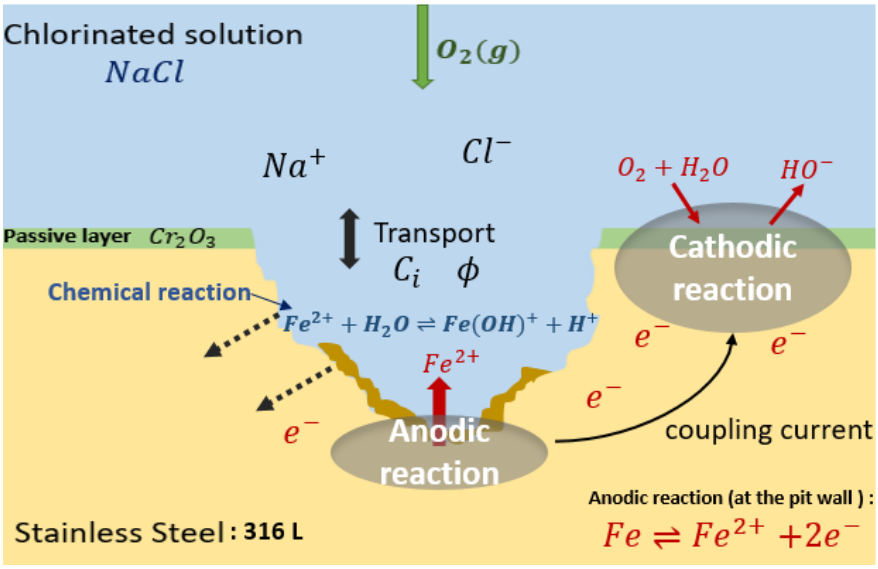

Figure 1.1.2: Schéma d'une piqûre de corrosion.

Comme le montre la Figure 1.1.2, une piqûre de corrosion constitue effectivement un problème multiphysique complexe qui peut être décrit par les étapes réactionnelles suivantes:

- la dissolution de métal;
- le transport des espèces chimiques dans la solution de la piqûre sous champs de concentration (diffusion) et de potentiel (migration);
  - la diffusion et la migration des ions sont deux phénomènes fondamentaux de la corrosion par piqûre. La diffusion est un phénomène qui tend à uniformiser la composition du milieu en tout point. Ainsi, il provoque le transfert de matière de la région la plus concentrée vers la moins concentrée, d'où le transport de masse vers l'extérieur,
  - la migration décrit le déplacement des ions sous l'effet d'un champ électrique.

  Il existe donc un gradient de concentration d'ions et un gradient de potentiel électrostatique dans la piqûre;
- les réactions chimiques (formation de complexes dissous et de précipités). Ces réactions sont responsables de l'évolution de la composition de la solution de la piqûre. Une réaction

importante dans la piqûre est la réaction d'hydrolyse des cations qui génère des ions H^+ dans la solution. Par exemple, dans le cas de la dissolution du fer, la réaction d'hydrolyse est décrite par la réaction suivante (voir Figure 1.1.2) :

$$Fe^{2+} + H_2O \rightleftharpoons Fe(OH)^+ + H^+.$$

Les ions H^+ sont responsables de l'acidification locale du milieu, cause proposée par certains auteurs pour expliquer la stabilisation des piqûres [71, 72]. Ce même phénomène a lieu pour les aciers inoxydables (Fe-Cr-Ni) avec l'hydrolyse des cations de chrome, Cr^{3+}, entrainant des pH encore plus faibles. L'hydrolyse des cations de chrome, Cr^{3+}, est décrite par la réaction suivante

$$Cr^{3+} + H_2O \rightleftharpoons Cr(OH)^{2+} + H^+.$$

Pouvoir simuler le développement au cours du temps d'une piqûre (conditions chimiques et géométriques nécessaires pour stabiliser une piqûre, vitesse de propagation, morphologie de propagation) représente depuis toujours et principalement depuis ces 50 dernières années un enjeu primordial. Dans ce cadre, de nombreux modèles cinétiques de propagation ont déjà été développés. Parmi ceux-ci, on peut citer des anciens travaux de Scharland 1988-1989 [64, 67, 68], Turnbull 1982-1993 [80, 82], Walton 1990-1996 [84, 85], Laycock and al. 1997-2014 [40, 43, 44],..., ainsi que des récents travaux de Tricoit 2012 [79], Srinivasan and al. 2015-2017 [73–75], Chadwick and al. 2018 [10], Jafarzadeh and al. 2019 [35].

Tout d'abord, différentes techniques, hypothèses et approximations ont été faites dans leurs modèles (géométrie de la piqûre, espèces chimiques considérées, conditions limites du système). Ensuite, différentes méthodes numériques ont été utilisées pour la résolution du système d'équations obtenu. A partir de l'ensemble des résultats de ces études, et en ayant identifié les avantages et inconvénients des différents modèles, le CEA a choisi de développer son propre modèle de propagation de piqûre.

C'est dans ce contexte que s'inscrit ce projet de thèse intitulé: « Modélisation et simulation numérique de la propagation d'une piqûre de corrosion dans un acier inoxydable ».

1.2 Objectifs de la thèse

Les objectifs scientifiques de cette thèse sont relatifs à la modélisation physico-chimique de la corrosion par piqûre, l'analyse mathématique et les simulations numériques.

1.2.1 Modélisation

Un des objectifs principaux est de modéliser le développement d'une piqûre (stabilité et cinétique de propagation) à partir d'un certain nombre de phénomènes physiques impliqués: réactions anodiques de dissolution, diffusion et migration des espèces, réactions chimiques en solution, avancée de la frontière mobile.

Il s'agit de décrire précisément l'évolution de la propagation d'une piqûre de corrosion en s'approchant au plus près de la réalité physique. Il est donc important de comprendre physiquement et chimiquement ce phénomène complexe. L'une des démarches suivies pour connaître le comportement à long terme d'ouvrages métalliques est le développement de modèles utilisant une approche mécaniste. L'approche mécaniste est basée sur une démarche déterministe qui présuppose de décrire le système métal-environnement par un système plus ou moins complexe d'équations physico-chimiques.

Cette approche revient à développer un modèle mathématique sous la forme d'un système d'équations aux dérivées partielles prenant en compte :

- la chimie de l'environnement ;
- les propriétés électrochimiques du matériau ;
- les différentes étapes physiques impliquées dans son développement (dissolution anodique, réactions, transports, électroneutralité locale de la solution,...) ;
- le mouvement de l'interface liquide/solide qui décrit l'évolution de la profondeur de la piqûre en fonction du temps.

Les contraintes qui doivent être respectées par le système sont :

- la conservation de la masse : tout ce qui se dissout se retrouve dans la solution ;
- l'électroneutralité locale de la solution : en tout point de la solution de la piqûre, la somme des charges est nulle. Pour cette raison, lors de la dissolution du métal, des cations sont injectés dans la solution et des anions (Cl^-, ...) sont transportés dans la piqûre pour respecter l'électroneutralité locale ;
- la conservation de la charge : ici on parle d'une part de l'électroneutralité locale de la solution de la piqûre pour avoir une somme des charges nulle au niveau de la piqûre et d'autre part une somme des charges nulle au niveau de l'acier par le couplage entre la réaction anodique qui a lieu au fond de la piqûre et la réaction cathodique qui a lieu majoritairement à la surface de la piqûre de l'acier, c'est-à-dire que tout électron produit par l'oxydation du métal doit être consommé par la réaction cathodique de réduction du milieu. On parle ici d'une corrosion ¨naturelle˝;
- le mouvement de l'interface métal/électrolyte (solution de la piqûre) pour décrire la morphologie de la piqûre dans le temps.

1.2.2 Approximations numériques et simulations

Un autre objectif est également de proposer une méthode de résolution numérique du système d'EDP non linéaire et fortement couplé obtenu après modélisation. Cette méthode doit être précise, robuste et présenter des temps de calculs raisonnables. Il a été choisi d'implémenter cette méthode de résolution dans un code écrit dans le langage PYTHON. L'utilisation de Python permet de maîtriser toutes les entrées et sorties du code, d'avoir la main sur la méthode de résolution numérique et enfin d'avoir un code le plus flexible possible en terme de modification. Le code doit permettre dans un premier temps:

- de simuler la vitesse de propagation de la piqûre de corrosion,
- de prévoir la composition chimique de la solution de piqûre,
- d'identifier les facteurs critiques importants pour assurer sa stabilité.

Il est important de souligner que le modèle est développé pour la propagation de piqûre mais s'applique également à la corrosion par crevasse dont la propagation implique la même physique.

Les chapitres liés à l'étude physique du phénomène sont:
le chapitre 2, le chapitre 3 et le chapitre 6. Davantage de détails sur le contenu de ces chapitres sont présentés dans la section 1.3 intitulée "Description de la thèse".

1.2.3 Analyse mathématique

On étudiera également un problème à frontière libre simplifié de la corrosion par piqûre, présenté dans le chapitre 3. Ce problème sera transformé à l'aide d'un changement de variable approprié en un problème de Stefan classique. On étudiera en particulier la stabilisation en temps long vers un profil auto-similaire de la solution d'une forme équivalente au problème physique à frontière libre, connue dans la littérature sous le nom de problème de Stefan.

Cela fera l'objet du chapitre 4. Dans le chapitre 5, on propose une méthode de résolution numérique efficace pour ce problème de Stefan. Ainsi, on introduit la méthode numérique ALE (Arbitrary-Lagrangian-Eulerian) qui est bien adaptée à ce type de phénomènes évolutifs en temps, pour lesquels une régularisation du maillage est nécessaire à chaque instant pour décrire le mouvement de l'interface. La même méthode numérique a été adoptée pour la résolution numérique des modèles plus complexes introduits par la suite.

On étudiera également dans le chapitre 7, un modèle réduit qui est dérivé du modèle original de diffusion-convection introduit dans le chapitre 6.

1.3 Description de la thèse

Au regard de la complexité du problème, le travail a été découpé en différentes étapes et basé sur la construction d'un modèle à complexité physique croissante permettant d'identifier l'influence des différentes hypothèses physiques du modèle.

Cette thèse comporte donc une double approche physico-mathématique qui est développée étape par étape au travers de huit chapitres qui sont présentés brièvement dans la suite de cette partie. Ici, uniquement le chapitre 4 est très détaillé. On détaillera les résultats des autres chapitres dans la Section 8.1 du Chapitre 8 (Conclusions et Perspectives).

1.3.1 Chapitre 2 : Analyse bibliographique

Une étude bibliographique est présentée dans le deuxième chapitre. Elle présente une revue des différents modèles numériques de propagation d'une piqûre qui ont été développés dans la littérature. D'autre part, nous détaillons dans ce chapitre les deux facteurs critiques qui sont proposés dans la littérature pour assurer la stabilité d'une piqûre. Ces deux facteurs sont une concentration critique en cations metalliques C_{crit} et le pH de la solution de la piqûre.

1.3.2 Chapitre 3 : Description d'un modèle simplifié à frontière libre: Dissolution du fer

Un premier modèle de dissolution du fer pur a été étudié afin d'introduire la démarche de résolution d'un système à frontière libre. Il s'agit d'un système en dimension 1 d'espace où seule l'espèce chimique fer non chargée est prise en compte. La concentration des cations fer en bouche de piqûre est égale à zéro et celle en fond de piqûre est égale à la limite de solubilité des chlorures de fer $FeCl_2$. Dans ce système, un sel métallique de chlorure de fer est formé et stable à tout instant en fond de piqûre.

Le modèle physique est décrit par le problème à frontière libre suivant:

$$\begin{cases} \dfrac{\partial C}{\partial t} = D\,\dfrac{\partial^2 C}{\partial x^2}, & t>0,\ 0<x<x_d(t), \\ C(0,t) = 0, & t>0, \\ C(x_d(t),t) = C_{\text{sat}}, & t>0, \\ \dfrac{dx_d(t)}{dt} = \dfrac{D}{C_{\text{solid}}-C_{\text{sat}}}\,\dfrac{\partial C(x_d(t),t)}{\partial x}, & t>0. \end{cases} \tag{1.3.1}$$

Ce système comporte deux inconnues: le profil de concentration du fer $C = C(x,t)$ et la profondeur de la piqûre $x_d(t)$. La concentration de fer C satisfait l'équation de la chaleur dans la solution de la piqûre, une condition de Dirichlet homogène au point $x = 0$ (bouche de la piqûre)et une condition de Dirichlet homogène $C = C_{\text{sat}}$, au fond de la piqûre en $x = x_d(t)$. La vitesse de propagation de l'interface mobile est contrôlée par la diffusion des cations du fond de piqûre vers l'extérieur. On parle d'un régime de dissolution-diffusion.

En s'appuyant sur le changement de variable

$$y = \frac{C_{\text{solid}}-C_{\text{sat}}}{\sqrt{D}}\,x, \quad s(t) = \frac{C_{\text{solid}}-C_{\text{sat}}}{\sqrt{D}}\,x_d(t) \ \text{ pour tout } \ t>0,$$

et en posant

$$u(y,t) = C_{\text{sat}} - C(x,t) \ \text{ pour tout } \ t>0, 0\leqslant x\leqslant x_d(t) \ \text{ et } \ y = \frac{C_{\text{solid}}-C_{\text{sat}}}{\sqrt{D}}\,x,$$

on transforme le problème physique (1.3.1) en un problème de Stefan unidimensionel à une phase. C'est ce problème qui sera étudié au chapitre 4.

1.3.3 Chapitre 4 : Convergence vers un profil auto-similaire de la solution d'un problème unidimensionnel de Stefan à une phase

Nous étudions le problème unidimensionnel de Stefan à une phase avec une condition au limite de type Dirichlet en $x = 0$ comme indiqué dans le livre d'Avner Friedman sur les équations paraboliques [24]. Ce problème est donné par:

$$\begin{cases} u_t = u_{xx}, & t>0, 0<x<s(t), \\ u(0,t) = h, & t>0, \\ u(s(t),t) = 0, & t>0, \\ \dfrac{ds(t)}{dt} = -u_x(s(t),t), & t>0, \\ s(0) = b_0, & \\ u(x,0) = u_0(x), & 0<x<b_0. \end{cases} \tag{1.3.2}$$

où $x = s(t)$ désigne la frontière libre et où h et b_0 sont des constantes positives. Les inconnues du système sont la fonction $u = u(x,t)$ et l'interface $s = s(t)$. La fonction initiale u_0 satisfait l'hypothèse
$\mathbf{H}_0$: $u_0 \in \mathbb{W}^{1,\infty}(0,b_0)$, $u_0(0) = h$, $u_0(x) = 0$ pour tout $x \geqslant b_0$ et $0 \leqslant u_0 \leqslant h(1-\dfrac{x}{\sqrt{2h}})$ pour tout $0 \leqslant x \leqslant b_0$.

Avec des hypothèses un peu moins restrictives sur la condition initiale, Friedman [24] a prouvé que le problème (1.3.2) posséde une solution classique unique. De plus, Schaeffer [59] et Friedman [22] ont démontré que $s \in C^\infty(0,\infty)$ et que u est indéfiniment différentiable jusqu'à la frontière

libre s.

Le but de ce chapitre est d'étudier le comportement en temps long de la solution (u,s). Plus précisément, nous démontrons que la solution (u,s) converge vers un profil auto-similaire quand $t \to +\infty$.

Le profil auto-similaire est défini de la façon suivante : on introduit la variable auto-similaire $\eta = \dfrac{x}{\sqrt{t+1}}$ et on recherche une solution auto-similaire sous la forme

$$u(x,t) = U(\frac{x}{\sqrt{t+1}}) = U(\eta).$$

On démontre que

$$U(\eta) = h\left[1 - \frac{\int_0^\eta e^{-\frac{s^2}{4}} ds}{\int_0^a e^{-\frac{s^2}{4}} ds}\right] \quad \text{pour} \quad \text{tout} \quad \eta \in (0,a), \tag{1.3.3}$$

où a est l'unique solution de l'équation non linéaire:

$$h = \frac{a}{2} e^{\frac{a^2}{4}} \int_0^a e^{-\frac{s^2}{4}} ds. \tag{1.3.4}$$

Dans le but de réécrire le problème (1.3.2) en terme de η et de t, on définit:

$$\begin{cases} V(\eta,t) = u(x,t), \\ a(t) = \dfrac{s(t)}{\sqrt{t+1}}. \end{cases} \tag{1.3.5}$$

L'équation aux dérivées partielles pour V fait intervenir explicitement la variable temporelle t. Elle est donnée par:

$$(t+1)V_t = V_{\eta\eta} + \frac{\eta}{2} V_\eta, \quad t > 0, \quad 0 < \eta < a(t). \tag{1.3.6}$$

Dans le but d'obtenir une équation aux dérivées partielles autonome, on pose $\tau = \ln(t+1)$ et $W(\eta,\tau) = u(x,t)$. On obtient donc le problème

$$\begin{cases} W_\tau = W_{\eta\eta} + \dfrac{\eta}{2} W_\eta, & \tau > 0, \quad 0 < \eta < b(\tau), \\ W(0,\tau) = h, & \tau > 0, \\ W(b(\tau),\tau) = 0, & \tau > 0, \\ \dfrac{db(\tau)}{d\tau} + \dfrac{b(\tau)}{2} = -W_\eta(b(\tau),\tau), & \tau > 0, \\ b(0) = b_0, & \\ W(\eta,0) = u_0(\eta), & 0 \le \eta < b_0. \end{cases} \tag{1.3.7}$$

où $b(\tau) = a(t)$.

Nous désignerons par $\Big(W(\eta,\tau,(u_0,b_0)), b(\tau,(u_0,b_0))\Big)$ la solution de (1.3.7) avec la condition initiale (u_0,b_0).

C'est dans les coordonnées η et τ que nous caractérisons rigoureusement le comportement en temps long de la solution (W,b). Cependant, pour des raisons techniques, nous devons parfois utiliser des variables différentes, soit (y,τ) avec $y = \dfrac{\eta}{b(\tau)}$ pour tout $\eta \in (0,b(\tau))$. Le problème est alors transformé en un problème sur un domaine fixe.

L'organisation de ce chapitre est la suivante :

Dans la section 2, nous introduisons le problème de Stefan [23] et rappelons des résultats connus d'existence, d'unicité et de régularité de la solution [22, 59]. En utilisant le principe du maximum [24], nous montrons que si u_0 est borné, alors la solution u est également bornée.

Dans la section 3, nous commençons par définir une notion de sur- et sous-solutions pour le problème (1.3.2). Nous démontrons ensuite un principe de comparaison dans les coordonnées (x,t).

Dans la section 4, nous construisons la solution auto-similaire (U,a). Nous montrons que U est donné par (1.3.3) et que a est caractérisé comme la solution unique de l'équation non linéaire (1.3.4).

Dans la section 5, nous transformons le problème (1.3.2) exprimé en coordonnées (x,t) pour obtenir un problème équivalent, le problème (1.3.7), exprimé en coordonnées (η,τ) où la solution devient (W,b). Nous présentons un principe de comparaison équivalent dans ces coordonnées.

Nous construisons ensuite une classe de fonctions qui inclus à la fois des sous- et sur-solutions. Nous utilisons la notation $(\bar{\mathcal{W}},\bar{b})$ pour la sur-solution, respectivement $(\underline{\mathrm{W}}_\lambda,\underline{\mathrm{b}}_\lambda)$ pour la sous-solution où λ est un paramètre positive ou nul et nous construisons une fonction (W_λ,b_λ) telle que

$$(W_\lambda,b_\lambda) \text{ est } \begin{cases} \text{une sur-solution} & \text{si } 0 \leqslant \lambda \leqslant 1, \\ \text{une sous-solution} & \text{si } \lambda \geqslant 1. \end{cases} \tag{1.3.8}$$

Ensuite, nous prouvons la monotonie en temps de la solution (W,b) du problème d'évolution en temps (1.3.7) avec les deux conditions initiales $(\bar{\mathcal{W}},\bar{b})$ et $(\underline{\mathrm{W}}_\lambda,\underline{\mathrm{b}}_\lambda)$. En d'autres termes, nous montrons qu'à partir d'une sous-solution, la solution $\underline{\mathrm{W}}(\eta,\tau) := W(\eta,\tau,(\underline{\mathrm{W}}_\lambda,\underline{\mathrm{b}}_\lambda))$ croît en temps et converge vers une fonction limite ψ quand $\tau \to \infty$ et que la frontière libre correspondante $\underline{\mathrm{b}}(\tau) := b(\tau,(\underline{\mathrm{W}}_\lambda,\underline{\mathrm{b}}_\lambda))$ converge vers une limite $\underline{\mathrm{b}}_\infty$ quand $\tau \to \infty$. De même, on peut montrer qu'à partir d'une sur-solution, la solution décroît vers une autre fonction limite ϕ quand $\tau \to \infty$ et la frontière libre correspondante $\bar{b}$ converge vers une limite $\bar{b}_\infty$. À la fin de cette section, nous montrons que les fonctions (W_λ,b_λ) sont des fonctions ordonnées. Cependant, nous ne savons pas encore si ψ et ϕ coïncident avec le profil auto-similaire U et si $\underline{\mathrm{b}}_\infty$ et $\bar{b}_\infty$ coïncident avec le point a. Afin de prouver ces résultats, nous devons d'abord présenter des estimations a priori supplémentaires, ce qui fait l'objet de la section suivante.

Dans la section 6, nous prouvons un certain nombre d'estimations a priori, certaines dans le domaine mobile et d'autres dans le domaine fixe. En effet, nous passons temporairement au domaine fixe $(y,\tau) \in (0,1) \times \mathbb{R}^+$ pour éviter des problèmes techniques liés à la caractérisation des limites $\underline{\mathrm{b}}_\infty$ et $\bar{b}_\infty$. En d'autres termes, nous devons montrer que $\underline{\mathrm{W}}_\eta(\underline{\mathrm{b}}(\tau),\tau)$ converge vers $\psi_\eta(\underline{\mathrm{b}}_\infty)$ quand $\tau \to \infty$. Il s'agit de prouver la convergence uniforme de $\underline{\mathrm{W}}_\eta(\eta,\tau)$ vers sa limite quand $\tau \to \infty$, ce que nous pouvons faire plus facilement dans les coordonnées du domaine fixe. Plus précisément, nous prouvons que

$$\frac{\underline{\mathrm{b}}_\infty}{2} = -\psi_\eta(\underline{\mathrm{b}}_\infty), \quad \psi(0) = h \quad \text{et} \quad \psi(\underline{\mathrm{b}}_\infty) = 0.$$

Nous prouvons ensuite que ψ satisfait l'équation différentielle ordinaire

$$\psi_{\eta\eta} + \frac{\eta}{2}\psi_\eta = 0,$$

d'où on conclut que $(\psi,\underline{\mathrm{b}}_\infty) = (U,a)$. De façon similaire, on conclut que $(\phi,\bar{b}_\infty) = (U,a)$ où (U,a) est la solution unique du problème

$$\begin{cases} U_{\eta\eta} + \dfrac{\eta}{2}U_\eta = 0, & 0 < \eta < a, \\ U(0) = h, & U(a) = 0, \\ \dfrac{a}{2} = -U_\eta(a). \end{cases} \tag{1.3.9}$$

Pour formuler avec précision les résultats de ce chapitre, il est plus facile d'utiliser la variable y. Dans les variables (y,η), le problème pour $(\widehat{W}(y,\tau),b(\tau)) = (W(\eta,\tau),b(\tau))$ est donné par

$$\begin{cases} \widehat{W}_\tau(y,\tau) = \dfrac{1}{b^2(\tau)}\widehat{W}_{yy}(y,\tau) + y\left(\dfrac{d\,\ln\left(b(\tau)\right)}{d\tau} + \dfrac{1}{2}\right)\widehat{W}_y(y,\tau), & \tau>0,\ 0<y<1, \\ \widehat{W}(0,\tau) = h, & \tau>0, \\ \widehat{W}(1,\tau) = 0, & \tau>0, \\ \dfrac{1}{2}\dfrac{db^2(\tau)}{d\tau} + \dfrac{b^2(\tau)}{2} = -\widehat{W}_y(1,\tau), & \tau>0, \\ b(0) = b_0, & \\ \widehat{W}(y,0) = u_0(b_0\,y), & 0\le y<1. \end{cases} \tag{1.3.10}$$

Le résultat principal de ce chapitre est le suivant.

Theorem 1.3.1. *Supposons que u_0 satisfait l'hypothèse $\boldsymbol{H}_0$. La solution unique $(\widehat{W},b)$ du problème (1.3.10) est telle que*

$$\lim_{\tau\to+\infty} ||\widehat{W}(.,\tau) - \widehat{U}||_{C([0,1])} = 0, \tag{1.3.11}$$

$$\lim_{\tau\to+\infty} b(\tau) = a, \tag{1.3.12}$$

où $(\widehat{U},a)$ est la solution unique du problème

$$\begin{cases} \dfrac{1}{a^2}\widehat{U}_{yy} + \dfrac{y}{2}\widehat{U}_y = 0, & 0<y<1, \\ \widehat{U}(0) = h, \quad \widehat{U}(1) = 0, & \\ \dfrac{a^2}{2} = -\widehat{U}_y(1) & \end{cases} \tag{1.3.13}$$

qui est équivalent au problème (1.3.9).

Ce chapitre 4 est l'objet d'un article en collaboration avec Danielle Hilhorst, Yasuhito Miyamoto et Jean-François Scheid.

1.3.4 Chapitre 5 : Schéma numérique pour la résolution du problème de Stefan

Dans ce chapitre, on introduit la méthode ALE (Arbitrary-Lagrangian-Eulerian method) adaptée à la résolution de problèmes évolutifs. Puis, on décrit un schéma numérique basé sur une formulation ALE pour résoudre le problème de Stefan. On s'appuie ainsi sur un maillage adaptatif. Finalement, on présente des simulations numériques illustrant la stabilisation en temps long d'une solution de ce problème à frontière libre vers le profil auto-similaire. On choisit les données initiales (u_0,b_0) vérifiant l'hypothèse $\mathbf{H}_0$ et on montre numériquement la convergence vers la solution auto-similaire (U,a).

1.3.5 Chapitre 6 : Dissolution anodique d'un acier inoxydable dans un milieu chloruré sous contrôle potentiostatique: modèle mathématique avec une interface mobile

Très souvent, la propagation d'une piqûre est étudiée dans la littérature sous contrôle potentiostatique. Dans ce cas, un potentiel électrique ϕ_m est imposé à la surface du métal. Cette situation de corrosion ne correspond pas à un cas de corrosion naturelle mais elle permet néanmoins d'envisager le cas le plus défavorable de la vie d'un matériau. Dans ce chapitre, le cas de la propagation d'une piqûre sur du fer pur dans une solution de NaCl est traité.

D'un point de vue mathématique, ce problème fait intervenir des inconnues multiples et il a la forme d'un système de réaction-migration-diffusion avec une interface mobile (problème de type Stefan).

Dans un premier temps, le travail a porté sur la résolution numérique d'un système de diffusion-migration pour trois espèces chimiques (Fe^{2+}, Na^{+}, Cl^{-}). Les trois inconnues du système qui dépendent du temps et/ou de l'espace sont :

- le profil des concentrations des espèces chimiques chargées $C_i(x,t)$ pour i $\in \{1,2,3\}$;
- le potentiel de la piqûre $\phi(x,t)$;
- la profondeur $x_d(t)$.

Le mouvement de l'interface mobile est proportionnel au taux de dissolution donné par l'équation de Butler-Volmer.

Nous proposons une méthode de résolution numérique performante pour ce système d'équations aux dérivées partielles non linéaires fortement couplées. En particulier, la résolution de ce système par la méthode des différences finies apparaît, ici, très appropriée. Nous avons développé un schéma numérique implicite en temps en nous appuyant sur la méthode ALE (Arbitrary-Lagrangian-Eulerian) décrite au chapitre 5.

Nous avons ensuite effectué une étude paramétrique afin d'examiner le comportement du système au regard des variations de certains paramètres (potentiel imposé, concentration en NaCl, profondeur initiale de la piqûre, ...) pour identifier les facteurs critiques influençant la vitesse de dissolution du métal.

Le développement du modèle s'est ensuite poursuivi par la prise en compte de la réaction d'hydrolyse des ions fers. Nous présentons une méthodologie de résolution d'un système de diffusion-migration-réaction.

Ce chapitre 6 est en collaboration avec Danielle Hilhorst, Florence Lequien, Hiroshi Matano, Fabien Rouillard et Jean-François Scheid.

1.3.6 Chapitre 7 : Une approximation quasi-stationnaire du modèle de diffusion-migration

Il n'est généralement pas possible de trouver une solution explicite au modèle complexe fortement couplé de diffusion-migration développé dans le chapitre 6. C'est pourquoi le présent chapitre a pour but de déterminer une limite singulière de ce modèle dont la solution représente une approximation du modèle complet sous certaines conditions.

Ce système limite est obtenu en utilisant un nouveau changement de variable en temps et en faisant tendre la concentration représentative C_0 vers zéro. Ensuite, deux approximations majeures permettent de trouver analytiquement une solution approchée au modèle réduit.

Nous comparons ensuite cette solution approchée avec les résultats des simulations numériques. Il s'avère que la solution numérique correspond extrêmement bien à la solution approchée de la limite singulière.

Le modèle réduit permet de valider le schéma numérique développé pour décrire ce phénomène complexe.

Ce chapitre 7 est en collaboration avec Hiroshi Matano et Yoichiro Mori.

1.3.7 Chapitre 8 : Conclusions et perspectives

Le dernier chapitre synthétise les résultats obtenus numériquement. Il permet de montrer l'importance des simulations numériques pour pouvoir prédire la vitesse de propagation de la corrosion par piqûre d'un acier inoxydable en milieu chloruré et identifier les principaux facteurs critiques pour assurer la stabilité de la piqûre. Finalement, nous aborderons les différentes perspectives qu'ouvre ce travail multidisciplinaire.

Chapter 2

State of the art and relevant anodic-dissolution models

2.1 Corrosion of stainless steel

2.1.1 Stainless steels

In metallurgy, stainless steels also known as inox steel or inox from French word «inoxydable» are usually alloys of iron (Fe) and chromium (Cr) with the addition of other alloying elements used to modify their structure and properties. Generally based on Fe–Cr, Fe–Cr–C or Fe–Cr–Ni models, they contain at least 11% chromium as the main alloying element. This chemical composition is necessary to develop a chromium oxide layer of a few nanometres of thickness, which acts as a barrier, preventing the metal surface from staining or corroding in an atmospheric or aqueous environment. This chromium oxide layer Cr_2O_3 as shown in Figure 2.1.1 forms spontaneously in contact with oxygen. It has the particular ability to self repair in presence of oxygen, so stainless steels have poor corrosion resistance in poor circulation environments and in low-oxygen [3]. Its stability can be limited by inclusions and it may show some mechanical or chemical deterioration, depending on environmental conditions [3]. For example, in the environment containing chloride solution such as a sea water, chloride induces localized corrosion of stainless steel, which may develop under certain conditions by breaking down the passive layer as shown in Figure 2.1.1.

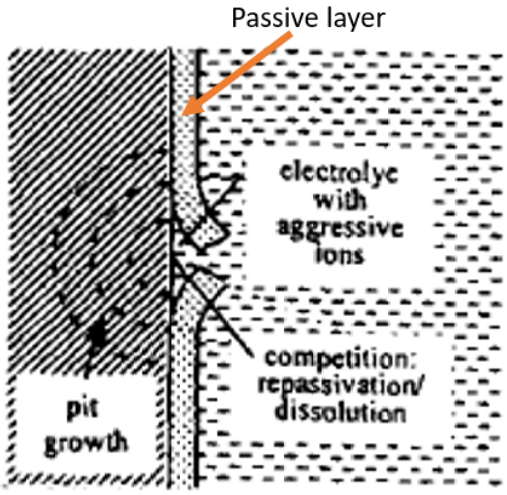

Figure 2.1.1: Passive layer (chromium oxide layer Cr_2O_3) breaking mechanism.

Stainless steels comprise a large group of alloys with a wide range of chemical compositions involving many different elements. This variety produces alloys with widely differing micro-structures and distinct mechanical properties. In the literature, their micro-structure is normally classified into five main types: ferritic, austenitic, martensitic, duplex and precipitation hardening stainless steel [3].

Austenitic stainless steels form the largest and most important group, known for their formability and resistance to corrosion, they are the most widely used grade of stainless steel. For example, they are used in a variety of engineering applications such as in nuclear power plants, boiler market, aeronautics, electronic components, railway equipment, tubes, chemical tanks, food vats and marine applications ... They are also proposed for the nuclear waste repository packages and they can be considered as primary containers.

As mentioned above, stainless steels are nevertheless susceptible by reaction with their aggressive environments to many forms of corrosion. This attack leads to changes in the metal's properties and affect the material performance and therefore their corrosion resistance.

2.1.2 Forms of Corrosion

Corrosion can be defined as deterioration of the integrity of stainless steel through the action of the surrounding environments that are contaminated, especially with chloride ions, alone, or in conjunction with mechanical forces. The process begins with a chemical or electrochemical reaction on the surface of the alloy. It will sustain an oxidation phenomena.

In general, in terms of environmental conditions, corrosion is classified as either dry or wet (aqueous) and as high or low temperature corrosion.

It can occur in many forms. Such forms are pictured schematically in Figure 2.1.2.

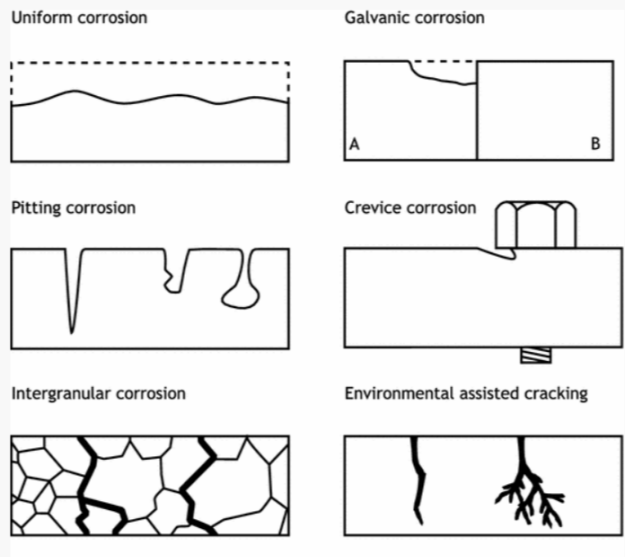

Figure 2.1.2: Figure showing typical corrosion forms occurring on metals [56].

Therefore, it is essential to accurately identify the type of corrosion to establish the mechanism and apply the appropriate protective procedures. Each type of corrosion has particular characteristics. It is classified as general or localized, depending on how it attacks the material. Uniform or general corrosion is a type of corrosion that occurs evenly across the surface of a metal, associated with

uniform metal dissolution. Atmospheric corrosion is perhaps the most common example of uniform corrosion. By contrast, **a localized attack** happens in the presence of certain aggressive ions such as chlorides in a restricted area. It leads to the formation of small isolated holes that may reach considerable depth. In this case, the corrosion rate is often high and is generally higher than that for uniform corrosion. Such localized attack is more detrimental to the integrity of stainless steel and usually involves one or more of crevice corrosion, pitting corrosion...[3, 29]. We recall that stainless steels have a good resistance to uniform corrosion because they naturally form thin protective films on the surface (at the nanometric scale) which strongly reduce their corrosion rate in their exposure environment.

There are several similarities between the mechanism of pitting corrosion and crevice corrosion. Both are insidious and unexpected and often share similar growth processes. Some researchers like Wilde and Willams assume that a propagating pit is a special form of crevice corrosion for solutions containing NaCl (in seawater) and that crevices are big pits [87].

In the present study, we are interested, in particular, in the phenomenon of **pit corrosion**.

In the next section, the pitting process is described.

2.2 Phenomenology of Pitting Corrosion of stainless steel

One of the very major failure mechanisms **in aggressive aqueous solution** is **pitting corrosion**. It is generally associated to the presence of a particular anion, notably the chloride ion. Pitting occurs when the protective passive layer, described in Subsection 2.1.1, breaks down in small isolated spots. Once started, the corrosion may accelerate because of differences in the potential between the large area of passive surface and the active pit [83]. Then, it leads to the formation of small isolated holes that may reach considerable depth. Therefore, the life cycle of stainless alloy decreases. Examples of various pitting modes are shown in Figure 2.2.1.

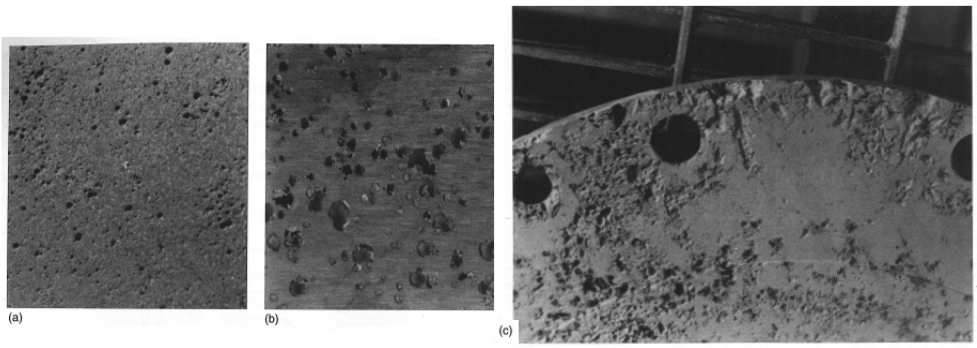

Figure 2.2.1: Examples of pitting in stainless steel (a) shallow pits; (b) deep pits; (c) deep closely spaced pits bordering on an irregular type of uniform corrosion in some areas. (From A. I. Asphahani and W. L. Silence, Metals Handbook, Vol.13, Corrosion, 9th ed., ASM, Metals Park, OH, p.113, 1987) [38].

Then, depending on the metallurgy of the alloy and the chemistry of the environment, several typical pit morphologies are possible. Figure 2.2.2 shows examples of various pit morphologies found in the literature. The local degradation of the passive layer formed on the metal surface leads to a physical separation of the anodic sites that describe the pit and cathodic sites that describe the stainless steel surface (passive layer) as shown in Figure 2.2.2.

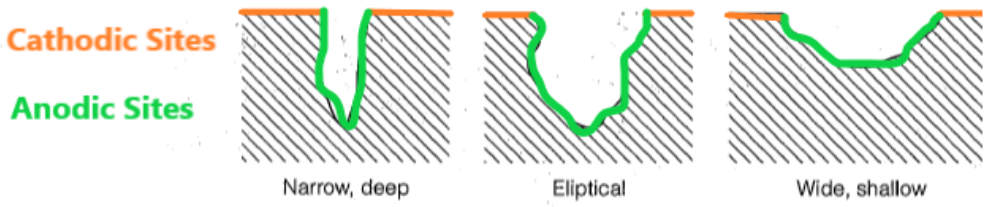

Figure 2.2.2: Pit morphologies, cathodic and anodic sites [38].

2.2.1 Mechanisms of pit corrosion

Pitting corrosion is a complex phenomenon. It can be divided into three distinct stages as shown in Figure 2.2.3. The **initiation** of pitting corrosion consists in local rupture of the passive layer which leads to the creation of a pit embryo, «a nano-sized defect». Then, depending on the chemistry of the environment, either the passive layer reforms (this is called **repassivation**) or the underlying steel corrodes (this is called **propagation**).

Once the pit is repassivated, the passive layer is again susceptible to deterioration leading to the re-initiation of the pit. Therefore, it constitutes a pitting corrosion cycle. In this subsection, we will summarize the literature's knowledge about these three steps of pitting corrosion.

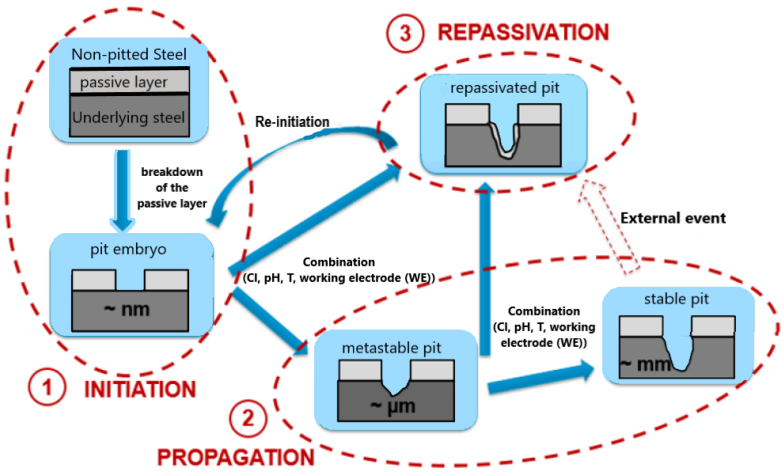

Figure 2.2.3: Diagram of the various stages of pitting corrosion on stainless steel [30].

2.2.1.1 Pitting initiation process

The process of pitting corrosion has been described as random and stochastic while the prediction of time and location of events remains extremely difficult. Therefore, pitting corrosion is treated as a time-dependent stochastic damage process characterized by an exponential or logarithmic pit growth [5]. Thus, the initiation of the pit is stochastic [69]. This is reflected in the uncertainty of the criteria characteristic of initiation and the number of theories of initiation that are discussed in literature [30, 70]. This process is very dependent on the protection capacity of the passive film which depends strongly on its composition.

2.2.1.2 Pit propagation

After the initiation stage, if the occluded cell (the pit nuclei) is sufficiently developed, to avoid any instantaneous repassivation, the propagation of the pit occurs.

There are two types of pit propagation in literature [77]:

- Metastable propagation for short periods of time where the pit still has a strong possibility to repassivate,
- Stable propagation for long periods of time where maintaining critical conditions inside the pit prevents its repassivation.

Many metastable pits of the order of a tenths or hundreds of nanometers are initiated, propagated for a period of less than a second and sometimes even a millisecond. Then, they repassivate because they do not maintain the necessary conditions for their propagation. However, the pit can survive after the metastable stage if sufficient conditions in terms of chemistry or potential are developed inside the pit to prevent its repassivation.

A model describing the stabilization and growth of a localized pit corrosion can be reduced to two steps :

❶ The first step leading to the evolution of the chemistry within the occluded cell is the local disappearance of the dissolved oxidizing species (usually oxygen), which is rapidly consumed by corrosion and cannot be regenerated due to the very low diffusional exchange with the external environment.

➥ The consequence of this step is the disappearance of the cathodic reaction which is necessary for the equilibrium of the dissolution process. As a result, it follows a separation between anodic and cathodic reactions with a dominant anodic reaction in the occluded cell, and a dominant cathodic reaction on its external surface.

❷ The second step leading to the local environment evolution within the occluded cell is carried out by the following processes (see Figure 2.2.4):

- The production of cations and H^+ **ions** in the occluded cell by hydrolysis of the metallic cations.
- The migration of negative charged ions such as chlorides ions to the anode zone in order to ensure local electroneutrality of the pit solution (occluded cell).

➥ As a result, the pit solution becomes concentrated in complex metal chlorides and its pH decreases significantly. In literature, **the pH of the pit solution** and **the high concentration of metallic cations** are considered to be the two main factors to ensure the pit stability [71].

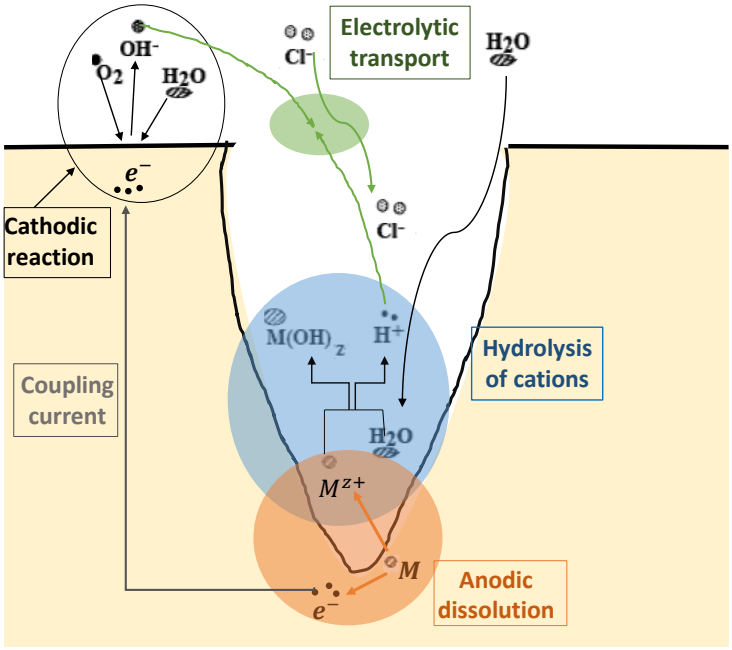

Figure 2.2.4: Main processes involved in the evolution of the environment in an occluded cell exposed to a NaCl solutions.

Diffusion and migration of ions are two fundamental phenomena involved in pitting corrosion. On one hand, the diffusion is a phenomenon that tends to unify the composition of the electrolyte at any point. Thus, it induces the transfer of mass from the most concentrated region to the least concentrated, hence the transport of mass outside the pit solution. On the other hand, the migration describes the movement of ions under the effect of an electric field. Here, we consider the migration of aggressive ions such as chloride ions to the inside of the pit.

The local electroneutrality of the pit solution is maintained by the migration of chlorides ions to the anodic region where cations are accumulated.

Finally, during pitting propagation, the anodic and cathodic reactions are coupled, i.e. any electrons produced by the oxidation of the metal must be consumed by a reduction reaction, often the reduction of oxygen outside of the pit on the passivated surface.

2.2.1.3 Pit repassivation

The repassivation occurs when the stability of the pit is lost. In this case, an oxide layer is formed on the active surface of the pit. This process will take place in the case of the dilution of the concentrated solution present in the propagation phase.

2.2.2 Review of critical factors proposed for pit stability

In this thesis, we will focus only on the **pit propagation** stage. Therefore, in this section, we are interested to identify the main criteria proposed in literature to ensure long-term pit propagation.

Many numerical models focus only on the stable growth stage of pitting corrosion [10, 44, 51, 71–75]. Srinivasan and Kelly discussed the critical electrochemical conditions describing the transition of

a corroding surface from active dissolution to repassivation [73]. They stated that pit propagation required the presence of a concentrated solution of cationic chlorides at the corroding site. This concentrated local chemistry, which is a consequence of the anodic dissolution of the metal and cation hydrolysis, is followed by chloride migration from the bulk into the occluded geometry of the pit to maintain the local electroneutrality of the solution. This local acidic environment promotes continued corrosion. Then, they conclude that a minimum aggressive chemistry is required to sustain pitting. This chemistry is described in terms of **a critical concentration of metal cations** and in terms of the pit solution **pH**. If these minimum conditions are not met, the chemistry in the pit becomes unfavorable toward continued dissolution and repassivation starts [73]. Quantification of these two parameters was proposed for 316L stainless steel.

Similarly, Sridhar made a review about the pit stability criteria proprosed in literature [71]. He shows that advances in modeling and analytical techniques provide two criteria which are generally used for solution-chemistry effects on localized corrosion propagation and repassivation. This two criteria are: the critical pH and the critical concentration of metal-anion complexes. In fact, he discussed the role of acidification as the mechanism of pit stabilization. Next, he discussed the approaches in understanding local chemistry changes during repassivation, with an emphasis on the role of metal-anion complexes in localized corrosion. He considered that the formation of metal-salt layer at the corroding interface may prevent repassivation. In the other hand, repassivation can occur at much lower concentrations of metal cations with respect to salt film saturation. Finally, since the metal-salt complex formation and the acidification resulting from hydrolysis are coupled, it is often difficult to distinguish these two mechanisms purely from artificial pit techniques [71]. Thus, we can deduce that there is a strong link between this two criteria for pit stability.

Finally, Laycock and White have modeled and simulated the pit propagation in stainless steel under potentiostatic conditions based on a critical metallic concentration in the pit [44]. Their model shows good qualitative agreement with experimental results concerning pit morphology and propagation stability at least for short time scales.

In conclusion, two main criteria for pit stability have been proposed in literature: **the critical concentration of metal cations** and the **pH** of the pit solution. These criteria will be used and discussed in subsection 6.5.4 of Chapter 6.

2.3 Review of anodic-dissolution models

2.3.1 Introduction

Since many decades, several computational models have been developed to study and predict the time evolution of pitting corrosion. The objective from these models is to provide powerful means to simulate the initiation and the propagation of localized corrosion in various environments, and to reduce its impact.

In this section, we focus on reviewing several corrosion models developed to describe anodic-dissolution. The main characteristics of each model are presented. These models start from mathematical formulations for electro-chemico-mechanical phenomena ; the authors then use various numerical methods to describe the progression of the pitting process such as : the evolution of the localized corrosion (pit or crevice) shape and morphology, the concentration of different chemical species inside and outside the pit, the electric potential distribution over the domain of interest, etc.. Reaction kinetics at the corrosion front and the transport kinetics of the chemical species inside the pits are usually taken as the basis for these models [35].

The developed models are mainly intended for modeling both pit corrosion and crevice corrosion.

Thereafter, all the discussed models describe the propagation of pit or crevice.

Crevice corrosion versus pit corrosion:

Let us define the main differences between these two phenomena. The main and first corrosion phenomenon which was modeled is «crevice corrosion» [66, 80]. **Crevice corrosion** occurs when two zones of a metallic component are clearly separated geometrically (see Figure 2.3.1). It starts when there is in the steel a free zone which penetrates deeply into the material (several millimeters for example). Due to this initial geometry, two zones are clearly distinguished: the surface metallic zone and the zone inside the steel (crevice). Oxygen cannot enter the crevice easily, so that this zone becomes an anodic zone (which cannot passivate and, as a consequence, dissolves). The other parts at the surface of the steel, where oxygen can access, easily passivate which leads to the formation of an oxide layer. Thus, there is a zone which mainly produces electrons in the crevice (oxidation of the steel) and a zone which mainly consumes electrons (oxygen reduction).

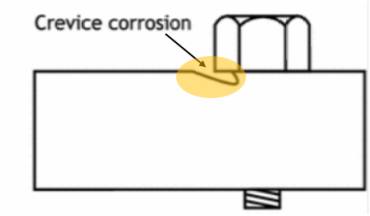

Figure 2.3.1: Example of crevice corrosion.

The initial state of the crevice solution taken in almost all models is the initial chemistry composition (as in the bulk). The initial dimension of the crevice is around a few millimeters.

Pitting corrosion is quite different in its starting geometrical configuration. A pit is initiated on an imperfection existing on an initial flat stainless steel surface. The initial size of a pit is only a few micrometers in all directions. Moreover, it is proposed in the pitting theory that the initial solution chemistry in contact with the metal is not identical to the bulk chemistry. However, it should be very concentrated in aggressive species which prevent stainless steel to passivate as we have shown previously. Moreover, initially, the pit mouth is always covered by a metallic cap as schown in Figure 2.3.2 which allows the existence of this aggressive solution [44]. Without this cap, it is not possible to justify the existence of such an aggressive solution because the solution would be diluted very fast and passivation would occur from the first instants [44].

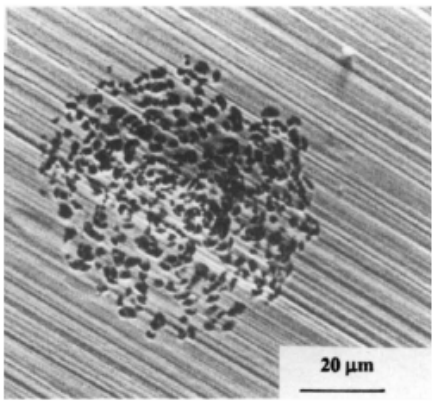

Figure 2.3.2: Covered pit on 2304 SS, showing a more complete cover with many tiny perforations [45].

2.3.2 Localized corrosion modeling

The task of developing reliable growth laws is huge because of the complex nature of localized corrosion processes. This makes the prediction of localized chemistry within the pit a very difficult task. In this context, several approaches are used to model the pit propagation kinetics in literature.

First of all, Turnbull has discussed both empirical and mechanistically based models of pit propagation kinetics in a literature review article [80]:

1. Empirical models of pit growth kinetics are based on experimental measurements. Turnbull shows that these empirical models have an important limitation in that only average properties are measured and hence the results do not reflect the distributed behavior of pitting in real systems.

2. Turnbull shows that mechanistically based models can assess the effect of a wide variation of parameters, providing understanding and guidance in testing and interpretation of results and aiding judgment. However, he shows that absolute prediction of pit growth kinetics based only on mechanistic modeling is uncertain because of specific limitations in the input data and the need to make assumptions in some cases about the effect on parameters such as the diffusion coefficient of precipitate products formed within the pit [80].

3. Finally, Turnbull proposes that the complementary use of empirical modeling methods and the more sophisticated mechanistically based models provides an effective method for predicting pit growth kinetics [80].

Moreover, Turnbull enumerates the main physical phenomena which should be considered to well describe the propagation of localized corrosion (reactions, transport by diffusion, electromigration,...) [80].

Next, based on deterministic modeling methods, we discuss the fundamentals needed to describe localized corrosion kinetics.

2.3.2.1 Corrosion kinetics basics: reaction kinetics and transport kinetics in the electrolyte

Basics for pit growth models include both the dissolution kinetics at the corrosion front and the transport kinetics of the species inside the electrolyte [35].

Reaction kinetics:

Pit growth in localized corrosion in metals exposed to aqueous solution can be reduced to the anodic reaction at the pit surface, since it is the reaction responsible for dissolution. As a result, the produced electrons in the anodic reaction travel in the solid metal, reach out the surface at a point, and participate in the cathodic reactions (see Figure 1.1.2 and Figure 2.3.3). The results of the cathodic reactions are corrosion products (H_2 gas or precipitated solid products) [35].

Figure 2.3.3 shows the localized metal dissolution by the anodic reaction in the presence of the electrolyte.

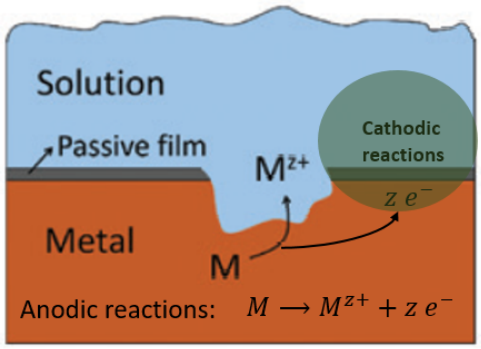

Figure 2.3.3: Schematic of anodic dissolution of some metal atom (M) and its dissolved state in the solution with $+z$ charge number: M^{z+} [35].

The anodic reaction rate can be expressed by [35] (cf. Appendix A)

$$i_a = i_0 \exp\left(\frac{\alpha \eta z F}{RT}\right), \tag{2.3.1}$$

where i_a is the anodic current density, z the charge number of the dissolved metal ion, η the overpotential (cf. Appendix A), F Faraday's constant, R the gas constant, T the absolute temperature, α the transfer coefficient and i_0 the exchange current density.

When the corrosion rate only depends on the anodic reaction and follows equation (2.3.1), the corrosion regime is called **activation-controlled** [35] (such a case is described in Chapter 6).

When the reaction rate is higher than the diffusion rate in the electrolyte, the dissolved ions M^{z+} accumulate near the corroding surface, and once their molar concentration C, reaches the saturation value C_{sat}, the solution cannot sustain a higher amount of M^{z+}. The excess of the ions precipitate as salt molecules and form a salt layer. Such a situation occurs at the pit bottom. The salt layer thickness increases until the potential drop through the thickness balances the dissolution rate with the diffusion rate in the electrolyte. Then, the corrosion rate is not controlled by the applied potential but by the diffusion rate inside the electrolyte. This corrosion regime is referred to as **the diffusion-controlled** mode [35] (such a case is described in Chapter 3). Since ion transport can affect the corrosion rate, we conclude on the importance of transport kinetic effects within the solution.

Figure 2.3.4 shows a schematic description of diffusion-controlled corrosion in comparison with the activation-controlled regime. In Figure 2.3.4 (A) in the activation-controlled regime, the anodic dissolution rate which can be given by the molar dissolution flux $\mathbf{J}_{diss}$, satisfies

$$\mathbf{J}_{diss} = \frac{i_a}{zF} = \mathbf{J}(\eta), \tag{2.3.2}$$

where i_a is given by (2.3.1). However, in Figure 2.3.4 (B), which describes the diffusion-controlled regime, the anodic dissolution rate satisfies

$$\mathbf{J}_{\text{diss}} = \mathbf{J}_{\text{trans}}, \tag{2.3.3}$$

where $\mathbf{J}_{\text{trans}}$ is the transport molar flux near the corrosion front.

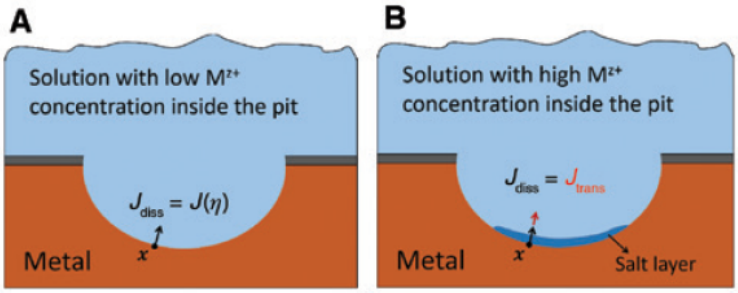

Figure 2.3.4: Schematic of metal (M) anodic dissolution in pitting corrosion under (A) activation-controlled and (B) diffusion-controlled corrosion regimes [35].

Transport kinetics in the electrolyte :

Nernst-Plank equation is commonly used to describe the transport of chemically charged ions. It describes the conservation of mass during the corrosion process. It is given by

$$\frac{\partial C_i}{\partial t} = -\nabla . \mathbf{J_i} + \mathcal{R}_i, \tag{2.3.4}$$

where C_i is the molar concentration of the ith species, $\mathbf{J_i}$ its molar flux, t the time and $\mathcal{R}_i$ the reaction term [35, 64]. The molar flux can be expressed as

$$\mathbf{J_i} = -[D_i \nabla C_i + z_i F \frac{D_i}{RT} C_i \nabla \phi - \overrightarrow{\nu} C_i], \tag{2.3.5}$$

where D_i is the diffusion coefficient of the ith species (assumed to be constant in most models, but in general it can vary in space), $\overrightarrow{\nu}$ the velocity and ϕ the electric potential.

The first term on the right-hand-side of (2.3.5) is the **diffusion flux**, the second term presents the **electromigration flux** and the third term expresses the **advection flux**.
An additional equation is required in order to find the electrical potential ϕ. A Poisson-type equation is usually used for finding ϕ; this equation is then reduced to the local electroneutrality equation given by ([35, 64])

$$\sum_i z_i C_i = 0. \tag{2.3.6}$$

Most of the computational models for pitting corrosion are based on the equations (2.3.1)–(2.3.6).

2.3.2.2 Computational models for localized corrosion

Most models in literature are based on solving the classical transport equation (2.3.4) (simplified version of the Nernst Planck equation) with a numerical method to compute the transport kinetics in the electrolyte. Moreover, they use an additional technique to solve the moving boundary (separately) such as updating the domain and remeshing the updated geometry [35].

In the following table, we compare some of these models proposed in literature and we identify the main characteristics of each of them. Of course, this Table has not the objective of being exhaustive. The only purpose is to cite several of them which appear relevant for the proposed work in this PhD. In general, the models are developed in dimension 1 or 2 in space. Most of these models are developed to describe pit/crevice corrosion in diluted solutions. In this case, the concentration of species are employed instead of their activities. Moreover, time evolution transport equations are considered to describe the evolution of the pit/crevice chemistry within the cavity of the localized corrosion with time. The transport is ensured by diffusion or electromigration or both. Finally, except the first model of Sharland, all models consider a moving boundary.

Once the different assumptions and approximations were made in these models (geometry of the pit, chemical species considered, boundary conditions of the system), different numerical methods were used as well for the resolution of the obtained system of equations.

Table 1: Comparaison between models proposed in literature to describe pit/crevice propagation.

Model	Year	Numerical method	Transport phenomena	Chemical Species or Electrolyte or Metal	Geometry	Boundary of the pit or crevice	Wall of the pit or crevice	Precipi-tation	Cathodic reaction in the bottom	Solution	Variable
Sharland and Tasker [66]	1988	Finite Element Method (FEM)	steady state transport equation including: diffusion electromigration and reaction	Fe^{2+} OH^- Na^+ Cl^- H^+ $Fe(OH)^+$	rectangular pit or crevice (fixed geometry) (1D in the case of passive walls)	fixed	passive and active	yes	reduction of water and hydrogen ions	diluted	concent-ration
Walton [81]	1990	Finite Difference Method (FDM)		Acetate and Sulfuric acid electrolyte					not included	diluted	concent-ration
Walton et al. [82]	1996									concent-rated	activity
Laycock et al. [42]	1998	(FEM) Dirichlet-type boundary condition on the pit boundary	time evolution transport equation including: diffusion	304 stainless steel	axisymmetric domain (2D) (evolving geometry with perforated (lacy) covers in the entrance of the pit)	moving	—			diluted	concent-ration
Laycock and White [41]	2001	(FEM) Neumann-type boundary condition on the pit boundary									
Xiao and Chaudhuri [86]	2011	COMSOL multiphysics software and a separate MATLAB program.	time evolution transport eq. : diffusion electromigration and reaction	aluminum alloys	axisymmetric domain (2D)	moving	—	not included	The four-electron O_2 reduction	diluted	concent-ration

Conclusion: From the models which have been already developed, several recommendations can be proposed for the strategy when developing another model :

1. transport equation: use of classical transport equation (Nernst-Plank equation) ;
2. numerical method employed: finite element method (FEM) is relevant for multidimensional modeling [46] ;
3. boundary condition at the pit bottom : the moving boundary according to Stefan-type condition is an essential part to describe the evolution of the morphology of the localized corrosion. It should not be ignored.

The advantages of such classical models are that they can assess the effect of a wide variation of parameters, providing understanding and guidance in the interpretation of results. These models are the ones used in commercialized software such as COMSOL. However, the disadvantages of such classical models are that the boundary tracking and the domain updating are required (complex and costly) [35].

2.4 Conclusion

This chapter introduces the phenomenology of pitting corrosion and presented several models developed for describing pit propagation. First, we described the distinct stages which may define the life cycle of the pit. To do so, three main mechanisms have been proposed: pitting initiation process, pit propagation and pit repassivation. We have centered our study on the propagation phase. Therefore, to ensure a long-term pit propagation, we have reviewed the main critical factors proposed in literature to ensure the stability of the pit. Two main criteria are derived: the critical concentration of metal cations and the pH of the pit solution. In the last section, we presented several anodic-dissolution models to describe pit or crevice propagation. We detailed the basics for pit growth models which include the dissolution kinetics at the corrosion front and the transport kinetics of species inside the electrolyte. Finally, we compared different computational models for pit propagation introduced in literature.

As we have shown in this chapter, pit corrosion is a complex phenomenon. The study of such corrosion problems requires multidisciplinary knowledge, including electrochemistry, thermodynamics, kinetics...

From this non-exhaustive literature review, the main objectives of this thesis become

a) to derive a relevant anodic-dissolution model to describe pit/crevice propagation,

b) to propose a performant numerical solution method for the strongly coupled nonlinear mathematical system. The numerical scheme will be implemented in an open source software (Python). The advantages of such software are multiple :

   - a complete mastering of all the input variables. Thus, we can examine the behavior of the mathematical system with respect to the variation of certain physical/chemical parameters,
   - a complete mastering of the numerical scheme and the described physics to provide a more accurate description of the physical reality,
   - the control of the numerical scheme in order to optimize the computation time/ accuracy of results.

In view of literature, one of the most relevant approach is to consider a sophisticated mechanistically based models with the complementary use of empirical results. The mechanistic approach is based on a deterministic approach which requires a description of the metal environment system by a complex system of physico-chemical equations.

Thus, we have chosen to use such an approach to describe the phenomenon of pit/crevice propagation in a stainless steel taking into account the complexity of its development (anodic dissolution, diffusion, migration and reactions). From a mathematical point of view, this problem can be identified as a Stefan problem involving a convection-reaction-diffusion system.

Due to the complexity of the problem, we chose to start in one-space dimension to create a relevant and efficient numerical scheme which will allow us to simulate the time evolution of pit propagation. The model will be developed step by step to gradually integrate the complexity of the chemical system.

Therefore, first, we will study a pit propagation model to describe a diffusion-controlled regime. The corresponding mathematical system is a one-dimensional problem including :

- a partial differential equation: to describe transport by diffusion of a non charged metal ion ;
- appropriate boundary conditions of Dirichlet type ;
- a boundary condition to describe the moving interface.

This is the subject of the next Chapter 3.

Next, we develop a more complicated coupled system for concentrations and potential to describe pit/crevice propagation. The concentration system will incorporate a diffusion term, a migration term (convection term related to the potential difference) and a reaction term into the partial differential equation. We define an appropriate Robin-type boundary conditions as well as a boundary condition to describe the moving interface. This is the subject of Chapter 6.

Chapter 3

Description of a Simple Moving Boundary Model: Iron Dissolution

3.1 Introduction

The first deterministic model for pit propagation we are dealing with is described by the following two references: [61, 62].

Scheiner and Hellmich [61, 62] derived their model to describe a stable pitting corrosion as an activation-controlled dissolution process (potential-dependent electrochemical kinetics law for the dissolution reaction) or as a diffusion-controlled dissolution process (potential-independent electrochemical kinetics law for the dissolution reaction). In fact, as long as the electrolyte solution adjacent to the electrode boundary does not reach its saturation level, they used the Butler-Volmer-type dissolution kinetics law to describe the dissolution rate, and Fick's law to describe the concentration distribution in the electrolyte solution. In this case, it is an activation-controlled corrosion mechanism. However, once the saturation level is reached at the electrode boundary, the pit depth evolution is governed by the diffusion of ions from the electrode boundary into the pit solution. In this case, it is a diffusion-controlled corrosion mechanism [61]. In the next section we present a brief summary of the modeling of this system for the two cases given above (for more details, see [61, 62]).

We restrict our study to the stage of pit propagation in order to describe a stable pitting corrosion of a pure iron steel. Here, only the bottom of the pit is active which give rise to an anodic metal dissolution. The cathodic reaction in the metal surface is neglected.

3.2 Governing model equation

3.2.1 Presentation of the mathematical model in two cases: activation- and diffusion- controlled dissolution processes

In this subsection, we describe the mathematical model for a stable pitting corrosion in one space dimension. The domain of study is given by the pit solution $(0,x_d(t))$ where $x_d(t)$ indicates the position of the moving boundary at time $t > 0$.

For suitable initial and boundary conditions, the model given by Scheiner and Hellmich [61, 62] is based on the mass conservation law

$$\frac{\partial C(x,t)}{\partial t} + \frac{\partial \mathbf{J}(x,t)}{\partial x} = 0 \quad \text{for all } t > 0, 0 < x < x_d(t), \tag{3.2.1}$$

and on the interface condition, also called jump or Rankine-Hugoniot condition [61] given by

$$\mathbf{J}(x,t) + [C_{\text{solid}} - C(x,t)]v(x,t) = 0 \quad \text{for all } t > 0, x = x_d(t), \tag{3.2.2}$$

where $\mathbf{J}$ is the ion flux and v is the velocity of the moving interface.

Next, we assume that once the iron ions are dissolved, their movement in the pit solution will be primarily driven by diffusion, according to the Fick's law

$$\mathbf{J}(x,t) = -D\frac{\partial C(x,t)}{\partial x} \quad \text{for all } t > 0, 0 < x < x_d(t), \tag{3.2.3}$$

where D is the diffusion coefficient of the iron ions.

Two possible cases can take place during the pit propagation. In the first case, we assume that the electrolyte solution adjacent to the electrode boundary does not reach its saturation level so that $C\left(x_d(t),t\right) < C_{\text{sat}}$ for all $t > 0$: this case is described as an activation-controlled corrosion mechanism. According to Scheiner and Hellmich [61], in view of (3.2.3), (3.2.2) becomes

$$-D\frac{\partial C(x,t)}{\partial x} + [C_{\text{solid}} - C(x,t)]\left(\frac{A_{\text{diss}}}{C_{\text{solid}}}\exp\left[\frac{zF(E_{\text{corr}} + \epsilon\,\eta_a)}{RT}\right]\right) = 0 \quad \text{for all } t > 0, x = x_d(t), \tag{3.2.4}$$

where A_{diss} is the dissolution affinity, R the universal gas constant, E_{corr} the corrosion potential, z the average charge number of the dissolving metal, F the Faraday's constant, ϵ the transfer coefficient and η_a is the system overpotential as the applied potential E deviates from E_{corr}, $\eta_a = E - E_{\text{corr}}$ [61].

This is a Butler-Volmer type condition for metal dissolution. Such a case is studied in Chapter 6 since this is the most complicated physical situation.

In the second case, we assume that the saturation level is reached at the electrode boundary, so that, $C\left(x_d(t),t\right) = C_{\text{sat}}$ for all $t > 0$: this case is described as a diffusion-controlled corrosion mechanism and according to Scheiner and Hellmich [61], in view of (3.2.3), (3.2.2) becomes

$$-D\frac{\partial C(x,t)}{\partial x} + [C_{\text{solid}} - C_{\text{sat}}]\frac{dx(t)}{dt} = 0 \quad \text{for all } t > 0, x = x_d(t). \tag{3.2.5}$$

3.2.2 Model representation of the stable pitting corrosion: case of a diffusion-controlled dissolution process

In order to study the diffusion–controlled dissolution regime, we consider an experimental case where the pit is as described in Figure 3.2.1.

Figure 3.2.1(b) shows an "artificial pit" which preserves the one-dimensional configuration. It is the simplest experimental means to simulate pitting corrosion [62]. The corroding steel wire with a diameter of 50 µm was wrapped up with epoxy resin, and only the wire face was in contact with the aqueous solution (1 M NaCl) of the bulk solution.

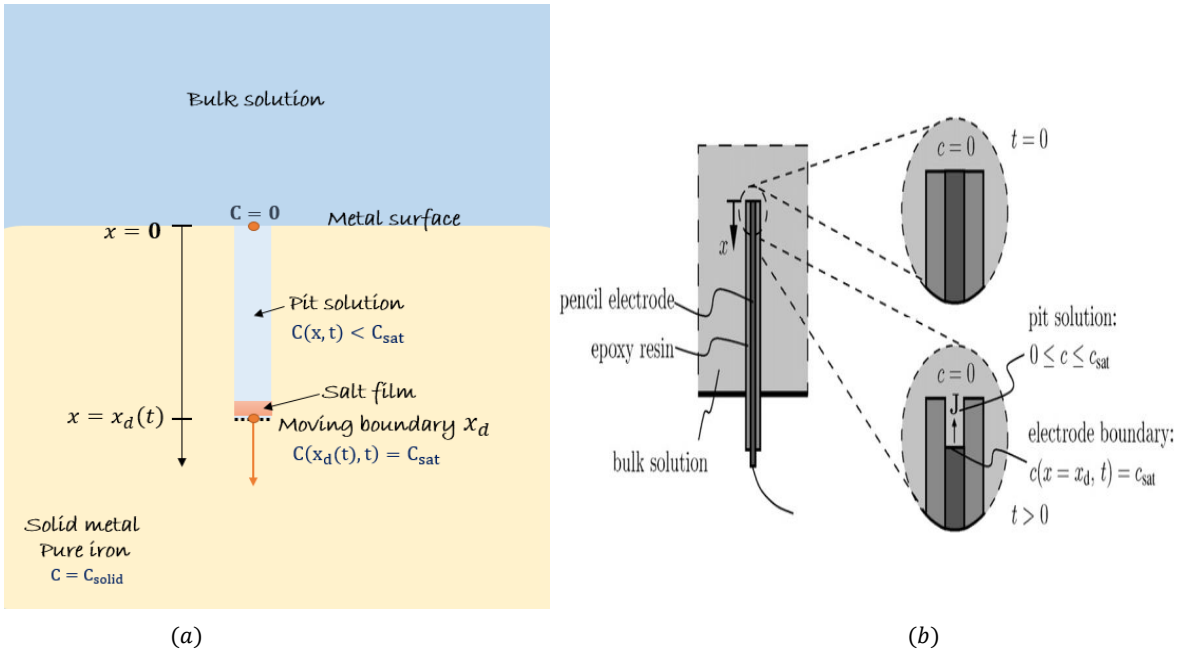

Figure 3.2.1: One space dimension pit: (a) domains of the stable pit, (b) Setup for the measurement of the current density at a pencil electrode [62].

The pit growing in stable corrosion mode is represented by the following domains (see Figure 3.2.1(a)):

(i) Solid metal: the first domain is related to the solid metal with temporally and spatially constant metal atom concentration. We consider pure iron Fe. In the following, we represent the metal atom concentration by C_{solid}.

(ii) Salt film at the pit bottom: the second domain takes place at the anode. The metal ions released from the solid electrode combines with chlorides in the solution, forming metal chloride salt. The more ions released, the more salt is formed, until the saturation concentration of the salt is reached [62]. Thus, in the bottom of the pit, the iron ion concentration remains constant and equal to the saturation limit C_{sat}.

(iii) Pit solution: the third domain relates to the pit solution with temporally and spatially varying concentration of dissolved iron ions. Their concentration is laying below the saturation concentration: $C(x,t) < C_{\text{sat}}$.

(iv) Bulk solution: the fourth domain relates to the bulk solution outside of the pit, characterized by the vanishing iron ion concentration $C = 0$.

The depth of the pit results from:

(i) the diffusion rate of dissolved iron ions outside of the pit;

(ii) the dissolution rate of the metal at the electrode boundary.

The boundary motion has to comply with the mass conservation law.

Finally, the one-dimensional mathematical model which describes a stable pitting corrosion in

the case of a diffusion controlled dissolution process is given by

$$\begin{cases} \dfrac{\partial C(x,t)}{\partial t} = D\,\dfrac{\partial^2 C(x,t)}{\partial x^2}, & t>0,\ 0<x<x_d(t), \\ C(0,t)=0, & t>0, \\ C(x_d(t)^-,t)=C_{\text{sat}}, & t>0, \\ \dfrac{dx_d(t)}{dt} = \dfrac{D}{C_{\text{solid}}-C_{\text{sat}}}\,\dfrac{\partial C(x_d(t)^-,t)}{\partial x}, & t>0, \end{cases} \tag{3.2.6}$$

together with suitable initial conditions for x_d and C, where $x_d(t)^-$ refers to the liquid side of the moving boundary, $D>0$ and $C_{\text{solid}}>C_{\text{sat}}$.

3.3 Analytical solution for the diffusion-controlled dissolution process

The goal of this part is to find an explicit solution of Problem (3.2.6) which defines the depth of the pit for a given time. To do so, we introduce the self-similar variable

$$\xi = \frac{x}{\sqrt{D(t+1)}}, \tag{3.3.1}$$

and the dimensionless variables

$$\widetilde{C}(\xi) = \frac{C(x,t)}{C_{sat}}, \varepsilon = \frac{C_{\text{sat}}}{C_{\text{solid}}-C_{\text{sat}}}. \tag{3.3.2}$$

Now, we look for a special solution of Problem (3.2.6) in the form

$$\begin{cases} C(x,t) = C_{sat}\,\widetilde{C}(\xi) = C_{sat}\,\widetilde{C}\left(\dfrac{x}{\sqrt{D(t+1)}}\right), \\ x_d(t) = \xi_d\,\sqrt{D\,(t+1)}, \end{cases} \tag{3.3.3}$$

for some positive constant ξ_d still to be determined.

Hereafter we use the following symbols for notational simplicity:

$$\square_x := \frac{\partial \square}{\partial x}, \quad \square_{xx} := \frac{\partial^2 \square}{\partial x^2}, \quad \square_t := \frac{\partial \square}{\partial t}.$$

In view of (3.3.2), it follows that

$$C_t = -\frac{C_{\text{sat}}\,\xi}{2(t+1)}\widetilde{C}_\xi, \quad C_x = \frac{C_{\text{sat}}\,\widetilde{C}_\xi}{\sqrt{D(t+1)}}, \quad C_{xx} = \frac{C_{\text{sat}}\,\widetilde{C}_{\xi\xi}}{D\,(t+1)},$$

and deduce that

$$\begin{cases} \widetilde{C}_{\xi\xi} + \dfrac{\xi}{2}\,\widetilde{C}_\xi = 0, & 0<\xi<\xi_d, \\ \widetilde{C}(0)=0, & \widetilde{C}(\xi_d)=1. \end{cases} \tag{3.3.4}$$

In turn, (3.3.4) implies that

$$\widetilde{C}_\xi(\xi) = \widetilde{C}_\xi(0)e^{-\frac{\xi^2}{4}} \quad \text{for all} \quad \xi\in(0,\xi_d), \tag{3.3.5}$$

so that

$$\widetilde{C}(\xi) = \widetilde{C}(0) + \widetilde{C}_\xi(0)\int_0^\xi e^{-\frac{s^2}{4}}ds \quad \text{for all} \quad \xi\in(0,\xi_d). \tag{3.3.6}$$

Using the boundary condition at the point $\xi = 0$ yields

$$\widetilde{C}(\xi) = \widetilde{C}_\xi(0) \int_0^\xi e^{-\frac{s^2}{4}} ds \quad \text{for} \quad \text{all} \quad \xi \in (0,\xi_d). \tag{3.3.7}$$

Next, we use the boundary condition at $\xi = \xi_d$ to deduce that

$$\widetilde{C}(\xi_d) = 1 = \widetilde{C}_\xi(0) \int_0^{\xi_d} e^{-\frac{s^2}{4}} ds, \tag{3.3.8}$$

so that

$$\widetilde{C}_\xi(0) = \frac{1}{\int_0^{\xi_d} e^{-\frac{s^2}{4}} ds}, \tag{3.3.9}$$

and consequently, substituting (3.3.9) into (3.3.7), we deduce that

$$\widetilde{C}(\xi) = \frac{\int_0^\xi e^{-\frac{s^2}{4}} ds}{\int_0^{\xi_d} e^{-\frac{s^2}{4}} ds} \quad \text{for} \quad \text{all} \quad \xi \in (0,\xi_d). \tag{3.3.10}$$

It remains to determine the constant ξ_d. We write that

$$x_d'(t) = \frac{D\,\xi_d}{2\sqrt{D(t+1)}} = \frac{D}{C_{\text{sol}} - C_{\text{sat}}}\, C_x(x_d(t),t) = \frac{D}{C_{\text{sol}} - C_{\text{sat}}} \frac{C_{\text{sat}}\, \widetilde{C}_\xi\left(\dfrac{x_d(t)}{\sqrt{D(t+1)}}\right)}{\sqrt{D(t+1)}}, \tag{3.3.11}$$

which implies that

$$\frac{\xi_d}{2} = \varepsilon\, \widetilde{C}_\xi(\xi_d), \tag{3.3.12}$$

so that ξ_d is characterized as the unique solution of the equation

$$\varepsilon = \frac{\xi_d}{2} e^{\frac{\xi_d^2}{4}} \int_0^{\xi_d} e^{-\frac{s^2}{4}} ds. \tag{3.3.13}$$

Finally, a special solution of Problem (3.2.6) is given by

$$C(x,t) = C_{\text{sat}} \frac{\displaystyle\int_0^{\frac{x}{\sqrt{D(t+1)}}} e^{-\frac{s^2}{4}} ds}{\displaystyle\int_0^{\frac{x_d(t)}{\sqrt{D(t+1)}}} e^{-\frac{s^2}{4}} ds} \quad \text{for} \quad \text{all} \quad t > 0, x \in (0,x_d(t)), \tag{3.3.14}$$

while the moving boundary x_d is given by the nonlinear equation (3.3.13) where $x_d(t) = \xi_d\sqrt{D(t+1)}$.

All the numerical results presented in Section 3.4 and Section 3.5 have been obtained by numerically solving Problem 3.2.6 with a Finite Differences/ALE method. This numerical method is described in details in Chapter 5.

3.4 Parametric study of the diffusion-controlled corrosion mechanism by means of numerical simulations

It follows from the equality (3.2.5), namely

$$x_d'(t) = \frac{D}{C_{\text{solid}} - C_{\text{sat}}} C_x(x_d(t),t) \quad \text{for all } t > 0,$$

that the propagation velocity of the concentration front increases as the difference $(C_{\text{solid}} - C_{\text{sat}})$ decreases and increases with the diffusion coefficient D and with the concentration gradient of the dissolved metal ions at the liquid side of the dissolution front. While the concentration difference and the diffusion coefficients are material properties known a priori, the concentration gradient follows from the overall response of the system.

In this section, we focus our study on the influence of two input parameters: the diffusion coefficient D and the saturated concentration C_{sat} in Problem 3.2.6. These two parameters play an important role to understand the evolution of the pit depth as a function of time.

3.4.1 Input parameters

In view of literature, we have found some possible values of D and C_{sat}. Indeed, it was mentioned that in the case of a one-dimensional pit, a reasonable approximation of the value of D is in the range $[7.10^{-6}, 10^{-5}]$ $(\text{cm}^2.\text{s}^{-1})$ [75] while the value of C_{sat} can be equal to 5.02 mol/L [75] or 4.2 mol/L [76]. In [62], these parameters were set at $0.85 \cdot 10^{-5}\,\text{cm}^2.\text{s}^{-1}$ for the diffusion coefficient and at 5.1 mol/L for the saturated concentration value. Thus, we will focus on these values to describe the evolution of the physics of our phenomenon. On the other hand, the value of the metal concentration will be set at 143 mol/L [62].

3.4.2 Effect of the diffusion coefficient on the evolution of the pit depth

In order to study the influence of the diffusion coefficient D on the propagation velocity, several computations are done in function of D for the following choice of the physical parameters

$$C_{\text{sat}} = 5{,}1\,\text{mol/L}, \quad C_{\text{solid}} = 143\,\text{mol/L} \tag{3.4.1}$$

with the initial values given by (see Figure 3.4.1):

- Initial pit depth: $x_d^0 = 1\mu\text{m}$.
- At the pit entrance $(x = 0)$: $C(0,0) = 10^{-6}$ mol/L.
- At the pit bottom $(x = x_d(0))$: $C(x_d(0),0) = 5.1$ mol/L.
- In the pit solution $(0 < x < x_d(0))$: $C(x,0)$ = linear profile from 10^{-6} mol/L at $x = 0$ to 5.1 mol/L at $x = x_d(0)$.

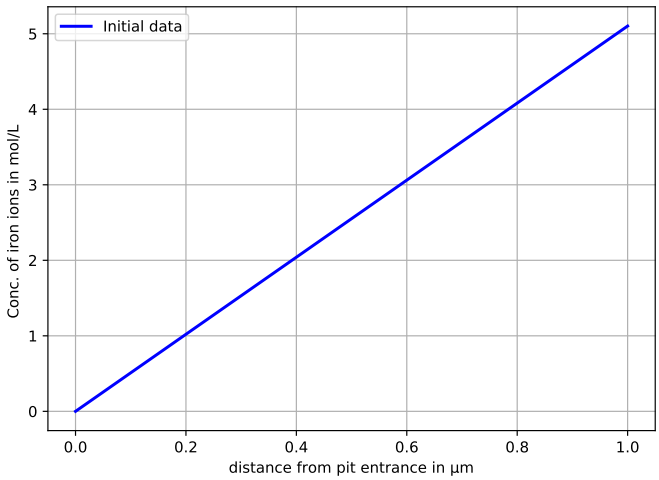

Figure 3.4.1: **Initial** distribution (at t=0) of the iron ions in the pit solution for initial pit depth $x_d(0) = 1$ µm.

Remark 3.4.1. *A detailed presentation of the numerical scheme is given in Chapter 5 for the equivalent problem expressed in different variables.*

Figure 3.4.2 shows the evolution of iron concentration in the pit solution after respectively 10 hours, 1013 hours and 5079 hours of pit propagation. Moreover, the CPU or execution time, which measures how much time the CPU spent on executing our program, is about 5 seconds. The evolution of the iron concentration with depth is linear for the three exposure times.

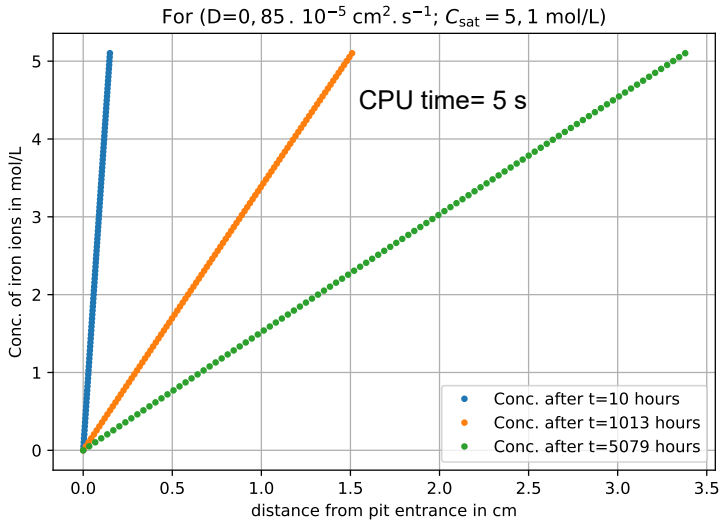

Figure 3.4.2: Evolution of the concentration of the iron ions in the pit solution at three different times.

Figure 3.4.3 illustrates the evolution of the pit depth for several values of the diffusion coefficient. We show that the depth increases when D increases.

In Figure 3.4.3a, we have fixed the final pit depth x_d^{Tf} at 35 mm; for D=8,5 $.10^{-5}$ cm^2.s^{-1}, the time required to reach this depth is about Tf_1=528,821 hours. However, for D=0,85 $.10^{-5}$ cm^2.s^{-1}, the time required to reach this depth is about Tf_2= 5288,21 hours. The ratio $\dfrac{\mathrm{Tf}_2}{\mathrm{Tf}_1} = 10$. Similarly,

for D=0,085 $.10^{-5}$ cm^2.s^{-1}, the time required to reach this depth is about Tf$_3$=52882,1 hours. It follows that $\dfrac{\text{Tf}_3}{\text{Tf}_2} = 10$.

We conclude that if the diffusion coefficient is decreased by a factor λ, the time needed to reach a given final pit depth is increased λ times.

Similarly, in Figure 3.4.3b, we shows that after Tf = 1000 hours of pit propagation, if the diffusion coefficient increases by factor λ, the pit depth increases $\approx \sqrt{\lambda}$ times.

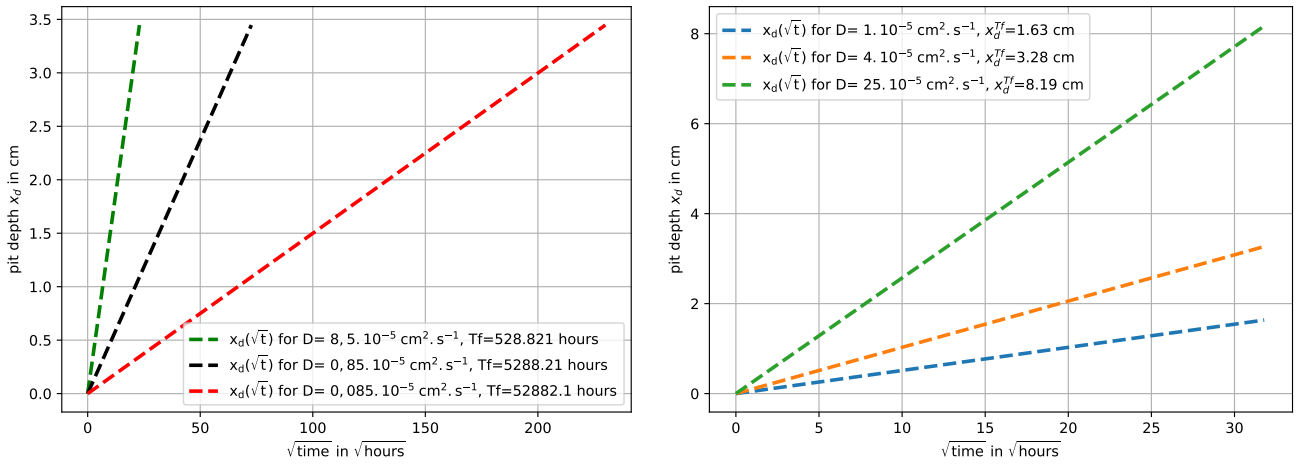

(a) for fixed final depth

(b) pit depth after 1000 hours of pit propagation

Figure 3.4.3: Evolution of the pit depth for several values of the diffusion coefficient.

Remark 3.4.2. *Let* $(C_1, x_{d,1})$ *be a solution of Problem* (3.2.6) *for* $D = 1$ *and an initial concentration* C_0*, then*

- $C_D(x,t) = C_1(x, Dt)$, $x_{d,D}(t) = x_{d,1}(Dt)$ *is a solution of Problem* (3.2.6)*. We find theoretically the multiplication by* D *of the time ;*
- $\tilde{C}_D(x,t) = C_1(\frac{x}{\sqrt{D}}, t)$, $\tilde{x}_{d,D} = \sqrt{D}\ x_{d,1}(t)$ *is a solution of Problem* (3.2.6) *with the initial condition* $C_0(\frac{x}{\sqrt{D}})$*. Since* C_0 *is close to zero in the numerical simulations, we find the factor* $\sqrt{D}$ *observed numerically.*

3.4.3 Effect of C_{sat} on the evolution of the pit depth

In the case where $D = 0{,}85\ .10^{-5}$ cm^2.s^{-1}, Figure 3.4.4 shows a comparison of the evolution of the pit depth during 1000 hours as a function of $\sqrt{\text{time}}$ (in $\sqrt{\text{hours}}$) for several values of C_{sat}.

The parameter C_{sat} has an influence on the evolution of the pit depth. Indeed, for a fixed time, the most important pit depth is the one computed for the largest value of C_{sat}.

Let us compare the two extremes values of C_{sat} where $C_{\text{sat},1} = 5{,}1$ mol/L and $C_{\text{sat},2} = 140{,}2$ mol/L after 1000 hours of pit propagation. For $C_{\text{sat},1} = 5{,}1$ mol/L, the pit depth is $\approx 1{,}51$ cm while for $C_{\text{sat},2} = 140{,}2$ mol/L is $\approx 18{,}71$ cm.

The ratio between the two depths is $\dfrac{18{,}71}{1{,}51} \approx 12{,}3$. So we deduce that even if the value of C_{sat} is very close to the value of C_{solid} (which is not real), the pit depth increases only 12 times comparing to the more realistic case where $C_{\text{sat}} = 5{,}1$ mol/L.

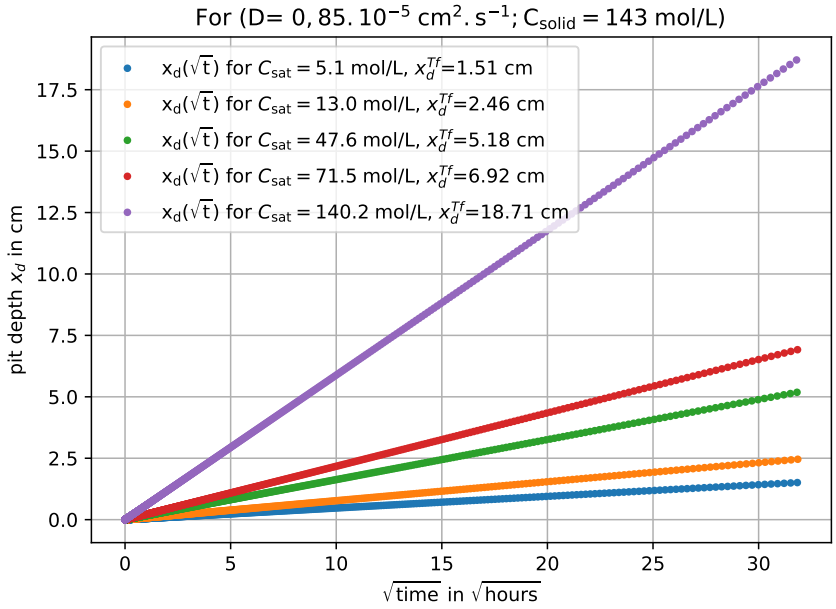

Figure 3.4.4: Evolution of the pit depth for several values of C_{sat} during 1000 hours.

The values x_d^{Tf} are those computed by the numerical code.

3.5 Numerical simulations for the convergence to the self similar solution

In this section, we present some numerical results which illustrate the convergence of the solution (C,x_d) of Problem 3.2.6 to the self-similar solution $(\widetilde{C},\xi_d)$ (a special solution) given by (see also (3.3.10)–(3.3.13))

$$\begin{cases} \widetilde{C}(\xi) = \dfrac{\int_0^{\xi} e^{-\frac{s^2}{4}}\,ds}{\int_0^{\xi_d} e^{-\frac{s^2}{4}}\,ds}, \\ 0 < \xi < \xi_d \end{cases} \tag{3.5.1}$$

with $\xi = \dfrac{x}{\sqrt{D(t+1)}}$ (see (3.3.1)), where ξ_d is the unique solution of the nonlinear equation (see (3.3.13))

$$\varepsilon = \frac{\xi_d}{2} e^{\frac{\xi_d^2}{4}} \int_0^{\xi_d} e^{-\frac{s^2}{4}}\,ds, \tag{3.5.2}$$

and ε is given by (3.3.2). This convergence turns out to hold when starting from rather general initial conditions (also see Chapter 4).

We set

$$\begin{cases} V(\xi,t) = C(x,t), \\ \xi_d(t) = \dfrac{x_d(t)}{\sqrt{D(t+1)}}. \end{cases} \tag{3.5.3}$$

Next, we show the numerical convergence to the self similar-solution for two arbitrary initial data. First, we consider the following initial data (C^0,x_d^0) given by

$$\begin{cases} x_d^0 := x_d(0) = 1\ \mu\text{m}, \\ C^0(x) := C(x,0) = \dfrac{C_{\text{sat}}}{x_d^0} x. \end{cases} \tag{3.5.4}$$

Figure 3.5.1a illustrates the convergence toward the self-similar solution $\tilde{C}$ given by (3.5.1). In the self-similar frame (ξ,t), we have that $t \mapsto V(\xi,t)$ tends to the stationary profile $\tilde{C}$ as t tends to $+\infty$. It shows that after only 0.8584 s of pit propagation, the numerical solution and the self-similar solution nearly coincide.

Figure 3.5.1c shows the time evolution of the free boundary x_d as well as the self-similar free boundary $\xi_d\sqrt{D(t+1)}$. Similarly, this is equivalent to show that $t \mapsto \xi_d(t)$ given by (3.5.3) tend to the self-similar constant ξ_d given by (3.5.2) as presented in Figure 3.5.1b.

Moreover, Figure 3.5.1c shows that the pit depth grows proportional to the square root of time $\sqrt{t}$.

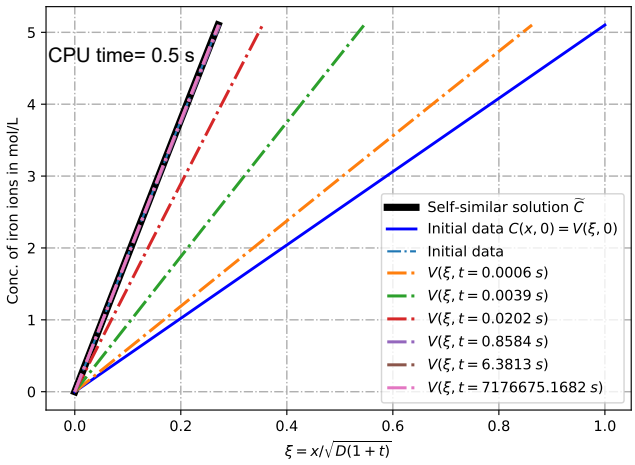

(a) Time evolution of the unknown function $V(\xi,t)$.

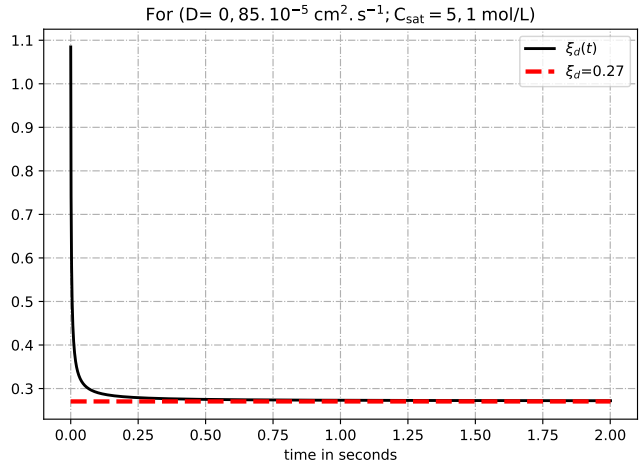

(b) Time evolution of the moving boundary $\xi_d(t)$.

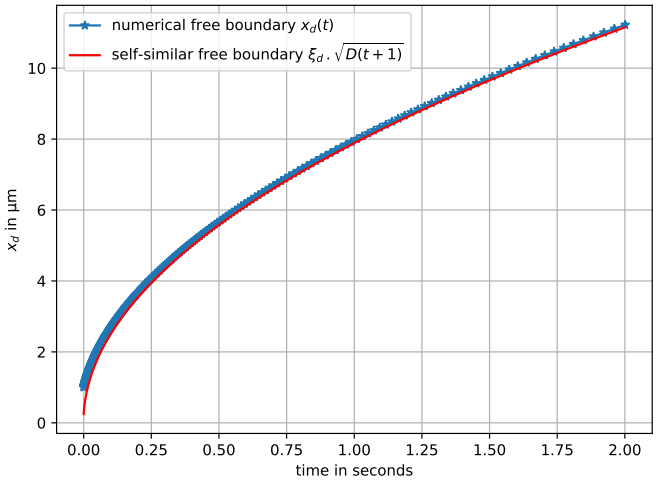

(c) Convergence of the numerical free boundary $x_d(t)$ to the self-similar free boundary $\xi_d\sqrt{D(t+1)}$.

Figure 3.5.1: Large time behavior of the solution pair (V,ξ_d).

Next, in Figure 3.5.2, we show the convergence to the self-similar solution for a more disturbed initial solution given by

$$\begin{cases} x_d^0 := x_d(0) = 5\ \mu\text{m}, \\ C^0(x) := C(x,0) = \dfrac{x\ C_{\text{sat}}}{2\,x_d^0}\left(1+\sin\left(\dfrac{2\pi x}{x_d^0}+\dfrac{\pi}{2}\right)\right). \end{cases} \tag{3.5.5}$$

The same observations are noted.

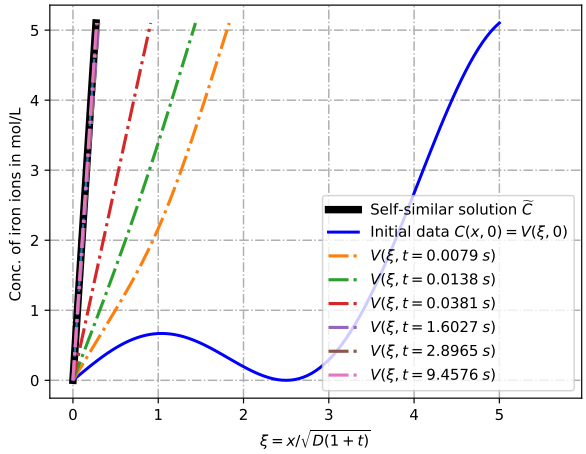

(a) Time evolution of the unknown function $V(\xi,t)$.

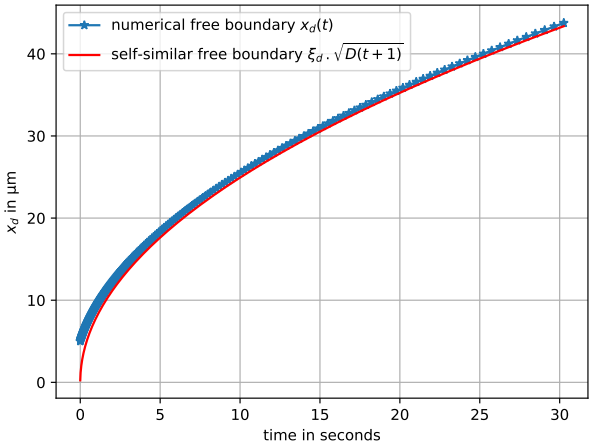

(b) Convergence of the numerical free boundary $x_d(t)$ to the self-similar free boundary $\xi_d\sqrt{D(t+1)}$.

Figure 3.5.2: Large time behavior of the solution.

3.6 From the physical problem to the classical Stefan problem

In this section, we show by means of a change of variables how the corrosion problem (3.2.6) can be reformulated as the standard Stefan classic problem as given in Avner Friedman's book on parabolic equations (Chapter 8 of [24, p.215]). Our starting point is Problem (3.2.6) which we rewrite below

$$\begin{cases} C_t = D\, C_{xx}, & t > 0,\ 0 \leqslant x \leqslant x_d(t), \\ C(0,t) = 0, & t > 0, \\ C(x_d(t)^-,t) = C_{\text{sat}}, & t > 0, \\ \dfrac{dx_d(t)}{dt} = \dfrac{D}{C_{\text{sol}} - C_{\text{sat}}}\, C_x(x_d(t)^-,t), & t > 0, \end{cases} \tag{3.6.1}$$

where $D > 0$ and $C_{\text{sol}} - C_{\text{sat}} > 0$. Next, we perform the change of variable

$$y = \frac{C_{\text{sol}} - C_{\text{sat}}}{\sqrt{D}}\, x, \quad s(t) = \frac{C_{\text{sol}} - C_{\text{sat}}}{\sqrt{D}}\, x_d(t) \ \text{ for all } \ t > 0, \tag{3.6.2}$$

and we define

$$u(y,t) = C_{\text{sat}} - C(x,t) \ \text{ for all } \ t > 0, 0 \leqslant x \leqslant x_d(t) \ \text{ and } \ y = \frac{C_{\text{sol}} - C_{\text{sat}}}{\sqrt{D}}\, x. \tag{3.6.3}$$

In what follows, we show how using the change of variable (3.6.2), Problem (3.6.1) becomes

$$\begin{cases} u_t = \alpha\, u_{yy}, & t > 0,\ 0 \leqslant y \leqslant s(t), \\ u(0,t) = C_{sat}, & t > 0, \\ u(s(t),t) = 0, & t > 0, \\ \dfrac{ds(t)}{dt} = -\sqrt{\alpha}\, u_y(s(t),t), & t > 0. \end{cases} \tag{3.6.4}$$

where

$$\alpha = (C_{\text{sol}} - C_{\text{sat}})^2. \tag{3.6.5}$$

Indeed, from (3.6.2) and (3.6.3), it follows that

$$C_x(x,t) = -\frac{dy}{dx}\, u_y(y,t), \tag{3.6.6}$$

so that

$$C_x(x,t) = -\frac{C_{\rm sol} - C_{\rm sat}}{\sqrt{D}}\, u_y(y,t), \tag{3.6.7}$$

and

$$C_{xx}(x,t) = -\frac{(C_{\rm sol} - C_{\rm sat})^2}{D}\, u_{yy}(y,t). \tag{3.6.8}$$

Also, we have that

$$C_t(x,t) = -u_t(y,t). \tag{3.6.9}$$

Then, since $C_t = D\, C_{xx}$, it follows from (3.6.8) and (3.6.9) that

$$u_t(y,t) = (C_{\rm sol} - C_{\rm sat})^2\, u_{yy}(y,t) \quad \text{for all} \quad t > 0,\, 0 < y < s(t). \tag{3.6.10}$$

Next, from (3.6.1) and (3.6.3), it follows that

$$u(0,t) = C_{\rm sat} \quad \text{and} \quad u(s(t),t) = 0. \tag{3.6.11}$$

From (3.6.1), we have that

$$\frac{dx_d(t)}{dt} = \frac{D}{C_{\rm sol} - C_{\rm sat}}\, C_x(x_d(t)^-,t), \quad \text{for all} \quad t > 0, \tag{3.6.12}$$

so that also in view of (3.6.2)

$$\frac{ds(t)}{dt} = \frac{C_{\rm sol} - C_{\rm sat}}{\sqrt{D}} \frac{D}{C_{\rm sol} - C_{\rm sat}}\, C_x(x_d(t)^-,t) \quad \text{for all} \quad t > 0. \tag{3.6.13}$$

Finally we deduce from (3.6.7) and (3.6.13) that

$$\frac{ds(t)}{dt} = -(C_{\rm sol} - C_{\rm sat})\, u_y(s(t),t) \quad \text{for all} \quad t > 0. \tag{3.6.14}$$

Problem (3.6.4) is then obtained as a combination of (3.6.10), (3.6.11) and (3.6.14).

Setting $\alpha = 1$ in Problem (3.6.4) yields the problem which we study in Chapter 4.

Chapter 4

Convergence to a self similar solution of a one-dimensional one-phase Stefan Problem

4.1 Introduction

In this Chapter, we revisit a standard one-dimensional one-phase Stefan problem. This free boundary problem arises in very simple physical situations and has been studied by numerous authors; in particular we should mention a chapter of the book of Avner Friedman on parabolic equations (Chapter 8 of [24, p.215]). This problem is given by

$$\begin{cases} u_t = u_{xx}, & t > 0, 0 < x < s(t), \\ u(0,t) = h, & t > 0, \\ u(s(t),t) = 0, & t > 0, \\ \dfrac{ds(t)}{dt} = -u_x(s(t),t), & t > 0, \\ s(0) = b_0, & \\ u(x,0) = u_0(x), & 0 < x < b_0 \end{cases} \tag{4.1.1}$$

where $x = s(t)$ is the unknown free boundary which is to be found together with $u(x,t)$.

Friedman [24] proves that this problem has a unique smooth classical solution $(u(x,t),s(t))$ in $Q := \{(x,t), t > 0, 0 < x < s(t)\}$. Moreover it follows from Schaeffer [59] and Friedman [22] that $s \in C^\infty(0,\infty)$ and that u is infinitely differentiable up to the free boundary s.

The purpose of this chapter is to study the large time behavior of the solution pair (u,s). Also let us mention some previous results from literature. Meirmanov [50] has proved that $\dfrac{s(t)}{\sqrt{t}} \to a$, where a is the unique solution of the nonlinear equation (4.1.3) below. Also, Ricci and Xie [58] have performed a stability analysis of some special solutions of a related one-phase Stefan problem on the semi-infinite interval $(s(t),\infty)$. In particular, they mention that the interface $s(t)$ behaves as $\beta\sqrt{t}$ for some positive constant β which they characterize. Moreover, Aiki and Muntean [1, 2], as mentioned in [90], have proved the existence of two positive constants c and C independent of t such that

$$c\,\sqrt{t} \leqslant s(t) \leqslant C\,\sqrt{t+1} \quad \text{for all} \quad t \geqslant 0,$$

in the case of a more complicated system.

In this chapter, we will prove that the solution pair (u,s) converges to a self-similar solution as $t \to \infty$.

First, let us define the self-similar solution. To do so, we introduce the self-similar variable $\eta = \frac{x}{\sqrt{t+1}}$. Then, the self-similar solution is given by

$$u(x,t) = U\left(\frac{x}{\sqrt{t+1}}\right) = U(\eta) = h\left[1 - \frac{\int_0^\eta e^{-\frac{s^2}{4}} ds}{\int_0^a e^{-\frac{s^2}{4}} ds}\right] \text{ for all } \eta \in (0,a), \tag{4.1.2}$$

where a is characterized as the unique solution of the nonlinear equation

$$h = \frac{a}{2} e^{\frac{a^2}{4}} \int_0^a e^{-\frac{s^2}{4}} ds. \tag{4.1.3}$$

In the first step, we will write the problem (4.1.1) in terms of η and t. To do so, we set

$$\begin{cases} V(\eta,t) = u(x,t), \\ a(t) = \dfrac{s(t)}{\sqrt{t+1}}. \end{cases} \tag{4.1.4}$$

However, the partial differential equation for V which we obtain explicitly involves the time variable t. It is given by

$$(t+1)V_t = V_{\eta\eta} + \frac{\eta}{2} V_\eta, \quad t > 0, \quad 0 < \eta < a(t). \tag{4.1.5}$$

This leads us to perform the change of time variable $\tau = \ln(t+1)$. A similar change of variables was performed by [31]. The full time evolution problem corresponding to the system (4.1.1) in coordinates η and τ is given by

$$\begin{cases} W_\tau = W_{\eta\eta} + \dfrac{\eta}{2} W_\eta, & \tau > 0, \quad 0 < \eta < b(\tau), \\ W(0,\tau) = h, & \tau > 0, \\ W(b(\tau),\tau) = 0, & \tau > 0, \\ \dfrac{db(\tau)}{d\tau} + \dfrac{b(\tau)}{2} = -W_\eta(b(\tau),\tau), & \tau > 0, \\ b(0) = b_0, & \\ W(\eta,0) = u_0(\eta), & 0 < \eta < b_0 \end{cases} \tag{4.1.6}$$

where $b(\tau) = a(t)$.

We shall denote by $(W(\eta,\tau,(u_0,b_0)), b(\tau,(u_0,b_0)))$ the solution pair of (4.1.6) with the initial conditions (u_0,b_0).

It is in the coordinates η and τ that we will rigorously characterize the large time behavior of the solution pair (W,b). However, for technical reasons, we sometimes have to use different variables, namely (y,τ) with $y = \dfrac{\eta}{b(\tau)}$ for all $0 < \eta < b(\tau)$. The problem is then transformed into a problem on a fixed domain.

Organization of this Chapter. In Section 2, we introduce the Stefan problem [23] and recall known well-posedness and regularity results [22, 59]. Using a maximum principle [24], we show that if u_0 is nonnegative and bounded then the solution u is also nonnegative and bounded.

In Section 3, we start by defining a notion of upper and lower solutions for Problem (4.1.1). Then, we prove a comparison principle in the (x,t) coordinates for a pair of upper and lower solutions of Problem (4.1.1).

In Section 4, we construct the self-similar solution (U,a). We will show that U is as given by (4.1.2) and a is characterized as the unique solution of the nonlinear equation (4.1.3).

In Section 5, we transform Problem (4.1.1) in coordinates (x,t) to obtain an equivalent problem, Problem (4.1.6), in coordinates (η,τ) where the solution pair becomes (W,b). We present an equivalent comparison principle in these coordinates and a class of functions which include both the lower and upper-solutions. We use the notation $(\bar{\mathcal{W}},\bar{b})$ for the upper-solution, respectively $(\underline{\mathcal{W}}_\lambda,\underline{b}_\lambda)$ for the lower-solution depending on a parameter $\lambda \geqslant 0$, and we construct a function (W_λ,b_λ) such that

$$(W_\lambda,b_\lambda) \text{ is } \begin{cases} \text{an upper solution} & \text{if } 0 \leqslant \lambda \leqslant 1, \\ \text{a lower solution} & \text{if } \lambda \geqslant 1. \end{cases} \tag{4.1.7}$$

Then, we prove the monotonicity in time of the solution pair (W,b) of the time evolution Problem (4.1.6) with the two initial conditions $(\bar{\mathcal{W}},\bar{b})$ and $(\underline{\mathcal{W}}_\lambda,\underline{b}_\lambda)$. In other words, we show that starting from a lower solution, the solution $\underline{\mathrm{W}}(\eta,\tau) := W\big(\eta,\tau,(\underline{\mathcal{W}}_\lambda,\underline{b}_\lambda)\big)$ increases in time as $\tau \to \infty$ to a limit function ψ and the corresponding moving boundary $\underline{b}(\tau) := b\big(\tau,(\underline{\mathcal{W}}_\lambda,\underline{b}_\lambda)\big)$ increases to a limit $\underline{b}_\infty$. Similarly, one can show that starting from an upper solution, the solution decreases to another limit function ϕ as $\tau \to \infty$ and the moving boundary $\bar{b}$ converges to a limit $\bar{b}_\infty$.

At the end of this section, we discuss some properties of upper and lower solutions to conclude that they are ordered functions. However, we do not know yet whether ψ and ϕ coincide with the self-similar profile U and whether $\underline{b}_\infty$ and $\bar{b}_\infty$ coincide with the point a. In order to prove these results we first have to show extra a priori estimates which we do in the following section.

In Section 6, we prove a number of a priori estimates some in the moving domain and some in the fixed domain. Indeed, we temporarily pass to fixed domain $(y,\tau) \in (0,1) \times \mathbb{R}^+$ to avoid technical problems related to the characterization of the limits $\underline{b}_\infty$ and $\bar{b}_\infty$. In other words, we need to show that $\underline{\mathrm{W}}_\eta(\underline{b}(\tau),\tau)$ converges to $\psi_\eta(\underline{b}_\infty)$ as $\tau \to \infty$. This requests to prove the uniform convergence of $\underline{\mathrm{W}}_\eta(\eta,\tau)$ to its limit as $\tau \to \infty$ which we can more easily do in the fix domain coordinates.

Section 7 is devoted to the study of the limits as $\tau \to \infty$. More precisely, we prove that $(\psi,\underline{b}_\infty)$ verifies the following conditions

$$\psi(0) = h, \quad \psi(\underline{b}_\infty) = 0, \quad \frac{\underline{b}_\infty}{2} = -\psi_\eta(\underline{b}_\infty).$$

and ψ satisfies the ordinary differential equation

$$\psi_{\eta\eta} + \frac{\eta}{2}\psi_\eta = 0.$$

Similarly, it turns out that $\Big(W\big(\eta,\tau,(\bar{\mathcal{W}},\bar{b})\big),b\big(\tau,(\bar{\mathcal{W}},\bar{b})\big)\Big)$ converges as $\tau \to \infty$ towards the unique solution $(\phi,\bar{b}_\infty)$ of the stationary problem corresponding to Problem (4.1.6). At the end of Section 7, we show that the solution pair $(\psi,\underline{b}_\infty)$ coincides with the unique solution (U,a) of Problem (4.4.4) which coincides also with the solution pair $(\phi,\bar{b}_\infty)$.

In the next chapter, we present the results of some numerical simulations. We choose the initial data (u_0,b_0) such that $\underline{b}_\lambda \leqslant b_0 \leqslant \bar{b}$ and $\underline{\mathcal{W}}_\lambda \leqslant u_0 \leqslant \bar{\mathcal{W}}$. Figure 4.1.1 shows the large time behavior of the solution pair (V,a) defined in (4.1.4).

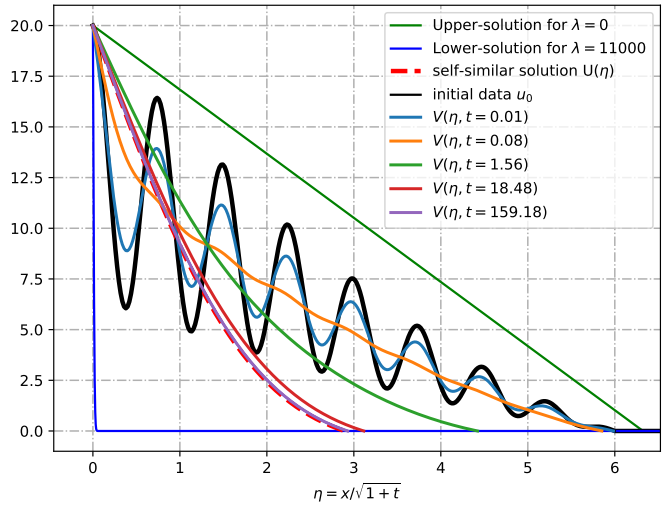

(a) Time evolution of the unknown function $V(\eta,t)$.

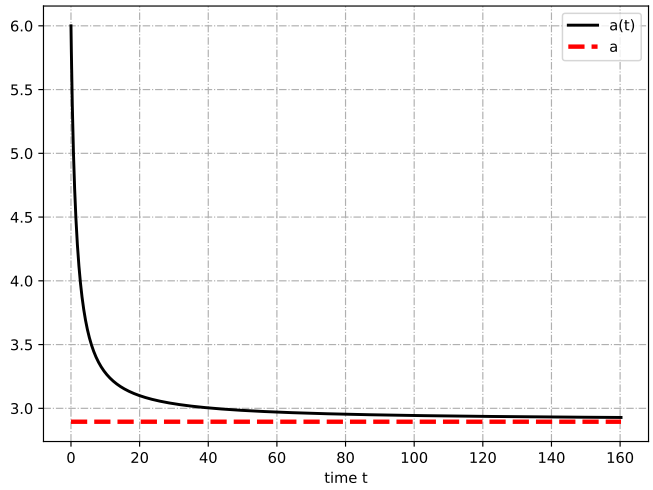

(b) Time evolution of the moving boundary $a(t)$.

Figure 4.1.1: Large time behavior of the solution pair (V,a).

To state an exact formulation of the results of this chapter, it is most convenient to use the variable y lying in $[0,1]$. In the variables (y,η), the problem for $(\hat{W}(y,\tau),b(\tau)) = (W(\eta,\tau),b(\tau))$ is given by

$$\begin{cases} \hat{W}_\tau(y,\tau) = \dfrac{1}{b^2(\tau)}\hat{W}_{yy}(y,\tau) + y\left(\dfrac{d\,\ln\left(b(\tau)\right)}{d\tau} + \dfrac{1}{2}\right)\hat{W}_y(y,\tau), & \tau > 0,\ 0 < y < 1, \\ \hat{W}(0,\tau) = h, & \tau > 0, \\ \hat{W}(1,\tau) = 0, & \tau > 0, \\ \dfrac{1}{2}\dfrac{db^2(\tau)}{d\tau} + \dfrac{b^2(\tau)}{2} = -\hat{W}_y(1,\tau), & \tau > 0, \\ b(0) = b_0, & \\ \hat{W}(y,0) = u_0(b_0 y), & 0 \leqslant y \leqslant 1. \end{cases} \tag{4.1.8}$$

The main result of this chapter is the following. We suppose that the initial data (u_0,b_0) satisfies the hypothesis:

$\mathbf{H}_0$: $b_0 \leqslant \bar{b}$ and $u_0 \in \mathbb{W}^{1,\infty}(0,b_0)$ with $u_0(0) = h$ and

$$\begin{aligned} &u_0(x) = 0 \quad \text{for all } x \geqslant b_0, \\ &0 \leqslant u_0(x) \leqslant h\left(1 - \frac{x}{\sqrt{2h}}\right) \quad \text{for all } 0 \leqslant x \leqslant b_0. \end{aligned}$$

Main Theorem 4.1.1. *Suppose that (u_0,b_0) satisfies the hypothesis $\boldsymbol{H}_0$. The unique solution $(\hat{W},b)$ of Problem (4.1.8) is such that*

$$\lim_{\tau\to+\infty} ||\hat{W}(.,\tau) - \hat{U}||_{C([0,1])} = 0, \tag{4.1.9}$$

$$\lim_{\tau\to+\infty} b(\tau) = a, \tag{4.1.10}$$

where $(\hat{U},a)$ is the unique solution of the stationary problem

$$\begin{cases} \dfrac{1}{a^2}\hat{U}_{yy} + \dfrac{y}{2}\hat{U}_y = 0, & 0 < y < 1, \\ \hat{U}(0) = h, \quad \hat{U}(1) = 0, & \\ \dfrac{a^2}{2} = -\hat{U}_y(1) & \end{cases} \tag{4.1.11}$$

which is equivalent to the stationary problem corresponding to Problem (4.1.6)

$$\begin{cases} U_{\eta\eta} + \dfrac{\eta}{2} U_\eta = 0, & 0 < \eta < a, \\ U(0) = h, \quad U(a) = 0, \\ \dfrac{a}{2} = -U_\eta(a), \end{cases} \tag{4.1.12}$$

for the self-similar solution of Problem (4.1.1).

Remark 4.1.1. *(4.1.10) is equivalent to the convergence result*

$$\frac{s(t)}{\sqrt{t+1}} \to a \ \text{ as } \ t \to +\infty, \tag{4.1.13}$$

which was already proved by Meirmanov [50].

4.2 Friedman's formulation

Let $h > 0$, $b > 0$. We define the function space

$$X^h(b) := \{u_0(x) \in C[0,\infty), \ \ u_0(0) = h, \, u_0(x) \geqslant 0 \text{ for } 0 \leqslant x < b, \, u_0(x) = 0 \text{ for } x \geqslant b\}$$

and we consider the problem

$$\begin{cases} u_t = u_{xx}, & t > 0, 0 < x < s(t), \\ u(0,t) = h, & t > 0, \\ u(s(t),t) = 0, & t > 0, \\ \dfrac{ds(t)}{dt} = -u_x(s(t),t), & t > 0, \\ s(0) = b_0, \\ u(x,0) = u_0(x) \in X^h(b_0). \end{cases} \tag{4.2.1}$$

Problem (4.2.1) is a free boundary problem where $x = s(t)$ is the free boundary to be found together with the unknown function $u(x,t)$.

Definition 4.2.1. *Let $T > 0$. We say that the pair (u,s) is a classical solution of Problem (4.2.1) if*

(i) *$s(t)$ is continuously differentiable for $0 \leqslant t \leqslant T$;*

(ii) *$u \in C(\overline{Q_T})$, where $Q_T := \{(x,t), t \in (0,T], 0 < x < s(t)\}$;*

(iii) *$u \in C^{2,1}(Q_T)$;*

(iv) *$u_x \in C(\overline{Q_T^\delta})$ for all $\delta > 0$ where $Q_T^\delta = \{(x,t), t \in (\delta,T], 0 < x < s(t)\}$;*

(v) *the equations of Problem (4.2.1) are satisfied.*

Let $(u(x,t),s(t))$ be a solution of (4.2.1) for all $0 \leqslant t \leqslant T$. We extend u by:

$$u(x,t) = 0 \text{ for } x \geqslant s(t), \tag{4.2.2}$$

so that $u(.,t)$ is defined for all $x \geqslant 0$.

Theorem 4.2.2 ([23, Theorem 1])**.** *Let $h > 0, b > 0$ and $u_0 \in X^h(b)$. Then, there exists a unique solution $(u(x,t),s(t))$ of (4.2.1) for all $t > 0$ in the classical sense. Moreover, the solution (u,s) is such that s is infinitely differentiable on $(0,\infty)$ and u is infinitely differentiable up to the free boundary for all $t > 0$ [22],[59]. Furthermore, the function $s(t)$ is strictly increasing in t.*

Proposition 4.2.3. *Let $h > 0, b > 0$ and $u_0 \in X^h(b)$ such that $0 \leqslant u_0 \leqslant h$. Then, the solution $(u(x,t),s(t))$ of (4.2.1) is such that $0 \leqslant u(x,t) \leqslant h$ for all $(x,t) \in Q_T$.*

Proof. We apply the strong maximum principle (Theorem 1 of [24, p.34]) which states that if u attains its minimum or its maximum in an interior point $(x^0,t^0) \in Q_T$, then u is constant in Q_{t^0}. However, since $u(0,t) = h > 0$ for $t \in (0,T]$ and $u(s(t),t) = 0$, $u(.,t)$ cannot be constant in space on $(0,s(t))$, so that u attains its minimum and its maximum on the boundary $\Gamma := \{(0,t), 0 \leqslant t \leqslant T\} \cup \{(x,0), 0 < x < b\} \cup \{(s(t),t), 0 \leqslant t \leqslant T\}$. As $0 \leqslant u_0 \leqslant h$, we conclude that $0 \leqslant u(x,t) \leqslant h$ for all $(x,t) \in Q_T$. □

4.3 Comparison principle

To begin with, we define a notion of lower and upper solutions.

Definition 4.3.1. *For $u \in C(\overline{Q_T}) \cap C^{2,1}(Q_T)$, we define $\mathcal{L}(u) := u_t - u_{xx}$.*
$(\underline{u},\underline{s})$ is a lower solution of the Problem (4.2.1) if it satisfies

$$\begin{cases} \mathcal{L}(\underline{u}) = \underline{u}_t - \underline{u}_{xx} \leqslant 0 \ \text{ in } Q_T, & \\ \underline{u}(0,t) = h, \quad \underline{u}(\underline{s}(t),t) = 0, & t > 0, \\ \dfrac{d\underline{s}(t)}{dt} = -\underline{u}_x(\underline{s}(t),t), & t > 0, \\ \underline{s}(0) \leqslant b_0, & \\ \underline{u}(x,0) \leqslant u_0(x), & x \in (0,b_0). \end{cases} \tag{4.3.1}$$

$(\bar{u},\bar{s})$ is an upper solution of the Problem (4.2.1) if it satisfies (4.3.1) with all $\leqslant$ replaced by $\geqslant$.

Theorem 4.3.2 (Comparison principle)**.** *Let $(u_1(x,t),s_1(t))$ and $(u_2(x,t),s_2(t))$ be respectively lower and upper solutions of (4.2.1) corresponding respectively to the data (h_1,u_{01},b_1) and (h_2,u_{02},b_2).*

If $b_1 < b_2$, $h_1 \leqslant h_2$ and $u_{01} \leqslant u_{02}$, then $s_1(t) < s_2(t)$ for $t \geqslant 0$ and $u_1(x,t) \leqslant u_2(x,t)$ for $x \geqslant 0$ and $t \geqslant 0$.

In particular, $u_1(x,t) < u_2(x,t)$ for $0 < x \leqslant s_1(t)$ and $t > 0$.

Before proving Theorem 4.3.2, we first show the following result.

Lemma 4.3.3. *Any upper solution $(\bar{u},\bar{s})$ of Problem (4.2.1) is such that $\bar{u} > 0$ in Q_T.*

Proof. We first perform the change of function $\bar{u}(x,t) = \bar{v}(x,t)e^{\lambda t}$ where λ is a strictly positive constant. The function $\bar{v}$, as is easily seen, satisfies the inequality

$$(\bar{v}_t - \bar{v}_{xx} + \lambda\bar{v})e^{\lambda t} \geqslant 0 \ \text{ in } Q_T, \ \text{for all } \lambda > 0,$$

so that

$$\bar{v}_t - (\bar{v}_{xx} - \lambda\bar{v}) \geqslant 0 \ \text{ in } Q_T, \text{ for all } \lambda > 0.$$

Now, we prove that $\bar{v} \geqslant 0$ in $\overline{Q_T}$. Indeed, it follows from the weak maximum principle (Lemma 1 of [24, p.34]) that $\bar{v}$ cannot have a negative minimum in Q_T. Then, $\bar{v}$ attains its minimum on the boundary $\Gamma := \{(0,t), 0 \leqslant t \leqslant T\} \cup \{(x,0), 0 < x < b_0\} \cup \{(s(t),t), 0 \leqslant t \leqslant T\}$; since $\bar{v} \geqslant 0$ on Γ, it follows that $\bar{v} \geqslant 0$ in $\overline{Q_T}$ which implies that $\bar{u} \geqslant 0$ in $\overline{Q_T}$.

Next, we apply the strong maximum principle (Theorem 1 of [24, p.34]) which implies that if $\bar{v}$ attains its negative minimum at an interior point $(\bar{x},\bar{t}) \in Q_T$, then $\bar{v}$ is constant in $Q_{\bar{t}}$. However, since $\bar{v}(0,t) \geqslant h\ e^{-\lambda t} > 0$ for $t \in (0,T]$, we have reached a contradiction, so that we conclude that $\bar{v} > 0$ in Q_T. Then, we conclude that $\bar{u} > 0$ in Q_T. □

Proof of Theorem 4.3.2. Suppose that

$$\text{there exists } t_0 > 0 \text{ such that } s_1(t) < s_2(t) \text{ for } 0 \leqslant t < t_0 \text{ and } s_1(t_0) = s_2(t_0). \tag{4.3.2}$$

Let $x_0 := s_1(t_0)$. Since $s_1(t) < s_2(t)$ for $0 \leqslant t < t_0$, we see that

$$s_1'(t_0) \geqslant s_2'(t_0). \tag{4.3.3}$$

Let $D := \{(x,t)|\ 0 < t \leqslant t_0,\ 0 < x < s_1(t)\}$ and $\Gamma := \{(0,t)|\ 0 \leqslant t \leqslant t_0\} \cup \{(x,0)|\ 0 < x < b_1\} \cup \{(s_1(t),t)|\ 0 \leqslant t \leqslant t_0\}$. We introduce $w(x,t) := u_2(x,t) - u_1(x,t)$. We shall prove that $w > 0$ in D. Indeed, $w_t - w_{xx} \geqslant 0$ in D, it follows from the weak maximum principle that $w \geqslant 0$ in $\overline{D}$. Then, we remark that $w(s_1(t),t) = u_2(s_1(t),t)$ and according to Lemma 4.3.3 we have $u_2(s_1(t),t) > 0$, so that we deduce from the strong maximum principle that $w > 0$ in D.

Let $\xi > 0$, $\alpha := \xi^{-2}$,

$$\varphi(x,t) := e^{-\alpha(x-x_0+\xi)^2+\alpha(t-t_0)} - e^{-\alpha\xi^2} \tag{4.3.4}$$

and

$$\rho(x) := (x - x_0 + \xi)^2 - \xi^2 + t_0. \tag{4.3.5}$$

Let $\delta > 0$ be small (to be chosen later). We define

$$D(\delta) := \{(x,t)|\ x_0 - \delta < x < x_0,\ \rho(x) < t < t_0\}.$$

In this proof, the different domains of study are presented in Figure 4.3.1.

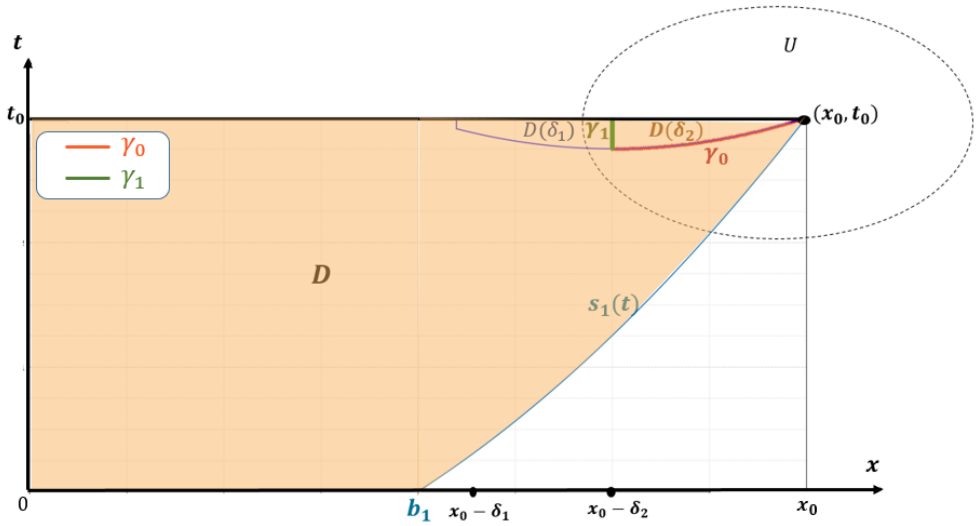

Figure 4.3.1: The domains of study D and $D(\delta)$.

Next we show that there exist a small $\xi > 0$ and a small $\delta_1 > 0$ such that $D(\delta_1) \subset D$, indeed since $0 < s_1'(t_0) < \infty$ and there exists a small $\xi > 0$ such that

$$s_1'(t_0) < \left.\frac{d\rho^{-1}(t)}{dt}\right|_{t=t_0} = \frac{1}{\rho'(x_0)} = \frac{1}{2\xi}.$$

It follows that if $\xi < \dfrac{1}{2s_1'(t_0)}$ then $D(\delta_1) \subset D$. Indeed, suppose that

$$\rho(x) := (x - x_0 + \xi)^2 - \xi^2 + t_0 = t.$$

Then

$$\frac{d\rho^{-1}(t)}{dt} = \frac{1}{\rho'(\rho^{-1}(t))} = \frac{1}{\rho'(x)},$$

where $\rho^{-1}(t)$ is the inverse function of $\rho(x)$ near $x = x_0$ and $\rho'(x) = 2(x - x_0 + \xi)$ which implies that $\rho'(x_0) = 2\xi$. By direct calculation, we shall prove that

$$\varphi_t(x_0,t_0) - \varphi_{xx}(x_0,t_0) = -e^{-1}\xi^{-2} < 0. \tag{4.3.6}$$

Indeed, from (4.3.4) we deduce that

$$\varphi_t(x,t) = \alpha e^{-\alpha(x-x_0+\xi)^2+\alpha(t-t_0)} = \alpha\varphi(x,t) + \alpha e^{-\alpha\xi^2}.$$

We remark that since $\varphi(x_0,t_0) = 0$, it follows that $\varphi_t(x_0,t_0) = \alpha e^{-\alpha\xi^2} = \xi^{-2}e^{-1}$. Next, we compute the space derivatives of φ :

$$\varphi_x(x,t) = -2\alpha(x - x_0 + \xi)e^{-\alpha(x-x_0+\xi)^2+\alpha(t-t_0)},$$

$$\varphi_{xx}(x,t) = -2\alpha e^{-\alpha(x-x_0+\xi)^2+\alpha(t-t_0)} + 4\alpha^2(x - x_0 + \xi)^2 e^{-\alpha(x-x_0+\xi)^2+\alpha(t-t_0)}.$$

Thus, $\varphi_{xx}(x_0,t_0) = -2\alpha e^{-\alpha\xi^2} + 4\alpha^2\xi^2 e^{-\alpha\xi^2}$ and since $\alpha = \xi^{-2}$, we have

$$\varphi_{xx}(x_0,t_0) = -2\xi^{-2}e^{-1} + 4\xi^{-2}e^{-1} = 2\xi^{-2}e^{-1},$$

which implies (4.3.6).

Since φ is smooth, and since φ satisfies (4.3.6), there exists a neighborhood U of (x_0,t_0) such that $\varphi_t - \varphi_{xx} < 0$ in U. We choose $\delta_2 \in (0,\delta_1)$ such that $D(\delta_2) \subset U$.

We define $z(x,t) := w(x,t) - \varepsilon\varphi(x,t)$, where $\varepsilon > 0$ will be chosen later. Then,

$$z_t - z_{xx} \geqslant 0 \text{ on } D(\delta_2). \tag{4.3.7}$$

Indeed, since $w_t - w_{xx} \geqslant 0$ in D, $\varphi_t - \varphi_{xx} < 0$ in U and $D(\delta_2) \subset U$, we have

$$z_t - z_{xx} = w_t - \varepsilon\varphi_t - w_{xx} + \varepsilon\varphi_{xx} = w_t - w_{xx} + \varepsilon(\varphi_{xx} - \varphi_t) \geqslant 0 + \varepsilon(\varphi_{xx} - \varphi_t) > 0 \text{ in } D(\delta_2).$$

Let

$$\gamma_0 := \{(x,t)|\ x_0 - \delta_2 \leqslant x \leqslant x_0,\ t = \rho(x)\}$$

and

$$\gamma_1 := \{(x,t)|\ x = x_0 - \delta_2,\ \rho(x_0 - \delta_2) \leqslant t < t_0\}.$$

In what follows, we use the notation $\partial(D(\delta_2)) := \gamma_0 \cup \gamma_1$ to denote the parabolic boundary of $D(\delta_2)$. Next, we show that $\varphi = 0$ on γ_0. Indeed $t = \rho(x)$ on γ_0 , we have that

$$\varphi(x,\rho(x)) = e^{-\alpha(x-x_0+\xi)^2+\alpha(x-x_0+\xi)^2}e^{-\alpha\xi^2} - e^{-\alpha\xi^2} = 0$$

and thus, $\varphi = 0$ on γ_0. Since $w \geq 0$ in $\overline{D}$ and $\gamma_0 \subset \overline{D}$, we deduce from the definition of z that $z = w \geqslant 0$ on γ_0.

Since $w > 0$ on γ_1, there exists a small $\varepsilon > 0$ such that $z \geqslant 0$ on γ_1. Indeed, $w > 0$ on D, so, there exists $\mu > 0$ such that $w \geqslant \mu$ in γ_1. Moreover, from (4.3.4) we deduce that

$$\varphi(x,t) \leqslant e^{-\alpha(x-x_0+\xi)^2+\alpha(t-t_0)}$$

so that $\varphi(x,t) \leqslant 1$ and $\varepsilon\,\varphi(x,t) \leqslant \varepsilon$. Therefore, if

$$\varepsilon \leqslant \frac{\mu}{2},$$

we have

$$w \geqslant \mu \geqslant \varepsilon\varphi(x,t)$$

which implies that $z \geqslant 0$ on γ_1. Using the fact that $\partial(D(\delta_2)) = \gamma_0 \cup \gamma_1$ and $z \geqslant 0$ on $\partial(D(\delta_2))$, we deduce from the weak maximum principle together with (4.3.7) that $z \geqslant 0$ in $\overline{D(\delta_2)}$ and hence $w(x,t_0) \geqslant \varepsilon\varphi(x,t_0)$ for $x_0 - \delta_2 \leqslant x \leqslant x_0$. Thus,

$$z(x,t_0) \geqslant 0 \text{ for all } x \in [x_0 - \delta_2, x_0]. \tag{4.3.8}$$

Moreover, since (x_0,t_0) both belongs to s_1 and s_2, it follows that

$$z(x_0,t_0) = w(x_0,t_0) = u_2(x_0,t_0) - u_1(x_0,t_0) = 0. \tag{4.3.9}$$

We deduce from (4.3.8) and (4.3.9) that $z_x(x_0,t_0) \leqslant 0$, or else,

$$w_x(x_0,t_0) \leqslant \varepsilon\varphi_x(x_0,t_0) = -2\varepsilon e^{-1}\xi^{-1} < 0,$$

and hence $u_{1x}(x_0,t_0) > u_{2x}(x_0,t_0)$. Because of (4.3.1), we see that $s_1'(t_0) < s_2'(t_0)$. This contradicts (4.3.3). Since we have obtained a contradiction, (4.3.2) cannot occur. We see that $s_1(t) < s_2(t)$ for all $t \geqslant 0$. By the weak maximum principle we see that $u_1(x,t) \leqslant u_2(x,t)$ for $x \geqslant 0$ and $t \geqslant 0$. It follows from the strong maximum principle that $u_1(x,t) < u_2(x,t)$ for $0 < x < s_1(t)$ and $t > 0$. □

Next we present an extension of Theorem 4.3.2 for the case that $b_1 \leqslant b_2$.

Corollary 4.3.4 (Extension of the comparison principle)**.** *Let $(u_1(x,t),s_1(t))$ and $(u_2(x,t),s_2(t))$ be respectively lower and upper solutions of (4.2.1) corresponding respectively to the data (h_1,u_{01},b_1) and (h_2,u_{02},b_2) such that u_{01} or u_{02} is a nonincreasing function.*

If $b_1 \leqslant b_2$, $h_1 \leqslant h_2$ and $u_{01} \leqslant u_{02}$, then $s_1(t) \leqslant s_2(t)$ for $t \geqslant 0$ and $u_1(x,t) \leqslant u_2(x,t)$ for $x \geqslant 0$ and $t \geqslant 0$.

Proof. The case where $b_1 < b_2$ has already been studied. It only remains to study the case "$b_1 = b_2$". We start to suppose that u_{01} is nonincreasing. The case where u_{02} is nonincreasing will be considered after.

We will construct a lower solution $(u_\varepsilon,s_\varepsilon)$, $0 < \varepsilon < 1$, of Problem (4.2.1) corresponding to the data $(h_1,b_{0\varepsilon},u_{0\varepsilon})$ such that $(b_{0\varepsilon},u_{0\varepsilon})$ satisfies

$$\begin{cases} b_{0\varepsilon} < b_2 \quad \text{and} \quad b_{0\varepsilon} \to b_1 = b_2 \ \text{ as } \ \varepsilon \to 1, \\ u_{0\varepsilon} \leqslant u_{02}, \end{cases} \tag{4.3.10}$$

and

$$\begin{cases} s_\varepsilon(t) \underset{\varepsilon\to 1}{\longrightarrow} s_1(t), & t \geqslant 0, \\ u_\varepsilon(x,t) \underset{\varepsilon\to 1}{\longrightarrow} u_1(x,t), & x \geqslant 0, t \geqslant 0. \end{cases} \tag{4.3.11}$$

Then, it follows from (4.3.10) and Theorem 4.3.2 that

$$\begin{cases} s_\varepsilon(t) < s_2(t), & t \geqslant 0, \\ u_\varepsilon(x,t) \leqslant u_2(x,t), & x \geqslant 0, t \geqslant 0. \end{cases} \tag{4.3.12}$$

Letting $\varepsilon \to 1$, we obtain

$$\begin{cases} s_1(t) \leqslant s_2(t), & t \geqslant 0, \\ u_1(x,t) \leqslant u_2(x,t), & x \geqslant 0, t \geqslant 0. \end{cases} \tag{4.3.13}$$

Next, we complete the proof by the construction of a lower solution $(u_\varepsilon, s_\varepsilon)$ which satisfies (4.3.11) with data $(h_1, u_{0\varepsilon}, b_{0\varepsilon})$ such that $(u_{0\varepsilon}, b_{0\varepsilon})$ satisfies (4.3.10).

Construction of the lower solution $(u_\varepsilon, s_\varepsilon)$. We choose

$$\begin{cases} s_\varepsilon(t) = \varepsilon \, . \, s_1\left(\dfrac{t}{\varepsilon^2}\right), & t \geqslant 0, \\ \\ u_\varepsilon(x,t) = u_1\left(\dfrac{x}{\varepsilon}, \dfrac{t}{\varepsilon^2}\right), & x \geqslant 0, t \geqslant 0. \end{cases} \tag{4.3.14}$$

We first check that $(u_\varepsilon, s_\varepsilon)$ corresponding to the data $(h_1, u_{0\varepsilon}, b_{0\varepsilon})$ is a lower solution of (4.2.1). Indeed, since u_1 is a lower solution of (4.2.1), it follows that

$$\mathcal{L}(u_\varepsilon) = \frac{1}{\varepsilon^2}\left(u_{1,t}\left(\frac{x}{\varepsilon}, \frac{t}{\varepsilon^2}\right) - u_{1,xx}\left(\frac{x}{\varepsilon}, \frac{t}{\varepsilon^2}\right)\right) \leqslant 0, \tag{4.3.15}$$

$$u_\varepsilon(0,t) = u_1(0, \frac{t}{\varepsilon^2}) = h_1 \leqslant h, \tag{4.3.16}$$

$$u_\varepsilon(s_\varepsilon(t),t) = u_1\left(s_1\left(\frac{t}{\varepsilon^2}\right), \frac{t}{\varepsilon^2}\right) = 0, \tag{4.3.17}$$

$$\frac{ds_\varepsilon(t)}{dt} = \frac{1}{\varepsilon}\frac{d}{dt}s_1\left(\frac{t}{\varepsilon^2}\right) = \frac{-1}{\varepsilon}\, u_{1,x}\left(s_1\left(\frac{t}{\varepsilon^2}\right), \frac{t}{\varepsilon^2}\right) = -u_{\varepsilon,x}(s_\varepsilon(t),t). \tag{4.3.18}$$

Next, we choose data $(h_1, u_{0\varepsilon}, b_{0\varepsilon})$ such that $(u_{0\varepsilon}, b_{0\varepsilon})$ satisfies (4.3.10). We set

$$b_{0\varepsilon} := \varepsilon b_1. \tag{4.3.19}$$

Then, it follows from (4.3.19) and $0 < \varepsilon < 1$ that

$$s_\varepsilon(0) = \varepsilon s_1(0) = \varepsilon b_1 =: b_{0\varepsilon} < b_1. \tag{4.3.20}$$

Finally, we should check that $u_\varepsilon(x,0) := u_{0\varepsilon}$ satisfies the second condition of (4.3.10). Indeed, we have

$$u_\varepsilon(x,0) = u_1(\frac{x}{\varepsilon}, 0) = u_{01}(\frac{x}{\varepsilon}). \tag{4.3.21}$$

Since u_{01} is a nonincreasing function and $0 < \varepsilon < 1$, it follows that

$$u_{01}(\frac{x}{\varepsilon}) \leqslant u_{01}(x) \quad \text{for } x \geqslant 0. \tag{4.3.22}$$

We deduce from (4.3.22) that

$$u_\varepsilon(x,0) := u_{0\varepsilon}(x) = u_{01}(\frac{x}{\varepsilon}) \leqslant u_{01}(x) \leqslant u_{02}(x) \quad \text{for } x \geqslant 0. \tag{4.3.23}$$

Therefore,$(u_\varepsilon, s_\varepsilon)$ satisfies (4.3.15)-(4.3.18) and corresponds to data $(h_1, u_{0\varepsilon}, b_{0\varepsilon})$ such that $(u_{0\varepsilon}, b_{0\varepsilon})$ satisfies (4.3.10). Thus, it is a lower solution of (4.2.1).

Now, we consider the case where the function u_{02} is nonincreasing. We can proceed exactly as before by considering the upper solution $(u_\varepsilon, s_\varepsilon)$ of Problem (4.2.1) with $\varepsilon > 1$, given by

$$\begin{cases} s_\varepsilon(t) = \varepsilon \, . \, s_2\left(\dfrac{t}{\varepsilon^2}\right), & t \geqslant 0, \\ \\ u_\varepsilon(x,t) = u_2\left(\dfrac{x}{\varepsilon}, \dfrac{t}{\varepsilon^2}\right), & x \geqslant 0, t \geqslant 0. \end{cases} \tag{4.3.24}$$

The corresponding initial datum $b_{0\varepsilon} = s_\varepsilon(0)$ and $u_{0\varepsilon} = u_\varepsilon(x,0)$ verify

$$\begin{cases} b_1 < b_{0\varepsilon} \quad \text{and} \quad b_{0\varepsilon} \to b_2 = b_1 \quad \text{as} \quad \varepsilon \to 1, \\ u_{01} \leqslant u_{0\varepsilon}, \end{cases} \tag{4.3.25}$$

and

$$\begin{cases} s_\varepsilon(t) \xrightarrow[\varepsilon\to 1]{} s_2(t), & t \geqslant 0, \\ u_\varepsilon(x,t) \xrightarrow[\varepsilon\to 1]{} u_2(x,t), & x \geqslant 0, t \geqslant 0. \end{cases} \tag{4.3.26}$$

Then, the result follows from the use of Theorem 4.3.2 with (4.3.25) and letting $\varepsilon \to 1$. □

4.4 Self-similar solution

We now look for a self-similar solution of the problem

$$\begin{cases} u_t = u_{xx}, & t > 0, \quad 0 < x < s(t), \\ u(0,t) = h, & t > 0, \\ u(s(t),t) = 0, & t > 0, \\ \dfrac{ds(t)}{dt} = -u_x(s(t),t), & t > 0, \end{cases} \tag{4.4.1}$$

in the form

$$\begin{cases} u(x,t) = U\left(\dfrac{x}{\sqrt{t+1}}\right), \\ s(t) = a\sqrt{t+1}, \end{cases} \tag{4.4.2}$$

for some positive constant a still to be determined. We set

$$\eta := \frac{x}{\sqrt{t+1}}. \tag{4.4.3}$$

and deduce that

$$\begin{cases} U_{\eta\eta} + \dfrac{\eta}{2} U_\eta = 0, & 0 < \eta < a, \\ U(0) = h, & U(a) = 0. \end{cases} \tag{4.4.4}$$

The unique solution of (4.4.4) is given by

$$U(\eta) = h\left[1 - \frac{\int_0^\eta e^{-\frac{s^2}{4}} ds}{\int_0^a e^{-\frac{s^2}{4}} ds}\right] \quad \text{for all } \eta \in (0,a). \tag{4.4.5}$$

It remains to determine the constant a. We write that

$$s'(t) = \frac{a}{2\sqrt{t+1}} = -u_x(s(t),t) = -\frac{U_\eta\left(\dfrac{s(t)}{\sqrt{t+1}}\right)}{\sqrt{t+1}}, \tag{4.4.6}$$

which implies that

$$\frac{a}{2} = -U_\eta(a), \tag{4.4.7}$$

so that a is characterized as the unique solution of the equation

$$h = \frac{a}{2} e^{\frac{a^2}{4}} \int_0^a e^{-\frac{s^2}{4}} ds. \tag{4.4.8}$$

We remark that the function $a = a(h)$ is strictly increasing, which in turn implies that the functional $h \to U$ is strictly increasing.

We conclude that the self-similar solution of Problem (4.4.1) coincides with the unique solution (U,a) of Problem (4.1.12).

4.5 New coordinates, upper and lower solutions

We set

$$\begin{cases} V(\eta,t) = u(x,t), \\ a(t) = \dfrac{s(t)}{\sqrt{t+1}}, \end{cases} \tag{4.5.1}$$

and obtain the problem

$$\begin{cases} (t+1)V_t = V_{\eta\eta} + \dfrac{\eta}{2}V_\eta, & t>0, \quad 0<\eta<a(t), \\ V(0,t) = h, \quad V(a(t),t) = 0, & t>0, \\ (t+1)\dfrac{da(t)}{dt} + \dfrac{a(t)}{2} = -V_\eta(a(t),t), & t>0. \end{cases} \tag{4.5.2}$$

Finally we set

$$\tau = \ln(t+1).$$

The equations in the system (4.5.2) read as

$$\begin{cases} W_\tau = W_{\eta\eta} + \dfrac{\eta}{2}W_\eta, & \tau>0, \quad 0<\eta<b(\tau), \\ W(0,\tau) = h, \quad W(b(\tau),\tau) = 0, & \tau>0, \\ \dfrac{db(\tau)}{d\tau} + \dfrac{b(\tau)}{2} = -W_\eta(b(\tau),\tau), & \tau>0, \end{cases} \tag{4.5.3}$$

where we have set

$$V(\eta,t) = W(\eta,\tau),\ a(t) = b(\tau).$$

Next, we write the full time evolution problem corresponding to the system (4.5.3). It is given by

$$\begin{cases} W_\tau = W_{\eta\eta} + \dfrac{\eta}{2}W_\eta, & \tau>0, \quad 0<\eta<b(\tau), \\ W(0,\tau) = h, & \tau>0, \\ W(b(\tau),\tau) = 0, & \tau>0, \\ \dfrac{db(\tau)}{d\tau} + \dfrac{b(\tau)}{2} = -W_\eta(b(\tau),\tau), & \tau>0, \\ b(0) = b_0, & \\ W(\eta,0) = u_0(\eta), & 0\leqslant\eta\leqslant b_0. \end{cases} \tag{4.5.4}$$

Finally, we note that the stationary solution of Problem (4.5.4) coincides with the unique solution of Problem (4.1.12), or in other words, the self-similar solution of Problem (4.1.1).

Definition 4.5.1. *We define the linear operator* $\mathcal{L}(W) := W_\tau - W_{\eta\eta} - \dfrac{\eta}{2}W_\eta$.
$(\underline{W},\underline{b})$ *is a lower solution of Problem (4.5.4) if it satisfies:*

$$\begin{cases} \mathcal{L}(\underline{W}) = \underline{W}_\tau - \underline{W}_{\eta\eta} - \dfrac{\eta}{2}\underline{W}_\eta \leqslant 0, & \tau>0, \quad 0<\eta<\underline{b}(\tau), \\ \underline{W}(0,\tau) = h, \quad \underline{W}(\underline{b}(\tau),\tau) = 0, & \tau>0, \\ \dfrac{d\underline{b}(\tau)}{d\tau} + \dfrac{\underline{b}(\tau)}{2} = -\underline{W}_\eta(\underline{b}(\tau),\tau), & \tau>0, \\ \underline{b}(0) \leqslant b_0, & \\ \underline{W}(\eta,0) \leqslant u_0(\eta), & 0\leqslant\eta\leqslant\underline{b}(0). \end{cases} \tag{4.5.5}$$

$(\bar{W},\bar{b})$ *is an upper solution of the Problem (4.5.4) if it satisfies Problem* (4.5.5) *with all* $\leqslant$ *replaced with* $\geqslant$.

Finally, we deduce from Corollary 4.3.4 that the following comparison principle holds.

Theorem 4.5.2. *Let $(W_1(\eta,\tau),b_1(\tau))$ and $(W_2(\eta,\tau),b_2(\tau))$ be respectively lower and upper solutions of (4.5.4) corresponding respectively to the data (h_1,u_{01},b_{01}) and (h_2,u_{02},b_{02}) such that u_{01} or u_{02} is a nonincreasing function.*

If $b_{01} \leqslant b_{02}$, $h_1 \leqslant h_2$ and $u_{01} \leqslant u_{02}$, then $b_1(\tau) \leqslant b_2(\tau)$ for $\tau \geqslant 0$ and $W_1(\eta,\tau) \leqslant W_2(\eta,\tau)$ for $\eta \geqslant 0$ and $\tau \geqslant 0$.

Throughout this chapter, we will also make use of the explicit notation $W(\eta,\tau,(u_0,b_0))$ and $b(\tau,(u_0,b_0))$ for the solution pair associated with the initial data (u_0,b_0).

4.5.1 Construction of upper and lower solutions

In this section, we construct ordered upper and lower solutions for Problem (4.5.4). For $\lambda \geqslant 0$, we consider (W_λ,b_λ) the unique solution of the problem

$$\begin{cases} W_{\eta\eta} + \dfrac{\lambda\eta}{2} W_\eta = 0, & 0 < \eta < b, \\ W(0) = h, \quad W(b) = 0, \\ \dfrac{b}{2} = -W_\eta(b), \end{cases} \tag{4.5.6}$$

which is given by

$$W_\lambda(\eta) = h\left[1 - \frac{\int_0^\eta e^{-\frac{\lambda s^2}{4}} ds}{\int_0^{b_\lambda} e^{-\frac{\lambda s^2}{4}} ds}\right] \quad \text{for all } \eta \in (0,b_\lambda) \tag{4.5.7}$$

and b_λ is the unique solution of the equation

$$h = \frac{b_\lambda}{2} e^{\frac{\lambda b_\lambda^2}{4}} \int_0^{b_\lambda} e^{-\frac{\lambda s^2}{4}} ds. \tag{4.5.8}$$

We can easily show the following properties for (W_λ,b_λ).

Lemma 4.5.3. *We have that*

$$0 \leqslant W_\lambda(\eta) \leqslant h \quad \text{for all } \lambda \geqslant 0 \text{ and } 0 \leqslant \eta \leqslant b_\lambda, \tag{4.5.9}$$

$$W_{\lambda,\eta}(\eta) \leqslant 0 \quad \text{for all } \lambda \geqslant 0 \text{ and } 0 \leqslant \eta \leqslant b_\lambda \tag{4.5.10}$$

and

$$W_{\lambda,\eta\eta}(\eta) \geqslant 0 \quad \text{for all } \lambda \geqslant 0 \text{ and } 0 \leqslant \eta \leqslant b_\lambda. \tag{4.5.11}$$

In particular,

$$W_\lambda \text{ is } \begin{cases} \text{a linear function} & \text{if } \lambda = 0, \\ \text{a convex function} & \text{if } \lambda > 0, \end{cases} \tag{4.5.12}$$

and

$$b_\lambda = \begin{cases} \sqrt{2h} & \text{if } \lambda = 0, \\ \text{satisfies the equation (4.5.8)} & \text{if } \lambda > 0. \end{cases} \tag{4.5.13}$$

Lower solution. We suppose that

$$\lambda \geqslant 1, \tag{4.5.14}$$

then (W_λ,b_λ) is a lower solution for Problem (4.5.4). Indeed, we easily check that W_λ satisfies the following property

$$-W_{\lambda,\eta\eta} - \frac{\eta}{2} W_{\lambda,\eta} \leqslant 0 \quad \text{if and only if} \quad \lambda \geqslant 1. \tag{4.5.15}$$

We define $(\underline{\mathcal{W}}_\lambda,\underline{b}_\lambda)$ by

$$\underline{b}_\lambda = b_\lambda \quad \text{and} \quad \underline{\mathcal{W}}_\lambda(\eta) := \begin{cases} W_\lambda(\eta) & \text{if } 0 \leqslant \eta \leqslant \underline{b}_\lambda, \\ 0 & \text{if } \eta > \underline{b}_\lambda. \end{cases} \tag{4.5.16}$$

The pair $(\underline{\mathcal{W}}_\lambda,\underline{b}_\lambda)$ is a lower solution for Problem (4.5.4).

We assume the following condition on the initial data (u_0,b_0):

$$\underline{\mathcal{W}}_\lambda(\eta) \leqslant u_0(\eta) \quad \text{for all } 0 \leqslant \eta \leqslant b_0, \quad \underline{b}_\lambda \leqslant b_0. \tag{4.5.17}$$

According to (4.5.10), $\underline{\mathcal{W}}_\lambda$ is a nonincreasing function and then, in view of the comparison principle Theorem 4.5.2, it follows that

$$\underline{b}_\lambda \leqslant b(\tau,(u_0,b_0)) \quad \text{and} \quad \underline{\mathcal{W}}_\lambda(\eta) \leqslant W\big(\eta,\tau,(u_0,b_0)\big) \text{ for all } \tau \geqslant 0, \eta \geqslant 0. \tag{4.5.18}$$

Upper solution. Now, we suppose that

$$0 \leqslant \lambda \leqslant 1. \tag{4.5.19}$$

We define $(\bar{\mathcal{W}}_\lambda,\bar{b}_\lambda)$ by

$$\bar{b}_\lambda = b_\lambda \quad \text{and} \quad \bar{\mathcal{W}}_\lambda(\eta) := \begin{cases} W_\lambda(\eta) & \text{if } 0 \leqslant \eta \leqslant \bar{b}_\lambda, \\ 0 & \text{if } \eta > \bar{b}_\lambda. \end{cases} \tag{4.5.20}$$

In view of (4.5.15), the pair $(\bar{\mathcal{W}}_\lambda,\bar{b}_\lambda)$ is an upper solution for Problem (4.5.4). We now suppose that $\lambda = 0$ and define the corresponding upper solution by $(\bar{\mathcal{W}},\bar{b})$

$$\bar{b} = \sqrt{2h} \quad \text{and} \quad \bar{\mathcal{W}}(\eta) := \begin{cases} W_0(\eta) & \text{if } 0 \leqslant \eta \leqslant \bar{b}, \\ 0 & \text{if } \eta > \bar{b}, \end{cases} \tag{4.5.21}$$

where $W_0(\eta) = h\big(1 - \dfrac{\eta}{\sqrt{2h}}\big)$ for all $0 < \eta < \bar{b}$.

We assume the following condition on the initial data (u_0,b_0):

$$u_0(\eta) \leqslant \bar{\mathcal{W}}(\eta) \quad \text{for all } 0 \leqslant \eta \leqslant \bar{b}, \quad b_0 \leqslant \bar{b}. \tag{4.5.22}$$

According to (4.5.10), $\bar{\mathcal{W}}$ is a nonincreasing function and then, in view of the comparison principle Theorem 4.5.2, it follows that

$$b(\tau,(u_0,b_0)) \leqslant \bar{b} \quad \text{and} \quad W\big(\eta,\tau,(u_0,b_0)\big) \leqslant \bar{\mathcal{W}}(\eta) \text{ for all } \tau \geqslant 0, \eta \geqslant 0. \tag{4.5.23}$$

Next, we prove the monotonicity in time of the solution pair (W,b) of the time evolution Problem (4.5.4) with the two initial conditions $(\bar{\mathcal{W}},\bar{b})$ and $(\underline{\mathcal{W}}_\lambda,\underline{b}_\lambda)$.

Lemma 4.5.4. *Suppose that the initial data (u_0,b_0) satisfies (4.5.17) and (4.5.22). Let $(\underline{\mathcal{W}}_\lambda,\underline{b}_\lambda)$ and $(\bar{\mathcal{W}},\bar{b})$ be defined by (4.5.16) and (4.5.21).*

(i) *The functions $W\big(\eta,\tau,(\bar{\mathcal{W}},\bar{b})\big)$ and $b\big(\tau,(\bar{\mathcal{W}},\bar{b})\big)$ are nonincreasing in time. Furthermore, there exist a positive constant $\bar{b}_\infty$ and a function $\phi \in L^\infty(0,\bar{b}_\infty)$ such that*

$$\lim_{\tau\to+\infty} W\big(\eta,\tau,(\bar{\mathcal{W}},\bar{b})\big) = \phi(\eta) \quad \textit{for all } \eta \in (0,\bar{b}_\infty), \tag{4.5.24}$$

$$\lim_{\tau\to+\infty} b\big(\tau,(\bar{\mathcal{W}},\bar{b})\big) = \bar{b}_\infty. \tag{4.5.25}$$

(ii) *The function* $W(\eta,\tau,(\underline{\mathcal{W}}_\lambda,\underline{b}_\lambda))$ *and* $b(\tau,(\underline{\mathcal{W}}_\lambda,\underline{b}_\lambda))$ *are nondeacreasing in time. Furthermore, there exist a positive constant* $\underline{b}_\infty$ *and a function* $\psi \in L^\infty(0,\underline{b}_\infty)$ *such that*

$$\lim_{\tau\to+\infty} W(\eta,\tau,(\underline{\mathcal{W}}_\lambda,\underline{b}_\lambda)) = \psi(\eta) \quad \textit{for all } \eta \in (0,\underline{b}_\infty), \tag{4.5.26}$$

$$\lim_{\tau\to+\infty} b(\tau,(\underline{\mathcal{W}}_\lambda,\underline{b}_\lambda)) = \underline{b}_\infty. \tag{4.5.27}$$

Proof. Applying repeatedly Theorem 4.5.2, one can show that $W(\eta,\tau,(\bar{\mathcal{W}},\bar{b}))$ and $b(\tau,(\bar{\mathcal{W}},\bar{b}))$ are nonincreasing in time and that $W(\eta,\tau,(\underline{\mathcal{W}}_\lambda,\underline{b}_\lambda))$ and $b(\tau,(\underline{\mathcal{W}}_\lambda,\underline{b}_\lambda))$ are nondeacreasing in time. Indeed, from (4.5.23) we have that

$$b(\tau,(u_0,b_0)) \leqslant \bar{b} \text{ and } W(\eta,\tau,(u_0,b_0)) \leqslant \bar{\mathcal{W}}(\eta) \text{ for all } \tau \geqslant 0 \text{ and } \eta \geqslant 0.$$

In particular, with $u_0 = \bar{\mathcal{W}}$ and $b_0 = \bar{b}$, we get

$$b(\tau,(\bar{\mathcal{W}},\bar{b})) \leqslant \bar{b} \text{ and } W(\eta,\tau,(\bar{\mathcal{W}},\bar{b})) \leqslant \bar{\mathcal{W}}(\eta) \quad \text{for all } \tau \geqslant 0 \text{ and } \eta \geqslant 0. \tag{4.5.28}$$

From (4.5.9), we have that

$$0 \leqslant \bar{\mathcal{W}}(\eta) \leqslant h.$$

Then, it follows from Proposition 4.2.3 that

$$0 \leqslant W(\eta,\tau,(\bar{\mathcal{W}},\bar{b})) \leqslant h \quad \text{for all } \tau \geqslant 0 \text{ and } \eta \geqslant 0. \tag{4.5.29}$$

Let $\sigma > 0$ be fixed. Due to (4.5.10), $\bar{\mathcal{W}}$ is a nonincreasing function, then we apply Theorem 4.5.2 for (4.5.28) to obtain

$$b(\tau+\sigma,(\bar{\mathcal{W}},\bar{b})) \leqslant b(\sigma,(\bar{\mathcal{W}},\bar{b})) \text{ and } W(\eta,\tau+\sigma,(\bar{\mathcal{W}},\bar{b})) \leqslant W(\eta,\sigma,(\bar{\mathcal{W}},\bar{b})) \text{ for all } \tau \geqslant 0 \text{ and } \eta \geqslant 0.$$

Thus for each $\eta, W(\eta,\tau,(\bar{\mathcal{W}},\bar{b}))$ is nonincreasing in τ and from (4.5.29), it is bounded from below by zero. Therefore it has a limit ϕ as $\tau \to \infty$.

Also $b(\tau,(\bar{\mathcal{W}},\bar{b}))$ is nonincreasing in τ and from (4.5.18) we deduce that it is bounded from below by $\underline{b}_\lambda$. Therefore it has a limit $\bar{b}_\infty$ as $\tau \to \infty$.

The same reasoning can be applied to prove that $W(\eta,\tau,(\underline{\mathcal{W}}_\lambda,\underline{b}_\lambda))$ and $b(\tau,(\underline{\mathcal{W}}_\lambda,\underline{b}_\lambda))$ are nondecreasing in time. Thus for each $\eta, W(\eta,\tau,(\underline{\mathcal{W}}_\lambda,\underline{b}_\lambda))$ is nondecreasing in τ and it is bounded from above by the constant function h as follows from Proposition 4.2.3. Therefore it has a limit ψ as $\tau \to \infty$. Also, $b(\tau,(\underline{\mathcal{W}}_\lambda,\underline{b}_\lambda))$ is nondecreasing in τ and bounded from above by $\bar{b}$ thanks to (4.5.23). Therefore it has a limit $\underline{b}_\infty$as $\tau \to \infty$. □

Later we will show that ϕ and ψ coincide with the unique solution of Problem (4.1.12). To that purpose, we will derive in the Section 6 estimates for the free boundary Problem (4.5.4) in both moving and fixed domains.

4.5.2 Properties of a family of upper and lower solutions

In this subsection, we establish some further properties of upper and lower solutions through successive lemmas.

Lemma 4.5.5. *The following properties hold for* b_λ *satisfying* (4.5.8).

(i) b_λ *is a decreasing function of* λ.

(ii) $b_\lambda \to 0$ *as* $\lambda \to +\infty$.

Proof. We start to prove (i). We define $\mathcal{F}$ as the function given by

$$\mathcal{F}(\lambda,b_\lambda) = \frac{b_\lambda}{2}\int_0^{b_\lambda} e^{\frac{\lambda(b_\lambda^2 - s^2)}{4}} ds - h \tag{4.5.30}$$

and consider the equation $\mathcal{F}(\lambda,b_\lambda) = 0$. We compute the differential of $\mathcal{F}$ through partial derivatives given by

$$d\mathcal{F} = \frac{\partial \mathcal{F}}{\partial \lambda} d\lambda + \frac{\partial \mathcal{F}}{\partial b_\lambda} db_\lambda. \tag{4.5.31}$$

From (4.5.30), it follows that

$$\frac{\partial \mathcal{F}}{\partial \lambda} = \frac{b_\lambda}{2}\int_0^{b_\lambda} \frac{(b_\lambda^2 - s^2)}{4} e^{\frac{\lambda(b_\lambda^2 - s^2)}{4}} ds \quad > 0 \text{ for all } b_\lambda > 0 \tag{4.5.32}$$

and

$$\frac{\partial \mathcal{F}}{\partial b_\lambda} = \frac{1}{2}\int_0^{b_\lambda} e^{\frac{\lambda(b_\lambda^2 - s^2)}{4}} ds + \frac{b_\lambda}{2}\left(1 + \int_0^{b_\lambda} \frac{2b_\lambda \lambda}{4} e^{\frac{\lambda(b_\lambda^2 - s^2)}{4}} ds\right) > 0 \text{ for all } b_\lambda > 0. \tag{4.5.33}$$

Since $\mathcal{F}(\lambda,b_\lambda) = 0$, it follows from (4.5.31) that

$$\frac{\partial \mathcal{F}(\lambda,b_\lambda)}{\partial \lambda} d\lambda + \frac{\partial \mathcal{F}(\lambda,b_\lambda)}{\partial b_\lambda} db_\lambda = 0. \tag{4.5.34}$$

Thus, since $\dfrac{\partial \mathcal{F}}{\partial b_\lambda} \neq 0$, it follows from (4.5.32),(4.5.33) and (4.5.34) that

$$\frac{db_\lambda}{d\lambda} = -\frac{\dfrac{\partial \mathcal{F}(\lambda,b_\lambda)}{\partial \lambda}}{\dfrac{\partial \mathcal{F}(\lambda,b_\lambda)}{\partial b_\lambda}} < 0, \tag{4.5.35}$$

which completes the proof of (i).

Now, we turn to the proof of (ii). For $\lambda \geqslant 0$, we have $b_\lambda > 0$ and b_λ is a decreasing function of λ. Hence, there exists $\alpha \geqslant 0$ such that $b_\lambda \to \alpha$ as $\lambda \to +\infty$ and $b_\lambda \geqslant \alpha$ for all $\lambda \geqslant 0$. We shall prove that $\alpha = 0$. This fact mainly relies on the following inequality which will be proved later on. Let $a \geqslant 0$. For $\lambda \geqslant 0$ large enough, the following inequality holds:

$$\int_0^a e^{-\frac{\lambda s^2}{4}} ds \geqslant a(1 + \frac{\lambda}{4}a^2)e^{-\frac{\lambda a^2}{4}}. \tag{4.5.36}$$

Since $b_\lambda \geqslant \alpha$ for all $\lambda \geqslant 0$, we deduce from (4.5.8) that

$$h \geqslant \frac{\alpha}{2} e^{\frac{\lambda \alpha^2}{4}} \int_0^\alpha e^{-\frac{\lambda s^2}{4}} ds. \tag{4.5.37}$$

For λ large enough we infer from the estimate (4.5.36) that

$$h \geqslant \frac{\alpha^2}{2}(1 + \frac{\lambda}{4}\alpha^2). \tag{4.5.38}$$

Letting $\lambda \to +\infty$ in (4.5.38), we see that we necessarily have $\alpha = 0$. It remains to prove that the inequality (4.5.36) holds for λ large enough. We only have to consider the case where $a > 0$ since (4.5.36) is trivially true for $a = 0$. Let us introduce $f(x) = e^{-\frac{\lambda x^2}{4}}$. We have $f''(x) = \frac{\lambda}{2}(\frac{\lambda}{2}x^2 - 1)e^{-\frac{\lambda x^2}{4}}$. We choose $\lambda > 0$ large enough to have $0 < \sqrt{\frac{2}{\lambda}} < a$ and then f is convex in $[\sqrt{\frac{2}{\lambda}}, a]$. Therefore, for all $x \in [\sqrt{\frac{2}{\lambda}}, a]$ we have

$$f(x) \geqslant g(x) := f(a) + (x - a)f'(a) \tag{4.5.39}$$

that is

$$e^{-\frac{\lambda x^2}{4}} \geqslant \left(1+\frac{\lambda}{2}a(a-x)\right)e^{-\frac{\lambda a^2}{4}}, \quad \text{for all } x \in \left[\sqrt{\frac{2}{\lambda}}, a\right]. \tag{4.5.40}$$

Next we prove that (4.5.39) also holds for $x \in [0,\sqrt{\frac{2}{\lambda}}]$. Indeed, we have

$$\max_{x\in\left[0,\sqrt{\frac{2}{\lambda}}\right]} g(x) = g(0) = (1+\frac{\lambda}{2}a^2)e^{-\frac{\lambda a^2}{4}}$$

and

$$\min_{x\in\left[0,\sqrt{\frac{2}{\lambda}}\right]} f(x) = f\left(\sqrt{\frac{2}{\lambda}}\right) = e^{-\frac{1}{2}}.$$

Since $g(0) \to 0$ as $\lambda \to +\infty$, we get, for λ large enough

$$\max_{\left[0,\sqrt{\frac{2}{\lambda}}\right]} g = g(0) \leq \min_{\left[0,\sqrt{\frac{2}{\lambda}}\right]} f = e^{-\frac{1}{2}} \tag{4.5.41}$$

and then

$$g(x) \leqslant f(x), \text{ for all } x \in \left[0,\sqrt{\frac{2}{\lambda}}\right] \tag{4.5.42}$$

Combining (4.5.39) with (4.5.42) leads to $f(x) \geqslant g(x)$ for all $x \in [0,a]$, that is

$$e^{-\frac{\lambda x^2}{4}} \geqslant \left(1+\frac{\lambda}{2}a(a-x)\right)e^{-\frac{\lambda a^2}{4}}, \text{ for all } x \in [0,a]. \tag{4.5.43}$$

Integrating (4.5.43) over $[0,a]$ leads to the desired inequality (4.5.36). □

Next, we prove the following result.

Lemma 4.5.6. *Let λ_1 and λ_2 be such that $\lambda_1 < \lambda_2$, then it follows that*

$$b_{\lambda_1} > b_{\lambda_2}, \tag{4.5.44}$$

and

$$W_{\lambda_1}(\eta) \geqslant W_{\lambda_2}(\eta) \text{ for all } 0 \leqslant \eta \leqslant b_{\lambda_2}. \tag{4.5.45}$$

Proof. From Lemma 4.5.5, since $\lambda_1 < \lambda_2$, it follows that $b_{\lambda_1} > b_{\lambda_2}$. Then, (4.5.44) holds. Next, we show (4.5.45). To do so, let the pair $(W_{\lambda_i}, b_{\lambda_i})_{i\in\{1,2\}}$ be the unique solution of the problem

$$\begin{cases} W_{\lambda_i,\eta\eta} + \dfrac{\lambda_i \eta}{2} W_{\lambda_i,\eta} = 0, & 0 < \eta < b_{\lambda_i}, \\ W_{\lambda_i}(0) = h, \quad W_{\lambda_i}(b_{\lambda_i}) = 0. \end{cases} \tag{4.5.46}$$

Then, we recall that for $i \in \{1,2\}$ the solution pair $(W_{\lambda_i}, b_{\lambda_i})$ is given by

$$W_{\lambda_i}(\eta) = h\left[1 - \frac{\int_0^\eta e^{-\frac{\lambda_i s^2}{4}} ds}{\int_0^{b_{\lambda_i}} e^{-\frac{\lambda_i s^2}{4}} ds}\right] \quad \text{for all } 0 \leqslant \eta \leqslant b_{\lambda_i}, \tag{4.5.47}$$

with also

$$W_{\lambda_i,\eta}(\eta) = \frac{-h\, e^{-\frac{\lambda_i \eta^2}{4}}}{\int_0^{b_{\lambda_i}} e^{-\frac{\lambda_i s^2}{4}} ds} \quad \text{for all } 0 \leqslant \eta \leqslant b_{\lambda_i}. \tag{4.5.48}$$

Next, we define the linear operator $\mathcal{L}(W) := W_{\eta\eta} + \dfrac{\lambda_1\,\eta}{2} W_\eta$ for all $0 \leqslant \eta \leqslant b_{\lambda_2}$. We compute $\mathcal{L}(W_{\lambda_2} - W_{\lambda_1})$ to obtain

$$\mathcal{L}(W_{\lambda_2} - W_{\lambda_1}) = W_{\lambda_2,\eta\eta} + \frac{\lambda_1\,\eta}{2} W_{\lambda_2,\eta} - W_{\lambda_1,\eta\eta} - \frac{\lambda_1\,\eta}{2} W_{\lambda_1,\eta} \text{ for all } 0 \leqslant \eta \leqslant b_{\lambda_2}. \tag{4.5.49}$$

Then, from (4.5.46), we have that

$$W_{\lambda_2,\eta\eta}(\eta) = -\frac{\lambda_2\,\eta}{2} W_{\lambda_2,\eta} \text{ for all } 0 \leqslant \eta \leqslant b_{\lambda_2}. \tag{4.5.50}$$

We substitute (4.5.50) in (4.5.49). Then, since $(W_{\lambda_1}, b_{\lambda_1})$ is a solution of problem (4.5.46), (4.5.49) becomes

$$\mathcal{L}(W_{\lambda_2} - W_{\lambda_1}) = \frac{(\lambda_1 - \lambda_2)\,\eta}{2} W_{\lambda_2,\eta}. \tag{4.5.51}$$

Since $\lambda_1 < \lambda_2$, by (4.5.48) and (4.5.51), we deduce that

$$\mathcal{L}(W_{\lambda_2} - W_{\lambda_1}) \geqslant 0 \text{ for all } 0 \leqslant \eta \leqslant b_{\lambda_2}. \tag{4.5.52}$$

Then, from (4.5.46), since

$$(W_{\lambda_2} - W_{\lambda_1})(0) = h - h = 0$$

and

$$(W_{\lambda_2} - W_{\lambda_1})(b_{\lambda_2}) = 0 - W_{\lambda_1}(b_{\lambda_2}) < 0,$$

we deduce from the one-dimensional maximum principle (Theorem 1 of [57, p.2]) that the function $W_{\lambda_2} - W_{\lambda_1}$ attains its maximum on the boundary. This implies that

$$W_{\lambda_2}(\eta) - W_{\lambda_1}(\eta) \leqslant 0 \text{ for all } 0 \leqslant \eta \leqslant b_{\lambda_2},$$

which completes the proof of Lemma 4.5.6. □

The next result ensures that the assumption made in (4.5.17) on the initial datum is fulfilled for λ large enough.

Lemma 4.5.7. *Let $u_0 \in X^h(b_0) \cap \mathbb{W}^{1,\infty}(0,b_0)$ and $(\underline{\mathcal{W}}_\lambda, \underline{b}_\lambda)$ defined by (4.5.16). There exists $\lambda \geqslant 1$ large enough such that $\underline{\mathcal{W}}_\lambda \leqslant u_0$ in $[0,b_0]$ and $\underline{b}_\lambda \leqslant b_0$.*

Proof. According to (4.5.12), W_λ is a convex function. Thus, we have

$$W_\lambda(\eta) \leqslant \frac{h}{b_\lambda}(b_\lambda - \eta) \quad \text{for all } 0 \leqslant \eta \leqslant b_\lambda. \tag{4.5.53}$$

From the identity $u_0(\eta) = h + \displaystyle\int_0^\eta \frac{du_0}{d\eta}(s)ds$ for $0 \leqslant \eta \leqslant b_0$, we deduce that

$$u_0(\eta) \geqslant h - M\eta \quad \text{for all } 0 \leqslant \eta \leqslant b_0 \tag{4.5.54}$$

where $M = \|\dfrac{du_0}{d\eta}\|_{L^\infty(0,b_0)}$. From Lemma 4.5.5 (ii), $b_\lambda \to 0$ as $\lambda \to +\infty$. Then we can choose $\lambda \geqslant 1$ large enough so that

$$b_\lambda \leqslant \min(\frac{h}{M}, b_0). \tag{4.5.55}$$

Estimate (4.5.54) then becomes

$$u_0(\eta) \geqslant h - \frac{h}{b_\lambda}\eta \quad \text{for all } 0 \leq \eta \leqslant b_0$$

and we deduce from (4.5.53) that

$$u_0(\eta) \geqslant W_\lambda(\eta) \quad \text{for all } 0 \leqslant \eta \leqslant b_\lambda. \tag{4.5.56}$$

Defining $\underline{\mathcal{W}}_\lambda = W_\lambda$ and $\underline{b}_\lambda = b_\lambda$ as in (4.5.16), we deduce that the pair $(\underline{\mathcal{W}}_\lambda, \underline{b}_\lambda)$ is a lower solution for Problem (4.5.4). □

4.6 A priori estimates for the solution of Problem (4.5.4)

4.6.1 A priori estimates for the solution of Problem (4.5.4) on the moving domain

Definition 4.6.1. *We define*

$$\underline{b}(\tau) := b(\tau,(\underline{\mathcal{W}}_\lambda,\underline{b}_\lambda))) \text{ and } \underline{W}(\eta,\tau) := W(\eta,\tau,(\underline{\mathcal{W}}_\lambda,\underline{b}_\lambda)) \text{ for all } \tau > 0, 0 \leqslant \eta \leqslant \underline{b}(\tau).$$

We start by showing successive lemmas for the function pair $(\underline{\mathrm{W}},\underline{\mathrm{b}})$.

Lemma 4.6.2. *We have the following uniform bounds in time*

$$\underline{b}_\lambda \leqslant \underline{b}(\tau) := b(\tau,(\underline{\mathcal{W}}_\lambda,\underline{b}_\lambda)) \leqslant \underline{b}_\infty \leqslant \bar{b} \quad \text{for all} \quad \tau \geqslant 0. \tag{4.6.1}$$

and

$$0 \leqslant \underline{W}(\eta,\tau) := W(\eta,\tau,(\underline{\mathcal{W}}_\lambda,\underline{b}_\lambda)) \leqslant h \text{ for all } \tau \geqslant 0, 0 \leqslant \eta \leqslant \bar{b}. \tag{4.6.2}$$

Proof. It follows from (4.5.18) and (4.5.23) that

$$\underline{b}_\lambda \leqslant b(\tau,(u_0,b_0)) \leqslant \bar{b} \text{ for all } \tau \geqslant 0.$$

In particular, for $(u_0,b_0) = (\underline{\mathcal{W}}_\lambda, \underline{b}_\lambda)$, we obtain

$$\underline{b}_\lambda \leqslant \underline{b}(\tau) := b(\tau,(\underline{\mathcal{W}}_\lambda,\underline{b}_\lambda)) \leqslant \bar{b} \text{ for all } \tau \geqslant 0.$$

We conclude from (4.5.27) that

$$\underline{b}_\lambda \leqslant \underline{b}(\tau) \leqslant \underline{b}_\infty \leqslant \bar{b},$$

then (4.6.1) holds.

Now we prove (4.6.2). Indeed, we know from (4.5.9) and (4.5.16) that $0 \leqslant \underline{\mathcal{W}}_\lambda(\eta) \leqslant h$ for all $\eta \in (0,\bar{b})$, which by Proposition 4.2.3 implies that

$$0 \leqslant \underline{\mathrm{W}}(\eta,\tau) := W(\eta,\tau,(\underline{\mathcal{W}}_\lambda,\underline{b}_\lambda)) \leqslant h \quad \text{for all } \tau \geqslant 0, 0 \leqslant \eta \leqslant \bar{b},$$

so that (4.6.2) holds. □

Next we prove the following result.

Lemma 4.6.3. *Let $\sigma > 0$. For all $\tau > 0$, we have that*

$$\| \underline{W}_\eta(\,\cdot\,,\,\cdot\,+\tau)\|^2_{L^2(\Omega_{\sigma,\tau})} \leqslant C(\sigma), \tag{4.6.3}$$

for some positive constant $C(\sigma)$ which does not depend on τ and where

$$\Omega_{\sigma,\tau} := \{(\eta,S); 0 < \eta < \underline{b}(S+\tau), S \in (0,\sigma)\}. \tag{4.6.4}$$

Proof. We have

$$\underline{\mathrm{W}}_\tau(\eta,\tau) = \underline{\mathrm{W}}_{\eta\eta}(\eta,\tau) + \frac{\eta}{2}\underline{\mathrm{W}}_\eta(\eta,\tau) \text{ for all } \tau > 0 \text{ and } 0 < \eta < \underline{b}(\tau),$$

Then,

$$(\underline{\mathrm{W}}-h)_\tau(\eta,\tau)(\underline{\mathrm{W}}-h)(\eta,\tau) = \underline{\mathrm{W}}_{\eta\eta}(\eta,\tau)(\underline{\mathrm{W}}-h)(\eta,\tau) + \frac{\eta}{2}\underline{\mathrm{W}}_\eta(\eta,\tau)(\underline{\mathrm{W}}-h)(\eta,\tau). \tag{4.6.5}$$

A direct computations yields

$$\frac{d}{d\tau}\int_0^{\underline{b}(\tau)}\left(\underline{\mathrm{W}}(\eta,\tau)-h\right)^2 d\eta=\frac{d\underline{b}(\tau)}{d\tau}\left(\underline{\mathrm{W}}(\underline{b}(\tau),\tau)-h\right)^2+2\int_0^{\underline{b}(\tau)}\left(\underline{\mathrm{W}}-h\right)_\tau(\eta,\tau)(\underline{\mathrm{W}}-h)(\eta,\tau)d\eta.$$

Since $\underline{\mathrm{W}}(\underline{b}(\tau),\tau)=0$, we obtain

$$\int_0^{\underline{b}(\tau)}\left(\underline{\mathrm{W}}-h\right)_\tau(\eta,\tau)(\underline{\mathrm{W}}-h)(\eta,\tau)d\eta=\frac{1}{2}\frac{d}{d\tau}\int_0^{\underline{b}(\tau)}\left(\underline{\mathrm{W}}(\eta,\tau)-h\right)^2 d\eta-\frac{1}{2}\frac{d\underline{b}(\tau)}{d\tau}h^2. \tag{4.6.6}$$

Then, we deduce from (4.6.5) and (4.6.6) that

$$\int_0^{\underline{b}(\tau)}\underline{\mathrm{W}}_{\eta\eta}(\eta,\tau)(\underline{\mathrm{W}}-h)(\eta,\tau)d\eta+\int_0^{\underline{b}(\tau)}\frac{\eta}{2}\underline{\mathrm{W}}_\eta(\eta,\tau)(\underline{\mathrm{W}}-h)(\eta,\tau)d\eta= \tag{4.6.7}$$

$$\frac{1}{2}\frac{d}{d\tau}\int_0^{\underline{b}(\tau)}\left(\underline{\mathrm{W}}(\eta,\tau)-h\right)^2 d\eta-\frac{1}{2}\frac{d\underline{b}(\tau)}{d\tau}h^2.$$

Next, we integrate by parts the first term on the left-hand-side of (4.6.7) and we use $\underline{\mathrm{W}}(\underline{b}(\tau),\tau)=0$ and $\underline{\mathrm{W}}(0,\tau)=h$ to obtain

$$\int_0^{\underline{b}(\tau)}\underline{\mathrm{W}}_{\eta\eta}(\eta,\tau)(\underline{\mathrm{W}}-h)(\eta,\tau)d\eta=-\underline{\mathrm{W}}_\eta(\underline{b}(\tau),\tau)h-\int_0^{\underline{b}(\tau)}|\underline{\mathrm{W}}_\eta|^2 d\eta. \tag{4.6.8}$$

Due to Lemma 4.6.2, we have $\left|\underline{\mathrm{W}}(\eta,\tau)-h\right|\leqslant h$ and $0\leqslant\eta\leqslant\bar{b}$. It follows that

$$\int_0^{\underline{b}(\tau)}\frac{\eta}{2}\underline{\mathrm{W}}_\eta(\eta,\tau)(\underline{\mathrm{W}}-h)(\eta,\tau)d\eta\leqslant\frac{\bar{b}}{2}\,h\int_0^{\underline{b}(\tau)}|\underline{\mathrm{W}}_\eta|d\eta. \tag{4.6.9}$$

Then, we deduce from (4.6.7), (4.6.8) and (4.6.9) that

$$\frac{1}{2}\frac{d}{d\tau}\int_0^{\underline{b}(\tau)}\left(\underline{\mathrm{W}}(\eta,\tau)-h\right)^2 d\eta-\frac{1}{2}\frac{d\underline{b}(\tau)}{d\tau}h^2\leqslant-\underline{\mathrm{W}}_\eta(\underline{b}(\tau),\tau)h-\int_0^{\underline{b}(\tau)}|\underline{\mathrm{W}}_\eta|^2 d\eta+\frac{\bar{b}}{2}\,h\int_0^{\underline{b}(\tau)}|\underline{\mathrm{W}}_\eta|d\eta. \tag{4.6.10}$$

Moreover, it follows from Cauchy-Schwarz's and Young's inequalities that

$$\int_0^{\underline{b}(\tau)}|\underline{\mathrm{W}}_\eta||1|d\eta\leqslant\frac{1}{2\varepsilon}\int_0^{\underline{b}(\tau)}|\underline{\mathrm{W}}_\eta|^2 d\eta+\frac{\varepsilon}{2}\int_0^{\underline{b}(\tau)}|1|^2 d\eta \tag{4.6.11}$$

for all $\varepsilon>0$. Since $-\underline{\mathrm{W}}_\eta(\underline{b}(\tau),\tau)=\dfrac{d\underline{b}(\tau)}{d\tau}+\dfrac{\underline{b}(\tau)}{2}$ and in view of (4.6.11), (4.6.10) becomes

$$\frac{1}{2}\frac{d}{d\tau}\int_0^{\underline{b}(\tau)}(\underline{\mathrm{W}}-h)^2 d\eta-\frac{h^2}{2}\frac{d\underline{b}(\tau)}{d\tau}+\int_0^{\underline{b}(\tau)}|\underline{\mathrm{W}}_\eta|^2 d\eta\leqslant \tag{4.6.12}$$

$$\left(\frac{d\underline{b}(\tau)}{d\tau}+\frac{\underline{b}(\tau)}{2}\right)h+\frac{\bar{b}\,h}{4}\left(\frac{1}{\varepsilon}\int_0^{\underline{b}(\tau)}|\underline{\mathrm{W}}_\eta|^2\,d\eta\;+\varepsilon\underline{b}(\tau)\right).$$

Let $\sigma>0$; we integrate both sides of the inequality (4.6.12) on $(\tau,\tau+\sigma)$ to obtain

$$\frac{1}{2}\int_\tau^{\tau+\sigma}\frac{d}{ds}\int_0^{\underline{b}(s)}(\underline{\mathrm{W}}-h)^2\,d\eta ds-\frac{h^2}{2}\int_\tau^{\tau+\sigma}\frac{d\underline{b}(s)}{ds}ds+\int_\tau^{\tau+\sigma}\int_0^{\underline{b}(s)}|\underline{\mathrm{W}}_\eta|^2\,d\eta ds\leqslant$$

$$\int_\tau^{\tau+\sigma}\left(\frac{d\underline{b}(s)}{ds}+\frac{\underline{b}(s)}{2}\right)h\,ds+\frac{\bar{b}\,h}{4}\int_\tau^{\tau+\sigma}\frac{1}{\varepsilon}\int_0^{\underline{b}(s)}|\underline{\mathrm{W}}_\eta|^2\,d\eta ds+\frac{\bar{b}\,h\,\varepsilon}{4}\int_\tau^{\tau+\sigma}\underline{b}(s)ds.$$

Then, it follows that

$$\frac{1}{2}\int_0^{\underline{b}(\tau+\sigma)}\left(\underline{\mathrm{W}}(\eta,\tau+\sigma)-h\right)^2 d\eta-\frac{1}{2}\int_0^{\underline{b}(\tau)}\left(\underline{\mathrm{W}}(\eta,\tau)-h\right)^2 d\eta-\frac{h^2}{2}\left(\underline{b}(\tau+\sigma)-\underline{b}(\tau)\right)+$$

$$\Big(1-\frac{\bar{b}\,h}{4\,\varepsilon}\Big)\int_{\tau}^{\tau+\sigma}\int_{0}^{\underline{b}(s)}|\underline{\mathrm{W}}_{\eta}|^{2}\,d\eta ds\leqslant\Big(\underline{b}(\tau+\sigma)-\underline{b}(\tau)\Big)h+\frac{h(2+\varepsilon\,\bar{b})}{4}\int_{\tau}^{\tau+\sigma}\underline{b}(s)ds.$$

For $\varepsilon=\dfrac{\bar{b}h}{2}$, we obtain

$$\frac{1}{2}\int_{\tau}^{\tau+\sigma}\int_{0}^{\underline{b}(s)}|\underline{\mathrm{W}}_{\eta}|^{2}\,d\eta ds\ \leqslant$$

$$\frac{1}{2}\int_{0}^{\underline{b}(\tau)}\Big(\underline{\mathrm{W}}(\eta,\tau)-h\Big)^{2}d\eta+\Big(h+\frac{h^{2}}{2}\Big)\Big(\underline{b}(\tau+\sigma)-\underline{b}(\tau)\Big)+\frac{h(4+\bar{b}^{2}h)}{8}\int_{\tau}^{\tau+\sigma}\underline{b}(s)ds.$$

Since $\underline{b}(\tau)\leqslant\bar{b}$ for all $\tau>0$ and $\big|\underline{\mathrm{W}}(\eta,\tau)-h\big|\leqslant h$, it follows that

$$\int_{\tau}^{\tau+\sigma}\int_{0}^{\underline{b}(s)}|\underline{\mathrm{W}}_{\eta}|^{2}\,d\eta ds\leqslant h^{2}\bar{b}+\Big(2h+h^{2}\Big)\bar{b}+\frac{h(4+\bar{b}^{2}h)}{4}\,\sigma\,\bar{b}.$$

We conclude that

$$\int_{\tau}^{\tau+\sigma}\int_{0}^{\underline{b}(s)}|\underline{\mathrm{W}}_{\eta}|^{2}\,d\eta ds\leqslant C(\sigma)\ \text{ for some positive constant } C(\sigma). \tag{4.6.13}$$

Next we perform the change of variable $S=s-\tau$; then

$$\int_{0}^{\sigma}\int_{0}^{\underline{b}(S+\tau)}|\underline{\mathrm{W}}_{\eta}(\eta,S+\tau)|^{2}\,d\eta dS\leqslant C(\sigma)\ \text{ for all } \tau\geqslant 0,$$

which implies that

$$\|\underline{\mathrm{W}}_{\eta}(.,.+\tau)\|^{2}_{L^{2}(\Omega_{\sigma,\tau})}\leqslant C(\sigma), \tag{4.6.14}$$

for some positive constant $C(\sigma)$ which does not depend on τ. This completes the proof of Lemma 4.6.3. □

Next we show the following result.

Lemma 4.6.4. *Let $\sigma>0$. For all $\tau>0$, we have that*

$$\|\,\underline{W}_{\eta\eta}(.,.+\tau)\|^{2}_{L^{2}(\Omega_{\sigma,\tau})}\leqslant C(\sigma), \tag{4.6.15}$$

for some positive constant $C(\sigma)$ which does not depend on τ.

Before proving Lemma 4.6.4, we will recall the following result.

Lemma 4.6.5 (The Uniform Gronwall Lemma (Lemma 1.1 of [78, p.89]))**.** *Let g and y be two positive locally integrable functions on $(0,+\infty)$ such that $\dfrac{dy}{dt}$ is locally integrable on $(0,\infty)$, which satisfy the inequalities*

$$\frac{dy}{dt}\leqslant g\,y\qquad \textit{for all } t\geqslant 0, \tag{4.6.16}$$

$$\int_{t}^{t+r}g(s)ds\leqslant a_{1},\ \int_{t}^{t+r}y(s)ds\leqslant a_{2}\ \textit{ for all } t\geqslant 0, \tag{4.6.17}$$

where r,a_{1},a_{2}, are positive constants which do not depend in t. Then

$$y(t+r)\leqslant\frac{a_{2}}{r}\exp(a_{1}),\qquad \textit{for all } t\geqslant 0. \tag{4.6.18}$$

Proof of Lemma 4.6.4. We define

$$Z(\eta,\tau) := \underline{\mathrm{W}}_{\eta}(\eta,\tau) \text{ for all } \tau > 0 \text{ and } 0 < \eta < \underline{b}(\tau), \tag{4.6.19}$$

where $\underline{\mathrm{W}}(\eta,\tau)$ is defined in Definition 4.6.1. From Problem (4.5.4), we have

$$(\underline{\mathrm{W}}_{\eta})_{\tau} = (\underline{\mathrm{W}}_{\eta})_{\eta\eta} + \frac{\eta}{2}(\underline{\mathrm{W}}_{\eta})_{\eta} + \frac{\underline{\mathrm{W}}_{\eta}}{2}, \quad \tau > 0, \quad 0 < \eta < \underline{b}(\tau),$$

so that

$$Z_{\tau} = Z_{\eta\eta} + \frac{\eta}{2}Z_{\eta} + \frac{Z}{2}, \quad \tau > 0, \quad 0 < \eta < \underline{b}(\tau). \tag{4.6.20}$$

Next we show that $Z_{\eta}(0,\tau) = 0$ and that $Z_{\eta}(\underline{b}(\tau),\tau) = Z^2(\underline{b}(\tau),\tau)$. Indeed, we have that $\left(\underline{\mathrm{W}}(0,\tau)\right)_{\tau} = (h)_{\tau} = 0$ and $\left(\underline{\mathrm{W}}(0,\tau)\right)_{\tau} = \underline{\mathrm{W}}_{\tau}(0,\tau) = (\underline{\mathrm{W}}_{\eta})_{\eta}(0,\tau) + \frac{0}{2}\underline{\mathrm{W}}_{\eta}(0,\tau)$. Then

$$Z_{\eta}(0,\tau) = 0. \tag{4.6.21}$$

Moreover, we have

$$\Big(\underline{\mathrm{W}}(\underline{b}(\tau),\tau)\Big)_{\tau} = \frac{d\underline{b}(\tau)}{d\tau}\underline{\mathrm{W}}_{\eta}(\underline{b}(\tau),\tau) + \underline{\mathrm{W}}_{\tau}(\underline{b}(\tau),\tau) = 0, \tag{4.6.22}$$

and

$$\underline{\mathrm{W}}_{\tau}(\underline{b}(\tau),\tau) = (\underline{\mathrm{W}}_{\eta})_{\eta}(\underline{b}(\tau),\tau) + \frac{\underline{b}(\tau)}{2}\underline{\mathrm{W}}_{\eta}(\underline{b}(\tau),\tau). \tag{4.6.23}$$

We substitute (4.6.23) in (4.6.22) to obtain

$$(\underline{\mathrm{W}}_{\eta})_{\eta}(\underline{b}(\tau),\tau) + \frac{\underline{b}(\tau)}{2}\underline{\mathrm{W}}_{\eta}(\underline{b}(\tau),\tau) + \frac{d\underline{b}(\tau)}{d\tau}\underline{\mathrm{W}}_{\eta}(\underline{b}(\tau),\tau) = 0,$$

so that

$$Z_{\eta}(\underline{b}(\tau),\tau) + \frac{\underline{b}(\tau)}{2}Z(\underline{b}(\tau),\tau) + \frac{d\underline{b}(\tau)}{d\tau}Z(\underline{b}(\tau),\tau) = 0. \tag{4.6.24}$$

Since $\dfrac{d\underline{b}(\tau)}{d\tau} + \dfrac{\underline{b}(\tau)}{2} = -\underline{\mathrm{W}}_{\eta}(\underline{b}(\tau),\tau) = -Z(\underline{b}(\tau),\tau)$ then (4.6.24) becomes

$$Z_{\eta}(\underline{b}(\tau),\tau) = Z^2(\underline{b}(\tau),\tau). \tag{4.6.25}$$

Therefore, from (4.6.20), (4.6.21) and (4.6.25), the time evolution Problem (4.5.4) leads to

$$\begin{cases} Z_{\tau} = Z_{\eta\eta} + \dfrac{\eta}{2}Z_{\eta} + \dfrac{Z}{2}, & \tau > 0, \quad 0 < \eta < \underline{b}(\tau), \\ Z_{\eta}(0,\tau) = 0, & \tau > 0, \\ Z_{\eta}(\underline{b}(\tau),\tau) = Z^2(\underline{b}(\tau),\tau), & \tau > 0, \\ \dfrac{d\underline{b}(\tau)}{d\tau} + \dfrac{\underline{b}(\tau)}{2} = -Z(\underline{b}(\tau),\tau), & \tau > 0, \\ \underline{\mathrm{b}}(0) = \underline{\mathrm{b}}, & \\ Z(\eta,0) = \underline{\mathrm{W}}_{\lambda,\eta}(\eta), & 0 \leqslant \eta \leqslant \underline{b}_{\lambda}, \end{cases} \tag{4.6.26}$$

where $\underline{\mathrm{W}}_{\lambda,\eta}(\eta) = \dfrac{-h\, e^{-\frac{\lambda\eta^2}{4}}}{\int_0^{\underline{b}_{\lambda}} e^{-\frac{\lambda s^2}{4}}\, ds}$ with $\lambda \geqslant 1$. We consider the function F defined by

$$F(\tau) = \int_0^{\underline{b}(\tau)} Z^2(\eta,\tau)\, \mathrm{d}\eta. \tag{4.6.27}$$

Then, we compute $\dfrac{dF(\tau)}{d\tau} = \dfrac{d\underline{b}(\tau)}{d\tau}\, Z^2(\underline{b}(\tau),\tau) + 2\displaystyle\int_0^{\underline{b}(\tau)} Z_\tau(\eta,\tau)Z(\eta,\tau)\,\mathrm{d}\eta$, so that

$$\int_0^{\underline{b}(\tau)} Z_\tau(\eta,\tau)Z(\eta,\tau)\,\mathrm{d}\eta = \frac{1}{2}\frac{d}{d\tau}\int_0^{\underline{b}(\tau)} Z^2(\eta,\tau)\,\mathrm{d}\eta - \frac{1}{2}\frac{d\underline{b}(\tau)}{d\tau}\, Z^2(\underline{b}(\tau),\tau). \tag{4.6.28}$$

We multiply (4.6.20) by Z and integrate in space between 0 en $\underline{b}(\tau)$ to obtain

$$\int_0^{\underline{b}(\tau)} Z_\tau(\eta,\tau)Z(\eta,\tau)\,\mathrm{d}\eta = \int_0^{\underline{b}(\tau)} Z_{\eta\eta}(\eta,\tau)Z(\eta,\tau)\,\mathrm{d}\eta + \int_0^{\underline{b}(\tau)} \frac{\eta}{2} Z_\eta(\eta,\tau)Z(\eta,\tau)\,\mathrm{d}\eta + \int_0^{\underline{b}(\tau)} \frac{Z^2(\eta,\tau)}{2}\,\mathrm{d}\eta. \tag{4.6.29}$$

We integrate by parts the first term on the right-hand-side of (4.6.29) and using $Z_\eta(0,\tau) = 0$ and $Z_\eta(\underline{b}(\tau),\tau) = Z^2(\underline{b}(\tau),\tau)$, we deduce that

$$\int_0^{\underline{b}(\tau)} Z_{\eta\eta}(\eta,\tau)Z(\eta,\tau)\,\mathrm{d}\eta = Z^3(\underline{b}(\tau),\tau) - \int_0^{\underline{b}(\tau)} \left|Z_\eta(\eta,\tau)\right|^2 \mathrm{d}\eta. \tag{4.6.30}$$

Next, since $0 \leqslant \eta \leqslant \bar{b}$, it follows that

$$\int_0^{\underline{b}(\tau)} \frac{\eta}{2} Z_\eta(\eta,\tau)Z(\eta,\tau)\,\mathrm{d}\eta \leqslant \frac{\bar{b}}{2}\int_0^{\underline{b}(\tau)} \left|Z_\eta(\eta,\tau)\right|\left|Z(\eta,\tau)\right|\mathrm{d}\eta. \tag{4.6.31}$$

Using the Cauchy-Schwarz inequality with the Young inequality, we obtain that

$$\int_0^{\underline{b}(\tau)} \frac{\eta}{2} Z_\eta(\eta,\tau)Z(\eta,\tau)\,\mathrm{d}\eta \leqslant \frac{\bar{b}}{4\varepsilon}\int_0^{\underline{b}(\tau)} |Z_\eta(\eta,\tau)|^2 d\eta + \frac{\bar{b}\varepsilon}{4}\int_0^{\underline{b}(\tau)} |Z(\eta,\tau)|^2 d\eta \tag{4.6.32}$$

for all $\varepsilon > 0$. Next, combining (4.6.28), (4.6.29), (4.6.30) and (4.6.32) we deduce that

$$\frac{1}{2}\frac{d}{d\tau}\int_0^{\underline{b}(\tau)} Z^2(\eta,\tau)\,\mathrm{d}\eta - \frac{1}{2}\frac{d\underline{b}(\tau)}{d\tau}\, Z^2(\underline{b}(\tau),\tau) \leqslant \tag{4.6.33}$$

$$Z^3(\underline{b}(\tau),\tau) - \int_0^{\underline{b}(\tau)} \left|Z_\eta(\eta,\tau)\right|^2 \mathrm{d}\eta + \frac{\bar{b}}{4\varepsilon}\int_0^{\underline{b}(\tau)} |Z_\eta(\eta,\tau)|^2 d\eta + \frac{\bar{b}\varepsilon}{4}\int_0^{\underline{b}(\tau)} |Z(\eta,\tau)|^2 d\eta + \int_0^{\underline{b}(\tau)} \frac{Z^2(\eta,\tau)}{2}\,\mathrm{d}\eta.$$

Since $\dfrac{d\underline{b}(\tau)}{d\tau} + \dfrac{\underline{b}(\tau)}{2} = -Z(\underline{b}(\tau),\tau)$, then

$$\frac{-1}{2}\frac{d\underline{b}(\tau)}{d\tau}\, Z^2(\underline{b}(\tau),\tau) = \frac{1}{2}Z^3(\underline{b}(\tau),\tau) + \frac{\underline{b}(\tau)}{4}\, Z^2(\underline{b}(\tau),\tau).$$

So, (4.6.33) becomes

$$\frac{1}{2}\frac{d}{d\tau}\int_0^{\underline{b}(\tau)} Z^2(\eta,\tau)\,\mathrm{d}\eta + \frac{4\varepsilon - \bar{b}}{4\varepsilon}\int_0^{\underline{b}(\tau)} |Z_\eta(\eta,\tau)|^2 d\eta \leqslant \tag{4.6.34}$$

$$\frac{1}{2}Z^3(\underline{b}(\tau),\tau) - \frac{\underline{b}(\tau)}{4}\, Z^2(\underline{b}(\tau),\tau) + \frac{\bar{b}\varepsilon + 2}{4}\int_0^{\underline{b}(\tau)} \left|Z(\eta,\tau)\right|^2 d\eta.$$

From (4.6.49) below, we have $Z(\underline{b}(\tau),\tau) = \underline{\mathrm{W}}_\eta(\underline{b}(\tau),\tau) \leqslant 0$; setting $\varepsilon = \dfrac{\bar{b}}{2}$ then yields

$$\frac{1}{2}\frac{d}{d\tau}\int_0^{\underline{b}(\tau)} Z^2(\eta,\tau)\,\mathrm{d}\eta + \frac{1}{2}\int_0^{\underline{b}(\tau)} \left|Z_\eta(\eta,\tau)\right|^2 \mathrm{d}\eta \leqslant \frac{\bar{b}^2 + 4}{8}\int_0^{\underline{b}(\tau)} \left|Z(\eta,\tau)\right|^2 \mathrm{d}\eta. \tag{4.6.35}$$

It follows from (4.6.35), (4.6.13) and the uniform Gronwall Lemma 4.6.5 that there exists some positive constant $C(\sigma)$ which does not depend on τ such that

$$\int_0^{\underline{b}(\tau+\sigma)} Z^2(\eta,\tau+\sigma)\,\mathrm{d}\eta \leqslant C(\sigma) \quad \text{for all} \quad \tau > 0. \tag{4.6.36}$$

Next, we integrate both sides of the inequality (4.6.35) on $(\tau,\tau+\sigma)$ to obtain

$$\frac{1}{2}\int_{\tau}^{\tau+\sigma}\frac{d}{ds}\int_{0}^{\underline{b}(s)} Z^2(\eta,s)\,d\eta ds+\frac{1}{2}\int_{\tau}^{\tau+\sigma}\int_{0}^{\underline{b}(s)}\left|Z_\eta(\eta,s)\right|^2 \mathrm{d}\eta\,\mathrm{d}s\leqslant\frac{\bar{b}^2+4}{8}\int_{\tau}^{\tau+\sigma}\int_{0}^{\underline{b}(s)}\left|Z(\eta,s)\right|^2\mathrm{d}\eta\,\mathrm{d}s. \tag{4.6.37}$$

Then, in view of (4.6.36) and the fact that $\underline{b}$ is nondecreasing, (4.6.37) becomes

$$\frac{1}{2}\int_{0}^{\underline{b}(\tau+\sigma)} Z^2(\eta,\tau+\sigma)\,\mathrm{d}\eta-\frac{1}{2}\int_{0}^{\underline{b}(\tau)} Z^2(\eta,\tau)\,\mathrm{d}\eta+\frac{1}{2}\int_{\tau}^{\tau+\sigma}\int_{0}^{\underline{b}(s)}\left|Z_\eta(\eta,s)\right|^2\mathrm{d}\eta\,\mathrm{d}s\leqslant\frac{(\bar{b}^2+4)\,\sigma\,C(\sigma)}{8}, \tag{4.6.38}$$

so that also

$$\int_{\tau}^{\tau+\sigma}\int_{0}^{\underline{b}(s)}\left|Z_\eta(\eta,s)\right|^2\mathrm{d}\eta\,\mathrm{d}s\leqslant C(\sigma)+\frac{(\bar{b}^2+4)\,\sigma\,C(\sigma)}{4}. \tag{4.6.39}$$

Next, we perform the change of variable $S=s-\tau$, then

$$\int_{0}^{\sigma}\int_{0}^{\underline{b}(S+\tau)}\left|Z_\eta(\eta,S+\tau)\right|^2\mathrm{d}\eta\,\mathrm{d}S\leqslant C(\sigma)+\frac{(\bar{b}^2+4)\,\sigma\,C(\sigma)}{4}\quad\text{for all }\tau>0$$

which implies that

$$\left\|Z_\eta(.,.+\tau)\right\|^2_{L^2(\Omega_{\sigma,\tau})}\leqslant C(\sigma)+\frac{(\bar{b}^2+4)\,\sigma\,C(\sigma)}{4}. \tag{4.6.40}$$

This completes the proof of Lemma 4.6.4. □

Next we deduce the following Corollary.

Corollary 4.6.6. *Let $\sigma>0$. For all $\tau>0$, we have that*

$$\left\|\underline{W}_\eta(.,.+\tau)\right\|_{L^2\left(0,\sigma;C^{\frac{1}{2}}(\overline{\Omega_\tau})\right)}\leqslant C(\sigma), \tag{4.6.41}$$

for some positive constant $C(\sigma)$ which does not depend on τ and where

$$\Omega_\tau:=\{\eta;0<\eta<\underline{b}(S+\tau),S\in(0,\sigma)\}. \tag{4.6.42}$$

Proof. From Lemmas 4.6.3 and 4.6.4, we deduce that there exists some positive constant $\tilde{\tilde{C}}(\sigma)$ which does not depend on τ such that

$$\left\|\underline{W}_\eta(.,.+\tau)\right\|^2_{L^2\left(0,\sigma;H^1(\Omega_\tau)\right)}\leqslant\tilde{\tilde{C}}(\sigma). \tag{4.6.43}$$

Then, since $H^1(\Omega_\tau)\subset C^{\frac{1}{2}}(\overline{\Omega}_\tau)$, (4.6.41) follows from (4.6.43). □

Uniform estimate of $\underline{W}(.,.+\tau)$ in $C^{\frac{1}{2},\frac{1}{4}}(\overline{\Omega}_{\sigma,\tau})$.

Lemma 4.6.7. *There exists some positive constant C which does not depend on τ such that*

$$\left\|\underline{W}(.,.+\tau)\right\|_{C^{\frac{1}{2},\frac{1}{4}}(\overline{\Omega}_{\tau,\sigma})}\leqslant C, \tag{4.6.44}$$

where $\Omega_{\sigma,\tau}:=\{(\eta,S);0<\eta<\underline{b}(S+\tau),S\in(0,\sigma)\}$.

Proof. There exists some positive constant $C_1(\sigma)$ which does not depend on τ such that

$$\left\|\underline{W}_\tau(.,.+\tau)\right\|_{L^2(\Omega_{\sigma,\tau})}\leqslant C_1(\sigma). \tag{4.6.45}$$

Indeed, we have that

$$\underline{W}_\tau(\eta,\tau)=\underline{W}_{\eta\eta}(\eta,\tau)+\frac{\eta}{2}\underline{W}_\eta(\eta,\tau)\text{ for all }\tau>0\text{ and }0<\eta<\underline{b}(\tau),$$

and from Lemmas 4.6.3 and 4.6.4, we have that

$$\|\underline{\mathrm{W}}_\eta(.,.+\tau)\|^2_{L^2(\Omega_{\sigma,\tau})} \leqslant C_2(\sigma) \text{ for some positive constant } C_2(\sigma),$$

and

$$\|\underline{\mathrm{W}}_{\eta\eta}(.,.+\tau)\|^2_{L^2(\Omega_{\sigma,\tau})} \leqslant C_3(\sigma) \text{ for some positive constant } C_3(\sigma).$$

Since $\eta \leqslant \bar{b}$, it follows that

$$\frac{\eta}{2}\underline{\mathrm{W}}_\eta(.,.+\tau) \in L^2(\Omega_{\sigma,\tau}).$$

Finally, we conclude from the partial differential equation for $\underline{\mathrm{W}}$ that the estimate (4.6.45) holds, so that $\underline{\mathrm{W}}(.,.+\tau) \in \mathbb{W}_2^{2,1}(\Omega_{\sigma,\tau})$. From (Lemma 3.5 of [8, p.207]), we have that

$$\mathbb{W}_2^{2,1}(\Omega_{\sigma,\tau}) \subset C^{\frac{1}{2},\frac{1}{4}}(\overline{\Omega}_{\sigma,\tau}), \tag{4.6.46}$$

so that (4.6.44) holds. □

Next we show the following result.

Lemma 4.6.8. *The function $\underline{W}_\eta$ is such that $\underline{W}_\eta(\eta,\tau) \leqslant 0$ for all $\tau > 0$ and $0 < \eta < \underline{b}(\tau)$.*

Proof. We recall that $Z(\eta,\tau) := \underline{\mathrm{W}}_\eta(\eta,\tau)$ for all $\tau > 0$ and $0 < \eta < \underline{b}(\tau)$ as defined in (4.6.19). From (4.6.26), Z satisfies the partial differential equation

$$Z_\tau = Z_{\eta\eta} + \frac{\eta}{2}Z_\eta + \frac{Z}{2}, \quad \tau > 0, \quad 0 < \eta < \underline{b}(\tau).$$

We also have that

$$Z(0,\tau) \leqslant 0 \text{ for all } \tau > 0. \tag{4.6.47}$$

Indeed, since $0 \leqslant \underline{\mathrm{W}}(\eta,\tau) \leqslant h$ and $\underline{\mathrm{W}}(0,\tau) = h$, it follows that

$$\underline{\mathrm{W}}_\eta(0,\tau) \leqslant 0 \text{ for all } \tau > 0. \tag{4.6.48}$$

Next, we prove that

$$Z(\underline{b}(\tau),\tau) \leqslant 0. \tag{4.6.49}$$

Indeed, from Problem (4.5.4) and Lemma 4.5.4, we deduce that $\frac{d\underline{b}(\tau)}{d\tau} + \frac{\underline{b}(\tau)}{2} = -\underline{\mathrm{W}}_\eta(\underline{b}(\tau),\tau)$ and $\frac{d\underline{b}(\tau)}{d\tau} \geqslant 0$ for all $\tau > 0$; it follows that $\underline{\mathrm{W}}_\eta(\underline{b}(\tau),\tau) \leqslant 0$ for all $\tau > 0$. Next from (4.6.26), we have that

$$Z(\eta,0) = \underline{\mathrm{W}}_{\lambda,\eta}(\eta) = \frac{-h\, e^{-\frac{\lambda\eta^2}{4}}}{\int_0^{\underline{b}_\lambda} e^{-\frac{\lambda s^2}{4}} ds} \leqslant 0 \text{ for } 0 \leqslant \eta \leqslant \underline{b}_\lambda \text{ with } \lambda \geqslant 1. \tag{4.6.50}$$

Let $T > 0$, we define

$$\mathbf{Q}_T := \{(\eta,\tau), \tau \in (0,T), 0 < \eta < \underline{b}(\tau)\}. \tag{4.6.51}$$

Next, we perform the change of function $Z(\eta,\tau) = \tilde{Z}(\eta,\tau)e^{\alpha\tau}$ where $\alpha > \frac{1}{2}$. The function $\tilde{Z}$ satisfies, for all $\alpha > \frac{1}{2}$, the equality

$$\tilde{Z}_\tau\, e^{\alpha\tau} = \tilde{Z}_{\eta\eta}\, e^{\alpha\tau} + \frac{\eta}{2}\tilde{Z}_\eta\, e^{\alpha\tau} + (\frac{1}{2} - \alpha)\tilde{Z}\, e^{\alpha\tau} \text{ in } \mathbf{Q}_\mathrm{T},$$

so that

$$\tilde{Z}_\tau - \left(\tilde{Z}_{\eta\eta} + \frac{\eta}{2}\tilde{Z}_\eta + (\frac{1}{2} - \alpha)\tilde{Z}\right) = 0 \text{ in } \mathbf{Q}_\mathrm{T}, \text{ for all ff} > \frac{1}{2}.$$

Now, we prove that $\tilde{Z} \leqslant 0$ in $\overline{\mathbf{Q}_T}$. Indeed, it follows from the weak maximum principle (Lemma 1 of [24, p.34]) that $\tilde{Z}$ cannot have a positive maximum in $\mathbf{Q}_T$. Then, $\tilde{Z}$ attains its maximum on the boundary $\Gamma := \{(0,\tau), 0 \leq \tau \leq T\} \cup \{(\eta,0), 0 < \eta < \underline{b}(0)\} \cup \{(\underline{b}(\tau),\tau), 0 \leq \tau \leq T\}$.
Then, it follows from (4.6.47), (4.6.49) and (4.6.50) that $\tilde{Z} \leqslant 0$ on Γ, so that $\tilde{Z} \leqslant 0$ in $\overline{\mathbf{Q}_T}$ which implies that $Z \leqslant 0$ in $\overline{\mathbf{Q}_T}$. Thus, we deduce that

$$\underline{\mathrm{W}}_{\eta}(\eta,\tau) \leqslant 0, \quad \text{for all } \tau \geqslant 0,\ 0 \leqslant \eta \leqslant \underline{b}(\tau). \tag{4.6.52}$$

which completes the proof of Lemma 4.6.8. □

Lemma 4.6.9. *Let $\tau \geqslant 0$ be arbitrary. The function $\eta \to \underline{W}_{\eta}(\eta,\tau)$ is nondecreasing.*

Proof. To prove Lemma 4.6.9, we need to show that $\underline{\mathrm{W}}_{\eta\eta}(\eta,\tau) \geqslant 0$ for each $\tau \geqslant 0$. Indeed, we define

$$G(\eta,\tau) := Z_{\eta}(\eta,\tau) \text{ for all } \tau > 0 \text{ and } 0 < \eta < \underline{b}(\tau).$$

We recall that $Z(\eta,\tau) := \underline{\mathrm{W}}_{\eta}(\eta,\tau)$ for all $\tau > 0$ and $0 < \eta < \underline{b}(\tau)$ as defined in (4.6.19).
Now we derive the time evolution problem satisfied by G from the time evolution Problem (4.6.26) satisfied by Z. First, G satisfied the following boundary conditions

$$G(0,\tau) = 0, \quad G(\underline{b}(\tau),\tau) = Z^2(\underline{b}(\tau),\tau) \ \text{ for all } \ \tau > 0. \tag{4.6.53}$$

From Lemma (4.6.8), we have that $Z(\underline{b}(\tau),\tau) = \underline{\mathrm{W}}_{\eta}(\underline{b}(\tau),\tau) \leqslant 0$ for all $\tau > 0$. It follows that

$$Z(\underline{b}(\tau),\tau) = -\sqrt{G(\underline{b}(\tau),\tau)} \ \text{ for all } \ \tau > 0. \tag{4.6.54}$$

Straightforward computations give

$$\begin{cases} G_{\tau} = G_{\eta\eta} + \dfrac{\eta}{2} G_{\eta} + G, & \tau > 0, \quad 0 < \eta < \underline{b}(\tau), \\ G(0,\tau) = 0, & \tau > 0, \\ G(\underline{b}(\tau),\tau) = Z^2(\underline{b}(\tau),\tau), & \tau > 0, \\ \dfrac{d\underline{b}(\tau)}{d\tau} + \dfrac{\underline{b}(\tau)}{2} = \sqrt{G(\underline{b}(\tau),\tau)}, & \tau > 0, \\ \underline{b}(0) = \underline{b}, & \\ G(\eta,0) = \underline{\mathrm{W}}_{\lambda,\eta\eta}(\eta), & 0 \leqslant \eta \leqslant \underline{b}_{\lambda}. \end{cases} \tag{4.6.55}$$

where $G(\eta,0) = \underline{\mathrm{W}}_{\lambda,\eta\eta}(\eta) = \dfrac{\lambda\, \eta\, h\, e^{-\frac{\lambda\eta^2}{4}}}{2\int_0^{\underline{b}_{\lambda}} e^{-\frac{\lambda s^2}{4}} ds} \geqslant 0$ with $\lambda \geqslant 1$.
Finally, we use similar arguments as in the proof of Lemma 4.6.8 to deduce that

$$\underline{\mathrm{W}}_{\eta\eta}(\eta,\tau) \geqslant 0 \ \text{ for all } \tau \geqslant 0,\ 0 \leqslant \eta \leqslant \underline{b}(\tau). \tag{4.6.56}$$

This completes the proof of Lemma 4.6.9. □

Lemma 4.6.10. *Let $\sigma > 0$. For all $\tau > 0$, we have that*

$$\left\| \frac{d\underline{b}(.+\tau)}{d\tau} \right\|_{L^2(0,\sigma)} \leqslant C(\sigma), \tag{4.6.57}$$

for some positive constant $C(\sigma)$ which does not depend on τ, so that

$$\left\| \underline{b}(.+\tau) \right\|_{C^{0,\frac{1}{2}}([0,\sigma])} \leqslant \hat{C}(\sigma), \tag{4.6.58}$$

for some positive constant $\hat{C}(\sigma)$ which does not depend on τ.

Proof. We only have to show (4.6.57). We recall that $\underline{b}(.+\tau)$ satisfies the ODE

$$\frac{d\underline{b}(.+\tau)}{d\tau}+\frac{\underline{b}(.+\tau)}{2}=-\underline{\mathrm{W}}_\eta(\underline{b}(.+\tau),.+\tau)\quad \text{for all } \tau>0.$$

We have that

$$\int_0^\sigma \left|\underline{\mathrm{W}}_\eta(\underline{b}(s+\tau),s+\tau)\right|^2 ds \leqslant \int_0^\sigma \sup_{0\leqslant\eta\leqslant\underline{b}(.+\tau)} \left|\underline{\mathrm{W}}_\eta(\eta,s+\tau)\right|^2 ds = \left\|\underline{\mathrm{W}}_\eta(.,.+\tau)\right\|^2_{L^2\left(0,\sigma;C([0,\underline{b}(.+\tau)])\right)}. \tag{4.6.59}$$

From (4.6.59) and Corollary 4.6.6, we deduce that there exists some positive constant $C(\sigma)$ which does not depend on τ such that

$$\int_0^\sigma \left|\underline{\mathrm{W}}_\eta(\underline{b}(s+\tau),s+\tau)\right|^2 ds \leqslant C(\sigma),$$

which together with Lemma 4.6.2 implies that (4.6.57) holds. □

In the following subsection, we derive estimates for the free boundary Problem (4.5.4) in a fixed domain.

4.6.2 A Priori Estimates for the solution of Problem (4.5.4) on the fixed domain.

It will be necessary in the sequel to reason on a fixed domain. To do so, we start by giving the transformation to the fixed domain $\widehat{\Omega}:=\{(y,\tau)\in(0,1)\times(0,\infty)\}$. We set

$$y=\frac{\eta}{\underline{b}(\tau)},\ \ \hat{\underline{\mathrm{W}}}(y,\tau)=\underline{\mathrm{W}}(\eta,\tau)\ \text{ for all }\ \tau\geqslant 0, 0\leqslant\eta\leqslant\underline{b}(\tau). \tag{4.6.60}$$

Using this change of variable in the estimates obtained in Lemmas 4.6.3 and 4.6.4, with the bounds on $\underline{\mathrm{b}}$ in Lemma 4.6.2, we readily get the following uniform estimates for the function $\hat{\underline{\mathrm{W}}}$.

Lemma 4.6.11. *Let $\sigma>0$. For all $\tau\geqslant 0$, we have that*

$$\left\|\hat{\underline{\mathrm{W}}}_y(\ \cdot\ ,\ \cdot\ +\tau)\right\|_{L^2\left((0,1)\times(0,\sigma)\right)}\leqslant C(\sigma), \tag{4.6.61}$$

$$\left\|\hat{\underline{\mathrm{W}}}_{yy}(\ \cdot\ ,\ \cdot\ +\tau)\right\|_{L^2\left((0,1)\times(0,\sigma)\right)}\leqslant C(\sigma), \tag{4.6.62}$$

for some positive constant $C(\sigma)$ which does not depend on τ.

Next, we show the following result.

Lemma 4.6.12. *We have that*

$$\hat{\underline{\mathrm{W}}}_{yy}(y,\tau)\geqslant 0\ \ \textit{for all}\ \ \tau\geqslant 0, 0\leqslant y\leqslant 1, \tag{4.6.63}$$

and the function $y\mapsto\hat{\underline{\mathrm{W}}}_y(y,\tau)$ is nondecreasing for all $\tau\geqslant 0$. Moreover, there exists a positive constant C which does not depend on τ such that

$$\|\hat{\underline{\mathrm{W}}}_{yy}(.,\tau)\|_{L^1(0,1)}\leqslant C\ \ \textit{for all}\ \ \tau\geqslant 0. \tag{4.6.64}$$

Proof. From (4.6.56), we have that $\underline{\mathrm{W}}_{\eta\eta}(\eta,\tau)\geqslant 0,$ for all $\tau\geqslant 0,\ 0\leqslant\eta\leqslant\underline{b}(\tau)$. Since $\underline{\mathrm{W}}_{\eta\eta}(\eta,\tau)=\dfrac{1}{\underline{b}^2(\tau)}\hat{\underline{\mathrm{W}}}_{yy}(y,\tau)$, we deduce that (4.6.63) holds. Next, we prove that

$$\underline{\mathrm{W}}_{\eta\eta}(\eta,\tau)\text{ is uniformly bounded on }\ L^1([0,\underline{b}(\tau)])\text{ for all }\ \tau\geqslant 0. \tag{4.6.65}$$

From Lemma (4.6.8), we have that $Z(\underline{b}(\tau),\tau) = \underline{\mathrm{W}}_\eta(\underline{b}(\tau),\tau) \leqslant 0$ for all $\tau > 0$. Thus, we have

$$0 \leqslant \int_0^{\underline{b}(\tau)} \underline{\mathrm{W}}_{\eta\eta}(\eta,s)\,\mathrm{d}s = \underline{\mathrm{W}}_\eta(\underline{b}(\tau),\tau) - \underline{\mathrm{W}}_\eta(0,\tau) \leqslant -\underline{\mathrm{W}}_\eta(0,\tau). \tag{4.6.66}$$

We shall prove that $\underline{\mathrm{W}}_\eta(0,\tau)$ is bounded below for $\tau \geqslant 0$. Indeed, from Lemma 4.5.4, we know that $\underline{\mathrm{W}}$ is nondecreasing in time and since $\underline{\mathrm{W}}(0,\tau) = h$ for all $\tau \geqslant 0$, it follows that

$$\underline{\mathrm{W}}_\eta(0,0) \leqslant \underline{\mathrm{W}}_\eta(0,\tau) \text{ for all } \tau \geqslant 0. \tag{4.6.67}$$

We have that $\underline{\mathrm{W}}_\eta(0,0) = \underline{\mathrm{W}}_{\lambda,\eta}(0) = \dfrac{-h}{\int_0^{\underline{b}_\lambda} e^{-\frac{\lambda s^2}{4}} ds}$ with $\lambda \geqslant 1$, which implies together with (4.6.67) that $-\underline{\mathrm{W}}_\eta(0,\tau) \leqslant \dfrac{h}{\int_0^{\underline{b}_\lambda} e^{-\frac{\lambda s^2}{4}} ds}$, which in turn implies that

$$\int_0^{\underline{b}(\tau)} \underline{\mathrm{W}}_{\eta\eta}(\eta,s)\,\mathrm{d}s \leqslant \frac{h}{\int_0^{\underline{b}_\lambda} e^{-\frac{\lambda s^2}{4}} ds}. \tag{4.6.68}$$

Since $\underline{\mathrm{W}}_{\eta\eta}(\eta,s) = \dfrac{1}{\underline{b}^2(\tau)}\hat{\underline{\mathrm{W}}}_{yy}(y,s)$ and $\underline{b}(\tau) \leqslant \bar{b}$, we deduce that

$$\int_0^1 \hat{\underline{\mathrm{W}}}_{yy}(y,s)\,\mathrm{d}y = \|\hat{\underline{\mathrm{W}}}_{yy}(.,s)\|_{L^1(0,1)} \leqslant \frac{\bar{b}\,h}{\int_0^{\underline{b}_\lambda} e^{-\frac{\lambda s^2}{4}} ds}. \tag{4.6.69}$$

This complete the proof of (4.6.64). □

Now, we prove the following result.

Lemma 4.6.13. *There exists a positive constant C which does not depend on τ such that*

$$\|\hat{\underline{\mathrm{W}}}_y(.,\tau)\|_{L^1(0,1)} \leqslant C \quad \textit{for all } \tau \geqslant 0. \tag{4.6.70}$$

Proof. From Lemma 4.6.12, we have that the function $y \mapsto \hat{\underline{\mathrm{W}}}_y(y,\tau)$ is nondecreasing for all $\tau \geqslant 0$. Then, it follows that

$$\|\hat{\underline{\mathrm{W}}}_y(.,\tau)\|_{L^1(0,1)} = -\int_0^1 \hat{\underline{\mathrm{W}}}_y(y,\tau)\,dy = \hat{\underline{\mathrm{W}}}(0,\tau) - \hat{\underline{\mathrm{W}}}(1,\tau) = h \quad \text{for all } \tau \geqslant 0. \tag{4.6.71}$$

Indeed, from Problem (4.5.4), we have that $\underline{\mathrm{W}}(0,\tau) = h$ and $\underline{\mathrm{W}}(\underline{b}(\tau),\tau) = 0$ which implies that $\hat{\underline{\mathrm{W}}}(0,\tau) = h$ and $\hat{\underline{\mathrm{W}}}(1,\tau) = 0$ for all $\tau \geqslant 0$. This complete the proof of Lemma 4.6.13. □

4.7 Limit Problem as $\tau \to \infty$.

Theorem 4.7.1. *Let $(\psi, \underline{b}_\infty)$ be defined in Lemma 4.5.4. Then $(\psi, \underline{b}_\infty)$ is the unique stationary solution of Problem (4.1.12).*

Before proving this theorem, we need to show some preliminary results. Let $\hat{\underline{\mathrm{W}}}$ be defined as in (4.6.60). We also define

$$\hat{\psi}(y) = \psi(\eta), \quad y = \frac{\eta}{\underline{b}_\infty} \in [0,1] \quad \text{for} \quad 0 \leqslant \eta \leqslant \underline{b}_\infty. \tag{4.7.1}$$

We will derive estimates for $\hat{\psi}$. We start by showing the following result.

Lemma 4.7.1. *We have $\hat{\psi}, \hat{\psi}_y \in H^1(0,1) \subset C^{0,\frac{1}{2}}([0,1])$.*

Proof. Since $0 \leqslant \underline{W}(\eta,\tau) \leqslant h$ for all $\tau \geqslant 0$ and $\eta \in [0,\underline{b}(\tau)]$, we have that

$$0 \leqslant \hat{\underline{W}}(y,\tau) \leqslant h \text{ for all } \tau \geqslant 0,\ y \in [0,1]. \tag{4.7.2}$$

We deduce from (4.6.61) and (4.6.62) in Lemma 4.6.11 that there exists a constant $C(\sigma) > 0$ such that

$$\|\hat{\underline{W}}(\,\cdot\,,\,\cdot\,+\tau)\|_{L^2(0,\sigma;H^2(0,1))} \leqslant C(\sigma) \tag{4.7.3}$$

for all $\tau > 0$. Thus, there exists $v \in L^2\left(0,\sigma;H^2(0,1)\right)$ such that

$$\hat{\underline{W}}(\,\cdot\,,\,\cdot\,+\tau) \rightharpoonup v \text{ weakly in } L^2(0,\sigma;H^2(0,1)) \text{ as } \tau \to +\infty. \tag{4.7.4}$$

We shall prove that $v = \hat{\psi}$. First, since $\lim\limits_{\tau\to+\infty} \underline{W}(\eta,\tau) = \psi(\eta)$ for all $\eta \in \mathbb{R}^+$, it follows from (4.6.60) and (4.7.1) that

$$\lim_{\tau\to+\infty} \hat{\underline{W}}(y,\tau) = \hat{\psi}(y) \quad \text{for all } y \in [0,1], \tag{4.7.5}$$

and since $0 \leqslant \hat{\underline{W}} \leqslant h$, we deduce from Lebesgue Dominated Convergence Theorem that

$$\hat{\underline{W}}(\,\cdot\,,\,\cdot\,+\tau) \to \hat{\psi} \text{ in } L^1\left((0,1)\times(0,\sigma)\right) \text{ as } \tau \to +\infty. \tag{4.7.6}$$

Using again the uniform boundedness of $\hat{\underline{W}}$ and $\hat{\psi}$, we conclude that this convergence also holds in $L^p((0,1)\times(0,\sigma))$ for all $p \in [1,\infty)$. Hence, $v = \hat{\psi} \in H^2(0,1)$. This completes the proof of Lemma 4.7.1. □

Proposition 4.7.2. *The sequence*

$$\{\hat{\underline{W}}_y(\,\cdot\,,\tau)\} \text{ converges to } \hat{\psi}_y \text{ in } L^2(0,1) \text{ as } \tau \to +\infty. \tag{4.7.7}$$

Proof. From the Lemmas 4.6.12 and 4.6.13, we deduce that there exists a positive constant C independent of τ such that

$$\|\hat{\underline{W}}_y(\,\cdot\,,\tau)\|_{\mathbb{W}^{1,1}(0,1)} \leqslant C \text{ for all } \tau \geqslant 0. \tag{4.7.8}$$

The space $\mathbb{W}^{1,1}(0,1)$ is compactly embedded in $L^2(0,1)$ (see for instance the proof of Lemma 2.7 in [6, p.86]). Thus, it follows that there exist a subsequence $\{\hat{\underline{W}}_y(\,\cdot\,,\tau_n)\}_{n=0}^{n=\infty}$ and a function $\chi \in L^2(0,1)$ such that

$$\hat{\underline{W}}_y(\,\cdot\,,\tau_n) \to \chi \text{ strongly in } L^2(0,1) \text{ as } \tau \to \infty. \tag{4.7.9}$$

Now, we prove that $\chi = \hat{\psi}_y$. From (4.7.9), it follows that

$$\int_0^1 \hat{\underline{W}}_y(y,\tau)\varphi(y)\,dy \to \int_0^1 \chi(y)\varphi(y)\,dy \text{ as } \tau \to \infty \text{ for all } \varphi \in H_0^1(0,1). \tag{4.7.10}$$

We also have that for all $\varphi \in H_0^1(0,1)$

$$\int_0^1 \hat{\underline{W}}_y(y,\tau)\ \varphi(y)\,dy = -\int_0^1 \hat{\underline{W}}(y,\tau)\ \varphi_y(y)\,dy. \tag{4.7.11}$$

We then deduce from (4.7.6) that

$$-\int_0^1 \hat{\underline{W}}(y,\tau)\varphi_y(y)\,dy \to -\int_0^1 \hat{\psi}(y)\ \varphi_y(y)\,dy = \int_0^1 \hat{\psi}_y(y)\varphi(y)\,dy \text{ as } \tau \to \infty \tag{4.7.12}$$

for all $\varphi \in H_0^1(0,1)$. We finally deduce from (4.7.10), (4.7.11) and (4.7.12) that $\chi = \hat{\psi}_y$ and then (4.7.9) becomes

$$\hat{\underline{W}}_y(\,\cdot\,,\tau_n) \to \hat{\psi}_y \text{ strongly in } L^2(0,1) \text{ as } \tau \to \infty, \tag{4.7.13}$$

which completes the proof of Proposition 4.7.2. □

Next we show the following result.

Proposition 4.7.3 (Application of Second Dini's Theorem)**.** *We have that*

$$\hat{\underline{\mathrm{W}}}_y(\ \cdot\ ,\tau) \ \textit{converges uniformly to}\ \hat{\psi}_y \ \ \textit{as}\ \tau \to \infty\ \textit{on}\ \ [0,1]. \tag{4.7.14}$$

Proof. From Lemma 4.6.12, we have that the function $y \mapsto \hat{\underline{\mathrm{W}}}_y(y,\tau)$ is nondecreasing for all $\tau \geqslant 0$. In view of Lemma 4.6.7, we recall that $\hat{\underline{\mathrm{W}}}_y(\ \cdot\ ,\tau)$ is a continuous function for all $\tau \geq 0$. From Proposition 4.7.2, we have that $\hat{\underline{\mathrm{W}}}_y(.,\tau)$ converges to $\hat{\psi}_y$, as $\tau \to +\infty$, a.e. in (0,1) and from Lemma 4.7.1, we have that $\hat{\psi}_y \in C^{0,\frac{1}{2}}([0,1])$. It follows from applying the second Dini's Theorem (Theorem 10.32 of [86, p. 454]) which states that "if a sequence of monotone continuous functions converges pointwise on (0,1) and if the limit function is continuous in [0,1], then the convergence is uniform", which completes the proof of Proposition 4.7.3. □

Corollary 4.7.4. $\lim\limits_{\tau \to +\infty} ||\hat{\underline{\mathrm{W}}}(.,\tau) - \hat{\psi}||_{C^1([0,1])} = 0.$

Proof. It remains to show that $\hat{\underline{\mathrm{W}}}(.,\tau)$ converges uniformly to $\hat{\psi}$ as $\tau \to \infty$. We have that

$$||\hat{\underline{\mathrm{W}}}(.,\tau) - \hat{\psi}||_{C^0([0,1])} = \sup_{y\in[0,1]} \left| \int_0^y \hat{\underline{\mathrm{W}}}_y(s,\tau)ds + h - \int_0^y \hat{\psi}_y(s)ds - h \right| \tag{4.7.15}$$

$$= \sup_{y\in[0,1]} \left| \int_0^y \hat{\underline{\mathrm{W}}}_y(s,\tau)ds - \int_0^y \hat{\psi}_y(s)ds \right| \leqslant ||\hat{\underline{\mathrm{W}}}_y(.,\tau) - \hat{\psi}_y||_{L^1(0,1)} \to 0 \ \text{ as } \ \tau \to \infty.$$

□

Next, we prove Theorem 4.7.1.

Proof of Theorem 4.7.1. The proof will be done through successive Lemmas. The first step of the proof consists in showing the following result.

Lemma 4.7.5. *We have* $\psi(0) = h$ *and* $\psi(\underline{b}_\infty) = 0$.

Proof. We start by showing that $\psi(0) = h$. Indeed, we have that (recall that $\underline{\mathrm{W}}$ is nondecreasing in time)

$$\underline{\mathcal{W}}_\lambda(\eta) = \underline{\mathrm{W}}(\eta,0) \leqslant \underline{\mathrm{W}}(\eta,\tau) \leqslant h. \tag{4.7.16}$$

Letting τ tend to $+\infty$, we deduce that

$$\underline{\mathcal{W}}_\lambda(\eta) \leqslant \psi(\eta) \leqslant h \quad \text{for all } \eta \in [0,\underline{b}_\infty].$$

Then, for $\eta = 0$, we obtain $\underline{\mathcal{W}}_\lambda(0) = h \leqslant \psi(0) \leqslant h$, that is $\psi(0) = h$.

Next, we prove that $\psi(\underline{b}_\infty) = 0$. We deduce from Corollary 4.7.4 that

$$\hat{\underline{\mathrm{W}}}(1,\tau) \to \hat{\psi}(1) \ \text{ as } \ \tau \to \infty, \tag{4.7.17}$$

which is equivalent to

$$\underline{\mathrm{W}}(\underline{b}(\tau),\tau) \to \psi(\underline{b}_\infty) \ \text{ as } \ \tau \to \infty. \tag{4.7.18}$$

Since,

$$\underline{\mathrm{W}}(\underline{b}(\tau),\tau) = 0 \ \text{ for all } \ \tau > 0, \tag{4.7.19}$$

we deduce that indeed $\psi(\underline{b}_\infty) = 0$. □

The following result holds.

Lemma 4.7.6. *We have*

$$\frac{\underline{b}_\infty}{2} = -\psi_\eta(\underline{b}_\infty). \tag{4.7.20}$$

Proof. First, we prove the corresponding relation for $\hat{\psi}_y(1)$ and then we will conclude the result for ψ_η. We recall that

$$\frac{d\underline{b}(\tau)}{d\tau} + \frac{\underline{b}(\tau)}{2} = -\underline{\mathrm{W}}_\eta(\underline{b}(\tau),\tau) \quad \text{for all } \tau > 0. \tag{4.7.21}$$

In view of the change of variables (4.6.60) for $\hat{\underline{\mathrm{W}}}$, the equation (4.7.21) becomes

$$\frac{1}{2}\frac{d\underline{b}^2(\tau)}{d\tau} + \frac{\underline{b}^2(\tau)}{2} = -\hat{\underline{\mathrm{W}}}_y(1,\tau), \text{ for all } \tau > 0. \tag{4.7.22}$$

Integrating (4.7.22) in time between τ and $\tau+\sigma$ and performing the change of variable $S = s - \tau$, we obtain

$$\frac{1}{2}(\underline{b}^2(\tau+\sigma) - \underline{b}^2(\tau)) + \frac{1}{2}\int_0^\sigma \underline{b}^2(S+\tau)\,\mathrm{d}S = -\int_0^\sigma \hat{\underline{\mathrm{W}}}_y(1,S+\tau)\,\mathrm{d}S. \tag{4.7.23}$$

Then, we deduce from Proposition 4.7.3 that $\hat{\underline{\mathrm{W}}}_y(1,S+\tau)$ converges to $\hat{\psi}_y(1)$ as $\tau \to +\infty$ and recall that $\underline{b}(\tau) \to \underline{b}_\infty$ as $\tau \to +\infty$. Passing to the limit as $\tau \to +\infty$ in (4.7.23), we conclude that

$$\frac{\underline{b}_\infty^2}{2} = -\hat{\psi}_y(1). \tag{4.7.24}$$

Now, since $\psi_\eta(\eta) = \dfrac{1}{\underline{b}_\infty}\hat{\psi}_y(y)$, $y = \dfrac{\eta}{\underline{b}_\infty}$ for all $0 \leqslant \eta \leqslant \underline{b}_\infty$ (see (4.7.1)), the relation (4.7.24) becomes

$$\frac{\underline{b}_\infty}{2} = -\psi_\eta(\underline{b}_\infty), \tag{4.7.25}$$

which completes the proof of Lemma 4.7.6. □

The last step of the proof of Theorem 4.7.1 consists in the following result.

Proposition 4.7.7. *The function $\psi \in C^\infty([0,\underline{b}_\infty])$ and satisfies the equation*

$$\psi_{\eta\eta} + \frac{\eta}{2}\psi_\eta = 0 \quad \text{in } (0,\underline{b}_\infty).$$

We will prove Proposition 4.7.7 by means of several lemmas.

Lemma 4.7.8. *Let $\widetilde{\varphi} \in \mathcal{D}(0,\underline{b}_\infty)$ be arbitrary. Then there exists a class of functions φ satisfying the following properties*

(i) $\varphi \in C^\infty\big([0,\underline{b}_\infty] \times \mathbb{R}^+\big)$,

(ii) $\varphi(0,\tau) = 0$, $\varphi(\underline{b}(\tau),\tau) = 0$ *and* $\varphi_\eta(0,\tau) = 0$ *for all* $\tau \geqslant 0$,

(iii) $\lim\limits_{\tau\to+\infty} \varphi_\tau(\eta,\tau) = 0$ *for all* $\eta \in [0,\underline{b}_\infty]$,

(iv) $\lim\limits_{\tau\to+\infty} \varphi(\eta,\tau) = \widetilde{\varphi}(\eta)$ *for all* $\eta \in [0,\underline{b}_\infty]$.

Proof. Let $\widetilde{\varphi} \in \mathcal{D}(0,\underline{b}_\infty)$ be given. We define the function $\varphi \in C^\infty\big([0,\underline{b}_\infty] \times \mathbb{R}^+\big)$ such that

$$\varphi(\eta,\tau) = \widetilde{\varphi}(\underline{b}_\infty\, y),\ y = \frac{\eta}{\underline{b}(\tau)} \text{ for all } \tau \geqslant 0, 0 \leqslant \eta \leqslant \underline{b}(\tau), \tag{4.7.26}$$

and $\varphi(\eta,\tau) = 0$ for all $\tau > 0$ and $\underline{b}(\tau) \leqslant \eta \leqslant \underline{b}_\infty$. Next, we show that φ satisfies the properties (i)-(iv).The function φ obviously satisfies (i). Property (ii) readily holds because we have $\varphi(0,\tau) =$

$\widetilde{\varphi}(0) = 0$, $\varphi(\underline{b}(\tau),\tau) = \widetilde{\varphi}(\underline{b}_\infty) = 0$ and $\varphi_\eta(0,\tau) = \dfrac{\underline{b}_\infty}{\underline{b}(\tau)}\,\widetilde{\varphi}_y(0) = 0$. Now, we turn to (iii). We have that

$$\lim_{\tau\to+\infty} \varphi_\tau(\eta,\tau) = \lim_{\tau\to+\infty} \frac{-\eta\,\underline{b}_\infty \dfrac{d\underline{b}(\tau)}{d\tau}}{\underline{b}^2(\tau)}\,\widetilde{\varphi}_y(\underline{b}_\infty\, y). \tag{4.7.27}$$

Since $\dfrac{d\underline{b}(\tau)}{d\tau} + \dfrac{\underline{b}(\tau)}{2} = -\dfrac{1}{\underline{b}(\tau)}\hat{\mathrm{W}}_y(1,\tau)$ for all $\tau > 0$, we obtain

$$\lim_{\tau\to+\infty} \frac{-\eta\,\underline{b}_\infty \dfrac{d\underline{b}(\tau)}{d\tau}}{\underline{b}^2(\tau)}\,\widetilde{\varphi}_y(\underline{b}_\infty\, y) = \lim_{\tau\to+\infty} \left(\frac{\eta\,\underline{b}_\infty}{2\underline{b}(\tau)} + \frac{\eta\,\underline{b}_\infty \hat{\mathrm{W}}_y(1,\tau)}{\underline{b}^3(\tau)}\right)\widetilde{\varphi}_y(\underline{b}_\infty\, y) \quad \text{for all} \quad 0 \leqslant \eta \leqslant \underline{b}(\tau).$$

From Proposition 4.7.3 and (4.7.24), we deduce that $\lim\limits_{\tau\to+\infty} \hat{\mathrm{W}}_y(1,\tau) = \hat{\psi}_y(1) = \dfrac{-\underline{b}_\infty^2}{2}$, which implies that

$$\lim_{\tau\to+\infty} \left(\frac{\eta\,\underline{b}_\infty}{2\underline{b}(\tau)} + \frac{\eta\,\underline{b}_\infty \hat{\mathrm{W}}_y(1,\tau)}{\underline{b}^3(\tau)}\right)\widetilde{\varphi}_y(\underline{b}_\infty\, y) = \left(\frac{\eta}{2} - \frac{\eta}{2}\right)\widetilde{\varphi}_y(\underline{b}_\infty\, y) = 0.$$

Thus, we obtain

$$\lim_{\tau\to+\infty} \varphi_\tau(\eta,\tau) = 0.$$

Finally, we show that (iv) holds; indeed we have that

$$\lim_{\tau\to+\infty} \varphi(\eta,\tau) = \lim_{\tau\to+\infty} \widetilde{\varphi}\left(\frac{\eta\,\underline{b}_\infty}{\underline{b}(\tau)}\right) = \widetilde{\varphi}(\eta).$$

This completes the proof of Lemma 4.7.8. □

Lemma 4.7.9. *The function ψ satisfies*

$$\int_0^{\underline{b}_\infty} \psi(\eta)\left(\widetilde{\varphi}_{\eta\eta} - \frac{\eta}{2}\widetilde{\varphi}_\eta - \frac{\widetilde{\varphi}}{2}\right)(\eta)\,\mathrm{d}\eta = 0 \tag{4.7.28}$$

for all test functions $\widetilde{\varphi} \in \mathcal{D}(0,\underline{b}_\infty)$.

Proof. Let φ satisfying the properties (i)-(iv) of Lemma 4.7.8 and let $\sigma > 0$ be fixed. Recall that $(\underline{\mathrm{W}},\underline{\mathrm{b}})$ satisfies Problem 4.5.4, in particular we have

$$\underline{\mathrm{W}}_\tau(\eta,\tau) = \underline{\mathrm{W}}_{\eta\eta}(\eta,\tau) + \frac{\eta}{2}\underline{\mathrm{W}}_\eta(\eta,\tau), \quad 0 < \eta < \underline{b}(\tau),\ \tau > 0. \tag{4.7.29}$$

By integrations by parts, we obtain

$$\int_\tau^{\tau+\sigma}\int_0^{\underline{b}(s)} \left(\underline{\mathrm{W}}_{\eta\eta}(\eta,s) + \frac{\eta}{2}\underline{\mathrm{W}}_\eta(\eta,s)\right)\varphi(\eta,s)\,\mathrm{d}\eta\,\mathrm{d}s$$
$$= \int_\tau^{\tau+\sigma}\int_0^{\underline{b}(s)} \underline{\mathrm{W}}(\eta,s)\left(\varphi_{\eta\eta} - \frac{\eta}{2}\varphi_\eta - \frac{\varphi}{2}\right)(\eta,s)\,\mathrm{d}\eta\,\mathrm{d}s. \tag{4.7.30}$$

Moreover, we have, on the one hand

$$\int_\tau^{\tau+\sigma} \frac{d}{ds}\int_0^{\underline{b}(s)} \underline{\mathrm{W}}(\eta,s)\varphi(\eta,s)\mathrm{d}\eta\mathrm{d}s = \int_0^{\underline{b}(\tau+\sigma)} \underline{\mathrm{W}}(\eta,\tau+\sigma)\varphi(\eta,\tau+\sigma)\mathrm{d}\eta - \int_0^{\underline{b}(\tau)} \underline{\mathrm{W}}(\eta,\tau)\varphi(\eta,\tau)\,\mathrm{d}\eta \tag{4.7.31}$$

and on the other hand,

$$\int_\tau^{\tau+\sigma} \frac{d}{ds} \int_0^{\underline{b}(s)} \underline{\mathrm{W}}(\eta,s)\varphi(\eta,s)\mathrm{d}\eta\mathrm{d}s = \int_\tau^{\tau+\sigma} \left(\int_0^{\underline{b}(s)} (\underline{\mathrm{W}}_s(\eta,s)\varphi(\eta,s) + \underline{\mathrm{W}}(\eta,s)\varphi_s(\eta,s))\mathrm{d}\eta \right.$$
$$\left. + \underline{\mathrm{W}}(\underline{b}(s),s)\varphi(\underline{b}(s),s)\frac{d\underline{b}(s)}{ds} \right) \mathrm{d}s$$
$$= \int_\tau^{\tau+\sigma} \int_0^{\underline{b}(s)} (\underline{\mathrm{W}}_s(\eta,s)\varphi(\eta,s) + \underline{\mathrm{W}}(\eta,s)\varphi_s(\eta,s))\mathrm{d}\eta\mathrm{d}s. \quad (4.7.32)$$

Combining (4.7.31) with (4.7.32) yields

$$\int_\tau^{\tau+\sigma} \int_0^{\underline{b}(s)} \underline{\mathrm{W}}_s(\eta,s)\varphi(\eta,s)\mathrm{d}\eta = -\int_\tau^{\tau+\sigma} \int_0^{\underline{b}(s)} \underline{\mathrm{W}}(\eta,s)\varphi_s(\eta,s)\mathrm{d}\eta$$
$$+ \int_0^{\underline{b}(\tau+\sigma)} \underline{\mathrm{W}}(\eta,\tau+\sigma)\varphi(\eta,\tau+\sigma)\mathrm{d}\eta - \int_0^{\underline{b}(\tau)} \underline{\mathrm{W}}(\eta,\tau)\varphi(\eta,\tau)\,\mathrm{d}\eta. \quad (4.7.33)$$

We deduce from (4.7.29), (4.7.30) and (4.7.33) that

$$\int_0^{\underline{b}(\tau+\sigma)} \underline{\mathrm{W}}(\eta,\tau+\sigma)\varphi(\eta,\tau+\sigma)\mathrm{d}\eta - \int_0^{\underline{b}(\tau)} \underline{\mathrm{W}}(\eta,\tau)\varphi(\eta,\tau)\,\mathrm{d}\eta - \int_\tau^{\tau+\sigma} \int_0^{\underline{b}(s)} \underline{\mathrm{W}}(\eta,s)\varphi_s(\eta,s)\,\mathrm{d}\eta\,\mathrm{d}s$$
$$= \int_\tau^{\tau+\sigma} \int_0^{\underline{b}(s)} \underline{\mathrm{W}}(\eta,s)(\varphi_{\eta\eta} - \frac{\eta}{2}\varphi_\eta - \frac{\varphi}{2})(\eta,s)\mathrm{d}\eta\mathrm{d}s. \quad (4.7.34)$$

Thus, since $\underline{b}(\tau) \leqslant \underline{b}_\infty$ for all $\tau \geq 0$, we can write

$$\int_0^{\underline{b}_\infty} \chi_{\left[0,\underline{b}(\tau+\sigma)\right]} \underline{\mathrm{W}}(\eta,\tau+\sigma)\varphi(\eta,\tau+\sigma)\,\mathrm{d}\eta - \int_0^{\underline{b}_\infty} \chi_{\left[0,\underline{b}(\tau)\right]} \underline{\mathrm{W}}(\eta,\tau)\varphi(\eta,\tau)\mathrm{d}\eta$$
$$- \int_\tau^{\tau+\sigma} \int_0^{\underline{b}(s)} \underline{\mathrm{W}}(\eta,s)\varphi_s(\eta,s)\,\mathrm{d}\eta\,\mathrm{d}s = \int_\tau^{\tau+\sigma} \int_0^{\underline{b}(s)} \underline{\mathrm{W}}(\eta,s)(\varphi_{\eta\eta} - \frac{\eta}{2}\varphi_\eta - \frac{\varphi}{2})(\eta,s)\,\mathrm{d}\eta\,\mathrm{d}s. \quad (4.7.35)$$

Furthermore, according to Lemma 4.5.4, we recall that

$$\lim_{\tau\to+\infty} \underline{\mathrm{W}}(\eta,\tau) = \psi(\eta) \quad \text{for all } 0 < \eta < \underline{b}_\infty \text{ and } \lim_{\tau\to+\infty} \underline{b}(\tau) = \underline{b}_\infty.$$

Then, since φ satisfies property (iv), it follows that

$$\lim_{\tau\to+\infty} \chi_{\left[0,\underline{b}(\tau+\sigma)\right]} \underline{\mathrm{W}}(\eta,\tau+\sigma)\varphi(\eta,\tau+\sigma) = \psi(\eta)\widetilde{\varphi}(\eta).$$

Moreover, we have

$$\left| \chi_{\left[0,\underline{b}(\tau+\sigma)\right]} \underline{\mathrm{W}}(\eta,\tau+\sigma)\varphi(\eta,\tau+\sigma) \right| \leqslant h \left\|\varphi\right\|_{L^\infty\left((0,\underline{b}_\infty)\times\mathbb{R}^+\right)}.$$

According to Lebesgue's Dominated Convergence Theorem,

$$\int_0^{\underline{b}_\infty} \chi_{\left[0,\underline{b}(\tau+\sigma)\right]} \underline{\mathrm{W}}(\eta,\tau+\sigma)\varphi(\eta,\tau+\sigma)\,\mathrm{d}\eta \to \int_0^{\underline{b}_\infty} \psi(\eta)\widetilde{\varphi}(\eta)\,\mathrm{d}\eta \quad \text{as } \tau \to \infty. \quad (4.7.36)$$

Similarly, we also have that

$$\int_0^{\underline{b}_\infty} \chi_{\left[0,\underline{b}(\tau)\right]} \underline{\mathrm{W}}(\eta,\tau)\varphi(\eta,\tau)\,\mathrm{d}\eta \to \int_0^{\underline{b}_\infty} \psi(\eta)\widetilde{\varphi}(\eta)\,\mathrm{d}\eta \quad \text{as } \tau \to \infty. \quad (4.7.37)$$

Now, we turn to the right-hand-side of (4.7.35). With the change of variables $S = s - \tau$, we obtain

$$\int_0^\sigma \int_0^{\underline{b}_\infty} \chi_{\left[0,\underline{b}(S+\tau)\right]} \underline{\mathrm{W}}(\eta,S+\tau)(\varphi_{\eta\eta} - \frac{\eta}{2}\varphi_\eta - \frac{\varphi}{2})(\eta,S+\tau)\,\mathrm{d}\eta\,\mathrm{d}S$$
$$\to \int_0^\sigma \int_0^{\underline{b}_\infty} \psi(\eta)(\widetilde{\varphi}_{\eta\eta} - \frac{\eta}{2}\widetilde{\varphi}_\eta - \frac{\widetilde{\varphi}}{2})(\eta)\,\mathrm{d}\eta\,\mathrm{d}S \quad \text{as } \tau \to \infty. \tag{4.7.38}$$

Then, since φ satisfies the property (iii), we conclude from (4.7.35)–(4.7.38) that

$$\int_0^{\underline{b}_\infty} \psi(\eta)(\widetilde{\varphi}_{\eta\eta} - \frac{\eta}{2}\widetilde{\varphi}_\eta - \frac{\widetilde{\varphi}}{2})(\eta)\,\mathrm{d}\eta = 0 \tag{4.7.39}$$

for all test functions $\widetilde{\varphi} \in \mathcal{D}(0,\underline{b}_\infty)$ which yields the result of Lemma 4.7.9. □

Finally, we present the proof of Lemma 4.7.7.

Proof of Lemma 4.7.7. From Lemma 4.7.1, we have that $\psi \in H^2(0,\underline{b}_\infty)$. Then, by means of integration by parts, we obtain

$$\int_0^{\underline{b}_\infty} \psi(\eta)\widetilde{\varphi}_{\eta\eta}(\eta)\,\mathrm{d}\eta = \int_0^{\underline{b}_\infty} \psi_{\eta\eta}(\eta)\widetilde{\varphi}(\eta)\,\mathrm{d}\eta \tag{4.7.40}$$

and

$$\int_0^{\underline{b}_\infty} \psi(\eta)\frac{\eta}{2}\widetilde{\varphi}_\eta(\eta)\mathrm{d}\eta = -\int_0^{\underline{b}_\infty} \left(\psi_\eta(\eta)\frac{\eta}{2}\widetilde{\varphi}(\eta) + \frac{1}{2}\psi(\eta)\widetilde{\varphi}(\eta)\right)\mathrm{d}\eta \tag{4.7.41}$$

for all test function $\widetilde{\varphi} \in \mathcal{D}(0,\underline{b}_\infty)$. Hence, we deduce from (4.7.28) that

$$\int_0^{\underline{b}_\infty} \left(\psi_{\eta\eta}(\eta) + \frac{\eta}{2}\psi_\eta(\eta)\right)\widetilde{\varphi}(\eta)\,\mathrm{d}\eta = 0, \tag{4.7.42}$$

for all $\widetilde{\varphi} \in \mathcal{D}(0,\underline{b}_\infty)$. This finally implies that

$$\psi \in C^\infty([0,\underline{b}_\infty]) \text{ and } \psi_{\eta\eta} + \frac{\eta}{2}\psi_\eta = 0 \text{ for all } 0 < \eta < \underline{b}_\infty. \tag{4.7.43}$$

This completes the proof of Lemma 4.7.7. □

We conclude that the pair $\left(\underline{\mathrm{W}}(\eta,\tau) := W(\eta,\tau,(\underline{\mathcal{W}}_\lambda,\underline{b}_\lambda)),\, \underline{b}(\tau) := b(\tau,(\underline{\mathcal{W}}_\lambda,\underline{b}_\lambda))\right)$ converges to $(\psi,\underline{b}_\infty)$ as $\tau \to \infty$. Thanks to Lemma 4.7.5, Lemma 4.7.6 and Lemma 4.7.7, $(\psi,\underline{b}_\infty)$ satisfies Problem (4.1.12) and thus $(\psi,\underline{b}_\infty)$ coincides with the unique stationary solution (U,a) of Problem (4.1.12). This completes the proof of Theorem 4.7.1. □

Similarly, one can show that $\left(W(\eta,\tau,(\bar{\mathcal{W}},\bar{b})),b(\tau,(\bar{\mathcal{W}},\bar{b}))\right)$ converges as $\tau \to \infty$ to $(\phi,\bar{b}_\infty)$ which also coincides with the unique stationary solution (U,a) of Problem (4.1.12). Recalling Lemma 4.5.7, we obtain the following result.

Theorem 4.7.2. *Let $u_0 \in X^h(b_0) \cap \mathbb{W}^{1,\infty}(0,b_0)$ be such that $0 \leqslant u_0 \leqslant \bar{\mathcal{W}}$ in $[0,b_0]$ and $b_0 \leqslant \bar{b}$ where $(\bar{\mathcal{W}},\bar{b})$ is defined in (4.5.21). Let $(W,b) = \left(W(\,\cdot\,,\,\cdot\,,(u_0,b_0)), b(\,\cdot\,,(u_0,b_0))\right)$ be the solution of Problem (4.5.4) with the initial data (u_0,b_0). Then*

$$\lim_{\tau\to+\infty} W(\eta,\tau) = U(\eta) \quad \textit{for all } \eta \in (0,a) \tag{4.7.44}$$

and

$$\lim_{\tau\to+\infty} b(\tau) = a \tag{4.7.45}$$

where (U,a) is the unique solution of the stationary Problem (4.1.12).

Proof. For all $\tau > 0$ and $\eta \geqslant 0$, we have that

$$W(\eta,\tau,(\underline{\mathcal{W}}_\lambda,\underline{b}_\lambda)) \leqslant W(\eta,\tau,(u_0,b_0)) \leqslant W(\eta,\tau,(\bar{\mathcal{W}},\bar{b})) \tag{4.7.46}$$

and

$$b(\tau,(\underline{\mathcal{W}}_\lambda,\underline{b}_\lambda)) \leqslant b(\tau,(u_0,b_0)) \leqslant b(\tau,(\bar{\mathcal{W}},\bar{b})). \tag{4.7.47}$$

According to Lemma 4.5.4 together with the fact that $(\psi,\underline{b}_\infty) = (\phi,\bar{b}_\infty) = (U,a)$, we deduce that

$$\lim_{\tau\to+\infty} W(\eta,\tau,(\bar{\mathcal{W}},\bar{b})) = \lim_{\tau\to+\infty} W(\eta,\tau,(\underline{\mathcal{W}}_\lambda,\underline{b}_\lambda)) = U(\eta), \tag{4.7.48}$$

$$\lim_{\tau\to+\infty} b(\tau,(\bar{\mathcal{W}},\bar{b})) = \lim_{\tau\to+\infty} b(\tau,(\underline{\mathcal{W}}_\lambda,\underline{b}_\lambda)) = a. \tag{4.7.49}$$

The result of Theorem 4.7.2 then follows from (4.7.46) and (4.7.47). □

This completes the proof of Theorem 4.1.1 in the introduction section.

Chapter 5

A numerical scheme for solving the Stefan Problem

There is a large choice of methods for solving one-dimensional Stefan problems [9, 37, 41, 63]. In this chapter, we apply a special choice of an Arbitrary Lagrangian Eulerian (ALE) method. In literature, this method is usually referred to as the Variable Space Grid (VSG) method [41],[53].

5.1 ALE formulation

5.1.1 Introduction to ALE Method

We recall that the classical one-dimensional one phase Stefan problem (4.2.1) is given as follows: find a solution $u : \cup_{t\geq 0}[0,s(t)] \times \{t\} \to \mathbb{R}$ and an interface $s : \mathbb{R}^+ \to \mathbb{R}^+$ such that

$$(\mathcal{S}) \begin{cases} u_t = u_{xx}, & t > 0, 0 < x < s(t), \\ u(0,t) = h, & t > 0, \\ u(s(t),t) = 0, & t > 0, \\ s'(t) = \dfrac{ds(t)}{dt} = -u_x(s(t),t), & t > 0, \\ s(0) = b_0, \\ u(x,0) = u_0(x) \in X^h(b_0) \end{cases}$$

where $h > 0$, $b_0 > 0$ and

$$X^h(b) := \{u_0(x) \in C[0,\infty),\ \ u_0(0) = h,\ u_0(x) \geqslant 0 \text{ for } 0 \leqslant x < b,\ u_0(x) = 0 \text{ for } x \geqslant b\}.$$

In this chapter we describe the numerical method used to solve the Stefan problem $(\mathcal{S})$. In order to do so, we will consider an Arbitrary Lagrangian Eulerian (ALE) formulation of $(\mathcal{S})$. In fact, the ALE description is used as an adaptive technique to handle the displacement of the free boundary (see [13], [32]). Indeed, when dealing with the numerical computation of solutions of physical problems in a moving domain, a possible way to proceed consists in adapting the mesh in order to follow the boundary motion. One has to rewrite the PDE in a moving frame of reference, leading to the so called Arbitrary Lagrangian Eulerian (ALE) formulation. An early presentation of this technique may be found in the work of J. Donea [13]. It is based on the definition of a suitable mapping from a reference configuration to the current, moving domain [55].

The boundary is moved using the boundary condition

$$s'(t) = -u_x(s(t),t),\ t > 0.$$

The coordinate of the free boundary at time $t+\Delta t$ can be approximated by

$$s(t+\Delta t) \approx s(t) + \Delta t\, s'(t) = s(t) - \Delta t\, u_x(s(t),t),\ t>0.$$

Once the boundary is moved, u can be computed in the fixed new domain $(0,s(t+\Delta t))$ using the PDE

$$u_t(x,t) = u_{xx}(x,t),\ t>0, 0<x<s(t+\Delta t).$$

In the framework of Finite Differences schemes, the approximation of the time derivative u_t at time $t+\Delta t$ would involve the term

$$\frac{u(x,t+\Delta t)-u(x,t)}{\Delta t}$$

for x in $(0,s(t+\Delta t))$. However, $u(\ \cdot\ ,t)$ is defined on the interval $(0,s(t))$ but possibly not known even not well defined on $(0,s(t+\Delta t))$. On one hand, if $(0,s(t+\Delta t)) \subset (0,s(t))$ then $u(\ \cdot\ ,t)$ can be determined on $(0,s(t+\Delta t))$ at discrete space levels (i.e. at discrete points $x=x_i$) by *interpolation*. On the other hand, if $(0,s(t+\Delta t))$ is not contained into $(0,s(t))$, an *extrapolation* procedure is needed to define $u(\ \cdot\ ,t)$ in $(0,s(t+\Delta t))$. This usually leads to a meaningful loss of numerical accuracy. ALE methods avoid resorting to numerical interpolation or extrapolation procedures. The idea is to transform at each time t, the PDE initially posed on a domain depending on t into a new PDE posed on a domain which do not depend on t anymore (say the domain at an another fixed time t'). The new PDE involves a correction term of convection type (a Lagrangian velocity). In that way, the approximation of the time derivative of the new unknown will be everywhere well defined on this new domain, with no need of interpolation nor extrapolation. The mapping defining this domain transformation can be chosen arbitrary. This is why this method is called "Arbitrary Lagrangian Eulerian".

The numerical method which we use is based on a decoupling of the displacement of the free boundary from the numerical solution of the diffusion equation. The motion of the free boundary is numerical solved by an explicit Euler scheme whereas an implicit finite difference scheme is used for the discretization of the ALE formulation of the diffusion equation.

5.1.2 The ALE mapping

Between two consecutive times, the diffusion equation lying in the moving domain is transformed into a partial differential equation on a fixed space interval. Let $t' \geq 0$ be fixed. For $t \geq 0$, we define the ALE mapping

$$\varphi(\ \cdot\ ,t) : [0,s(t)] \to [0,s(t')] \tag{5.1.1}$$

such that $\varphi(\ \cdot\ ,t)$ is a smooth function from $[0,s(t)]$ into $[0,s(t')]$ with $\varphi_x(\ \cdot\ ,t)>0$, $\varphi(0,t)=0$ and $\varphi(s(t),t)=s(t')$ for all $t\geq 0$. The function φ is also smooth with respect to t. In $(\mathcal{S})$, we perform the change of unknown

$$\hat{u}(\hat{x},t) = u(x,t) \text{ with } \hat{x} = \varphi(x,t) \tag{5.1.2}$$

for $x \in [0,s(t)]$, $t\geq 0$. Then the function $\hat{u}(\hat{x},t)$ together with the (unchanged) function s satisfy the problem:

$$(\mathcal{S}_\varphi)\ \begin{cases} \hat{u}_t = (\varphi_x)^2 \hat{u}_{\hat{x}\hat{x}} - (\varphi_t - \varphi_{xx})\,\hat{u}_{\hat{x}}, & t>0, 0<\hat{x}<s(t') \\ \hat{u}(0,t) = h & t>0, \\ \hat{u}(s(t'),t) = 0 & t>0, \\ \hat{u}(\hat{x},0) = \hat{u}_0(\hat{x}), & \hat{x} \in (0,s(t')), \\ u(x,t) = \hat{u}(\hat{x},t), \quad \hat{x} = \varphi(x,t) & t>0, \\ s'(t) = -u_x(s(t),t) & t>0, \\ s(0) = b_0. \end{cases}$$

5.1.3 A special choice for the ALE mapping

We choose φ as a polynomial function of x. For a positive integer $p > 0$, we choose

$$\varphi(x,t) = s(t') \left(\frac{x}{s(t)} \right)^p . \tag{5.1.3}$$

The polynomial mappings which are interesting are concerned with the case $0 < p \leq 1$. In this case, the ALE mapping $\varphi(\,\cdot\,,t)$ has the effect to tighten and concentrate nodes close to the free boundary $s(t)$ when $p < 1$. For the rest of this chapter, we choose $p = 1$, so that,

$$\varphi(x,t) = \frac{s(t')}{s(t)} x. \tag{5.1.4}$$

In the literature, this case is usually referred to the Variable Space Grid (VSG) method [53],[41]. As we will see below, this mapping preserves the uniform discretization of the moving space interval $[0,s(t)]$ during the time evolution. The problem $(\mathcal{S}_\varphi)$ becomes

$$(\mathcal{S}') \begin{cases} \hat{u}_t = \mathcal{D}_1 \hat{u}_{\hat{x}\hat{x}} + \mathcal{D}_2 \hat{u}_{\hat{x}}, & t > 0, 0 < \hat{x} < s(t'), \\ \hat{u}(0,t) = h, & t > 0, \\ \hat{u}(s(t'),t) = 0, & t > 0, \\ \hat{u}(\hat{x},0) = \hat{u}_0(\hat{x}), & \hat{x} \in (0,s(t')), \\ u(x,t) = \hat{u}(\hat{x},t), \quad \hat{x} = \varphi(x,t), & t > 0, \\ s'(t) = -u_x(s(t),t), & t > 0, \\ s(0) = b_0 \end{cases}$$

with $\mathcal{D}_1 = \mathcal{D}_1(t) = \left(\dfrac{s(t')}{s(t)} \right)^2$ and $\mathcal{D}_2 = \mathcal{D}_2(\hat{x},t) = \dfrac{s'(t)}{s(t)} \hat{x}$.

5.2 Numerical scheme

In this section, we describe a numerical scheme for solving the ALE formulation $(\mathcal{S}')$.

5.2.1 Time discretization for a decoupling scheme of the ALE formulation $(\mathcal{S}')$

First, we describe the time approximation for the ALE formulation $(\mathcal{S}')$. Let $\Delta t > 0$ be the discretization time-step such that $T = M\Delta t$, $M \in \mathbb{N}^*$. We denote by $t^n = n\Delta t$ the discrete times for $n = 0,1,\cdots,M$ and we consider the approximations $u^n \simeq u(\,\cdot\,,t^n)$ and $s^n \simeq s(t^n)$ of the solution (u,s) of $(\mathcal{S})$ at time $t = t^n$. The approximate solution u^n is defined in the interval $[0,s^n]$. Starting with

$$s^0 = s(0) = b_0, \quad u^0 = u_0 \text{ in } [0,b_0], \tag{5.2.1}$$

we compute (u^{n+1},s^{n+1}) from (u^n,s^n) for $n \geq 0$, according to the following decoupling scheme of the ALE system $(\mathcal{S}')$.

Algorithm Semi-discretization in time for the one-phase one dimensional Stefan Problem with the ALE formulation $(\mathcal{S}')$: the discretization in time.

1. Interface displacement: computation of the new position s^{n+1} of the interface

$$s^{n+1} = s^n + v^n \Delta t \quad \text{with} \quad v^n = -u_x^n(s^n) \tag{5.2.2}$$

   i.e. with $v^n \simeq s'(t^n)$ (forward Euler).

2. Computation of $\hat{u}^n$ in $[0,s^{n+1}]$. We take $t' = t^{n+1}$ in (5.1.1), and define

$$\begin{array}{rcl} \varphi^{n+1} : [0,s^n] & \longrightarrow & [0,s^{n+1}] \\ x & \longmapsto & \hat{x} = \dfrac{s^{n+1}}{s^n} x \end{array} \tag{5.2.3}$$

   and

$$\hat{u}^n(\varphi^{n+1}(x)) = \hat{u}^n(\hat{x}) = u^n(x). \tag{5.2.4}$$

3. Computation of u^{n+1} in $[0,s^{n+1}]$. We take $t' = t^{n+1}$ in $(\mathcal{S}')$ at time $t = t^{n+1}$. We solve the following elliptic problem for u^{n+1}:

$$(\mathcal{P}^{n+1}) \quad \left\{ \begin{array}{l} \dfrac{u^{n+1} - \hat{u}^n}{\Delta t} = u_{xx}^{n+1} + \dfrac{v^n}{s^{n+1}} x\, u_x^{n+1}, \quad 0 < x < s^{n+1} \\ u^{n+1}(0) = h \\ u^{n+1}(s^{n+1}) = 0 \end{array} \right. \tag{5.2.5}$$

5.2.2 Well-posedness of $(\mathcal{P}^{n+1})$

We shall prove that the sequence $(u^n,s^n)_{n\geq 0}$ introduced in Algorithm 1 is well-defined. To do so, we first prove that Problem $(\mathcal{P}^{n+1})$ is well-posed. This problem can be written as

$$(\mathcal{P}^{n+1}) \left\{ \begin{array}{ll} -\Delta t\, u_{xx}^{n+1} - \dfrac{v^n\, \Delta t}{s^{n+1}} x\, u_x^{n+1} + u^{n+1} = \hat{u}^n, & 0 < x < s^{n+1} \quad (5.2.6) \\ u^{n+1}(0) = h > 0, \quad u^{n+1}(s^{n+1}) = 0. & (5.2.7) \end{array} \right.$$

It involves a linear differential equation for u^{n+1} with $\hat{u}^n$ and s^{n+1} known. The first result establishes that Problem $(\mathcal{P}^{n+1})$ is well-posed under a sign assumption on the coefficient of the differential equation.

Proposition 5.2.1. *We assume that $v^n > 0$. If $\hat{u}^n \in L^2(0,s^{n+1})$ then Problem $(\mathcal{P}^{n+1})$ admits a unique solution $u^{n+1} \in H^2(0,s^{n+1})$. In addition, if $\hat{u}^n \in C^k([0,s^{n+1}])$ for $k \in \mathbb{N}$ with $\hat{u}^n > 0$ in $(0,s^{n+1})$, then $u^{n+1} \in C^{2+k}([0,s^{n+1}])$ and we have*

$$u^{n+1} > 0 \text{ in } (0,s^{n+1}), \ v^{n+1} := -u_x^{n+1}(s^{n+1}) > 0. \tag{5.2.8}$$

Proof. In order to prove the existence and uniqueness of a weak solution u^{n+1}, we will apply the Lax-Milgram Theorem. We consider the change of variables

$$y = \frac{x}{s^{n+1}}, \ \tilde{u}(y) = u^{n+1}(x), \ f(y) = \hat{u}^n(x) \ \text{ for all } \ 0 < x < s^{n+1}, \tag{5.2.9}$$

and we define the positive constants

$$c_1 = \frac{\Delta t}{(s^{n+1})^2} \ \text{ and } \ c_2 = \frac{\Delta t\, v^n}{s^{n+1}} > 0. \tag{5.2.10}$$

Then, Problem $(\mathcal{P}^{n+1})$ [(5.2.6)–(5.2.7)] becomes

$$\begin{cases} -c_1\,\tilde{u}_{yy} - c_2\,y\,\tilde{u}_y + \tilde{u} = f, \quad 0 < y < 1, & (5.2.11)\\ \tilde{u}(0) = h > 0, \quad \tilde{u}(1) = 0. & (5.2.12) \end{cases}$$

Let $z(y) := h(1-y)$ and $w := \tilde{u} - z$ for all $0 < y < 1$. Then (5.2.11)–(5.2.12) become

$$\begin{cases} -c_1\,w_{yy} - c_2\,y\,(w_y - h) + w + h(1-y) = f, \quad 0 < y < 1, & (5.2.13)\\ w(0) = 0, \quad w(1) = 0. & (5.2.14) \end{cases}$$

The weak formulation of Problem (5.2.13) and (5.2.14) is:

$$\text{Find} \quad w \in H_0^1(0,1) \quad \text{such that} \quad a(w,v) = l(v) \quad \text{for all} \quad v \in H_0^1(0,1) \tag{5.2.15}$$

where we have defined

$$a(w,v) = c_1 \int_0^1 w_y v_y\,dy - c_2 \int_0^1 y\,w_y\,v\,dy + \int_0^1 w\,v\,dy \ \text{ for all } \ v \in H_0^1(0,1) \tag{5.2.16}$$

and

$$l(v) = \int_0^1 (f - h(1-y) - c_2\,h\,y)v\,dy \ \text{ for all } \ v \in H_0^1(0,1). \tag{5.2.17}$$

Now, we prove that the weak formulation (5.2.15) admits a unique solution.

To do so, let $v \in H_0^1(0,1)$; since $f \in L^2(0,1)$ it follows from (5.2.17) that there exists a constant $\widehat{C} > 0$ such that

$$|l(v)| \leqslant \widehat{C}||v||_{H_0^1(0,1)}. \tag{5.2.18}$$

Thus, l is a linear and continuous form on $H_0^1(0,1)$.

Next, we show that $a(\,\cdot\,,\,\cdot\,) : H_0^1(0,1) \times H_0^1(0,1) \to \mathbb{R}$ is a continuous and coercive bilinear form. Indeed, let $v, w \in H_0^1(0,1)$, from (5.2.16) it follows that

$$|a(w,v)| \leqslant c_1||w||_{H_0^1(0,1)}\,||v||_{H_0^1(0,1)} + c_2 \int_0^1 |w_y\,v|\,dy + ||w||_{H_0^1(0,1)}\,||v||_{H_0^1(0,1)}. \tag{5.2.19}$$

Next, using Cauchy-Schwarz inequality, we have that

$$\int_0^1 |w_y\,v|\,dy \leqslant ||w||_{H_0^1(0,1)}\,||v||_{H_0^1(0,1)}. \tag{5.2.20}$$

Then, we deduce from (5.2.19) and (5.2.20) that there exists a constant $\tilde{C} > 0$ such that

$$|a(w,v)| \leqslant \tilde{C}\,||w||_{H_0^1(0,1)}\,||v||_{H_0^1(0,1)} \ \text{ for all } \ w, v \in H_0^1(0,1), \tag{5.2.21}$$

which implies that $a(\,\cdot\,,\,\cdot\,)$ is continuous. Next, we check that $a(\,\cdot\,,\,\cdot\,)$ is coercive.
Let $v \in H_0^1(0,1)$. From (5.2.16), we have that

$$a(v,v) = c_1 \int_0^1 (v_y)^2\,dy - c_2 \int_0^1 y\,v_y\,v\,dy + \int_0^1 v^2\,dy. \tag{5.2.22}$$

By integration by parts, the second term on the right-hand-side of (5.2.22) becomes

$$\int_0^1 y\,v_y\,v\,dy = \int_0^1 \frac{y}{2}(v^2)_y\,dy = -\int_0^1 \frac{v^2}{2}\,dy. \tag{5.2.23}$$

Then, it follows from (5.2.22) and (5.2.23) that

$$a(v,v) = c_1 \int_0^1 (v_y)^2 \, dy + (\frac{c_2}{2} + 1) \int_0^1 v^2 \, dy. \tag{5.2.24}$$

We deduce that

$$a(v,v) \geqslant min\Big(c_1, (\frac{c_2}{2} + 1)\Big)\Big(\int_0^1 (v_y)^2 \, dy + \int_0^1 v^2 \, dy\Big), \tag{5.2.25}$$

so that

$$a(v,v) \geqslant min\Big(c_1, (\frac{c_2}{2} + 1)\Big)||v||_{H_0^1(0,1)} \ \text{ for all } \ v \in H_0^1(0,1), \tag{5.2.26}$$

so that $a(\,\cdot\,,\,\cdot\,)$ is coercive.

Finally, using (5.2.18), (5.2.21) and (5.2.26), we deduce from the Lax-Milgram theorem the existence of a unique solution $w \in H_0^1(0,1)$ which satisfies the weak formulation (5.2.15), and thus the existence of a unique solution $u^{n+1} \in H_0^1(0,s^{n+1})$ of Problem (5.2.13)–(5.2.14). Since, $\hat{u}^n \in L^2(0,s^{n+1})$, a standard regularity argument shows that $u^{n+1} \in H^2(0,s^{n+1})$. Moreover, if $\hat{u}^n \in C^k([0,s^{n+1}])$ with $k \geq 0$, a regularity argument for classical solution infers that $u^{n+1} \in C^{k+2}([0,s^{n+1}])$. To complete the proof of Proposition 5.2.1, it remains to prove that (5.2.8) holds under the

additional assumption that $\hat{u}^n > 0$. We apply the strong maximum principle (Theorem 3 of [57, p.6]) which states that if u^{n+1} reaches its nonpositive minimum at an interior point $x^* \in (0,s^{n+1})$, then u^{n+1} is constant in $[0,s^{n+1}]$. However, since $u^{n+1}(0) = h > 0$ and $u^{n+1}(s^{n+1}) = 0$, we have reached a contradiction, so that, we conclude that $u^{n+1} > 0$ in $(0,s^{n+1})$. Now, since $u^{n+1}(s^{n+1}) = 0$ and $u^{n+1} > 0$ in $(0,s^{n+1})$, it follows from the Hopf maximum principle [19, p.330] that $u_x^{n+1}(s^{n+1}) < 0$, so that $v^{n+1} > 0$ (see (5.2.2)). The proof of Proposition 5.2.1 is then completed.

□

Corollary 5.2.2. *If the initial data (b_0,u_0) in (6.4.27) is such that $u_0 \in C^k([0,b_0])$, $k \geq 0$ with $u_0 > 0$ in $(0,b_0)$ and $(u_0)_x < 0$, then the sequence $(u^n,s^n)_{n\geq 0}$ introduced in (6.4.27)–(6.4.33) (see Algorithm1) is well-defined for all $n \geq 0$. Moreover, we have that*

$$u^n > 0 \text{ in } (0,s^n), \ v^n > 0 \ \text{ and } \ s^{n+1} > s^n > b_0 > 0 \ \text{ for all } n \geq 0. \tag{5.2.27}$$

Proof. We easily check by induction on $n \geq 0$ with the use of Proposition 5.2.1 that the sequence (u^n,s^n) is well-defined for all $n \geq 0$. The property (5.2.27) immediately follows from (5.2.8) and (5.2.2). □

5.2.3 Time and space discretizations: the semi-implicit scheme

We use a finite difference scheme for the spatial approximation of (5.2.2)–(6.4.33), in particular for the discretization of Problem $(\mathcal{P}^{n+1})$. The space intervals (evolving with time) are uniformly discretized using a fix number $(N+2)$ of points. We consider the approximations $u_i^n \simeq u(x_i^n,t^n)$ for $i = 0,\cdots,N+1$ and $\tilde{s}^n \simeq s(t^n)$ of the solution (u,s) of $(\mathcal{S})$ at the time $t = t^n$.

We use the notation $\tilde{s}^n$ for the fully discretized scheme whereas s^n denotes the interface corresponding to the semi-discretized one.

The interval $[0,\tilde{s}^n]$ is uniformly discretized with the $(N+2)$ points

$$x_i^n = i\Delta x^n \ \text{ with } \ \Delta x^n = \frac{\tilde{s}^n}{N+1}, \tag{5.2.28}$$

for $i = 0,1,\cdots,N+1$. Starting with

$$\begin{cases} \tilde{s}^0 = s(0) = b_0, \\ u_i^0 = u_0(x_i^0) \ \text{ with } \ x_i^0 = i\Delta x^0 = i\dfrac{b_0}{N+1}, \ i = 0,\cdots,N+1, \end{cases} \tag{5.2.29}$$

we compute $(u_i^{n+1}, \tilde{s}^{n+1})$ from $(u_i^n, \tilde{s}^n)$ for $n \geq 0$ and $i = 0,\cdots,N+1$, according to the following decoupling semi-implicit Euler scheme of the ALE system form $(\mathcal{S}')$.

Algorithm An algorithm for the decoupled semi-implicit Euler scheme for the ALE formulation $(\mathcal{S}')$: time and space discretizations.

Suppose $(u_i^n, \tilde{s}^n)$, $i = 0,\cdots,N+1$, is known.

1. Interface displacement: computation of the new position $\tilde{s}^{n+1}$ of the interface.

$$\begin{cases} \tilde{v}^n = -\dfrac{(u_{N+1}^n - u_N^n)}{\Delta x^n} \ \text{ with } \ \Delta x^n = \dfrac{\tilde{s}^n}{N+1} \\ \tilde{s}^{n+1} = \tilde{s}^n + \tilde{v}^n \Delta t \end{cases} \tag{5.2.30}$$

   i.e. $v^n \simeq s'(t^n) = -u_x(s(t^n), t^n)$ (forward Euler approximation).

2. Computation of $\{u_i^{n+1}\}$ in $[0, \tilde{s}^{n+1}]$. Defining $\Delta x = \Delta x^{n+1} = \dfrac{\tilde{s}^{n+1}}{N+1}$, the implicit upwind scheme is given by:

$$(\mathcal{P}_{\Delta x}^{n+1}) \ \begin{cases} \dfrac{u_i^{n+1} - u_i^n}{\Delta t} = \dfrac{1}{\Delta x^2}\left(u_{i+1}^{n+1} - 2u_i^{n+1} + u_{i-1}^{n+1}\right) + \dfrac{\tilde{v}^n}{\tilde{s}^{n+1}} x_i^{n+1}\left(\dfrac{u_i^{n+1} - u_{i-1}^{n+1}}{\Delta x}\right) \\ \quad \text{for } i = 1,\cdots,N. \\ u_0^{n+1} = h, \ u_{N+1}^{n+1} = 0 \ \text{ (boundary conditions).} \end{cases} \tag{5.2.31}$$

Problem $(\mathcal{P}_{\Delta x}^{n+1})$ can be written as a linear combination of $\{u_i^{n+1}\}_{i\in\{0,\cdots,N+1\}}$:

$$\gamma u_{i-1}^{n+1} + \alpha_i u_i^{n+1} + \beta_i u_{i+1}^{n+1} = u_i^n \tag{5.2.32}$$

for $i = 1,\cdots,N$, with

$$\alpha_i = 1 + 2\frac{\Delta t}{\Delta x^2} + \frac{\Delta t}{\Delta x}\frac{v^n}{\tilde{s}^{n+1}} x_i^{n+1} \tag{5.2.33}$$

$$\beta_i = -\frac{\Delta t}{\Delta x^2} - \frac{\Delta t}{\Delta x}\frac{v^n}{\tilde{s}^{n+1}} x_i^{n+1} \tag{5.2.34}$$

$$\gamma = -\frac{\Delta t}{\Delta x^2} \tag{5.2.35}$$

together with the boundary conditions

$$u_0^{n+1} = h, \ u_{N+1}^{n+1} = 0. \tag{5.2.36}$$

Remark that, for all $i = 1,\cdots,N$, we have

$$\alpha_i + \beta_i + \gamma = 1. \tag{5.2.37}$$

Matrix form. The unknowns are gathered in the vector $\mathbf{u}^{n+1} = (u_0^{n+1}, \cdots, u_{N+1}^{n+1}) \in \mathbb{R}^{N+2}$. The system (5.2.32) with the boundary conditions (5.2.36) leads to

$$A\mathbf{u}^{n+1} = \mathbf{u}^n \tag{5.2.38}$$

where A is a tridiagonal matrix of order $(N+2)$ given by

$$A = \begin{pmatrix} 1 & 0 & & & 0 \\ \gamma & \alpha_1 & \beta_1 & & \\ & \ddots & \ddots & \ddots & \\ & & \gamma & \alpha_N & \beta_N \\ 0 & & & 0 & 1 \end{pmatrix}. \tag{5.2.39}$$

In view of (5.2.37), we easily see that A is a strictly diagonally dominant matrix and therefore A is invertible so that (5.2.38) (or equivalently problem $(\mathcal{P}_{\Delta x}^{n+1})$) possesses a unique solution $\mathbf{u^{n+1}}$.

Remark 5.2.3. *Since $\tilde{v}^n$ and $\tilde{s}^{n+1}$ are positive, we have used in $(\mathcal{P}_{\Delta x}^{n+1})$ the following upwind space approximation for the derivative u_x:*

$$u_x(x_i^{n+1},t^{n+1}) \simeq \frac{u_{i+1}^{n+1} - u_i^{n+1}}{\Delta x}. \tag{5.2.40}$$

Now, we give some basic monotonicity properties of the scheme (5.2.28)-(5.2.31). We recall that the initial condition is chosen such that $u_0 \geq 0$ in $[0,b_0]$.

Lemma 5.2.4. *Let $\mathbf{x} \in \mathbb{R}^N$,*

$$\mathbf{x} \geq 0 \Leftrightarrow \mathbf{x}_i \geqslant 0, i = 0,..., N-1.$$

Definition 5.2.5 (Monotone matrix [60])**.** *A matrix $\mathcal{A} \in \mathbb{R}^{N\times N}$ is monotone if $\mathcal{A}$ is invertible and $\mathcal{A}^{-1} \geqslant 0$, i.e all coefficients of $\mathcal{A}^{-1}$ are non-negative. Moreover, $\mathcal{A}$ is monotone if and only if $\{\mathcal{A}x \geqslant 0 \Rightarrow \mathbf{x} \geq 0\}$.*

Lemma 5.2.6.
i) The matrix A defined by (5.2.39) is monotone.

ii) Suppose that the sequence $(\{u_i^n\},\tilde{s}^n)_{n\geq 0}$ is obtained from the scheme (5.2.28)-(5.2.31). We have, for all $n \geq 0$,

$$\begin{aligned} &v^n \geq 0, \\ &u_i^n \geq 0,\ i = 0, \cdots, N+1, \end{aligned} \tag{5.2.41}$$

Proof. i) Let us denote by a_{ij} the coefficients of the matrix A. For all $i = 1, \cdots, N$, we have $\alpha_i > 0$, $\beta_i < 0$, $\gamma < 0$ and in view of (5.2.37), we deduce that

$$\begin{aligned} &a_{ij} \leq 0 \text{ for all } i \neq j, \\ &\sum_j a_{ij} > 0 \text{ for all } i. \end{aligned}$$

As a result, A is a M-matrix (see [4]) and in particular A is monotone.
ii) We proceed by induction on n. For $n = 0$, we have $u_i^0 \geq 0$ for all i since $u_0 \geq 0$. It follows from (5.2.30) that $\tilde{v}^0 = -\dfrac{(u_{N+1}^0 - u_N^0)}{\Delta x^0} = \dfrac{u_N^0}{\Delta x^0} \geq 0$.

Hence, (5.2.41) is true for $n = 0$. Now, suppose that the property (5.2.41) is true for n. We shall prove that it is also true for $n+1$. Since $A\mathbf{u^{n+1}} = \mathbf{u^n} \geq \mathbf{0}$ by assumption, we infer from the monotonicity property of A that $\mathbf{u}^{n+1} \geq 0$. Finally, since $\tilde{v}^{n+1} = -\dfrac{(u_{N+1}^{n+1} - u_N^{n+1})}{\Delta x} = \dfrac{u_N^{n+1}}{\Delta x} \geq 0$, the property (5.2.41) is true for $n+1$, so that the sequence $\{\tilde{s}^n\}$ is increasing.

□

5.3 Numerical results for the convergence to the self-similar profile

In this section, we present some numerical results which illustrate the convergence of the solution (u,s) of the Stefan problem (4.2.1) or $(\mathcal{S})$ to the self-similar solution (U,a) given by (see also (4.4.2),(4.4.5))

$$\begin{cases} U(\eta) = h\left(1 - \dfrac{\int_0^\eta e^{-\frac{s^2}{4}}ds}{\int_0^a e^{-\frac{s^2}{4}}ds}\right) \\ 0 < \eta < a. \end{cases} \tag{5.3.1}$$

with $\eta = \dfrac{x}{\sqrt{t+1}}$, where a is the unique solution of the nonlinear equation (see (4.4.8))

$$h = \frac{a}{2}e^{\frac{a^2}{4}}\int_0^a e^{-\frac{s^2}{4}}ds. \tag{5.3.2}$$

We remark that the upper and lower solutions are ordered according to the values of λ as shown in lemmas 4.5.5 and 4.5.6. So, the largest possible upper solution corresponds to value $\lambda = 0$ and it is given by (4.5.21)

$$\bar{\mathcal{W}}(\eta) = \begin{cases} h(1 - \dfrac{\eta}{\bar{b}}) & \text{for all } \ 0 \leqslant \eta \leqslant \bar{b}, \\ 0 & \text{for all } \ \eta \geqslant \bar{b}, \end{cases} \tag{5.3.3}$$

where $\bar{b}$ which is given also by (4.5.13), satisfies

$$\bar{b} = \sqrt{2h}. \tag{5.3.4}$$

Moreover, we choose a very small lower solution corresponding to a very large value for λ. We numerically obtain a possible lower solution by setting $\lambda = 11000$. It is given by (4.5.16)

$$\underline{b}_\lambda = b_\lambda \quad \text{and} \quad \underline{\mathcal{W}}_\lambda(\eta) := \begin{cases} W_\lambda(\eta) & \text{if } 0 \leqslant \eta \leqslant \underline{b}_\lambda, \\ 0 & \text{if } \eta > \underline{b}_\lambda. \end{cases}$$

where $W_\lambda(\eta)$ is given by (4.5.7)

$$W_\lambda(\eta) = h\left[1 - \frac{\int_0^\eta e^{-\frac{\lambda s^2}{4}}ds}{\int_0^{b_\lambda} e^{-\frac{\lambda s^2}{4}}ds}\right] \quad \text{for all } \eta \in (0,\underline{b}_\lambda)$$

and $\underline{b}_\lambda$ is given by (4.5.8) and is the unique solution of the equation

$$h = \frac{\underline{b}_\lambda}{2}e^{\frac{\underline{b}_\lambda^2}{4}}\int_0^{\underline{b}_\lambda} e^{-\frac{\lambda s^2}{4}}ds. \tag{5.3.5}$$

We set $h = 20$. Numerically solving (5.3.2), (5.3.4) and (5.3.5), we obtain respectively $a = 2.894$, $\bar{b} = 6.324$ and $\underline{b}_\lambda = 0.061$.

Next, we choose the initial data (u_0,b_0) such that $\underline{b}_\lambda \leqslant b_0 \leqslant \bar{b}$ and $\underline{\mathcal{W}}_\lambda \leqslant u_0 \leqslant \bar{\mathcal{W}}$. To do so, we set $b_0 = 6$ and we consider the following initial data

$$u_0(\eta) = \begin{cases} \dfrac{h}{3b_0^2}(b_0 - \eta)(2b_0 - \eta)\left(\dfrac{3}{2} - \sin^2\left(\dfrac{8\pi\,\eta}{b_0}\right)\right) & \text{if } \ 0 \leqslant \eta \leqslant b_0, \\ 0 & \text{if } \ \eta \geqslant b_0. \end{cases} \tag{5.3.6}$$

This initial data together with the self-similar solution U, and the upper and lower solutions are represented in Figure 5.3.1.

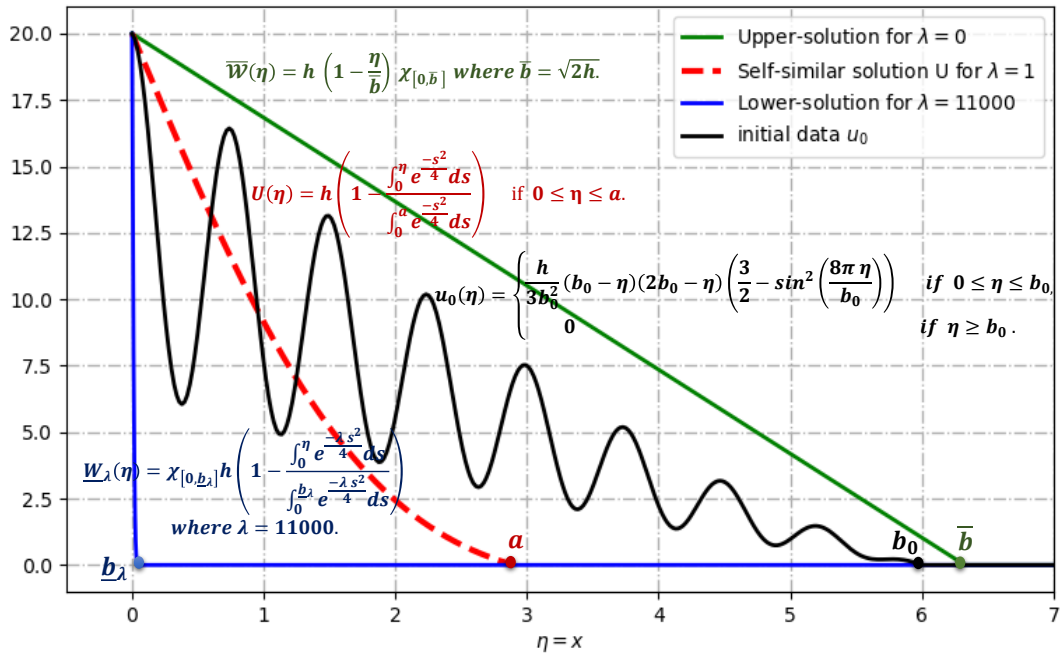

Figure 5.3.1: Initial data u_0, the self-similar solution U, and the upper and lower solutions.

We take $N = 300$ for the numerical simulations and we choose a variable time step depending on the mesh size Δx^n and the velocity v^n at each time iteration n, that is $\Delta t = \Delta x^n / v^n$. In Figure 5.3.2, the solution $\eta \mapsto V(\eta, t)$ with the variable $\eta = \dfrac{x}{\sqrt{t+1}}$ is drawn at different times t^n. We recall that the solution pair (V,a) is given by (4.5.1) as follows

$$\begin{cases} V(\eta,t) = u(x,t), \\ a(t) = \dfrac{s(t)}{\sqrt{t+1}}. \end{cases} \tag{5.3.7}$$

This illustrates the convergence toward the self-similar solution $U(\eta)$. In the self-similar frame (η,t), we have that $t \mapsto V(\eta,t)$ tend to the stationary profile U as t tends to $+\infty$.

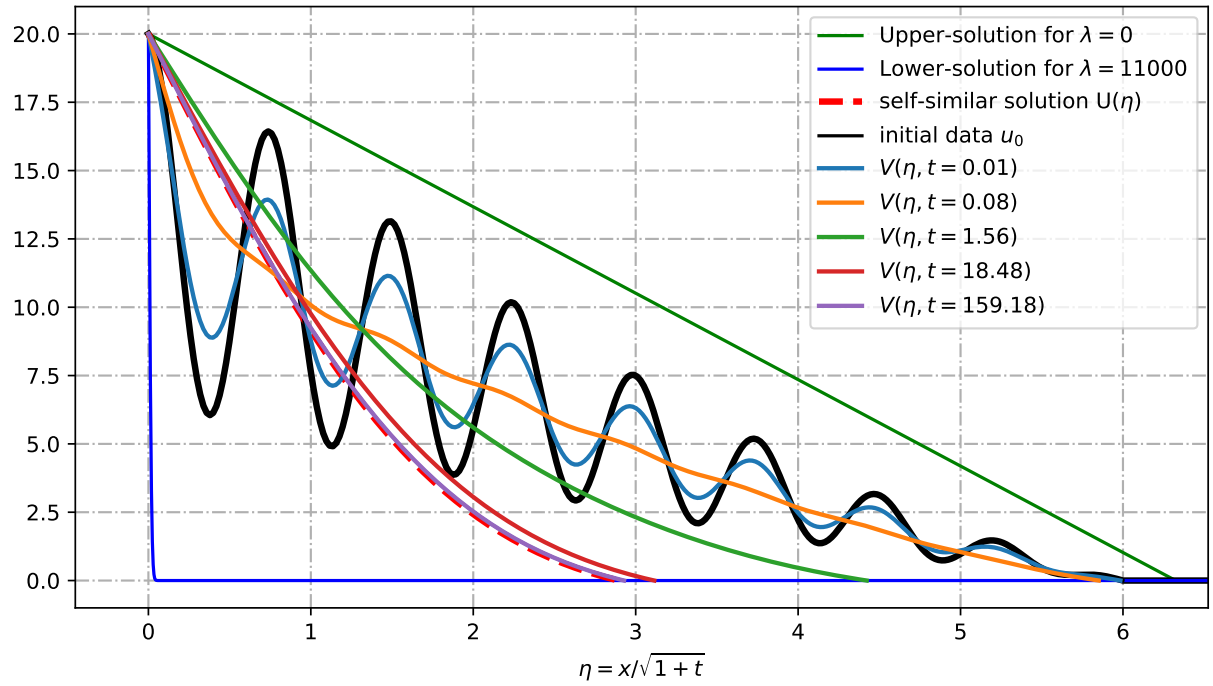

Figure 5.3.2: Solution $\eta \mapsto V(\eta,t)$ of the Stefan problem at different time instants t.

Figure 5.3.3 shows the time evolution of the free boundary s as well as the self-similar moving boundary $r(t) = a\sqrt{t+1}$. Similarly, this is equivalent to show that $t \mapsto a(t)$ given by (5.3.7) tend to the self-similar constant a given by (5.3.1) and (5.3.2).

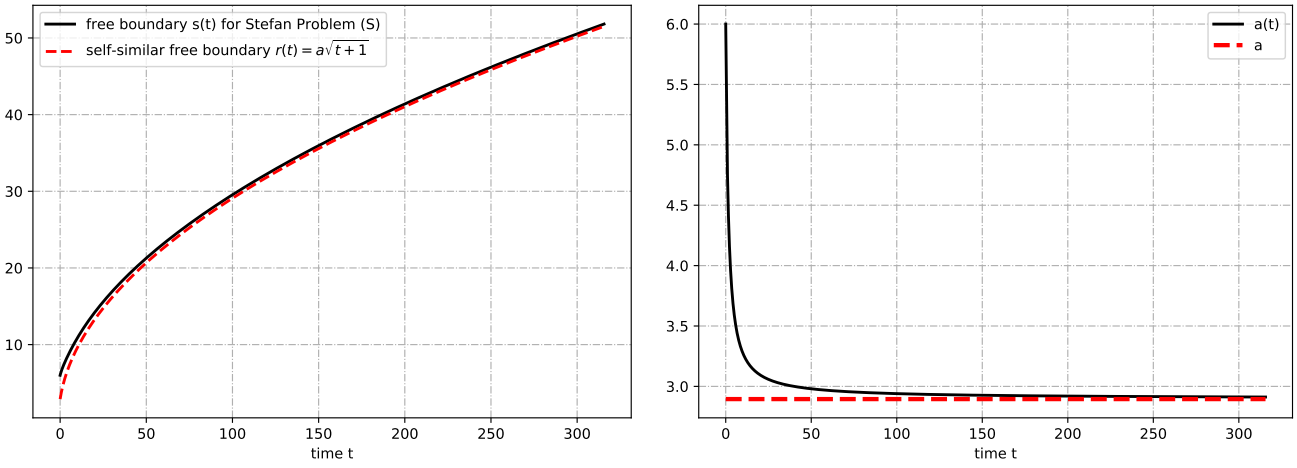

(a) Time evolution of the free boundary $s(t)$ and the self-similar free boundary $r(t) = a\sqrt{1+t}$.

(b) Time evolution of the moving boundary $a(t)$.

Figure 5.3.3: Large time behavior of the free boundary.

Figure 5.3.4 shows the time evolution of the relative difference

$$e_s(t) = \left| \frac{s(t) - r(t)}{r(t)} \right| \tag{5.3.8}$$

between $s(t)$ and the self-similar free boundary $r(t)$. The convergence to zero of the relative gap e_s is clearly highlighted in Figure 5.3.4. For $t = 56{,}94$, we obtain $e_s \simeq 2{,}60 \cdot 10^{-2}$.

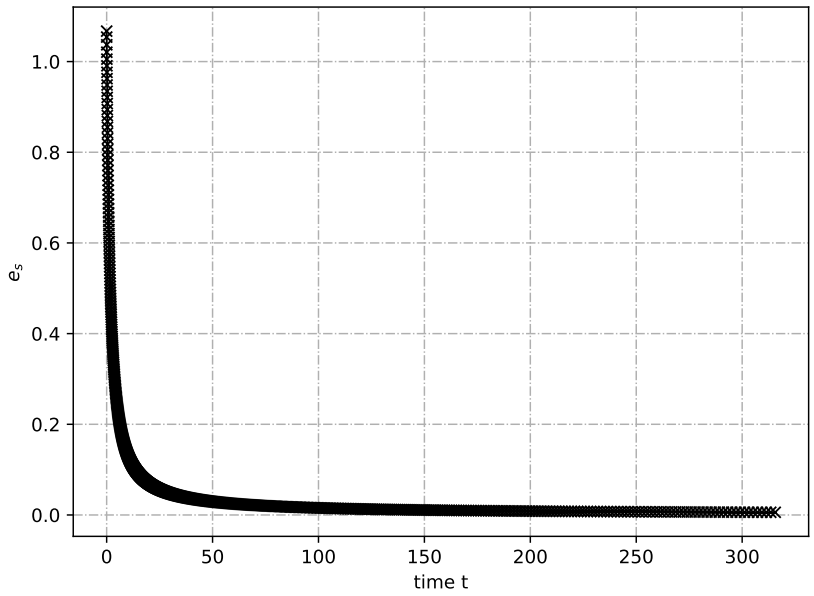

Figure 5.3.4: Time evolution of the relative gap $e_s(t) = \left|\dfrac{s(t) - r(t)}{r(t)}\right|$ between $s(t)$ and the self-similar free boundary $r(t)$.

We define $\|U - V(\,\cdot\,,t)\|_{\infty,\eta} = \sup_{\eta\in(0,a)} |U(\eta) - V(\eta,t)|$ and we consider the relative difference

$$e_u(t) = \frac{\|U - V(\,\cdot\,,t)\|_{\infty,\eta}}{\|U\|_{\infty,\eta}} \tag{5.3.9}$$

between the solution V and the self-similar profile U. The gap e_u is computed using the discrete L^∞-norms with $e_u(t^n) \simeq \dfrac{\max_i |U(\eta_i) - u_i^n|}{\max_i |U(\eta_i)|}$ where $\eta_i = \dfrac{i\,a}{N+1}$ for $i \in \{0, \cdots, N+1\}$. The convergence to zero of the relative gap e_u is exposed in Figure 5.3.5. For $t = 27{,}41$ we obtain $e_u \simeq 9{,}27 \cdot 10^{-4}$.

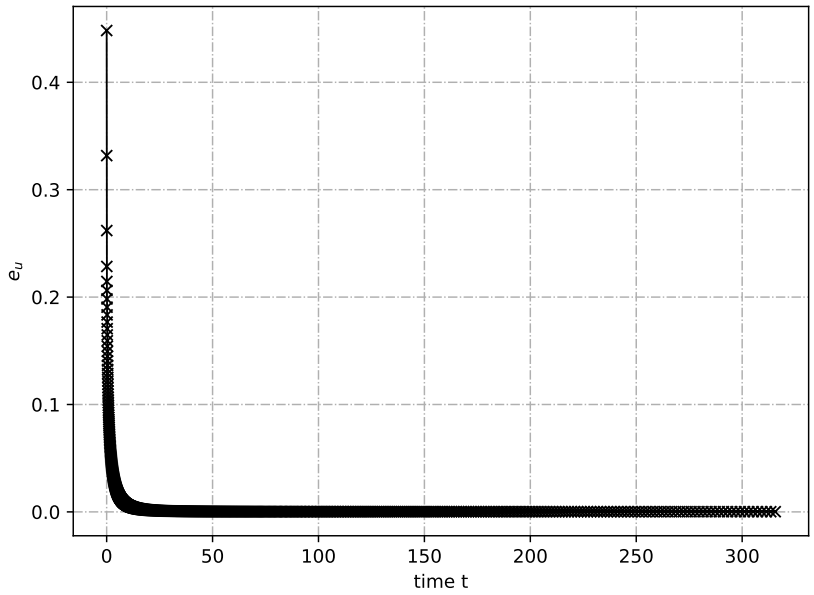

Figure 5.3.5: Time evolution of the relative gap $e_u(t) = \dfrac{\|U - V(\,\cdot\,,t)\|_{\infty,\eta}}{\|U\|_{\infty,\eta}}$ between the solution $V(\,\cdot\,,t)$ and the self-similar solution U.

Chapter 6

Anodic dissolution of stainless steel in aqueous NaCl-electrolytes under potentiostatic conditions: Mathematical model with moving interface

6.1 Introduction

The objective of the present chapter is to develop a mathematical model of partial differential equations to simulate the propagation of a corrosion pitting taking into account the complexity of its growth. This mathematical model will describe only anodic dissolution.

The work was performed in several steps. First, we propose a mathematical model based on all known physical phenomena; are involved anodic reactions of dissolution, transport of the aqueous chemical species in the pit solution by diffusion and migration, taking into account the moving interface to describe the kinetics of the pit propagation.

Then, we propose a performant numerical solution method for a strongly coupled nonlinear system of partial differential equations in one-space dimension. Therefore, we have developed a numerical scheme implicit in time based on the ALE method. Afterwards, for a complete mastering of all the input variables, this scheme was implemented in an open source software (Python). The behavior of our system is studied as a function of the input physical parameters such as the imposed potential or the initial concentration of NaCl. Then, we have identified the main critical factor that influences the dissolution rate in order to ensure the stability of the pit.

The physical and chemical parameters employed in this chapter and their values are summarized in Table 6.1.

Table 6.1: **Physical and chemical parameters.**

Parameter	**Name**	**Value**	**Unit**
C_i	Concentration of the ion species i	–	mol.m^{-3}
C_{ref}	The reference constant	1000	mol.m^{-3}
$\phi = \phi(x,t)$	The electrostatic potential in solution	–	V
$\boldsymbol{J}_i$	The ion flux	–	$\text{mol.m}^{-2}.s^{-1}$
$f_{\text{Fe}^{2+}}$	The corrosive ferrous ion flux	–	$\text{mol.m}^{-2}.s^{-1}$
D_i	Diffusion coefficient of the ion species i	–	$\text{m}^2.s^{-1}$
z_i	Valence of the ion species i	–	–
F	Faraday constant	96485,3321	C.mol^{-1}
T	Temperature	25°C + 273,15 298,15	Kelvin=K
R	The ideal gas constant	8,314	$\text{J.mol}^{-1}.\text{K}^{-1}$
$\gamma = \frac{\text{F}}{RT}$	-	38,9239	$\text{C.J}^{-1} = \text{V}^{-1}$
ϵ	The dielectric constant	$8{,}85\ .\ 10^{-12}$	F.m^{-1}
ϕ_m	The metal potential relative to NHE or SCE reference	–	V
Ω_{Fe}	The molar volume of solid iron	$7{,}095\ .\ 10^{-6}$	$\text{m}^3.\text{mol}^{-1}$
$N_{\text{Fe}} = \Omega_{Fe}^{-1}$	The concentration of ferrous atoms in solid iron	$140\ .\ 10^3$	mol.m^{-3}
k_a	The oxidation rate constant	89,0636	$\text{mol.m}^{-2}.\text{s}^{-1}$
k_c	The reduction rate constant	$1{,}1852\ .10^{-13}$	$\text{mol.m}^{-2}.\text{s}^{-1}$

Remark 6.1.1. *The determination of the rate constant values of oxidation k_a and reduction k_c is detailed in Appendix B.*

6.2 Diffusion-migration model with moving interface

6.2.1 Derivation of the equations

Let $\Omega = \Omega(t) \subset \mathbb{R}^3$ denote the domain representing the pit occupied by an aqueous electrolyte solution. The boundary of $\Omega(t)$ consists of the wall of the pit denoted by $\Gamma = \Gamma(t)$ and the entrance of the pit denoted by $\Gamma_0 = \Gamma_0(t)$ (see Figure 6.2.1).

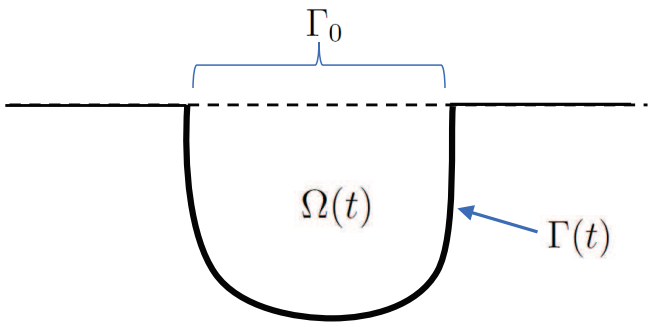

Figure 6.2.1: Picture of a *pit*

We suppose that the solution contains M species of ions, whose concentrations are given by $C_i = C_i(x,t)$ $(i = 1,\ldots,M)$, where $x := (x_1,x_2,x_3)$. The concentrations C_i and the electrostatic potential $\phi = \phi(x,t)$ satisfy the following *Poisson-Nernst-Planck* system:

$$\begin{cases} \dfrac{\partial C_i}{\partial t} = \nabla \cdot \left(D_i \Big(\nabla C_i + \dfrac{z_i F}{RT} C_i \nabla \phi \Big) \right), \quad i = 1,\ldots,M, \\ -\nabla \cdot (\epsilon \nabla \phi) = \displaystyle\sum_{i=1}^{M} z_i F C_i, \end{cases} \tag{6.2.1}$$

where D_i, z_i denote respectively the diffusion coefficient and the valence of the ion species i, F the Faraday constant, R the ideal gas constant, T the absolute temperature and ϵ the dielectric constant. If we consider the reactions between the ions, then the system is given by

$$\frac{\partial C_i}{\partial t} = \nabla \cdot \left(D_i \Big(\nabla C_i + \frac{z_i F}{RT} C_i \nabla \phi \Big) \right) + \mathcal{R}_i \left(\{C\} \right), \quad i = 1,\ldots,M, \tag{6.2.2a}$$

$$-\nabla \cdot (\epsilon \nabla \phi) = \sum_{i=1}^{M} z_i F C_i, \tag{6.2.2b}$$

where $\mathcal{R}_i(\{C\}) := \mathcal{R}_i(C_1,\ldots,C_M)$.

On the one hand, the time dependent form of the Nernst–Planck equation (6.2.2a) is a conservation of mass equation used to describe the motion of charged chemical species in the aqueous pit solution $\Omega(t)$. It extends the diffusion Fick's law to the case where the diffusing particles are also moved by electrostatic forces. These electrostatic forces are caused by the electric field $\boldsymbol{E} = -\nabla\phi$. On the other hand, the Poisson equation (6.2.2b) describes the electrical potential field $\boldsymbol{E}$ which results from the charge distribution in the pit solution.

To have a good understanding of the behavior of the above system, it is convenient to **make the above equations dimensionless**. This latter non-dimensional system is expressed with different parameters: the $\widehat{C_i}'$s denote dimensionless concentrations, obtained by normalizing the molar concentrations with a characteristic reference value C_0. The independent variables time and

space are also normalized by appropriate characteristic values τ and L respectively, where $\tau = \dfrac{L^2}{D_0}$ and D_0 denotes a characteristic diffusivity. The dimensionless potential is normalized by the ratio $\dfrac{RT}{F}$. We obtain

$$x = L\widehat{x}, \quad t = \frac{L^2}{D_0}\widehat{t}, \quad C_i = C_0\widehat{C}_i, \quad D_i = D_0\widehat{D}_i, \quad \phi = \frac{RT}{F}\widehat{\phi}. \tag{6.2.3}$$

Note that, in the above, the voltage $\widehat{\phi}$ is measured with respect to RT/F, known as the *thermal voltage* [39, p.202].

With the change of variables (6.2.3), the equation (6.2.2a) becomes

$$\frac{C_0 D_0}{L^2}\frac{\partial \widehat{C_i}}{\partial \widehat{t}} = \frac{1}{L}\widehat{\nabla} \cdot \left(\frac{D_0 C_0}{L}\widehat{D_i}\left(\widehat{\nabla}\widehat{C}_i + z_i \frac{F}{RT}\widehat{C_i}\frac{RT}{F}\widehat{\nabla}\widehat{\phi}\right)\right) + \mathcal{R}_i\left(\{C_0\widehat{C}\}\right),$$

so that the *Nernst-Planck* equation (6.2.2a) is converted into the following non-dimensional form:

$$\frac{\partial \widehat{C}_i}{\partial \widehat{t}} = \widehat{\nabla} \cdot \left(\widehat{D}_i\left(\widehat{\nabla}\widehat{C}_i + z_i\widehat{C}_i\widehat{\nabla}\widehat{\phi}\right)\right) + \widehat{\mathcal{R}}_i\left(\{\widehat{C}\}\right), \quad i = 1, \ldots, M, \tag{6.2.4}$$

where $\widehat{\nabla}$ denotes the divergence and gradient operators with respect to $\widehat{x}$ and

$$\widehat{\mathcal{R}}_i\left(\{\widehat{C}\}\right) = \frac{L^2}{D_0 C_0}\mathcal{R}_i\left(\{C_0\widehat{C}\}\right).$$

The non-dimensional form of the *Poisson* equation (6.2.2b) is given by

$$-\frac{1}{L}\widehat{\nabla} \cdot \left(\epsilon\frac{RT/F}{L}\widehat{\nabla}\widehat{\phi}\right) = F\sum_{i=1}^{M} z_i C_0 \widehat{C}_i,$$

so that

$$-\widehat{\nabla} \cdot \left(\frac{\epsilon RT/F}{L^2 F C_0}\widehat{\nabla}\widehat{\phi}\right) = \sum_{i=1}^{M} z_i \widehat{C}_i.$$

We deduce from the non-dimensionalization that the system (6.2.2) reduces to:

$$\begin{cases} \dfrac{\partial \widehat{C}_i}{\partial \widehat{t}} = \widehat{\nabla} \cdot \left(\widehat{D}_i\left(\widehat{\nabla}\widehat{C}_i + z_i\widehat{C}_i\widehat{\nabla}\widehat{\phi}\right)\right) + \widehat{\mathcal{R}}_i\left(\{\widehat{C}\}\right), \quad i = 1, \ldots, M, & \text{(6.2.5a)} \\ -\widehat{\nabla} \cdot \left(\delta^2\widehat{\nabla}\widehat{\phi}\right) = \displaystyle\sum_{i=1}^{M} z_i\,\widehat{C}_i. & \text{(6.2.5b)} \end{cases}$$

We use the symbol $\widehat{\cdot}$ for the non-dimensional variables. The reaction terms are also rescaled. Here the constant δ is given by

$$\delta = \frac{r_D}{L} \text{ with } r_D := \sqrt{\frac{\epsilon RT/F}{FC_0}}, \tag{6.2.6}$$

where r_D is the so-called *Debye length*[1], while L is, as mentioned above, the representative length scale of the phenomenon we want to describe. In the case where the representative concentration is around $C_0 = 0.001 \sim 1$ mol/L, one has $r_D = 0.0485 \sim 1.53$ nm, an extremely small value. On the other hand, the size of the pit is around $1 \sim 100$ μm. Therefore $r_D \ll L$, thus $\delta \approx 0$ ($\delta = 10^{-3} \sim 10^{-6}$ or smaller).

[1] reference: https://en.wikipedia.org/wiki/Debye_length#In_an_electrolyte_solution

Consequently, in view of (6.2.5b), we have

$$\sum_{i=1}^{M} z_i \widehat{C}_i \approx 0 \tag{6.2.7}$$

in the entire bulk of the solution, except possibly very near the boundary of the domain. In other words, the sum of the ionic charges at each point of the solution is nearly zero which means that the solution (water with ions) is nearly electrically neutral. The value is so small that one can even set

$$\sum_{i=1}^{M} z_i \widehat{C}_i = 0, \tag{6.2.8}$$

throughout the entire bulk. This equation describes the local electroneutrality condition. Thus one can always assume that the solution is completely electrically neutral in the bulk of the solution. In consequence, the Poisson equation (6.2.5b) is replaced by the local electroneutrality equation. The system (6.2.5) reduces to:

$$\begin{cases} \dfrac{\partial \widehat{C}_i}{\partial \hat{t}} = \widehat{\nabla} \cdot \left(\widehat{D}_i (\widehat{\nabla} \widehat{C}_i + z_i \widehat{C}_i \widehat{\nabla} \widehat{\phi}) \right) + \widehat{\mathcal{R}}_i \left(\{\widehat{C}\} \right) \quad \text{in } \widehat{\Omega}(\hat{t}), \;\; i = 1, \ldots, M, & \text{(6.2.9a)} \\ 0 = \displaystyle\sum_{i=1}^{M} z_i \widehat{C}_i \;\; \text{in } \widehat{\Omega}(\hat{t}), \quad \text{(local electroneutrality of the solution)} & \text{(6.2.9b)} \end{cases}$$

where $\widehat{\Omega}(\hat{t})$ is the non-dimensional domain derived from $\Omega(t)$ via the change of variables $x \mapsto \widehat{x}$ and $\mathrm{t} \mapsto \widehat{\mathrm{t}}$.

This last system is the system which we are going to study.

Next we multiply the equations in (6.2.9a) by z_i and sum them up for $i = 1, \ldots, M$. Note that, by (6.2.9b),

$$z_1 \frac{\partial \widehat{C}_i}{\partial \hat{t}} + \cdots + z_M \frac{\partial \widehat{C}_M}{\partial \hat{t}} = \frac{\partial}{\partial \hat{t}} \left(z_1 \widehat{C}_1 + \cdots + z_M \widehat{C}_M \right) = 0.$$

Note also that no electric charges are created or annihilated by the reactions, since in the present context, the reactions are just recombinations and dissociations of ions. Therefore

$$z_1 \widehat{\mathcal{R}}_1 + \cdots + z_M \widehat{\mathcal{R}}_M = 0 \quad \text{(conservation of electric charge)}.$$

Consequently, we have

$$\sum_{i=1}^{M} \widehat{\nabla} \cdot \left(\widehat{D}_i (z_i \widehat{\nabla} \widehat{C}_i + z_i^2 \widehat{C}_i \widehat{\nabla} \widehat{\phi}) \right) = 0.$$

This equation can be rewritten as

$$\widehat{\nabla} \cdot \left(\sigma \widehat{\nabla} \widehat{\phi} \right) + \sum_{i=1}^{M} \widehat{\nabla} \cdot \left(z_i \widehat{D}_i \widehat{\nabla} \widehat{C}_i \right) = 0 \quad \text{where} \quad \sigma := \sum_{i=1}^{M} z_i^2 \widehat{D}_i \widehat{C}_i, \tag{6.2.10}$$

and σ is the electrical conductivity of the ionic solution.
Since $\sigma > 0$, (6.2.10) is a partial differential equation of the **elliptic type** for $\widehat{\phi}$, and it can be solved if we impose appropriate boundary conditions. We can now rewrite system (6.2.9) as

$$\begin{cases} \dfrac{\partial \widehat{C}_i}{\partial \hat{t}} = \widehat{\nabla} \cdot \Big(\widehat{D}_i (\widehat{\nabla} \widehat{C}_i + z_i \widehat{C}_i \widehat{\nabla} \widehat{\phi}) \Big) + \widehat{\mathcal{R}}_i \Big(\{\widehat{C}\} \Big) \quad \text{in } \widehat{\Omega}(\hat{t}), \ \ i = 1, \ldots, M, & \text{(6.2.11a)} \\ \displaystyle\sum_{i=1}^{M} \widehat{\nabla} \cdot (z_i \widehat{D}_i \widehat{\nabla} \widehat{C}_i) + \widehat{\nabla} \cdot \Big(\sigma \widehat{\nabla} \widehat{\phi} \Big) = 0 \ \text{ in } \widehat{\Omega}(\hat{t}), \ \text{ where } \ \sigma := \displaystyle\sum_{i=1}^{M} z_i^2 \widehat{D}_i \, \widehat{C}_i. & \text{(6.2.11b)} \end{cases}$$

There are $M+1$ equations in the above system for the $M+1$ unknowns $\widehat{C}_i \, (i = 1, \ldots, M)$ and $\widehat{\phi}$. Therefore it is reasonable to expect that this system is solvable under appropriate boundary conditions.

Interpretation of (6.2.11b)

The equation (6.2.11b) (or (6.2.10)) for the electric potential $\widehat{\phi}$ can be rewritten as follows:

$$\widehat{\nabla} \cdot \left(\sum_{i=1}^{M} z_i \widehat{\boldsymbol{J}_i} \right) = \widehat{\nabla} \cdot \Big(\widehat{\boldsymbol{I}}_{\text{diff}} + \widehat{\boldsymbol{I}}_{\text{ohm}} \Big) = 0, \tag{6.2.12}$$

where $\widehat{\boldsymbol{J}_i} = -\widehat{D}_i (\widehat{\nabla} \widehat{C}_i + z_i \widehat{C}_i \widehat{\nabla} \widehat{\phi})$ is the ion flux, and

$$\widehat{\boldsymbol{I}}_{\text{diff}} = -\sum_{i=1}^{M} z_i \widehat{D}_i \widehat{\nabla} \widehat{C}_i, \quad \widehat{\boldsymbol{I}}_{\text{ohm}} = -\sigma \widehat{\nabla} \widehat{\phi}.$$

The ion flux $\widehat{\boldsymbol{J}_i} \, (i = 1, \ldots, M)$ consists of two parts. The first is the *diffusion flux* $-\widehat{D}_i \widehat{\nabla} \widehat{C}_i$, which is associated with the Fick's law, and the second term $-z_i \widehat{D}_i \widehat{C}_i \widehat{\nabla} \widehat{\phi}$ represents the flux caused by the electric field $\widehat{\boldsymbol{E}} = -\widehat{\nabla} \widehat{\phi}$.

Since $\widehat{\boldsymbol{J}_i}$ is the ion flux, $z_i \widehat{\boldsymbol{J}_i}$ is the electric current carried by the i-th ion species. The **dimensional form** of this electric current is given by $z_i F \boldsymbol{J}_i$ where

$$\boldsymbol{J}_i := -D_i \Big(\nabla C_i + \frac{z_i F}{RT} C_i \nabla \phi \Big) \ \ (\text{mol} \, / \, \text{m}^2 \text{s}).$$

The total electric current is divided into two parts: the diffusive component $\widehat{\boldsymbol{I}}_{\text{diff}}$ and the Ohmic component $\widehat{\boldsymbol{I}}_{\text{ohm}}$. The former is an electric current generated by the random motion of ions through a concentration gradient, while the latter is generated by the electric field $-\widehat{\nabla} \widehat{\phi}$. Here σ plays the role of the electric conductivity. The equation (6.2.12) expresses the **continuity of the electric current**.

Remark 6.2.1 (System equivalence)**.** System (6.2.11) has been derived from (6.2.9). Conversely, if we start from (6.2.11), then we easily see that $\partial_{\hat{t}} (z_1 \widehat{C}_1 + \cdots + z_M \widehat{C}_M) = 0$. Therefore, if the initial value satisfies the electroneutrality condition $z_1 \widehat{C}_1 + \cdots + z_M \widehat{C}_M = 0$ at $\hat{t} = 0$, then (6.2.9b) holds for all $\hat{t} > 0$. Hence the two systems (6.2.9) and (6.2.11) are equivalent, under the condition that the initial value satisfies the electroneutrality condition.

□

Remark 6.2.2 (Equation for $\widehat{\phi}$)**.** Since (6.2.9) implies (6.2.11), **in order to keep the electroneutrality of the solution, $\widehat{\phi}$ has to satisfy (6.2.11b) (or (6.2.10)).** In the special case where $\widehat{C}_i$ are spatially uniform (i.e. $\widehat{\nabla} \widehat{C}_i = 0 \ i = 1, \ldots, M$), equation (6.2.10) (or (6.2.11b)) reduces to Laplace's equation $\widehat{\Delta} \widehat{\phi} = 0$ (or $\widehat{\nabla}^2 \widehat{\phi} = 0$), hence $\widehat{\phi}$ is harmonic. However, apart from such special cases, $\widehat{\phi}$ is not harmonic in general. **The use of Laplace equation instead of the local electroneutrality condition equation is a common mistake which has been made in many papers [54].** □

6.2.2 Initial and Boundary conditions

Henceforth the system (6.2.11) is considered. Needless to say, (6.2.11) cannot be solved without specifying the boundary conditions as well as the initial condition at $\hat{t} = 0$. Since the domain $\widehat{\Omega}(\hat{t})$, which represents the pit, evolves along with $\{\widehat{C}_i\}$ and $\widehat{\phi}$, this is a **free boundary problem**. In other words, the unknowns are not just $\{\widehat{C}_i\}$ and $\widehat{\phi}$, but also $\widehat{\Omega}(\hat{t})$. It is therefore important to specify appropriate boundary conditions that govern the evolution of the domain $\widehat{\Omega}(\hat{t})$.
Once the boundary conditions are specified, the next step is to discuss how to solve the problem for a given initial data.

6.2.2.1 Initial conditions

Since we are considering a free boundary problem in which the spatial domain $\widehat{\Omega}(\hat{t})$ evolves as time passes, we have to first specify the initial shape of the domain. The initial conditions are given in the form:

$$\begin{cases} \widehat{\Omega}(0) = \widehat{\Omega}^0, \\ \widehat{C}_i(\hat{x},0) = \widehat{C}_i^0(\hat{x}) \ \text{ in } \ \widehat{\Omega}(0) \quad (i = 1,\dots,M), \end{cases} \tag{6.2.13}$$

where $\widehat{\Omega}^0$ is a bounded domain having the shape as shown in Figure 6.2.1, and $\widehat{C}_i^0(\hat{x})$ $(i = 1,\dots,M)$ are functions satisfying

$$\widehat{C}_i^0 \geq 0 \ \ (i = 1,\dots,M), \qquad z_1\widehat{C}_1^0 + \cdots + z_M\widehat{C}_M^0 = 0.$$

We do not specify the initial value of $\widehat{\phi}$, since $\widehat{\phi}$ is obtained by solving a boundary value problem as we shall see later.

6.2.2.2 Boundary conditions

To find appropriate boundary conditions is much more difficult as it reflects the complex mechanism of corrosion. To do so, we introduce the symbols $\widehat{\Omega}(\hat{t})$, $\widehat{\Gamma}_0(\hat{t})$ (the pit entrance), $\widehat{\Gamma}(\hat{t})$ (the pit wall), $V_{\widehat{\Gamma}}$(the velocity of the boundary $\widehat{\Gamma}(\hat{t})$), which denote the non-dimensional counterparts of $\Omega(t), \Gamma_0(t), \Gamma(t), V_\Gamma$ via the change of variable $x \mapsto \hat{x}$, $t \mapsto \hat{t}$, respectively.

Boundary conditions satisfied by $\{\widehat{\mathbf{C}}_\mathbf{i}\}_{\mathbf{i}\in(\mathbf{1},\cdots,\mathbf{M})}$ on the pit wall $\widehat{\Gamma}(\hat{t})$

There are two types of reactions that may occur during the development of corrosion pit which are chemical reactions and electrochemical reactions:

The chemical reactions take place in the pit solution $\Omega(t)$ to describe interactions between ions. It is given by the reactions term $\mathcal{R}_i$ in the Nernst-Planck equation (6.2.2a).

On the other hand, the electrochemical reactions occur only at the pit walls $\Gamma(t)$ (the surface of the steel). There are two types of electrochemical reaction: oxidation reaction (anodic reaction) and reduction reaction (cathodic reaction). For example, during corrosion, more than one oxidation and one reduction reaction may occur. Indeed, during oxidation of an alloy its component metal atoms go into solution as their respective ions. This process corresponds to the dissolution of metal which implies the liberation of electrons. However, during cathodic reactions these electrons will be consumed. Here, two cathodic reactions are possible to occur: the evolution of hydrogen and the reduction of oxygen.

For simplicity, in the present model, we only consider one electrochemical reaction. We neglect the cathodic reaction localized on the metal surface as mentioned above. Thus, we only consider

the anodic reaction of metal dissolution. In our case, the metal to be studied is pure iron. So, this anodic reaction is given by:

$$\mathrm{Fe} \quad \underset{k_c}{\overset{k_a}{\rightleftharpoons}} \quad \mathrm{Fe}^{2+} \; + \; 2\,\mathrm{e}^{-}.$$

In this subsection, we derive boundary conditions in their dimensional form and then deduce their dimensionless form. So, in what follows, to avoid confusion, we keep using the symbol $\widehat{\cdot}$ only for the non-dimensional expression.

To do so, with regards to the boundary conditions on the wall $\Gamma(t)$, we need to distinguish Fe^{2+} and other ions, so hereafter we let $i = 1$ represent Fe^{2+}, that is,

$$C_1 := C_{\mathrm{Fe}^{2+}}, \qquad z_1 := z_{Fe^{2+}} = +2.$$

Then the boundary conditions on $\Gamma(t)$ are given in the following dimensional form:

$$\begin{cases} \boldsymbol{J}_1 \cdot \boldsymbol{n} = -f_{\mathrm{Fe}^{2+}} + V_\Gamma C_1 \quad \text{on} \quad \Gamma(t), & \text{(6.2.14a)} \\ \boldsymbol{J}_i \cdot \boldsymbol{n} = V_\Gamma C_i \quad \text{on} \quad \Gamma(t) \quad (i = 2, \ldots, M), & \text{(6.2.14b)} \end{cases}$$

where

$\boldsymbol{J}_i = -D_i(\nabla C_i + \dfrac{z_i F}{RT} C_i \nabla\phi)$, $i = 1, \ldots, M$, are the ion flux,

$\boldsymbol{n}$ is the outward unit normal vector on $\Gamma(t)$ (pointing outside of $\Omega(t)$) and

V_Γ denotes the velocity of the boundary $\Gamma(t)$ in the outward normal direction, which we call the **corrosion rate**. V_Γ indicates how fast the pit grows. (Thus $V_\Gamma > 0$ if $\Omega(t)$ is expanding).

The boundary condition (6.2.14b) is the no-flux boundary condition for the case of a moving boundary. This condition implies that there is no inflow or outflow of ions through the boundary except for iron ions Fe^{2+}.
On the other hand, the boundary condition (6.2.14a) implies that there is inflow of iron ions from the boundary. This inflow $f_{\mathrm{Fe}^{2+}}$ denotes the **ferrous ion flux**, that is, the amount of the ferrous ions dissolving from the surface of the iron in the pit caused by the anodic reaction as mentioned above (per unit time, per unit area) minus the amount of the iron ions absorbed by the pit solution. For $f_{\mathrm{Fe}^{2+}}$, we adopt the **Butler-Volmer formula** given as follows:

$$f_{\mathrm{Fe}^{2+}}(\phi, C_{\mathrm{Fe}^{2+}}) = k_a \exp\Big(-\frac{F}{RT}(\phi - \phi_m)\Big) - k_c \frac{C_{\mathrm{Fe}^{2+}}}{C_{\mathrm{ref}}} \exp\Big(\frac{F}{RT}(\phi - \phi_m)\Big), \tag{6.2.15}$$

where k_a and k_c are positive constants that represent the speed of oxidation of iron and that of reduction, respectively ($\mathrm{mol/m^2 s}$). C_{ref} is a reference concentration which is usually set at $C_{\mathrm{ref}} = 1000\,\mathrm{mol/m^3} = 1\mathrm{mol/L}$ in ideal system, while ϕ_m denotes the electric potential applied on the iron steel surface (which is assumed to be constant) and ϕ, the electric potential of the aqueous solution in contact with the steel surface. **In this case, this pit corrosion phenomenon is considered to be under potentiostatic conditions.**

Physically, the first term on the right-hand side of (6.2.15) expresses the speed of dissolution of ferrous ions from the pit wall into the solution, and the second term expresses the speed of absorption of ferrous ions by the pit wall as shown in Figure 6.2.2.

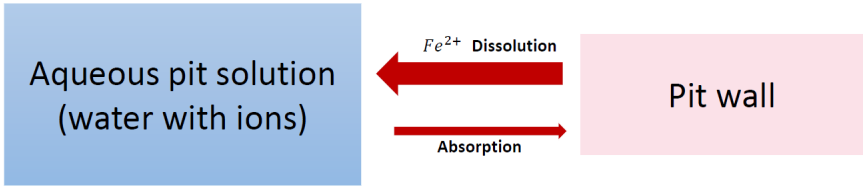

Figure 6.2.2: Butler-Volmer flux (Ferrous ions flux): $f_{\mathrm{Fe}^{2+}} = [\text{dissolution}] - [\text{absorption}]$

Here it is assumed that these speeds depend on the difference between the potential ϕ of the aqueous solution at the boundary $\Gamma(t)$ and the potential ϕ_m applied on the steel surface that is kept constant at all times. The speed of absorption of ferrous ions by the pit wall (the second term in (6.2.15)) depends also on the concentration of Fe^{2+} ions in the aqueous solution at the boundary $\Gamma(t)$.
The **corrosion speed** V_Γ, namely the normal velocity of the boundary $\Gamma(t)$ in the outward direction, is proportional to the flux $f_{\mathrm{Fe}^{2+}}$ through the following relationship:

$$f_{\mathrm{Fe}^{2+}} = N_{\mathrm{Fe}} V_\Gamma \ \ (\mathrm{mol/m^2 s}) \qquad \text{or} \qquad V_\Gamma = \Omega_{Fe}\, f_{\mathrm{Fe}^{2+}} \ \ (\mathrm{m/s}), \tag{6.2.16}$$

where $\Omega_{Fe} = N_{\mathrm{Fe}}^{-1}$ and N_{Fe} denotes the concentration of ferrous atoms in solid iron (thus Ω_{Fe} is the molar volume of solid iron).

$$N_{\mathrm{Fe}} = \frac{\text{Density of iron}}{\text{Molar mass of iron}} = \frac{7.87\ \mathrm{g/cm^3}}{55.845\ \mathrm{g/mol}} \approx 0.14\,\mathrm{mol/cm^3} = 140\,\mathrm{mol/L}$$

and $\Omega_{\mathrm{Fe}} \approx 7.095\ \mathrm{cm^3/mol} = 7.095\ 10^{-6}\ \mathrm{m^3/mol}$.

Next, we discuss the non-dimensional expressions of the above formulas (6.2.14). To this end, we use the change of variables (6.2.3) to obtain:

$$\begin{cases} \widehat{\boldsymbol{J}}_1 \cdot \boldsymbol{n} = -\widehat{f}_{\mathrm{Fe}^{2+}} + V_{\widehat{\Gamma}} \widehat{C}_1 \quad \text{on} \quad \widehat{\Gamma}(\hat{t}), & \text{(6.2.17a)} \\ \widehat{\boldsymbol{J}_i} \cdot \boldsymbol{n} = V_{\widehat{\Gamma}} \widehat{C}_i \quad \text{on} \quad \widehat{\Gamma}(t) \quad (i = 2, \ldots, M), & \text{(6.2.17b)} \end{cases}$$

Indeed, as for the ion flux, the relation between the dimensional and non-dimensional expressions is given by

$$\boldsymbol{J}_i := -D_i \Big(\nabla C_i + \frac{z_i F}{RT} C_i \nabla \phi \Big) \ \ \mathrm{mol}\,/\,\mathrm{m^2 s},$$

so that

$$\boldsymbol{J}_i := -D_0 \widehat{D}_i \Big(\frac{C_0}{L} \widehat{\nabla} \widehat{C}_i + \frac{z_i F}{RT} C_0 \widehat{C}_i \frac{RT}{FL} \widehat{\nabla} \widehat{\phi} \Big) \ \ \mathrm{mol}\,/\,\mathrm{m^2 s},$$

which implies that

$$\widehat{\boldsymbol{J}_i} = \frac{L}{D_0 C_0} \boldsymbol{J}_i \quad (i = 1, \ldots, M), \tag{6.2.18}$$

where

$$\widehat{\boldsymbol{J}_i} := -\widehat{D}_i (\widehat{\nabla} \widehat{C}_i + z_i \widehat{C}_i \widehat{\nabla} \widehat{\phi}).$$

The non-dimensional expression of the free boundary speed V_Γ becomes:

$$V_{\widehat{\Gamma}} = \frac{L}{D_0} V_\Gamma \quad \text{and} \quad V_\Gamma = \frac{D_0}{L} V_{\widehat{\Gamma}} \quad \mathrm{m/s}, \tag{6.2.19}$$

while the non-dimensional expression of the Butler-Volmer formula $f_{\mathrm{Fe}^{2+}}$ (6.2.15) is given by:

$$\widehat{f}_{\mathrm{Fe}^{2+}} = \frac{L}{D_0 C_0} f_{\mathrm{Fe}^{2+}} \tag{6.2.20}$$

where

$$\widehat{\phi}_m = \frac{F}{RT}\phi_m, \quad \widehat{k}_a = \frac{L}{D_0 C_0}\, k_a \quad \textit{and} \quad \widehat{k}_c = \frac{L}{D_0 C_0}\, k_c. \tag{6.2.21}$$

Indeed, from (6.2.15) we have that

$$f_{\mathrm{Fe}^{2+}}(\phi, C_{\mathrm{Fe}^{2+}}) = k_a \exp\Big(-\frac{F}{RT}(\phi-\phi_m)\Big) - k_c\, \frac{C_{\mathrm{Fe}^{2+}}}{C_{\mathrm{ref}}} \exp\Big(\frac{F}{RT}(\phi-\phi_m)\Big),$$

so that,

$$f_{\mathrm{Fe}^{2+}}(\phi, C_{\mathrm{Fe}^{2+}}) = k_a \exp\Big(-\frac{F}{RT}\frac{RT}{F}(\widehat{\phi}-\widehat{\phi}_m)\Big) - k_c\, \frac{C_0 \widehat{C}_{\mathrm{Fe}^{2+}}}{C_{\mathrm{ref}}} \exp\Big(\frac{F}{RT}\frac{RT}{F}(\widehat{\phi}-\widehat{\phi}_m)\Big). \tag{6.2.22}$$

Then from (6.2.16), (6.2.19) and since $N_{\mathrm{Fe}} = C_0 \widehat{N_{\mathrm{Fe}}}$ mol/m^3, we obtain

$$f_{\mathrm{Fe}^{2+}} = N_{\mathrm{Fe}} V_\Gamma = C_0 \widehat{N_{\mathrm{Fe}}}\, \frac{D_0}{L}\, V_{\widehat{\Gamma}} = \frac{C_0 D_0}{L}\, \widehat{N_{\mathrm{Fe}}}\, V_{\widehat{\Gamma}} = \frac{C_0 D_0}{L}\, \widehat{f}_{\mathrm{Fe}^{2+}}, \tag{6.2.23}$$

where

$$\widehat{f}_{\mathrm{Fe}^{2+}} = \widehat{N_{\mathrm{Fe}}}\, V_{\widehat{\Gamma}} \quad \text{and} \quad \widehat{\mathrm{N}_{\mathrm{Fe}}} = \frac{\mathrm{N}_{\mathrm{Fe}}}{\mathrm{C}_0}\,. \tag{6.2.24}$$

We deduce from (6.2.22) and (6.2.23) the non-dimensional form of $f_{\mathrm{Fe}^{2+}}$ which is

$$\widehat{f}_{\mathrm{Fe}^{2+}}\Big(\widehat{\phi}, \widehat{C}_{\mathrm{Fe}^{2+}}\Big) = \widehat{k}_a \exp\big(-(\widehat{\phi}-\widehat{\phi}_m)\big) - \widehat{k}_c\, \frac{C_0}{C_{\mathrm{ref}}}\, \widehat{C}_{\mathrm{Fe}^{2+}} \exp\big(\widehat{\phi}-\widehat{\phi}_m\big), \tag{6.2.25}$$

where the constants $\widehat{\phi}_m, \widehat{k}_a$ and $\widehat{\mathrm{k}}_{\mathrm{c}}$ in (6.2.25) are given in (6.2.21).

Boundary conditions satisfied by $\widehat{\phi}$ on the pit wall $\widehat{\Gamma}(\hat{t})$

We did not specify the boundary condition for $\widehat{\phi}$ on $\widehat{\Gamma}(\hat{t})$, but just as equation (6.2.11b) has been derived from (6.2.9), one can derive the boundary condition for $\widehat{\phi}$ on $\widehat{\Gamma}(\hat{t})$ from those for $\{\widehat{C}_i\}$ and the local electroneutrality condition (6.2.9b). To see this, let us multiply (6.2.17a), (6.2.17b) by z_i $(i = 1, \ldots, M)$ and sum them up, and use (6.2.9b). Then we obtain

$$\Big(\sigma \widehat{\nabla}\widehat{\phi} + \sum_{i=1}^{M} z_i \widehat{D}_i \widehat{\nabla}\widehat{C}_i\Big) \cdot \boldsymbol{n} = z_1 \widehat{f}_{\mathrm{Fe}^{2+}}(\widehat{\phi}, \widehat{C}_1) \quad \text{on} \quad \widehat{\Gamma}(\hat{t}), \tag{6.2.26}$$

where $\sigma = \displaystyle\sum_{i=1}^{M} z_i^2 \widehat{D}_i\, \widehat{C}_i$ and $z_1 = 2$. Here $\widehat{C}_i$, $i = 1, \ldots, M$, are regarded as given functions. One can rewrite (6.2.26) in the following equivalent form:

$$\sigma \frac{\partial \widehat{\phi}}{\partial \nu} + \sum_{i=1}^{M} z_i \widehat{D}_i \frac{\partial \widehat{C}_i}{\partial \nu} = 2 \widehat{f}_{\mathrm{Fe}^{2+}}(\widehat{\phi}, \widehat{C}_1) \quad \text{on} \quad \widehat{\Gamma}(\hat{t}), \tag{6.2.27}$$

where $\partial/\partial\nu$ denotes the outward normal derivative on the boundary $\widehat{\Gamma}(\hat{t})$. This is so-to-speak a **nonlinear Robin boundary conditions**. Note that we have

$$\frac{\partial}{\partial \widehat{\phi}} \widehat{f}_{\mathrm{Fe}^{2+}}(\widehat{\phi}, \widehat{C}) < 0, \qquad \frac{\partial}{\partial \widehat{C}} \widehat{f}_{\mathrm{Fe}^{2+}}(\widehat{\phi}, \widehat{C}) < 0 \tag{6.2.28}$$

Remark 6.2.3. Here we define the sign of $\widehat{f}_{\mathrm{Fe}^{2+}}$ as in Figure 6.2.2, so $\widehat{f}_{\mathrm{Fe}^{2+}} > 0$ **implies the expansion of the pit**. □

Boundary conditions satisfied by $\{\widehat{C}_i\}_{i\in(1,\cdots,M)}$ at the entrance of the pit $\widehat{\Gamma}_0(\hat{t})$

For the boundary conditions on $\widehat{\Gamma}_0(\hat{t})$ (the entrance of the pit), we suppose that the solution outside the pit is well stirred so that the concentration of each ion is always constant on $\widehat{\Gamma}_0(\hat{t})$. This implies the **Dirichlet boundary conditions on $\widehat{\Gamma}_0(\hat{t})$**, which are given in the form

$$\widehat{C}_i = \beta_i \quad \text{on} \quad \widehat{\Gamma}_0(\hat{t}),\ \hat{t} > 0 \quad (i = 1,2,\ldots,M), \tag{6.2.29}$$

where β_i $(i = 1,\ldots,M)$ are constants which satisfy the local electroneutrality condition $\sum_{i=1}^{M} z_i\beta_i = 0$.

Boundary conditions satisfied by $\widehat{\phi}$ at the entrance of the pit $\widehat{\Gamma}_0(\hat{t})$

Unlike the pit wall $\widehat{\Gamma}(\hat{t})$, where we do not specify the boundary condition for $\widehat{\phi}$, we need to specify the boundary condition for $\widehat{\phi}$ on $\widehat{\Gamma}_0(\hat{t})$ in order to determine $\widehat{\phi}$ in $\widehat{\Omega}(\hat{t})$. So, for the moment, we set

$$\widehat{\phi} = 0 \quad \text{on} \quad \widehat{\Gamma}_0(\hat{t}),\ \hat{t} > 0 \tag{6.2.30}$$

6.2.3 Procedure for solving the problem

The analysis in later sections will be done for the non-dimensionalized systems, but for notational simplicity we will drop the symbol $\widehat{\cdot}$. However, only in the Butler-Volmer formula, we keep using this symbol just for $f_{Fe^{2+}}, \phi_m, k_a, k_c$ and $\phi^* := \phi^{\text{eq}}$ (to be defined later). We keep write them as $\widehat{f}_{Fe^{2+}}, \widehat{\phi}_m, \widehat{k}_a, \widehat{k}_c$ and $\widehat{\phi^*}$ for the non-dimensional expression to avoid confusion later (especially in Chapter 7).

Now that we have specified the boundary conditions, we discuss how to solve the problem. It is an initial-boundary value problem for the system (6.2.11). Here is a sketch of the procedure.

- Step 1
  Specify the initial values of $\Omega(t)$ and $C_1,\ldots,C_M$ as in (6.2.13);
- Step 2
  Regard $\{C_i\}$ as given functions and solve equation (6.2.11b) under the boundary conditions for ϕ discussed above. This determines ϕ from the present values of $C_1,\ldots,C_M$;
- Step 3
  Input the above $\phi = \phi[C_1,\ldots,C_M]$ into (6.2.11a). Then we can delete ϕ from (6.2.11a) and regard (6.2.11a) as a system of equations for $C_1,\ldots.C_M$ only. We then solve this system under the boundary conditions for $\{C_i\}$ discussed above.

Let us explain the procedure in more details. The Step 2 amounts to solving the following boundary value problem:

$$\begin{cases} \nabla\cdot(\sigma\nabla\phi) + \sum_{i=1}^{M} \nabla\cdot(z_i D_i \nabla C_i) = 0 \quad \text{in} \quad \Omega(t) & \text{(6.2.31a)} \\ \sigma\dfrac{\partial\phi}{\partial\nu} + \sum_{i=1}^{M} z_i D_i \dfrac{\partial C_i}{\partial\nu} = 2\widehat{f}_{\text{Fe}^{2+}}(\phi, C_1) \quad \text{on} \quad \Gamma(t), & \text{(6.2.31b)} \\ \phi = 0 \quad \text{on} \quad \Gamma_0(t), & \text{(6.2.31c)} \end{cases}$$

where $\sigma := \sum_{i=1}^{M} z_i^2 D_i C_i$ and $\widehat{f}_{Fe^{2+}}(\phi, C_1)$ is given by (6.2.25).

As we mentioned before, (6.2.31a) is a second-order **elliptic PDE** for ϕ since $\sigma > 0$. The boundary condition is a mixture of a **nonlinear Robin boundary condition** (6.2.31b) and a **Dirichlet boundary condition** (6.2.31c). The condition (6.2.31b) is nonlinear, but since

$$\frac{\partial}{\partial \phi} \widehat{f}_{Fe^{2+}}(\phi, C_1) < 0, \tag{6.2.32}$$

it is most probable that the system (6.2.31) is solvable.
Next we discuss Step 3. This amounts to solving the following free boundary problem:

$$\begin{cases} \dfrac{\partial C_i}{\partial t} = \nabla \cdot \Big(D_i (\nabla C_i + z_i C_i \nabla \phi) \Big) + \mathcal{R}_i(\{C\}) \quad \text{in } \Omega(t), \ \ i = 1, \dots, M, & \text{(6.2.33a)} \\ D_1 \dfrac{\partial C_1}{\partial \nu} + 2 D_1 C_1 \dfrac{\partial \phi}{\partial \nu} = \widehat{f}_{Fe^{2+}}(\phi, C_1) - V_\Gamma C_1 \quad \text{on } \ \Gamma(t), & \text{(6.2.33b)} \\ D_i \dfrac{\partial C_i}{\partial \nu} + z_i D_i C_i \dfrac{\partial \phi}{\partial \nu} = -V_\Gamma C_i \quad \text{on } \ \Gamma(t), \ \ i = 2, \dots, M, & \text{(6.2.33c)} \\ C_i = \beta_i \quad \text{on } \ \Gamma_0(t), \ \ i = 1, \dots, M, & \text{(6.2.33d)} \end{cases}$$

along with the following free boundary condition that governs the speed of the boundary movement:

$$V_\Gamma = b \widehat{f}_{Fe^{2+}}(\phi, C_1) \quad \text{on } \ \Gamma(t), \tag{6.2.34}$$

where (6.2.34) is a non-dimensional expression of (6.2.16). It is the same equation as (6.2.24). The constant b is given by

$$b = \frac{C_0}{N_{Fe}} = \widehat{N_{Fe}}^{-1} \qquad (N_{Fe} \text{ is the concentration of atoms in solid iron}). \tag{6.2.35}$$

Finally, we substitute the solution of (6.2.31) into the function ϕ in the above system. The boundary condition (6.2.33b) is nonlinear for C_1, but since

$$\frac{\partial}{\partial C_1} \widehat{f}_{Fe^{2+}}(\phi, C_1) < 0, \tag{6.2.36}$$

the system (6.2.33) is most probable that it is solvable.

In the next section, we will study a one-dimensional model and we will discuss in more detail the procedure for solving the problem.

6.3 One-dimensional model with three ions

6.3.1 Model with Dirichlet boundary conditions at the entrance of the pit

We consider a simple situation where **corrosion only occurs at the bottom of the pit** and the pit has a **thin cylindrical shape**. We assume that the pit is so thin that the aqueous solution is well mixed by diffusion in the direction orthogonal to the axis of the cylinder. In such a situation it is reasonable to assume that the concentration of the ions and the potential ϕ only depend on one space variable, thus the system is reduced to a one-dimensional problem with only three ions, Na^+, Cl^- and Fe^{2+}, where the domain $\Omega(t)$ is an interval on the x-axis:

$$\Omega(t) := (0, x_d(t)), \quad \Gamma(t) = \{x_d(t)\}, \quad \Gamma_0(t) = \{0\}.$$

The normal velocity V_Γ of the boundary $\Gamma(t)$ is given by

$$V_\Gamma = \dot{x}_d(t) := \frac{d}{dt} x_d(t).$$

For notational simplicity, we set

$$C_1 := C_{\mathrm{Fe}^{2+}}, \quad C_2 := C_{\mathrm{Na}^{+}}, \quad C_3 := C_{\mathrm{Cl}^{-}}$$

$$z_1 = 2, \quad z_2 = 1, \quad z_3 = -1.$$

As for the diffusion coefficients [2], we set

$$D_1 = 0.719, \quad D_2 = 1.33, \quad D_3 = 2.03.$$

Note that these are non-dimensional values with the following choice of reference parameters:

$$D_0 = 1 \times 10^{-9}\ \mathrm{m}^2/\mathrm{s}, \quad L = 1\ \mu\mathrm{m}, \quad C_0 = 1000\ \mathrm{mol}/\mathrm{m}^3 = 1\,\mathrm{mol}/L.$$

At the pit entrance, we assume that the ionic concentrations are constant, so that we impose the Dirichlet boundary conditions. At the pit bottom, we adopt the Butler-Volmer formula (6.2.25) for the ferrous ion dissolution. Our system is thus the same as discussed in Subsection 6.2.3, except that the reaction terms $\mathcal{R}_i(\{C\})$ are not present. With this setting, systems (6.2.31) and (6.2.33) are written as follows:

System satisfied by the potential ϕ

$$\begin{cases} \dfrac{\partial}{\partial x}\left(\sigma \dfrac{\partial \phi}{\partial x}\right) + \displaystyle\sum_{i=1}^{3} \frac{\partial}{\partial x}\left(z_i D_i \frac{\partial C_i}{\partial x}\right) = 0, \quad t > 0,\ 0 < x < x_d(t), & \text{(6.3.1a)} \\ \sigma \dfrac{\partial \phi}{\partial x} + \displaystyle\sum_{i=1}^{3} z_i D_i \frac{\partial C_i}{\partial x} = 2\widehat{f}(\phi, C_1) \quad \text{at} \quad x = x_d(t), & \text{(6.3.1b)} \\ \phi(0,t) = 0, \quad t > 0, & \text{(6.3.1c)} \end{cases}$$

where $\sigma := \displaystyle\sum_{i=1}^{3} z_i^2 D_i C_i$ and $\widehat{f}(\phi, C_1)$ stands for the dimensionless $\widehat{f}_{\mathrm{Fe}^{2+}}(\phi, C_1)$ given in (6.2.25):

$$\widehat{f}\,(\phi, C_1) = \widehat{k}_a \exp\big(-(\phi - \widehat{\phi}_m)\big) - \widehat{k}_c \frac{C_0}{C_{\mathrm{ref}}} C_1 \exp\big(\phi - \widehat{\phi}_m\big), \tag{6.3.2}$$

where the constants $\widehat{\phi}_m, \widehat{k}_a$ and $\widehat{\mathrm{k}}_{\mathrm{c}}$ in (6.2.25) are given in (6.2.21). Here, we recall also that the reference concentration C_{ref} which appears in the Butler-Volmer formula (6.3.2) below is **always fixed at** $C_{\mathrm{ref}} = 1000\ \mathrm{mol}/\mathrm{m}^3 = 1\,\mathrm{mol}/\mathrm{L}$.

[2] reference: https://www.aqion.de/site/194.

System satisfied by the concentrations $\{C_i\}_{i=1,2,3}$

$$\begin{cases} \dfrac{\partial C_i}{\partial t} = \dfrac{\partial}{\partial x}\left(D_i\left(\dfrac{\partial C_i}{\partial x} + z_i C_i \dfrac{\partial \phi}{\partial x}\right)\right), \quad t>0,\ 0<x<x_d(t), \quad (i=1,2,3) & \text{(6.3.3a)} \\ D_1 \dfrac{\partial C_1}{\partial x} + 2D_1 C_1 \dfrac{\partial \phi}{\partial x} = -\dot{x}_d(t) C_1 + \widehat{f}(\phi, C_1) \quad \text{at} \quad x = x_d(t), & \text{(6.3.3b)} \\ D_i \dfrac{\partial C_i}{\partial x} + z_i D_i C_i \dfrac{\partial \phi}{\partial x} = -\dot{x}_d(t) C_i \quad \text{at} \quad x = x_d(t) \quad (i=2,3), & \text{(6.3.3c)} \\ C_i(0,t) = a_i, \quad t>0 \quad (i=1,2,3), & \text{(6.3.3d)} \end{cases}$$

along with the free boundary condition

$$\dot{x}_d(t) = b\widehat{f}\Big(\phi(x_d(t),t), C_1(x_d(t),t)\Big) \quad \text{on} \quad \Gamma(t), \tag{6.3.4}$$

where $b = C_0 N_{\mathrm{Fe}}^{-1}$ is the non-dimensional molar volume of solid iron (see (6.2.35)).

In the one-dimensional case, the equation (6.3.1) for the potential ϕ is rather easy to solve, as we explain below. This is a special feature of the one-dimensional problem.

Expression of the potential as a function of concentrations by solving (6.3.1):

As we explained in Section 6.2.3, the only unknown in (6.3.1) is the potential ϕ, as C_1, C_2, C_3, x_d are regarded as given functions at this stage. Integrating (6.3.1a) by x shows that

$$\sigma \frac{\partial \phi}{\partial x} + \sum_{i=1}^{3} z_i D_i \frac{\partial C_i}{\partial x}$$

is independent of x, hence, by (6.3.1b), we obtain

$$\sigma \frac{\partial \phi}{\partial x} + \sum_{i=1}^{3} z_i D_i \frac{\partial C_i}{\partial x} = 2\widehat{f}(P(t), C_1(x_d(t),t)) \quad \text{for} \quad 0 \le x \le x_d(t), \tag{6.3.5}$$

where

$$P(t) := \phi(x_d(t),t).$$

Hereafter we use the following symbols for notational simplicity:

$$\Box_x := \frac{\partial \Box}{\partial x}, \quad \Box_{xx} := \frac{\partial^2 \Box}{\partial x^2}, \quad \Box_t := \frac{\partial \Box}{\partial t}.$$

Then (6.3.5) can be rewritten as

$$\phi_x = -\frac{\sum_{i=1}^{3} z_i D_i (C_i)_x}{\sum_{i=1}^{3} z_i^2 D_i C_i} + \frac{2\widehat{f}(P(t), C_1(x_d(t),t))}{\sum_{i=1}^{3} z_i^2 D_i C_i}. \tag{6.3.6}$$

Integrating this equality from $x = 0$ to $x = x_d(t)$ and using (6.3.1c), we obtain

$$P(t) = -A(t) + 2\widehat{f}(P(t), C_1(x_d(t),t))B(t), \tag{6.3.7}$$

where

$$A(t) = \int_0^{x_d(t)} \frac{\sum_{i=1}^{3} z_i D_i (C_i)_x}{\sum_{i=1}^{3} z_i^2 D_i C_i} dx, \quad B(t) = \int_0^{x_d(t)} \frac{dx}{\sum_{i=1}^{3} z_i^2 D_i C_i} \left(= \int_0^{x_d(t)} \frac{dx}{\sigma(x,t)} \right).$$

Here $A(t)$, $B(t)$, $C_1(x_d(t),t)$ are treated as given functions.

We can **determine the value $P(t)$ uniquely from (6.3.7), since $\widehat{f}(\phi,C_1)$ is monotone decreasing in ϕ** as stated in (6.2.32) and since $B > 0$. Indeed, the left-hand side of (6.3.7) is monotone increasing in P while the right-hand side is monotone decreasing in P; therefore, as we vary the value of P from $-\infty$ to $+\infty$, the two sides must become equal at a unique value of P.

Remark 6.3.1. As we mentioned in the paragraph below (6.2.12), σ plays the role of electric conductivity, therefore $B(t)$ can be interpreted as the electric resistance of the aqueous solution between $x = 0$ and $x = x_d(t)$. Thus if we drop the term $A(t)$ from (6.3.7), it coincides with the usual Ohm's law

$$V = IR$$

where I is the current through the conductor pit solution in units of amperes, V is the voltage measured across the pit solution in units of volts, and R is the resistance of the pit solution in units of ohms. The formula (6.3.7) shows that Ohm's law **is violated in an aqueous solution due to the random motion of ions**, which the term $A(t)$ expresses.

□

Procedure for solving (6.3.3):

First we determine the potential at the pit bottom $P(t) = \phi(x_d(t),t)$ by solving the equation (6.3.7). Once the value of $P(t)$ is determined (from the given data of $\{C_i\}_{i\in\{1,2,3\}}$ and x_d), we can determine ϕ_x on the entire interval $0 \le x \le x_d(t)$ from (6.3.6). By substituting this ϕ_x into (6.3.3), we delete it from the equations. Then, we can determine the time derivative of concentrations in (6.3.3), since this equation is written in the form

$$(C_i)_t = \big(D_i\left((C_i)_x + z_i C_i \phi_x\right)\big)_x.$$

$$\boxed{\text{Present values of } C_i} \longrightarrow \boxed{P(t) = \phi(x_d(t),t)} \longrightarrow \boxed{\partial\phi/\partial x} \longrightarrow \boxed{\partial C_i/\partial t}.$$

Thus, on a formal level, the system looks solvable.

Note that the boundary conditions (6.3.3b), (6.3.3c) are written in the following slightly simpler form

$$\begin{cases} D_1(C_1)_x + 2D_1C_1\,\phi_x = (1 - b\,C_1)\widehat{f}\big(P(t),C_1\big) \quad \text{at} \quad x = x_d(t), & \text{(6.3.8a)} \\ D_i(C_i)_x + z_iD_iC_i\,\phi_x = -b\widehat{f}\big(P(t),C_1\big)C_i \quad \text{at} \quad x = x_d(t) \quad (i = 2,3). & \text{(6.3.8b)} \end{cases}$$

Since $b = C_0N_{\mathrm{Fe}}^{-1}$ is the molar volume of solid iron in its dimensionless form derived from (6.2.16), where N_{Fe} denotes the concentration of ferrous atoms in solid iron which is much denser than the ferrous ions in the aqueous solution and as the reference concentration C_0 is in the range of 10^{-3}mol/L and 1mol/L, we must have

$$bC_1 = bC_{\mathrm{Fe}^{2+}} = \frac{C_0C_{\mathrm{Fe}^{2+}}}{N_{\mathrm{Fe}}} < 1.$$

Therefore $1 - bC_1 > 0$ in (6.3.8a). This fact and the inequality (6.2.36) imply that the right-hand side of (6.3.8a) is strictly decreasing in C_1 so long as $\widehat{f}$ is not too much negative. The boundary condition (6.3.8a) is a nonlinear Robin boundary condition, so it is generally more difficult to handle than linear boundary conditions, but if the right-hand side of (6.3.8a) is monotone decreasing in C_1, there is a good chance that the system is solvable.

6.4 Numerical scheme for the one-dimensional model

6.4.1 Introduction

In this section we describe the numerical method used to solve the coupled system (6.3.1)–(6.3.3)–(6.3.4). As we have seen in Chapter 5, we will consider an Arbitrary Lagrangian Eulerian (ALE) formulation of the one-dimensional model in order to handle the displacement of the free boundary (6.3.4). We recall that this approach avoids resorting to numerical interpolations or extrapolations of the computed solution. The numerical method which we use is based on a decoupling of the displacement of the free boundary with the numerical solution of the system (6.3.3). The motion of the free boundary is numerically solved by an explicit Euler scheme whereas an implicit finite difference scheme is used for the spatial and time approximation of the ALE formulation of the diffusion-convection system (6.3.3).

In section, we rewrite the one-dimensional system by considering M chemical species instead of only three species.

The concentrations are given by $C^j = C^j(x,t) \quad (j = 0,..,M-1)$ where C^j is the concentration of the ion species j. If $j = 0$, it refers to the metal cation concentration.

Remark 6.4.1 (Equivalent systems)**.** *The full system* (6.3.1)–(6.3.2) *with* (6.3.3)–(6.3.4) *is equivalent to the system* (6.3.3)–(6.3.4)–(6.3.2) *with* (6.4.1) *below, i.e. where the potential system* (6.3.1) *has been replaced by the electroneutrality condition* (6.4.1a) *and* (6.4.1b)*.*

$$\begin{cases} \displaystyle\sum_{j=0}^{M-1} z_j C^j(x,t) = 0, \quad t > 0, \ 0 \leqslant x \leqslant x_d(t), & \text{(6.4.1a)} \\ \phi(0,t) = 0, \quad t > 0. & \text{(6.4.1b)} \end{cases}$$

In view of remark 6.4.1 and for simplicity, the numerical scheme will be derived to solve the coupled system (6.4.1)–(6.3.3)–(6.3.4) instead of the coupled system (6.3.1)–(6.3.3)–(6.3.4). However, we use the system (6.3.1) only at initial time (t=0) to determine the initial profile of potential (see subsection 6.4.3) by means of the procedure described in subsection 6.3.1.

6.4.2 ALE formulation of the one-dimensional model

An introduction to the ALE method is presented in Chapter 5 for the classical Stefan problem. As mentioned above, we consider an Arbitrary Lagrangian Eulerian (ALE) formulation of the system (6.4.1)–(6.3.3)–(6.3.4) in order to handle the displacement of the free boundary (6.3.4).

To do so, let $t' \geqslant 0$ be fixed. For $t \geqslant 0$, we define the ALE mapping (see Sections 5.1.2 and 5.1.3 of Chapter 5)

$$\psi(\,\cdot\,,t) : [0,x_d(t)] \to [0,x_d(t')] \qquad (6.4.2)$$

$$x \ \to \ \psi(x,t) = \frac{x_d(t')}{x_d(t)} x.$$

The function ψ is smooth with respect to t. We recall that this case is usually referred to the Variable Space Grid (VSG) method [53],[41]. This mapping preserves the uniform discretization of the moving space interval $[0,x_d(t)]$ during the time evolution.

In the system (6.4.1)–(6.3.3)–(6.3.4), we perform the change of unknowns

$$\widetilde{\phi}(\tilde{x},t) = \phi(x,t) \quad \text{and} \quad \widetilde{C}^j(\tilde{x},t) = C^j(x,t) \text{ with } \tilde{x} = \psi(x,t) \tag{6.4.3}$$

for $t \geq 0$, $x \in [0,x_d(t)]$.

Next, the functions $\widetilde{\phi}(\tilde{x},t)$ and $\widetilde{C}^j(\tilde{x},t)$ together with the (unchanged) function x_d satisfy the system:

System satisfied by the concentrations $\{\widetilde{C}^j\}_{j=0,\cdots,M-1}$ and $\widetilde{\phi}$

$$\begin{cases}
\dfrac{\partial \widetilde{C}^j}{\partial t} = \mathcal{F}_1 \dfrac{\partial}{\partial \tilde{x}} \left(D_j \left(\dfrac{\partial \widetilde{C}^j}{\partial \tilde{x}} + z_j \widetilde{C}^j \dfrac{\partial \widetilde{\phi}}{\partial \tilde{x}} \right) \right) + \mathcal{F}_2 \dfrac{\partial \widetilde{C}^j}{\partial \tilde{x}}, & \text{(6.4.4a)} \\
\qquad \text{for } t > 0,\ 0 < \tilde{x} < x_d(t'), j \in [\![0,M-1]\!], & \\
\sqrt{\mathcal{F}_1} \cdot \left(D_0 \dfrac{\partial \widetilde{C}^0}{\partial \tilde{x}} + z_0\, D_0\, \widetilde{C}^0 \dfrac{\partial \widetilde{\phi}}{\partial \tilde{x}} \right) = (1 - b\, \widetilde{C}^0) \widehat{f}(\widetilde{\phi},\widetilde{C}^0), & \text{(6.4.4b)} \\
\qquad \text{at } \tilde{x} = x_d(t') \quad (j = 0), & \\
\sqrt{\mathcal{F}_1} \cdot \left(D_j \dfrac{\partial \widetilde{C}^j}{\partial \tilde{x}} + z_j D_j \widetilde{C}^j \dfrac{\partial \widetilde{\phi}}{\partial \tilde{x}} \right) = -b\, \widetilde{C}^j\, \widehat{f}(\widetilde{\phi},\widetilde{C}^0), & \text{(6.4.4c)} \\
\qquad \text{at } \tilde{x} = x_d(t') \quad (j = 1,\cdots,M-1), & \\
\widetilde{C}^j(0,t) = a_j, \quad t > 0 \quad (j = 0,\cdots,M-1), & \text{(6.4.4d)} \\
\widetilde{C}^j(\tilde{x},0) = \widetilde{C}^{0,j}(\tilde{x}) \quad \tilde{x} \in (0,x_d(t')) \quad (j = 0,\cdots,M-1), & \text{(6.4.4e)}
\end{cases}$$

$$\begin{cases}
\displaystyle\sum_{j=0}^{M-1} z_j \widetilde{C}^j(\tilde{x},t) = 0, \quad t > 0,\ 0 \leqslant \tilde{x} \leqslant x_d(t'), & \text{(6.4.5a)} \\
\widetilde{\phi}(0,t) = 0, \quad t > 0, & \text{(6.4.5b)} \\
\widetilde{\phi}(\tilde{x},0) = \widetilde{\phi}^0(\tilde{x}), \quad \tilde{x} \in (0,x_d(t')), \text{(see subsection 6.4.3)}, & \text{(6.4.5c)}
\end{cases}$$

along with the free boundary condition

$$\dot{x}_d(t) = b\, \widehat{f}(\widetilde{\phi},\widetilde{C}^0) \text{ at } \tilde{x} = x_d(t'), \tag{6.4.6}$$

where $b = C_0 N_{\mathrm{Fe}}^{-1}$ is the non-dimensional molar volume of solid iron (see (6.2.35)),

$$\mathcal{F}_1 = \mathcal{F}_1(t) = \left(\frac{x_d(t')}{x_d(t)} \right)^2, \quad \mathcal{F}_2 = \mathcal{F}_2(\tilde{x},t) = \frac{x_d'(t)}{x_d(t)} \tilde{x}. \tag{6.4.7}$$

and $\widehat{f}(\widetilde{\phi},\widetilde{C}^0)$ is given in (6.2.25), namely

$$\widehat{f}(\widetilde{\phi},\widetilde{C}^0) = \widehat{k}_a \exp\left(-(\widetilde{\phi} - \widehat{\phi}_m) \right) - \widehat{k}_c \frac{C_0}{C_{\mathrm{ref}}} \widetilde{C}^0 \exp\left(\widetilde{\phi} - \widehat{\phi}_m \right), \tag{6.4.8}$$

where the constants $\widehat{\phi}_m, \widehat{k}_a$ and $\widehat{\mathrm{k}}_{\mathrm{c}}$ in (6.4.8) are given in (6.2.21).

Later, we describe a numerical scheme for solving the ALE formulation (6.4.4)–(6.4.5)–(6.4.6).

For notational simplicity we will drop the symbol $\widetilde{\ }$ from the notations $\widetilde{C}$, $\widetilde{\phi}$ and $\tilde{x}$.

6.4.3 Determination of the initial discrete profile of the potential

In this section, we determine the initial discrete profile of the potential ϕ^0 into the pit solution from a given initial concentration $(C^{0,j} := C^j(\,\cdot\,,0))_{j\in\{0,..,M-1\}}$ and initial pit depth x_d^0. The initial potential $(\phi^0 := \phi(\,\cdot\,,0))$ satisfies the system given by (6.3.1), namely

System satisfied by the initial potential ϕ^0

$$\begin{cases} \dfrac{\partial}{\partial x}\left(\sigma_1\dfrac{\partial\phi^0}{\partial x}\right) + \displaystyle\sum_{j=0}^{M-1}\frac{\partial}{\partial x}\left(z_jD_j\frac{\partial C^{0,j}}{\partial x}\right) = 0, \qquad 0 < x < x_d(0), & \text{(6.4.9a)}\\[2ex] \sigma_1\dfrac{\partial\phi^0}{\partial x} + \displaystyle\sum_{j=0}^{M-1} z_jD_j\frac{\partial C^{0,j}}{\partial x} = 2\widehat{f}(\phi^0,C^{0,0}), \qquad \text{at } x = x_d(0), & \text{(6.4.9b)}\\[2ex] \phi^0(0) = 0, & \text{(6.4.9c)} \end{cases}$$

where $\sigma_1 := \displaystyle\sum_{j=0}^{M-1} z_j^2D_j\,C^{0,j}$ and $C^{0,0}$ is the initial metallic cation concentration.

First, the space interval $[0,x_d^0]$ is uniformly discretized using (N+1) points. The equidistant grid points are given by

$$x_i^0 = i\,\Delta x \;\text{ for }\; i = 0,1,\cdots,N,\;\; \Delta x = \frac{x_N^0}{N} = \frac{x_d^0}{N} > 0. \tag{6.4.10}$$

We consider the approximations $\phi_i^0 \approx \phi^0(x_i^0)$, $C_i^{0,j} \approx C^{0,j}(x_i^0)$ for $i = 0,\cdots,N$ and $j = 0,\cdots,M-1$.

From (6.3.6) and (6.4.9), it follows that

$$\phi_x^0 = -\frac{\sigma_2}{\sigma_1} + \frac{2\widehat{f}(P(0),C^{0,0}(x_d^0))}{\sigma_1}, \tag{6.4.11}$$

where

$$\sigma_1 := \sum_{j=0}^{M-1} z_j^2D_j\,C^{0,j} \;\text{ and }\; \sigma_2 := \sum_{j=0}^{M-1} z_jD_j(C^{0,j})_x. \tag{6.4.12}$$

We have that

$$P(0) = \phi^0(x_d^0), \tag{6.4.13}$$

which satisfies (6.3.7), namely,

$$P(0) + A(0) - 2\widehat{f}(P(0),C^{0,0}(x_d^0))B(0) = 0 \tag{6.4.14}$$

where

$$A(0) = \int_0^{x_d^0}\frac{\sigma_2}{\sigma_1}dx, \quad B(0) = \int_0^{x_d^0}\frac{dx}{\sigma_1} \;\text{ and} \tag{6.4.15}$$

$$\widehat{f}\left(P(0),C^{0,0}(x_d^0)\right) = \widehat{k}_a\exp\left(-(P(0)-\widehat{\phi}_m)\right) - \widehat{k}_c\frac{C_0}{C_{\text{ref}}}C^{0,0}(x_d^0)\exp\left(P(0)-\widehat{\phi}_m\right).$$

Next, we consider the following approximations:

- We approximate the value of the potential at the pit bottom $P(0)$ defined in (6.4.13) by $P(0) \approx P_0$.

- We consider the approximations $\phi_x^0(x_i^0) \approx \delta\phi_i^0$, $\left(C^{0,j}\right)_x(x_i) \approx \delta C_i^{0,j}$, $\sigma_1(x_i^0) \approx \sigma_{1,i}$ and $\sigma_2(x_i^0) \approx \sigma_{2,i}$ for $i = 0, \cdots, N$.

Computation of $\sigma_{1,i}$ for $i = 0, \cdots, N$:

$$\sigma_{1,i} = \sum_{j=0}^{M-1} z_j^2 D_j C_i^{0,j}, \quad \text{for } i = 0, \cdots, N. \tag{6.4.16}$$

Computation of $\sigma_{2,i}$ for $i = 0, \cdots, N$:

In view of (6.4.12), it follows that

$$\sigma_{2,i} = \sum_{j=0}^{M-1} z_j D_j \, \delta C_i^{0,j}, \quad \text{for } i = 0, \cdots, N \tag{6.4.17}$$

where **for i=0** :

$$\delta C_0^{0,j} = \frac{-3C_0^{0,j} + 4C_1^{0,j} - C_2^{0,j}}{2\,\Delta x}, \tag{6.4.18}$$

for i= $1, \cdots, N-1$:

$$\delta C_i^{0,j} = \frac{C_{i+1}^{0,j} - C_{i-1}^{0,j}}{2\,\Delta x}, \tag{6.4.19}$$

for i=N : (cf. [25, 41])

$$\delta C_N^{0,j} = \frac{3C_N^{0,j} - 4C_{N-1}^{0,j} + C_{N-2}^{0,j}}{2\,\Delta x}. \tag{6.4.20}$$

Computation of A_0 **an approximate value of** $A(0)$ **(see**(6.4.15)**) :**

- σ_2 is approximated by the vector $\tilde{\sigma}_2 = (\sigma_{2,0}, \cdots, \sigma_{2,N})$ and σ_1 is approximated by the vector $\tilde{\sigma}_1 = (\sigma_{1,0}, \cdots, \sigma_{1,N})$.
- We interpolate $\dfrac{\tilde{\sigma}_2}{\tilde{\sigma}_1}$ by a cubic spline **s**.
- Finally, we deduce the value of A_0 by computing the integral $\displaystyle\int_0^{x_d^0} \mathbf{s}\, dx$ by an appropriate numerical method.

Similarly, we determine the value of B_0 an approximate value of $B(0)$ (see(6.4.15)).

Then, once A_0 and B_0 are known, the value P_0 is determined from (6.4.14) by using the Newton method. Here, only P_0 is unknown.

Next, once P_0 is known, it follows from (6.4.11) and (6.4.14) that

$$\delta\phi_i^0 = g_i = -\frac{\sigma_{2,i}}{\sigma_{1,i}} + \frac{P_0 + A_0}{B_0\,\sigma_{1,i}} \quad \text{for} \quad i = 0, \cdots, N-2, \tag{6.4.21}$$

where we have set

$$\delta\phi_i^0 := \begin{cases} \dfrac{-3\phi_0^0 + 4\phi_1^0 - \phi_2^0}{2\Delta x} & \text{for} \quad i = 0, \\ \dfrac{\phi_{i+1}^0 - \phi_{i-1}^0}{2\Delta x} & \text{for} \quad i = 1, \cdots, N-2. \end{cases} \tag{6.4.22}$$

We also have from (6.4.9c) that

$$\phi_0^0 = 0. \tag{6.4.23}$$

Finally, we deduce from (6.4.21), (6.4.22) and (6.4.23) the discretized profile of the initial potential $\phi^0 = (\phi_i^0)_{i\in\{0,\cdots,N\}}$ by solving the linear system

$$\begin{pmatrix} 4 & -1 & 0 & 0 & \cdots & 0 \\ 0 & 1 & 0 & 0 & \cdots & 0 \\ -1 & 0 & 1 & 0 & \ddots & \vdots \\ 0 & \ddots & \ddots & \ddots & \ddots & 0 \\ \vdots & \ddots & \ddots & \ddots & \ddots & 0 \\ 0 & \cdots & 0 & -1 & 0 & 1 \end{pmatrix} \begin{pmatrix} \phi_1^0 \\ \phi_2^0 \\ \phi_3^0 \\ \vdots \\ \vdots \\ \phi_{N-1}^0 \end{pmatrix} = 2\Delta x \begin{pmatrix} g_0 \\ g_1 \\ g_2 \\ \vdots \\ \vdots \\ g_{N-2} \end{pmatrix} + \begin{pmatrix} 3\phi_0^0 \\ \phi_0^0 \\ 0 \\ \vdots \\ \vdots \\ 0 \end{pmatrix}, \tag{6.4.24}$$

and

$$\phi_N^0 = P_0. \tag{6.4.25}$$

6.4.4 Time and space discretizations: the semi-implicit scheme

Now we describe the time and space approximations for the ALE formulation (6.4.4)–(6.4.5)–(6.4.6).

Let $\Delta t > 0$ be the discretization time step such that $t^n = n\ \Delta t$ be the discrete times for $n \in \mathbb{N}^*$. The time increment $\Delta t = t^n - t^{n-1}$ varies with n.

We use $(N+1)$ equidistant grid points:

$$x_i^n = i\ \Delta x \ \text{ for } \ i = 0,1,\cdots,N,\ \Delta x = \frac{x_N^n}{N} \ \text{ for } \ n \in \mathbb{N}^*. \tag{6.4.26}$$

Note here that Δx also depends on n, so that the equidistant grid points are moving in time.

We consider the approximations $C_i^{n,j} \simeq C^j(x_i^n,t^n)$ for j= 0,..,M-1, $\phi_i^n \simeq \phi(x_i^n,t^n)$ and $x_d^n = x_N^n \simeq x_d(t^n)$ of the solution $\left(\{C^j\}_{j=0,..,M-1},\ \phi,\ x_d\right)$ of (6.4.4)–(6.4.5)–(6.4.6) at time $t = t^n$.

Starting with

$$x_d^0 = x_d(0), \quad C_i^{0,j} = C^j(x_i,0) \ \text{ and } \ \phi^0 = \phi(x_i,0);\ i = 0,\cdots,N;\ j = 0,\cdots,M-1, \tag{6.4.27}$$

we compute $(\{C_i^{n+1,j}\}_{j=0,..,M-1},\phi_i^{n+1},x_d^{n+1})$ from $(\{C_i^{n,j}\}_{j=0,..,M-1},\phi_i^n,x_d^n)$ for $n \geq 0$ and $i = 0,\cdots,N$, according to the following decoupling scheme of the ALE system (6.4.4)–(6.4.5)–(6.4.6).

The initial potential ϕ^0 given in (6.4.27) is determined in subsection 6.4.3 above.

Define the forward and backward differencing operators:

$$\left(\mathcal{D}_{\Delta x}^+ u\right)_i = \frac{u_{i+1} - u_i}{\Delta x}, \quad \left(\mathcal{D}_{\Delta x}^- u\right)_i = \frac{u_i - u_{i-1}}{\Delta x}. \tag{6.4.28}$$

Algorithm Semi-discretization in time for the one dimensional model with the ALE formulation (6.4.4)–(6.4.5)–(6.4.6): the discretization in time.

1. Interface displacement : computation of the new position x_d^{n+1} of the interface using the Butler-Volmer formula

$$x_d^{n+1} = x_d^n + v^n \Delta t \quad \text{with} \quad v^n = b\,\widehat{f}(\phi_N^n, C_N^{n,0}) \quad \text{at} \quad x = x_d^n = x_N^n, \tag{6.4.29}$$

   i.e. with $v^n \simeq x_d'(t^n)$ (forward Euler), where $\widehat{f}(\phi_N^n, C_N^{n,0})$ is given by (see (6.4.8))

$$\widehat{f}(\phi_N^n, C_N^{n,0}) = \widehat{k}_a \exp\big(-(\phi_N^n - \widehat{\phi}_m)\big) - \widehat{k}_c \frac{C_0}{C_{\text{ref}}} C_N^{n,0} \exp(\phi_N^n - \widehat{\phi}_m). \tag{6.4.30}$$

   We choose Δt small enough so that $v^n \Delta t$ does not exceed Δx.

2. Computation of $\widetilde{C}_i^{n,j}$ for $j = 0, \cdots, M-1$. We take $t' = t^{n+1}$ in (6.4.2), and define

$$\begin{array}{rcl} \psi^{n+1} : [0, x_d^n] & \longrightarrow & [0, x_d^{n+1}] \\ x & \longmapsto & \tilde{x} = \dfrac{x_d^{n+1}}{x_d^n} x \end{array} \tag{6.4.31}$$

   and

$$\widetilde{C}_i^{n,j} \approx \widetilde{C}^j(\psi^{n+1}(x_i), t^n) = \widetilde{C}^j(\tilde{x}_i, t^n) = C^j(x_i, t^n) \approx C_i^{n,j}. \tag{6.4.32}$$

   We choose $\widetilde{C}_i^{n,j} = C_i^{n,j}$ for $i = 0, \cdots, N$ and $j = 0, \cdots, M-1$.

Algorithm Semi-discretization in time for the one dimensional model with the ALE formulation (6.4.4)–(6.4.5)–(6.4.6): the discretization in time. (Continuation)

3. Computation of $C_i^{n+1,j}$ and ϕ_i^{n+1} for $j = 0, \cdots, M-1$; $i = 0, \cdots, N$. We take $t' = t^{n+1}$ in (6.4.4) at time $t = t^{n+1}$. We solve the following problem for $C_i^{n+1,j}$ and ϕ_i^{n+1} for $i = 0, \cdots, N$:

   - The electrodiffusion equations (6.4.4a) are discretized as :

$$\frac{C_i^{n+1,j} - C_i^{n,j}}{\Delta t} = -\left(\mathcal{D}^-_{\Delta x}\mathbf{J}^{n+1,j}\right)_i + \frac{b\,\widehat{f}(\phi_N^{n+1},C_N^{n+1,0})}{x_d^{n+1}} x_i^{n+1}\left(\mathcal{D}^-_{\Delta x}C^{n+1,j}\right)_i, \quad (6.4.33)$$

$$\text{for } \; j = 0, \cdots, M-1, \text{and } i = 1, \cdots, N-1, \quad \text{where}$$

$$\mathbf{J}_i^{n+1,j} = -D_j\left(\left(\mathcal{D}^+_{\Delta x}C^{n+1,j}\right)_i + z_j\left(\frac{C_{i+1}^{n+1,j} + C_i^{n+1,j}}{2}\right)\left(\mathcal{D}^+_{\Delta x}\phi^{n+1}\right)_i\right) \quad \text{for } i = 1, \cdots, N-1. \quad (6.4.34)$$

   - The boundary condition at $x = x_N^{n+1} = x_d^{n+1}$ for the metallic cation (6.4.4b) is discretized as:

$$\mathbf{J}_N^{n+1,0} = -(1 - b\,C_N^{n+1,0})\;\widehat{f}(\phi_N^{n+1},C_N^{n+1,0}), \text{ for } j = 0. \quad (6.4.35)$$

   - The boundary condition at $x = x_N^{n+1} = x_d^{n+1}$ for the other ions (6.4.4c) is discretized as:

$$\mathbf{J}_N^{n+1,j} = b\,C_N^{n+1,j}\;\widehat{f}(\phi_N^{n+1},C_N^{n+1,0}), \text{ for } j = 1, \cdots, M-1, \quad \text{where} \quad (6.4.36)$$

$$\mathbf{J}_N^{n+1,j} = -D_j\left(\frac{3\,C_N^{n+1,j} - 4\,C_{N-1}^{n+1,j} + C_{N-2}^{n+1,j}}{2\Delta x} + z_j\,C_N^{n+1,j}\left(\frac{3\phi_N^{n+1} - 4\phi_{N-1}^{n+1} + \phi_{N-2}^{n+1}}{2\Delta x}\right)\right). \quad (6.4.37)$$

   - The boundary conditions at $x = x_0^{n+1} = 0$ (6.4.4d) and (6.4.5b) are given by

$$C_0^{n+1,j} = a_j \;\text{ such that }\; \sum_{j=0}^{M-1} z_j\,C_0^{n+1,j} = 0, \;\; \phi_0^{n+1} = 0. \quad (6.4.38)$$

   - The electroneutrality condition (6.4.5a) is dicretized as :

$$\sum_{j=0}^{M-1} z_j\,C_i^{n+1,j} = 0 \;\text{ for }\; i = 1, \cdots, N. \quad (6.4.39)$$

Note that, in the above condition (6.4.39), i runs from 1 to N.

The nonlinear problem (6.4.33)–(6.4.39) forms a system of $(M+1)\times(N+1)$ equations in $(M+1)\times(N+1)$ unknowns $\left(\{C_i^{n+1,j}\}_{j=0,\cdots,M-1}, \phi_i^{n+1} \;\text{ for }\; i = 0, \cdots, N\right)$. We use a **Newton method** to solve the above equations with $\left(\{C_i^{n,j}\}_{j=0,\cdots,M-1}, \phi_i^n \;\text{ for }\; i = 0, \cdots, N\right)$ as the initial guess.

6.4.4.1 Newton function

The problem (6.4.33)–(6.4.39) can be written as

$$\mathcal{F}(S) = 0, \quad (6.4.40)$$

where the unknowns are gathered in the vector S.

The vector S of the $(M+1)\times(N+1)$ unknowns is defined as follows

$$S_{j(N+1)+i} = C_i^{n+1,j} \quad \text{for} \quad j = 0,\cdots,M-1 \quad \text{and} \quad i = 0,\cdots N, \tag{6.4.41}$$

and

$$S_{M(N+1)+i} = \phi_i^{n+1} \quad \text{for} \quad i = 0,\cdots N. \tag{6.4.42}$$

$\mathcal{F}$ is a vector of $(M+1)\times(N+1)$ functions given as follows :

- Equations for all the species concentrations at the boundary $x = x_0^{n+1} = 0$ (see (6.4.38))

$$\mathcal{F}_j = C_0^{n+1,j} - a_j \quad \text{for} \quad j = 0,\cdots,M-1. \tag{6.4.43}$$

- Equations for the electrodiffusion of all the species at interior points (see (6.4.33), (6.4.28), (6.4.30) and (6.4.34))

$$\mathcal{F}_{M+j(N-1)+i-1} = \tag{6.4.44}$$

$$C_i^{n+1,j} - C_i^{n,j} + \Delta t\left(\mathcal{D}^-_{\Delta x}\mathbf{J}^{n+1,j}\right)_i - \Delta t\,\frac{b\,\widehat{f}(\phi_N^{n+1},C_N^{n+1,0})}{x_d^{n+1}}x_i^{n+1}\left(\mathcal{D}^-_{\Delta x}C^{n+1,j}\right)_i,$$

for $j = 0,\cdots,M-1$ and $i = 1,\cdots N-1$.

- Equation for the metallic cation concentration at the boundary $x = x_N^{n+1} = x_d^{n+1}$ (see(6.4.35), (6.4.30) and (6.4.37))

$$\mathcal{F}_{M+M(N-1)} = \mathbf{J}_N^{n+1,0} + (1 - b\,C_N^{n+1,0})\,\widehat{f}(\phi_N^{n+1},C_N^{n+1,0}). \tag{6.4.45}$$

- Equations for the other ions concentrations at the boundary $x = x_N^{n+1} = x_d^{n+1}$ (see(6.4.36), (6.4.30) and (6.4.37))

$$\mathcal{F}_{M+M(N-1)+j} = \mathbf{J}_N^{n+1,j} - b\,C_N^{n+1,j}\,\widehat{f}(\phi_N^{n+1},C_N^{n+1,0}) \quad \text{for} \quad j = 1,\cdots,M-1. \tag{6.4.46}$$

- Equation for the potential at the entrance of the pit $x = x_0^{n+1} = 0$ (see (6.4.38))

$$\mathcal{F}_{M+MN} = \phi_0^{n+1}. \tag{6.4.47}$$

- Equation for the electroneutrality at the pit solution (see (6.4.39))

$$\mathcal{F}_{M+MN+i} = \sum_{j=0}^{M-1} z_j\,C_i^{n+1,j} \quad \text{for} \quad i = 1,\cdots N. \tag{6.4.48}$$

6.4.4.2 The Jacobian matrix from the Newton function

Let $\mathcal{J}(S)$ with S given by (6.4.41)–(6.4.42) be the Jacobian matrix of the Newton function $\mathcal{F}$ given by (6.4.43)–(6.4.48).

The matrix $\mathcal{J}$ is of order $(M+1).(N+1)\times(M+1).(N+1)$. Next, we complete $\mathcal{J}$ as follows

- Derivative of $\{\mathcal{F}_j\}_{j=0,\cdots,M-1}$ (see (6.4.43)) with respect to $C_0^{n+1,j}$

$$\mathcal{J}_{j,j(N+1)} = 1 \quad \text{for} \quad j = 0,\cdots,M-1. \tag{6.4.49}$$

- Let α_j, k_1 and k_2 be defined as follows

$$\alpha_j := \frac{\Delta t\ D_j}{\Delta x^2}, \tag{6.4.50}$$

$$k_1 := M + j(N-1) + i - 1, \tag{6.4.51}$$

$$k_2 := j(N+1) + i, \tag{6.4.52}$$

$$k_3 := M(N+1) + i. \tag{6.4.53}$$

- The derivative of the Butler-Volmer flux $\widehat{f}(\phi_N^{n+1},C_N^{n+1,0})$
  - ✤ with respect to $C_N^{n+1,0}$

$$\partial_C \text{fBV} = -\widehat{k}_c \frac{C_0}{C_{\text{ref}}} \exp\left(\phi_N^{n+1} - \widehat{\phi}_m\right). \tag{6.4.54}$$

  - ✤ with respect to ϕ_N^{n+1}

$$\partial_\phi \text{fBV} = -\widehat{k}_a \exp\left(-\left(\phi_N^{n+1} - \widehat{\phi}_m\right)\right) - \widehat{k}_c \frac{C_0}{C_{\text{ref}}} C_N^{n+1,0} \exp\left(\phi_N^{n+1} - \widehat{\phi}_m\right). \tag{6.4.55}$$

- The derivative of $\{\mathcal{F}_{M+j(N-1)+i-1}\}$ (see (6.4.44)) for $j = 0,\cdots,M-1$ and $i = 1,\cdots,N-1$
  - ✓ with respect to $C_{i-1}^{n+1,j}$ for $(j,i) \in [\![0,M-1]\!] \times [\![1,N-1]\!]$

$$\mathcal{J}_{k_1,k_2-1} = \alpha_j\left(-1 + \frac{z_j \Delta x}{2}\left(\mathcal{D}^-_{\Delta x}\phi^{n+1}\right)_i\right) + \Delta t\ \frac{b\,\widehat{f}(\phi_N^{n+1},C_N^{n+1,0})}{x_d^{n+1}} x_i^{n+1}, \tag{6.4.56}$$

  - ✓ with respect to $C_i^{n+1,j}$ for $(j,i) \in [\![0,M-1]\!] \times [\![1,N-1]\!]$

$$\mathcal{J}_{k_1,k_2} = \tag{6.4.57}$$

$$1 - \alpha_j\left(-2 + \frac{z_j \Delta x}{2}\left(\left(\mathcal{D}^+_{\Delta x}\phi^{n+1}\right)_i - \left(\mathcal{D}^-_{\Delta x}\phi^{n+1}\right)_i\right)\right) - \Delta t\ \frac{b\,\widehat{f}(\phi_N^{n+1},C_N^{n+1,0})}{x_d^{n+1}} x_i^{n+1},$$

  - ✓ with respect to $C_{i+1}^{n+1,j}$ for $(j,i) \in [\![0,M-1]\!] \times [\![1,N-1]\!]$

$$\mathcal{J}_{k_1,k_2+1} = -\alpha_j\left(1 + \frac{z_j \Delta x}{2}\left(\mathcal{D}^+_{\Delta x}\phi^{n+1}\right)_i\right), \tag{6.4.58}$$

  - ✓ with respect to $C_N^{n+1,0}$ for $(j,i) \in [\![0,M-1]\!] \times [\![1,N-1]\!] \backslash \{(j,i) = (0,N-1)\}$

$$\mathcal{J}_{k_1,N} = \frac{-\Delta t\ x_i^{n+1}}{x_d^{n+1}}\ b\ \partial_C \text{fBV}\ \ \Delta x\ \left(\mathcal{D}^-_{\Delta x} C^{n+1,j}\right)_i, \tag{6.4.59}$$

  - ✓ with respect to ϕ_{i-1}^{n+1} for $(j,i) \in [\![0,M-1]\!] \times [\![1,N-1]\!]$

$$\mathcal{J}_{k_1,k_3-1} = -\alpha_j z_j \frac{C_i^{n+1,j} + C_{i-1}^{n+1,j}}{2}, \tag{6.4.60}$$

  - ✓ with respect to ϕ_i^{n+1} for $(j,i) \in [\![0,M-1]\!] \times [\![1,N-1]\!]$

$$\mathcal{J}_{k_1,k_3} = \alpha_j z_j \frac{C_{i-1}^{n+1,j} + 2\,C_i^{n+1,j} + C_{i-1}^{n+1,j}}{2}, \tag{6.4.61}$$

✓ with respect to ϕ_{i+1}^{n+1} for $(j,i) \in [\![0,M-1]\!] \times [\![1,N-1]\!]$

$$\mathcal{J}_{k_1,k_3+1} = -\alpha_j z_j \frac{C_{i+1}^{n+1,j} + C_i^{n+1,j}}{2}, \tag{6.4.62}$$

✓ with respect to ϕ_N^{n+1} for $(j,i) \in [\![0,M-1]\!] \times [\![1,N-2]\!]$

$$\mathcal{J}_{k_1,M(N+1)+N} = \frac{-\Delta t\ x_i^{n+1}}{x_d^{n+1}}\ b\ \partial_\phi \text{fBV}\ \ \Delta x\ \left(\mathcal{D}_{\Delta x}^- C^{n+1,j}\right)_i, \tag{6.4.63}$$

✓ with respect to ϕ_N^{n+1} for $(j,i) \in [\![0,M-1]\!] \times \{N-1\}$

$$\mathcal{J}_{l_1,l_2} = \tag{6.4.64}$$

$$-\alpha_j z_j \frac{C_N^{n+1,j} + C_{N-1}^{n+1,j}}{2} - \frac{\Delta t\ x_{N-1}^{n+1}}{x_d^{n+1}}\ b\ \partial_\phi \text{fBV}\ \ \Delta x\ \left(\mathcal{D}_{\Delta x}^- C^{n+1,j}\right)_{N-1},$$

where

$$l_1 = M + j(N+1) + N - 2 \quad \text{and} \quad l_2 = M(N+1) + N.$$

✓ with respect to $C_N^{n+1,0}$ for $(j,i) = (0,N-1)$

$$\mathcal{J}_{M+N-2,N} = \tag{6.4.65}$$

$$-\alpha_0\left(1 + \frac{z_0 \Delta x}{2}\ \left(\mathcal{D}_{\Delta x}^+ \phi^{n+1}\right)_{N-1}\right) - \frac{\Delta t\ x_{N-1}^{n+1}}{x_d^{n+1}}\ b\ \partial_C \text{fBV}\ \ \Delta x\ \left(\mathcal{D}_{\Delta x}^- C^{n+1,j}\right)_{N-1}.$$

- Let k_4 and k_5 be defined as follows

$$k_4 := M + M(N-1) + j, \tag{6.4.66}$$

$$k_5 := j(N+1). \tag{6.4.67}$$

- The derivative of $\{\mathcal{F}_{M+M(N-1)+j}\}$ for $j = 0, \cdots, M-1$ (see (6.4.45) and (6.4.46))

✓ with respect to $C_{N-2}^{n+1,j}$ for $j \in [\![0,M-1]\!]$

$$\mathcal{J}_{k_4,k_5+(N-2)} = \frac{D_j}{2\Delta x}, \tag{6.4.68}$$

✓ with respect to $C_{N-1}^{n+1,j}$ for $j \in [\![0,M-1]\!]$

$$\mathcal{J}_{k_4,k_5+(N-1)} = \frac{-4\ D_j}{2\Delta x}, \tag{6.4.69}$$

✓ with respect to $C_N^{n+1,j}$ for $j \in [\![0,M-1]\!]$

$$\mathcal{J}_{k_4,k_5+N} = \frac{3\ D_j}{2\Delta x} + \frac{z_j\ D_j}{2\Delta x}\left(3\phi_N^{n+1} - 4\phi_{N-1}^{n+1} + \phi_{N-2}^{n+1}\right) + b\ \widehat{f}(\phi_N^{n+1}, C_N^{n+1,0}), \tag{6.4.70}$$

✓ with respect to $C_N^{n+1,0}$ for $j \in [\![1, M-1]\!]$

$$\mathcal{J}_{k_4,N} = b\ C_N^{n+1,j}\ \partial_C \text{fBV}, \tag{6.4.71}$$

✓ with respect to ϕ_{N-2}^{n+1} for $j \in [\![0,M-1]\!]$

$$\mathcal{J}_{k_4,M(N+1)+(N-2)} = \frac{D_j\ z_j\ C_N^{n+1,j}}{2\Delta x}, \tag{6.4.72}$$

✓ with respect to ϕ_{N-1}^{n+1} for $j \in [\![0, M-1]\!]$

$$\mathcal{J}_{k_4, M(N+1)+(N-1)} = \frac{-4\, D_j\, z_j\, C_N^{n+1,j}}{2\Delta x}, \tag{6.4.73}$$

✓ with respect to ϕ_N^{n+1} for $j \in [\![1, M-1]\!]$

$$\mathcal{J}_{k_4, M(N+1)+N} = \frac{3\, D_j\, z_j\, C_N^{n+1,j}}{2\Delta x} + b\, C_N^{n+1,j}\, \partial_\phi \text{fBV}, \tag{6.4.74}$$

✓ with respect to ϕ_N^{n+1} for $j = 0$

$$\mathcal{J}_{M+M(N-1), M(N+1)+N} = \frac{3\, D_0\, z_0\, C_N^{n+1,0}}{2\Delta x} - (1 - b\, C_N^{n+1,0})\, \partial_\phi \text{fBV}, \tag{6.4.75}$$

✓ with respect to $C_N^{n+1,0}$ for $j = 0$

$$\mathcal{J}_{M+M(N-1), N} = \frac{3\, D_0}{2\Delta x} + \frac{z_0\, D_0}{2\Delta x}\left(3\phi_N^{n+1} - 4\phi_{N-1}^{n+1} + \phi_{N-2}^{n+1}\right) \tag{6.4.76}$$
$$+ b\, \widehat{f}(\phi_N^{n+1}, C_N^{n+1,0}) + (b\, C_N^{n+1,0} - 1)\, \partial_C \text{fBV}.$$

- The derivative of $\{\mathcal{F}_{M+MN}\}$ (see (6.4.47))

  ✓ with respect to ϕ_0^{n+1}

$$\mathcal{J}_{M+MN, M(N+1)} = 1. \tag{6.4.77}$$

- The derivative of $\{\mathcal{F}_{M+MN+i}\}$ for $j = 0, \cdots, M-1$ and $i = 1, \cdots, N$ (see (6.4.48))

  ✓ with respect to $C_i^{n+1,j}$

$$\mathcal{J}_{M+MN+i, j(N+1)+i} = z_j. \tag{6.4.78}$$

Once the Jacobian matrix $\mathcal{J} = \mathcal{J}(S)$ of $\mathcal{F}$ is known, the Newton method is built by introducing a sequence of vector $(S^k)_{k \geqslant 0}$ satisfying the linear system

$$\mathcal{J}(S^k)\,(S^{k+1} - S^k) = -\mathcal{F}(S^k) \tag{6.4.79}$$

with $\mathcal{J}(S^k)$ is the Jacobian matrix of $\mathcal{F}$ evaluated at $S = S^k$.

We obtain S^{k+1} from S^k by solving the linear system (6.4.79).

6.5 Numerical simulations for the three ions model

In this section, we present numerical simulations of solutions of the original system (6.3.1)–(6.3.3) along with the free boundary condition (6.3.4). The main objective of this section is to identify the major factors governing the propagation of the pit. We recall that the pit is subject to an anodic potentiostatic control as mentioned when we defined the Butler-Volmer formula (6.2.15). It is equivalent to a situation in which the cathodic reaction on the outer surface of the material is never rate limiting. This situation of corrosion does not correspond to reality, but it is nevertheless the most unfavorable case for the material; it indicates the most severe conditions under which the pitting is susceptible to propagate.

Remark 6.5.1. *The kinetic laws of iron oxidation remain multiple and uncertain [79]. Therefore, the objective of this section also includes the evaluation of the choice of the Butler-Volmer formula as an oxidation rate law on the corrosion propagation process. This formula in its dimensionless form is given by* (6.3.2).

6.5.1 Main features of the corrosion model to be studied

Next, we briefly recall the physical and mathematical characteristics of the model to be studied (6.3.1)–(6.3.3)–(6.3.4).

Remark 6.5.2. *The model* (6.3.1)–(6.3.3)–(6.3.4) *is only valid for dilute solutions.*

Physical characteristics:

- The physical system: pit propagation on **pure iron** (Fe) in aqueous sodium chloride (NaCl) solutions (**dilute-solutions**); case where the pit is always active (**dissolution part**).
- Geometry of the pit: **one-dimensional pit** where corrosion occurs only at the bottom of the pit (the walls of the pit are inert). Indeed, cracks are often viewed as being one-dimensional slots of length l, such that l is much greater than the opening displacement w [16]. In this case, only metal dissolution at the bottom is assumed. Please note that a one-dimensional pit should be represented as an interval with moving boundary $[0,x_d(t))$ but in order to indicate all the necessary physical parameters, we present it as shown in Figure 6.5.1 (as a rectangle).

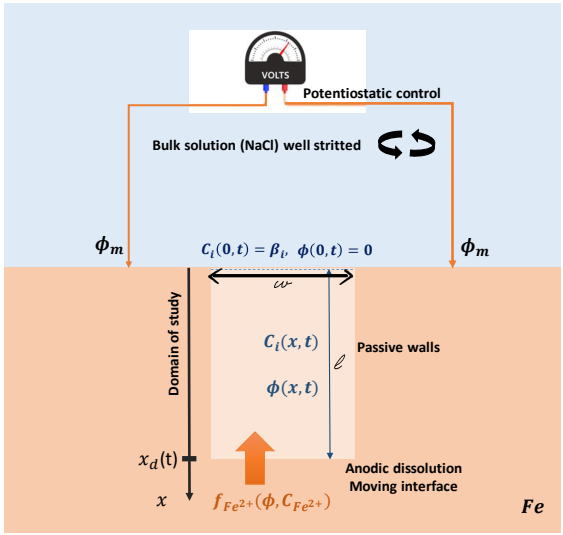

Figure 6.5.1: One space dimension pit for $l \gg w$.

- The model describes only **anodic dissolution** under **potentiostatic control** using the **Butler-Volmer formula**.
- Aqueous chemical species to be considered in the system: Fe^{2+}, Na^+ and Cl^-.
- Ionic transfer in the pit solution (transport mechanisms): ionic **diffusion** and **electromigration.**
- **Chemical reactions in the pit solution (hydrolysis of cations) are only considered in Section 6.6.**
- **Precipitation of the salt film is not considered in this chapter.**
- **The model approximates Poisson's equation with the equation of local electroneutrality.**

Mathematical characteristics:

- The domain of study is represented by the pit solution given by the interval $(0,x_d(t))$ where $x = 0$ denotes the entrance of the pit and $x_d(t)$ the bottom of the pit at time t.
- the unknowns of the system are: concentrations of chemical species in the pit solution $\{C_i\}_{i\in\{Fe^{2+},Na^{+},Cl^{-}\}}$, potential ϕ where all of them are functions of time and space and finally the bottom of the pit x_d which is a function of time.
- It is a parabolic problem for the concentrations $\{C_i\}$ and an elliptic one for the potential ϕ.
- We impose the Dirichlet boundary conditions at the entrance of the pit, so that, $C_{\mathrm{Fe}^{2+}}, C_{\mathrm{Na}^{+}}, C_{\mathrm{Cl}^{-}}, \phi$ always remain constant at $x = 0$.
- We consider Robin boundary conditions at the bottom of the pit for $\{C_i\}$ and ϕ.
- The corrosion speed $\dot{x}_d(t)$ is governed by the Butler-Volmer formula at the pit bottom to describe the moving motion.
- The mathematical model is a fully non-dimensional system given by (6.3.1)–(6.3.3)–(6.3.4); **it is a time evolution problem which describes a local electroneutrality–concentrations coupled system with moving interface.**

For numerical scheme, we have considered:

- an Arbitrary Lagrangian Eulerian (ALE) formulation of the system (6.3.1)–(6.3.3) to handle the displacement of the moving interface given by (6.3.4),
- an explicit Euler scheme for the displacement of the moving interface and a time implicit scheme for the diffusion-electromigration equations in an ALE framework,
- a full discretization scheme with finite differences in space and time,
- an adaptive time-step and uniformly discretized space intervals (evolving with time) using a fixed number N of intervals.

Finally, we have used Newton's method to solve the full system.

Main output of the pit model under potentiostatic condition:

- the distribution of potential $\phi(x,t)$ in the pit $(0,x_d(t))$,
- concentration profile $C_i(x,t)$ of each chemical species $i \in \{\mathrm{Fe}^{2+}, \mathrm{Na}^{+}, \mathrm{Cl}^{-}\}$ (chemistry of the solution),
- speed of propagation of the pit (rate of corrosion at any time).

After outlining the main characteristics of the model to be studied, we recall that the aim of this model is to be entirely self-consistent, predictive and to reproduce experimental data both accurately and consistently. In particular, the cavity growth rates and the solution chemistry should be reproduced, so that, after providing the mathematical details of the development of the pit corrosion model, the next step is to validate this model against similar previous studies.

6.5.2 Comparison of the numerical model with existing modeling results

To validate the mathematical model, the numerical simulations will be compared with similar one-dimensional models discussed in literature. Sharland [64, 66, 68] and Tasker [68] have developed a predictive mathematical model incorporating the **electrochemical, chemical and ionic migra -tion processes**. Their model predicts the **steady-state solution chemistry** and the **electrode potential** within **a corroding crevice or pit**.

In the case of **propagation of a crevice-type corrosion** with both passive and active walls, Sharland [64] solved her model using a number of mathematical approximations based on physical observations. In fact, she considered that the cavity propagation was slow compared to the ionic transport, so that the moving boundary effects was ignored. In other word, the geometry of the crevice was kept constant, which was a very rough approximation since a real crevice never reaches a steady state mainly because of its shape evolution [64, 68].

Mousson, Vuillemin, Oltra, Grusset, Santarini and Combrade [52] reproduced the same simulation to describe the propagation of a crevice corrosion in the case of active walls. Contrary to Sharland who solved her system using a number of mathematical approximations, Mousson and al. used a commercial code. This code was developed using the Chemical Engineering Module FEMLAB which is a MATLAB-based tool for finite element methods. They have shown the ability of this software to be used for crevice corrosion on iron by comparing their results with those of Sharland [64, 68].

Remark 6.5.3. ***In our case, our developed mathematical model*** (6.3.1)–(6.3.3) ***and*** (6.3.4) ***is able to describe the propagation of both pit and crevice corrosion.***

Before comparing the results given by our model (6.3.1)–(6.3.3)–(6.3.4) with those found by Sharland [68], we present the main differences between these models are presented in Table 6.2 :

	Sharland [64, 68]	Our model (6.3.1)–(6.3.3)–(6.3.4)
Crevice geometry	A fixed rectangular shaped crevice with a width "w" and a depth "l", with $l \gg w$. The depth of the crevice is kept constant.	A one-dimensional crevice where corrosion occurs only at the bottom. We consider a moving boundary.
Walls	Both passive and active walls.	Passive walls; only the base is active.
Aqueous chemical species considered in the system	$Fe^{2+}, Na^+, Cl^-, OH^-, H^+, Fe(OH)^+$.	Fe^{2+}, Na^+, Cl^-.
Transport equation	Steady-state transport equation.	Time evolution transport equation.
Homogeneous reactions	Two chemical reactions are considered: 1. $Fe^{2+} + H_2O \rightleftharpoons Fe(OH)^+ + H^+$, 2. $H^+ + OH^- \rightleftharpoons H_2O$.	Without reaction.
Electrochemical reactions and kinetics	Oxidation of iron: 1. $Fe \rightarrow Fe^{2+} + 2\ e^-$, reduction of water: 2. $H_2O + e^- \rightarrow OH^- + H$, the hydrogen discharge reaction: 3. $2H^+ + 2\ e^- \rightarrow H_2$. These electrochemical reactions are described using Tafel kinetics given in the form: $i = i_0 \exp\left(\frac{\alpha\, EF}{RT}\right)$ where α and i_0 are determined from empirical data and E is the electrode potential measured on the SCE scale.	Oxidation of iron: 1. $Fe \rightarrow Fe^{2+} + 2\ e^-$ The iron oxidation is described using Butler-Volmer kinetics $f_{Fe^{2+}}(\phi, C_{Fe^{2+}})$ given by (6.2.15).
Method for solving the system	Solving a coupled system of differential equations: series of algebraic equations using numerical approximations which limit the accuracy of the model's predictions [66].	Solving a coupled system of nonlinear partial differential equations with moving interface. The numerical scheme is described in Section 6.4.

Table 6.2: Comparison of the developed model (6.3.1)–(6.3.3)–(6.3.4) with previous studies to describe the propagation of a crevice under potentiostatic conditions.

Remark 6.5.4 (Comparison with Sharland model)**.** *The objective of this first comparison is to emphasize the importance of taking into account the interface motion for more accurate prediction results. The main profiles to be considered in this comparison are the evolution of both the solution chemistry and the potential drop in the crevice (i.e. the difference in potential between the solution at the cavity mouth and the potential in the solution at the cavity base).*

To be close to Sharland's model, we limit the comparison of the one-dimensional model (6.3.1)–(6.3.3)–(6.3.4) to only Sharland's simulations of the crevice propagation with passive walls. Distinctions between the two models are shown in Table 6.2 which is the origin of any slight difference in the simulation results. The two models are compared with each other with regard to the solution chemistry along the cavity and the potential drop.

Figure 6.5.2 shows the evolution of the solution chemistry along the cavity length for a metal potential ϕ_m of -0.2 V in relative to SCE reference. The initial data used in computation is given by

$$x_d^0 = 2 \text{ mm}, C_{Cl^-}^0 = C_{Na^+}^0 = 10^{-3} \text{ mol/L} \text{ and } C_{Fe^{2+}}^0 = 10^{-6} \text{ mol/L},$$

where x_d^0 is the initial depth of the crevice.

Comparison between a steady-state model (from literature) and our time evolution model:

Figure 6.5.2a shows the solution chemistry given by Sharland steady-state model where the moving boundary is ignored. According to her, this assumption is due to the fact that the cavity propagation is slow compared with the ionic transport. Here, there is no notion of time (time-invariant model which calculates the system at equilibrium). In fact, the geometry of the crevice is always kept constant. Similarly, the solution chemistry along the cavity length is always the same.

Unlike Figure 6.5.2a, Figure 6.5.2b shows our time-evolution system where the crevice depth increases as propagation proceeds. With this model, it is possible to follow the time evolution of the solution chemistry along the cavity length as well as the time evolution of the crevice depth. Evolution of Fe^{2+}, Cl^- and Na^+ concentration profiles are observed as time progresses. This is due to the accumulation of aqueous species in the cavity as time evolves. Therefore, our model (6.3.1)–(6.3.3)–(6.3.4) allows us to identify the time required for a crevice to obtain the solution chemistry presented by Sharland's model in Figure 6.5.2a. According to Figure 6.5.2b, the solution chemistry such as found by Sharland's model in Figure 6.5.2a is only obtained after 2,43 hours of propagation which corresponds to a depth of 2,35 mm. Besides, we note that the concentration of all species continues to increase with time.

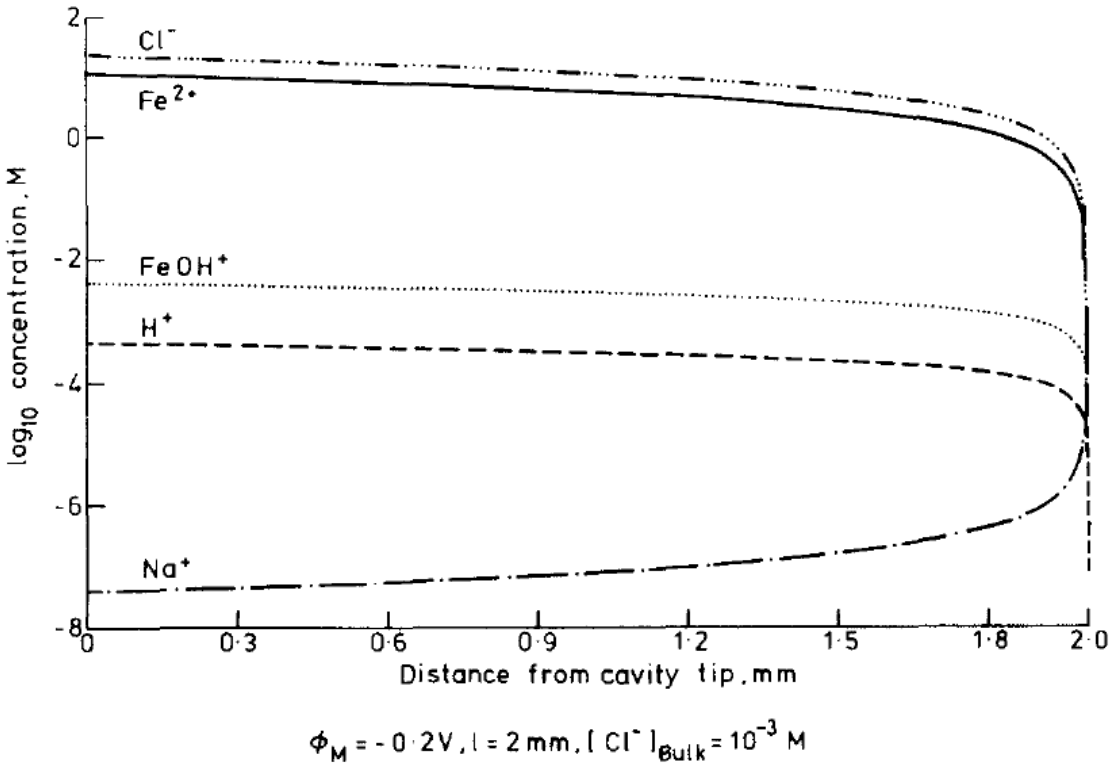

(a) Concentration profiles along the cavity length for a crevice with passive walls given by Sharland model [68].

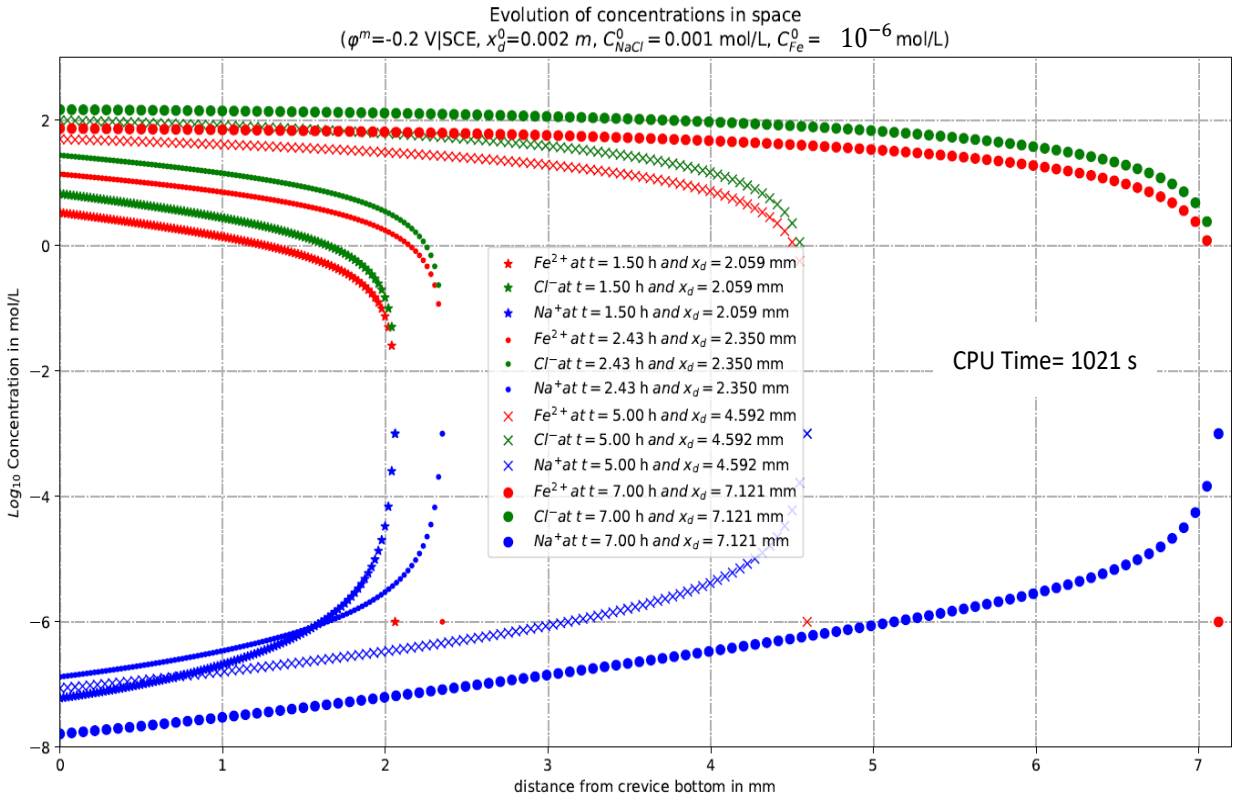

(b) Concentration profiles for a one-dimensional crevice given by the numercial scheme for the model (6.3.1)–(6.3.3)–(6.3.4) with the initial data $\phi_m = -0{,}2\ \mathrm{V}_{|\mathrm{SCE}}, C^0_{\mathrm{Fe}^{2+}} = 10^{-6}$ mol/L and $C^0_{\mathrm{NaCl}} = 10^{-3}$ mol/L.

Figure 6.5.2: Comparison between the solution chemistry in crevice given by our time evolution model (6.3.1)–(6.3.3) with the moving boundary condition (6.3.4) and the steady-state model developed by Sharland [64].

Figure 6.5.3 shows the potential drop within a corroding crevice for a metal potential ϕ_m of **-0.1** V relative to the SCE reference. We recall that the potential drop is the difference in potential between the solution at the cavity mouth and at the cavity base.

The initial data used in the computation is given by

$$x_d^0 = 2 \text{ mm}, C_{\text{Cl}^-}^0 = C_{\text{Na}^+}^0 = 2 \,.\, 10^{-3} \text{ mol/L} \text{ and } C_{\text{Fe}^{2+}}^0 = 10^{-6} \text{ mol/L},$$

where x_d^0 is the initial depth of the crevice.

Figure 6.5.3b shows a comparison of the potential profiles given by Sharland model for a static-geometry run and a moving-boundary run. Here, Sharland shows that the addition of the moving-boundary term has the effect of increasing the potential drop (and so decreasing the current in the crevice) which brings the model's predictions to more realistic values [66].

Figure 6.5.3a shows the time evolution of the potential drop which is close to the one found by Sharland's model with moving boundary.

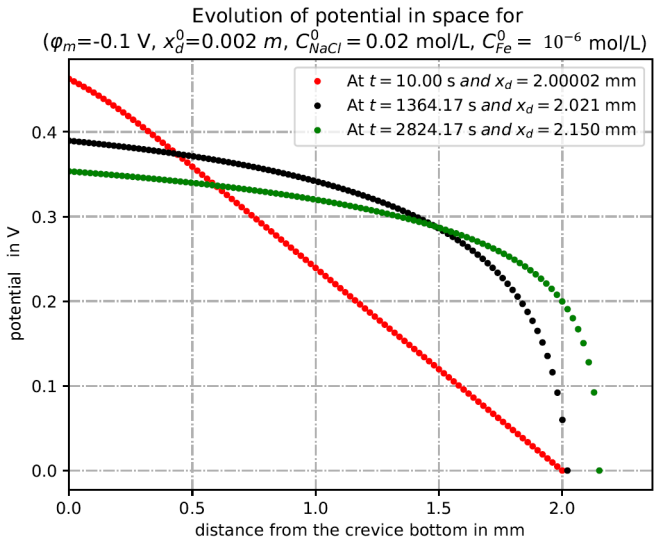

(a) Potential drop given by numercial scheme for the model (6.3.1)–(6.3.3)–(6.3.4) with the initial data $\phi_m = -0{,}1\ \mathrm{V}_{|\mathrm{SCE}}, C^0_{\mathrm{Fe}^{2+}} = 10^{-6}$ mol/L and $C^0_{\mathrm{NaCl}} = 2\ .\ 10^{-2}$ mol/L.

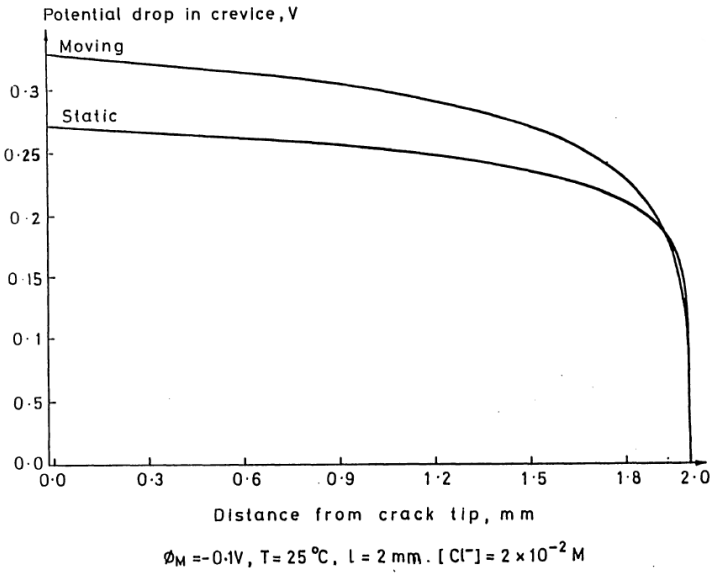

(b) Potential drop given by Sharland model [66].

Figure 6.5.3: Comparison between the potential drop within a corroding crevice given by our time evolution model (6.3.1)–(6.3.3) with the moving boundary condition (6.3.4) and the steady-state model developed by Sharland [64].

The conclusions that can be drawn from Figure 6.5.3 are as follows:

- Based on Sharland's observations, the addition of the moving boundary gives more realistic values to model predictions.
- The values of the potential drop given by Sharland's model and ours seem to be consistent despite the various distinctions between them cited in Table 6.2.
- From Figure 6.5.3a, we conclude that the potential drop decreases in time. In fact, due to the very slow moving boundary, it follows, as shown in Figure 6.5.2, an accumulation of chemical species in the pit solution which becomes more conductive with time. Therefore, the potential drop in the pit solution decreases in time.

Comparison of the theoretical prediction of our model (6.3.1)–(6.3.3)–(6.3.4) with experimental measurements from literature [82]

Remark 6.5.5 (Comparison with Turnbull model [82]). *Two main objectives to note for this second comparison are:*

- *to show the variation of the potential drop as a function of the metal potential ϕ_m,*
- *to compare the simulated results with the experimental measurements given in [82].*

Using an artificial crevice, Turnbull and Thomas [82] have presented a comparison of their theoretical prediction model with some experimental measurements for several metal potentials. They described the variation of the potential drop in different positions "x" of the crevice. The steel BS 4360 50D was used and the bulk solutions employed were 3.5% NaCl.

In order to compare their data with the one given by our model (6.3.1)–(6.3.3)–(6.3.4), the same initial data should be used. Thus, since the molarity of 3.5 % NaCl corresponds to an NaCl concentration of 0,61 mol/L, we have used the following initial data

$$x_d^0 = 33 \text{ mm}, C^0_{Cl^-} = C_{Na^+} = 0{,}6 \text{ mol/L} \text{ and } C^0_{Fe^{2+}} = 10^{-6} \text{ mol/L},$$

where x_d^0 is the initial depth of the crevice.

First, in the case of crevice propagation, to investigate the effect of metal potential in the potential drop, several simulations were performed. Using our model (6.3.1)–(6.3.3)–(6.3.4), Figure 6.5.4 shows the variation of the potential drop within a corroding crevice which reached a depth of 34 mm as a function of the metal potential ϕ_m. It shows that the potential drop becomes more significant for higher values of metal potentials.

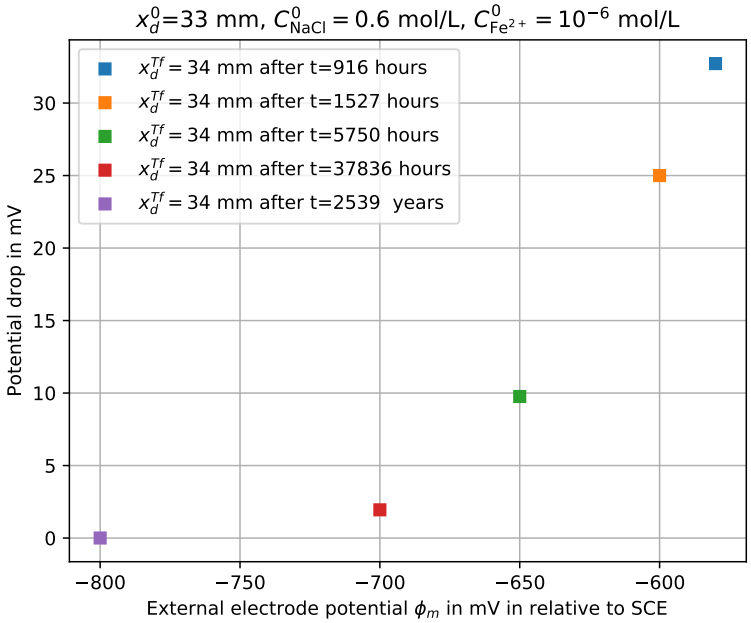

Figure 6.5.4: Variation of the potential drop in the crevice (initial length= 33 mm and final depth= 34 mm) in function of the external electrode potential ϕ_m using our model (6.3.1)–(6.3.3)–(6.3.4) .

The result seems to be basic, but, since the system is strongly coupled, it was not easy to identify the mechanism behind this behavior. We can explain the evolution of the potential drop

as given in Figure 6.5.4 for different values of ϕ_m as follows : let us fix two values of ϕ_m such that $\phi_m \in \{-600 \text{ mV}, -700 \text{ mV}\}$. Figure 6.5.5 shows that the crevice solution, for $\phi_m = -600$ mV, is more conductive (thus less resistive) than the one for $\phi_m = -700$ mV. According to Ohm's law which gives "potential drop= resistivity * density of current", the potential drop must be lower as the potential is increased. It is not the case which means that the influence of the current density (the second term in Ohm's law) is predominant in defining the evolution of the potential drop. The current density increases more strongly than the resistivity decreases when the potential is increased.

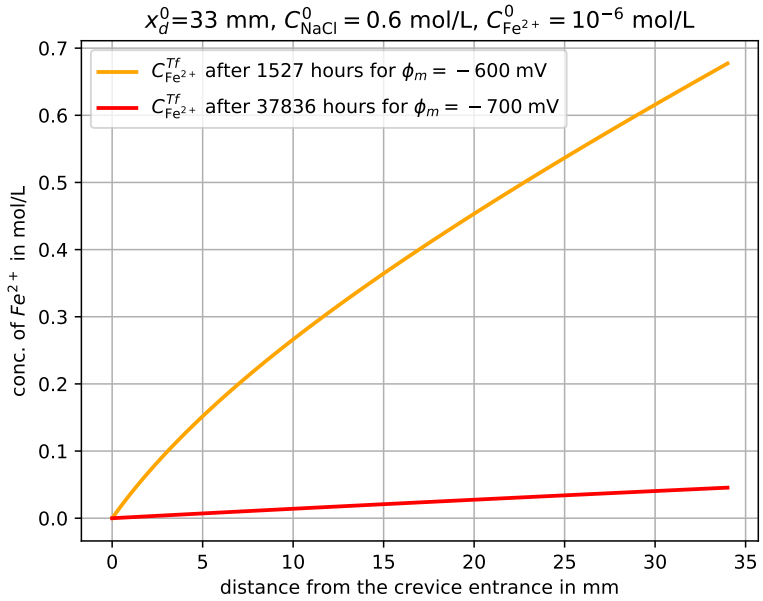

Figure 6.5.5: Evolution of the metallic cation concentrations $C_{Fe^{2+}}$ in the crevice for different ϕ_m values over a depth of 34 μm using our model (6.3.1)–(6.3.3)–(6.3.4) .

Next, we compare this result with similar results given by Turnbull model [82].

As it was done by Sharland, Turnbull considered a steady-state system and a fixed geometry which are a very rough approximation since a real crevice never reaches a steady state mainly because of its shape evolution. Turnbull showed in Figure 6.5.6a the variation of the potential drop at distance "x" from the crevice bottom for different metal potentials from his model and from experimental measurements. He showed that the potential drop increases with the metal potential and with depth. In other words, the potential drop becomes more significant close to the crevice bottom. Similar observations and conclusions are given by our model (6.3.1)–(6.3.3)–(6.3.4) according to Figure 6.5.6b.

The comparison between our model and Turnbull model gives a good qualitative agreement; the quantitative comparisons are less favorable. However, the most reasonable explanation for the quantitative difference between these results is mainly due to the difference in the assumptions used in the construction of the two models. In particular, as shown previously, the rate of dissolution which is proportional to the current density can play an important role in the evolution of the potential drop in the crevice. In fact, the kinetic parameters used in Turnbull model to describe the rate of dissolution are different from those used in our model. Indeed, Turnbull considers both anodic dissolution and cathodic reduction of hydrogen and water. However, in our model, we only use the Butler-Volmer formula to describe the anodic dissolution.

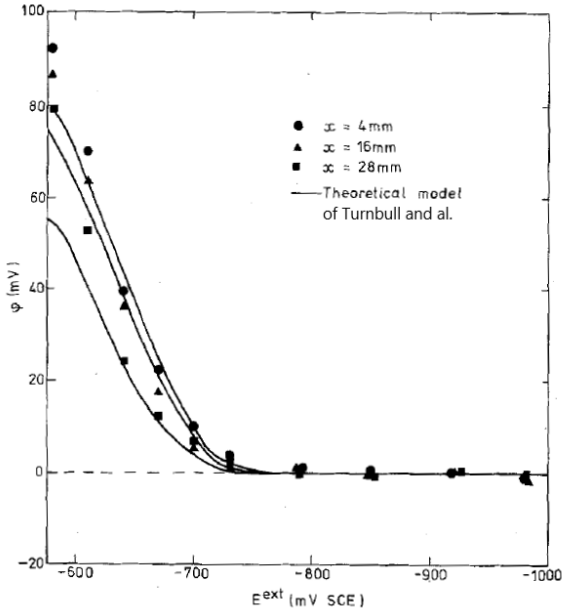

(a) Variation in potential drop in an artificial crevice with external potential at the distance x from the crevice tip (length = 33 mm, width = 150 μm): Experimental measurements compared with theoretical predictions of Turnbull model [82].

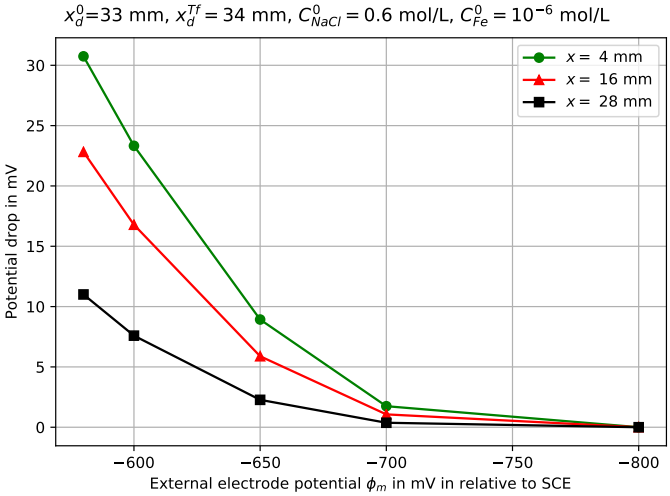

(b) Variation in potential drop with external potential ϕ_m at different positions "x" from the crevice bottom given by our model (6.3.1)–(6.3.3)–(6.3.4) .

Figure 6.5.6: Comparison of the potential drop for different metal potentials between our model (6.3.1)–(6.3.3)–(6.3.4) and the experimental measurements and the theoretical predictions of Turnbull model given in [82].

Conclusions:

The main conclusions that may be drawn from the comparison so far of our time evolution model (6.3.1)–(6.3.3)–(6.3.4) with moving boundary and the steady-state models with fixed geometry given in literature are as follows:

1. Our model is able to describe the propagation of a crevice, to identify the solution chemistry inside it as well as the distribution of potential and its propagation speed.

2. At high metal potential, neglecting the moving boundary is not valid as shown in Figure 6.5.2. In fact, unlike the steady-state model which indicates that the solution chemistry along the crevice length is constant, the time evolution model shows that the concentrations in the crevice solution of the various species, except the Na^+ concentration, increase in time as well as the depth of the crevice.

3. Comparison of our model (6.3.1)–(6.3.3)–(6.3.4) with similar previous studies shows a good qualitative agreement for certain aspects of the chemistry and electrochemistry within the crevice.

The aim of the next subsection is to examine the behavior of the solution of our system with respect to the variation of certain input physical parameters and to identify the critical factors that influence the oxidation rate of the metal.

6.5.3 Parametric study of the propagation of the unidimensional pit

The main objective of this part is to identify the critical factors that influence the oxidation rate of the metal using the numerical model. In the sequel, unless otherwise specified, the potential is

given relative to the NHE reference.

6.5.3.1 Choice of the ϕ_m value

To start simulation, it is necessary to impose a value of ϕ_m (the electric potential applied on the pure iron steel surface) such that the metal initially dissolves and does not re-deposit (absorption phase) (see Figure 6.2.2).

The minimum value to be imposed depends on the initial data. Let $\phi_m^{\min}$ be such a value. Then, $\phi_m^{\min}$ satisfies the **Nernst equation** (See Appendix A for more details) which is given in its dimensional form by:

$$\varepsilon^{eq} \quad (:= \phi_m^{min} - \phi^*) = E^0_{\mathrm{Fe}^{2+}/\mathrm{Fe}} + \frac{RT}{z_{\mathrm{Fe}^{2+}} F} \ln\left(\frac{C_{\mathrm{Fe}^{2+}}}{C_{\mathrm{ref}}}\right), \quad C_{\mathrm{ref}} = 1000\,\mathrm{mol/m^3} \tag{6.5.1}$$

where ε^{eq} is the electrode potential of iron in contact with the pit solution at equilibrium, $E^0_{\mathrm{Fe}^{2+}/\mathrm{Fe}}$ denotes the standard potential for $\mathrm{Fe}^{2+} \leftrightarrow \mathrm{Fe}$, which is known to be -0.44 V relative to the standard hydrogen electrode at room temperature.

The value ϕ^* is called ϕ^{eq} in literature (the potential at equilibrium). It denotes the potential at equilibrium for which the Butler-Volmer flux vanishes (see Figure 6.5.7).

Let $P(t) := \phi(x_d(t),t)$ be the potential at the bottom of the pit. Figure 6.5.7 shows a schematic image of the graph of $f_{Fe^{2+}}(P,C_{Fe^{2+}})$ for a fixed value of $C_{Fe^{2+}}$. There exists a unique value $\phi^* = \phi^*(C_{Fe^{2+}})$ at which $f_{Fe^{2+}}$ vanishes.

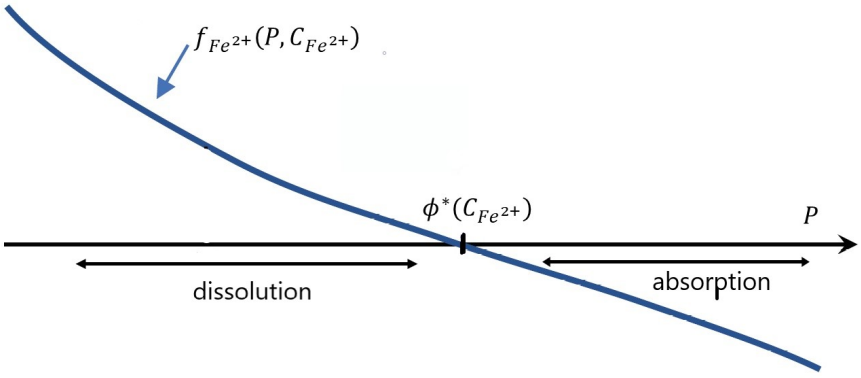

Figure 6.5.7: Graph of $f_{Fe^{2+}}(P,C_{Fe^{2+}})$ for a fixed value of $C_{Fe^{2+}}$

Then, we deduce that dissolution of the metal implies that

$$\phi_m^{\min} - P \geqslant \phi_m^{\min} - \phi^*. \tag{6.5.2}$$

In Figure 6.5.8, using (6.5.1), we plot the curve of $\phi_m^{\min} - \phi^*$ as a function of the initial concentration of the iron cations at the bottom of the pit $C^0_{Fe^{2+}}(x_d^0)$.

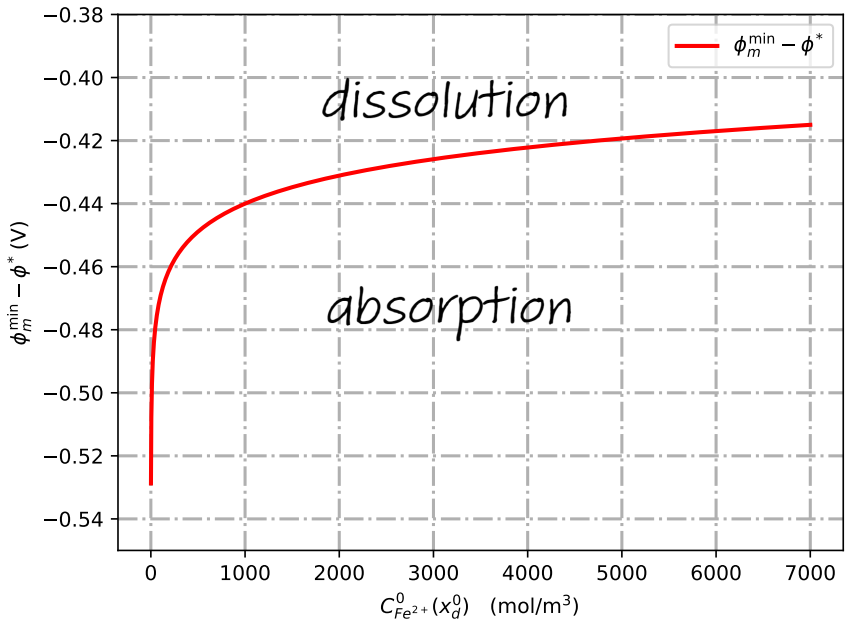

Figure 6.5.8: The curve of $\phi_m^{\min} - \phi^*$ in function of the initial concentration of iron cations at the bottom of the pit given by (6.5.1).

The right-hand side of (6.5.1) is calculated as follows for some sample values of $C_{\mathrm{Fe}^{2+}}$:

$$\phi_m^{min} - \phi^* = \begin{cases} -0.552873 \text{ V} & \text{if } C_{\mathrm{Fe}^{2+}} = 10^{-3} \text{ mol/L}, \\ -0.44 \text{ V} & \text{if } C_{\mathrm{Fe}^{2+}} = 1 \text{ mol/L}, \\ -0.42588 \text{ V} & \text{if } C_{\mathrm{Fe}^{2+}} = 3 \text{ mol/L}. \end{cases}$$

In the sequel, we show through an example how to approach the minimum value of the metal potential that ensures dissolution. To do so, we consider the initial data given by (the local electroneutrality of the solution should be respected):

$$\begin{cases} x_d^0 = 1 \text{ µm}, \\ C^0_{Fe^{2+}}(x) = 1 \text{ mol/L} & \text{for } 0 \leqslant x \leqslant x_d^0, \\ C^0_{Cl^-}(x) = 3 \text{ mol/L} & \text{for } 0 \leqslant x \leqslant x_d^0, \\ C^0_{Na^+}(x) = 1 \text{ mol/L} & \text{for } 0 \leqslant x \leqslant x_d^0. \end{cases} \tag{6.5.3}$$

Let ϕ_m be an arbitrary metal potential. For such initial data and ϕ_m, we calculate the potential at the bottom of the pit $P(t=0)$ by solving the system (6.3.1) as explained previously in subsection 6.3.1. Therefore, for $\phi_m \in \{-0.43 \text{ V}, -0.44 \text{ V}, -0.45 \text{ V}\}$, we obtain

	$P(0)$ V/NHE	ϕ^* V/NHE	$f_{Fe^{2+}}\left(P(0), C^0_{Fe^{2+}}(x_d^0)\right)$ mol.m^{-2}.s^{-1}
$\phi_m = -0.43$ V/NHE	1.293 . 10^{-8}	0.00999	2.593 . 10^{-6}
$\phi_m = -0.44$ V/NHE	0	0	0
$\phi_m = -0.45$ V/NHE	-1.293 . 10^{-8}	-0.00999	-2.593 . 10^{-6}

In the case of a constant initial data as in (6.5.3), we conclude that the region above the red curve corresponds to the range of ϕ_m where dissolution occurs ($\phi_m > \phi_m^{min} - \phi^*$) and the one below to an absorption field ($\phi_m < \phi_m^{min} - \phi^*$). To be close to equilibrium, the ϕ_m value needs to be close to the red curve ($\phi_m \approx \phi_m^{min} - \phi^*$).

6.5.3.2 System behavior towards the variation of certain parameters

The model set up makes it possible to describe the behavior of the system in presence of different variations of the physico-chemical parameters such that

- the impact of the potential applied to the surface of pure iron steel ϕ_m,
- the influence of the initial chloride concentration $C^0_{Cl^-}$ in the pit solution.

Remark 6.5.6. *The objective of this subsection is only to evaluate the influence of different parameters on the system without taking into account any passivation criteria. In other words, we do not consider any phenomenon of repassivation if the criterium of pit stability is not respected. In this context, independently of the value of the applied metal potential ϕ_m, we assume that the pit will always propagate even for low metallic cation concentration at the bottom of the pit as we will show later in Figure 6.5.10a.*

Next, we present **simulations for the case of a constant initial data.**

6.5.3.2.1 Influence of ϕ_m

In this paragraph we present numerical simulations of solutions of system (6.3.1)–(6.3.3)–(6.3.4) under the boundary condition $\phi = 0$ at the pit entrance. It is a one-dimensional pit grown in 1 mol/L NaCl which initially contains 10^{-6} mol/L of Fe^{2+}.

The computations are done for the following choice of reference parameters

$$D_0 = 1 \times 10^{-9}\ \mathrm{m}^2/\mathrm{s}, \quad \mathrm{L} = 1\ \mu\mathrm{m}, \quad \mathrm{C}_0 = 1000\ \mathrm{mol/m}^3 = 1\,\mathrm{mol/L}, \tag{6.5.4}$$

and for the following physical and chemical parameters[3]

$$D_{Fe^{2+}} = 7{,}19\ .\ 10^{-10}\ \mathrm{m}^2.\mathrm{s}^{-1}, D_{Cl^-} = 2{,}032\ .\ 10^{-9}\ \mathrm{m}^2.\mathrm{s}^{-1}, D_{Na^+} = 1{,}334\ .\ 10^{-9}\ \mathrm{m}^2.\mathrm{s}^{-1},$$

$$k_a = 89{,}0636\ \mathrm{mol.m}^{-2}.\mathrm{s}^{-1}, k_c = 1{,}1852\ .10^{-13}\ \mathrm{mol.m}^{-2}.\mathrm{s}^{-1} \quad \text{(see Appendix B)}$$

with the initial values given by

$x_d^0 := x_d(0)$	1 μm
$C^0_{Fe^{2+}}(x) := C_{Fe^{2+}}(x,0)$ for all $0 \leqslant x \leqslant x_d^0$	10^{-6} mol/L
$C^0_{Cl^-}(x) := C_{Cl^-}(x,0)$ for all $0 \leqslant x \leqslant x_d^0$	1,000002 mol/L
$C^0_{Na^+}(x) := C_{Na^+}(x,0)$ for all $0 \leqslant x \leqslant x_d^0$	1 mol/L

Table 6.3: Initial data for a one-dimensional pit grown in 1 mol/L NaCl.

Figure 6.5.9 presents a constant initial data. It shows the initial profiles of the chemical species concentrations present in the pit solution as given in Table 6.3. Here, the initial concentrations $C^0_{\mathrm{Cl}^-}$ (green) and $C^0_{\mathrm{Na}^+}$ (blue) are equal.

[3] reference: https://www.aqion.de/site/194.

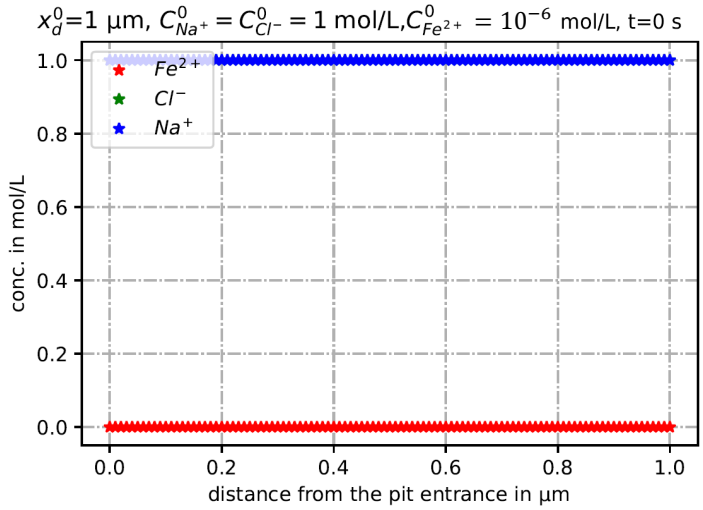

Figure 6.5.9: Initial profiles of concentrations in the pit solution; case of a constant initial data.

Next, as we have shown in paragraph 6.5.3.1, we first look for the smallest value of ϕ_m^{min} that ensures the dissolution of metal. By (6.5.1), we obtain

$$\phi_m^{min} - \phi^* \approx -0.617 \text{ V}.$$

Thus dissolution can occur only for

$$\phi_m \geqslant -0.617 \text{ V}. \tag{6.5.5}$$

Concentration profiles for $\phi_m = -0.3$ V|NHE and $\phi_m = -0.2$ V|NHE

Figure 6.5.10 shows that increasing the metal potential yields to some fairly high concentrations of aqueous species in the pit solution. In fact, Figures 6.5.10a and 6.5.10b show the graphs of $C_{\text{Fe}^{2+}}(x,t), C_{\text{Na}^+}(x,t), C_{\text{Cl}^-}(x,t)$ $(0 \leq x \leq x_d(t))$ at the time required to reach a final depth of 100 µm for two different metal potentials. It describes the concentration distribution of each ion in the pit: $C_{\text{Fe}^{2+}}$ (red), C_{Na^+} (blue), C_{Cl^-} (green).
In Figure 6.5.10b, for a sufficiently high metal potential $\phi_m = -0.2$ V, the metal dissolves faster than in the case where $\phi_m = -0.3$ V which leads to the accumulation of the iron cations Fe^{2+} in the pit solution. However, to maintain the local electroneutrality of the solution, the anions Cl^- are also accumulated. As a result, the pit reaches 100 µm faster (after 745 s).

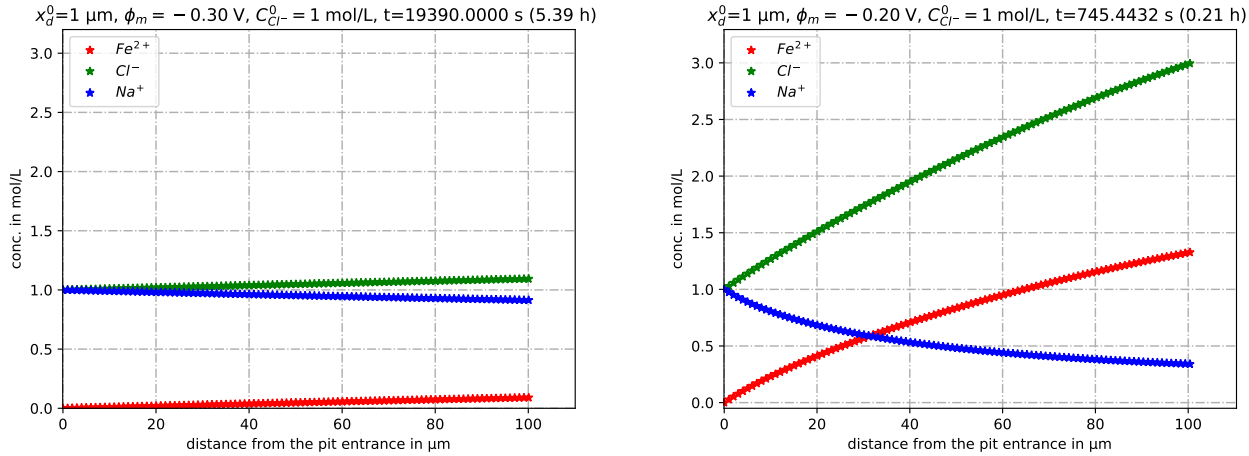

(a) Concentration profiles of the aqueous chemical species for $\phi_m = -0.3$V|NHE.

(b) Concentration profiles of the aqueous chemical species for $\phi_m = -0.2$V|NHE.

Figure 6.5.10: Influence of the metal potential on the evolution of the solution chemistry in the pit solution.

By setting the initial concentration of NaCl, C^0_{NaCl}, at 10^{-3} mol/L or 1 mol/L, Figure 6.5.11 shows that the potential drop in the pit solution increases with increasing ϕ_m. In fact, we have shown in Figure 6.5.10 that the conductivity in the pit solution increases with ϕ_m. However, according to Figure 6.5.11, the potential drop increases also with ϕ_m. Therefore, we deduce from the Ohm's law that for high values of ϕ_m, the current density is more important than the resistance (inverse of the conductivity) of the pit solution (as already explained previously).

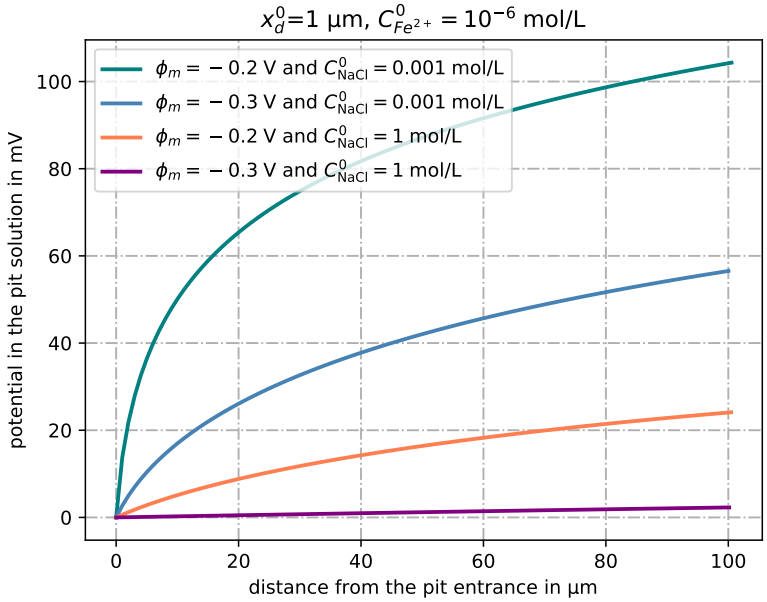

Figure 6.5.11: Influence of ϕ_m on the evolution of the potential drop along the pit solution over a depth of 100 µm.

Next, Figure 6.5.12 shows the graphs of the time evolution of pit depths for different values of ϕ_m. It illustrates the very high sensitivity of the propagation speed to the metal potential value ϕ_m. It shows that for lower values of ϕ_m, the evolution of the corrosion speed is constant. On

the other hand, it is clear that for high values of ϕ_m (for example, ϕ_m= -0.2 V) the pit cannot keep a constant speed of growth. By a very rough guess, we can suggest the following conjecture: the depth of the pit grows as $\mathcal{O}(\sqrt{t})$ for high values of ϕ_m. This implies that the evolution of the corrosion speed decreases with ϕ_m at large time. To validate this conjecture, we must study the long time behavior of the solution (not discussed in this thesis).

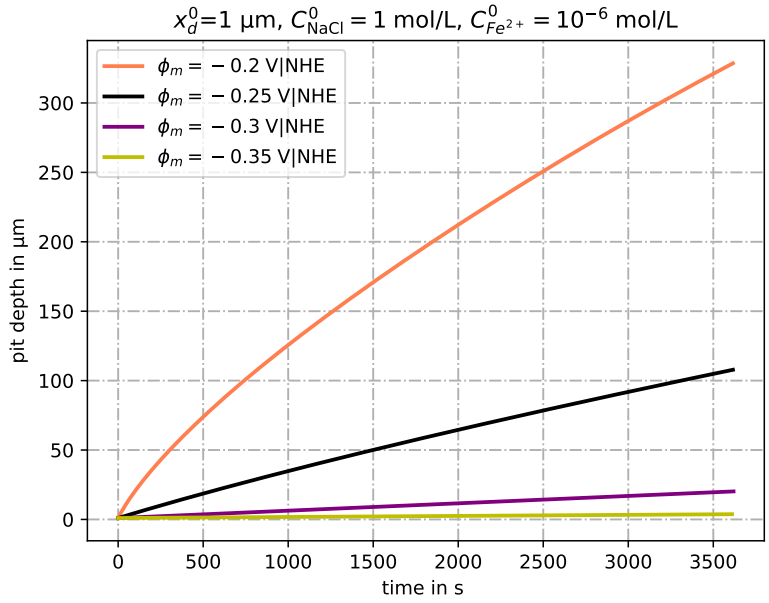

Figure 6.5.12: Evolution of the pit depth in time for different values of the metal potential.

Since the Butler-Volmer formula (6.2.15) describes the dissolution rate at the pit bottom, it follows that this flux incorporates the main factors that influence the corrosion speed. This flux is given as a function of the iron ions concentration and the potential drop at the pit bottom. So, in order to interpret physically the results of Figure 6.5.12, we have plotted in Figure 6.5.13 the evolution of the metallic cations concentration $C_{Fe^{2+}}$ at the pit bottom after ≈ 4,5 hours of pit propagation for several metallic potential values ϕ_m.

It shows that for $\phi_m = -0.2$ V, the concentration of the metallic cations at the bottom of the pit increases until reaching a quasi-stationary value ≈ 82,5 mol/L. This high concentration value was also reached for lower potential (-0.25 and -0.3V) but after much longer times. The transient time required to reach this near-equilibrium state decreases with increasing ϕ_m. Indeed, in the case ϕ_m= -0,2 V, this transient time (Figure 6.5.14a) is around 4 hours of pit propagation whereas in the case ϕ_m = -0,3 V (Figure 6.5.14e), it is around 1100 hours of pit propagation. It is obvious that this situation does not reflect reality because a precipitation of a salt film would occur if the metallic cations concentration $C_{Fe^{2+}}$ exceeds the saturation value of 5 mol/L at the pit bottom.

The potential drop, which coincides with the potential at the bottom of the pit $\phi(x_d(t),t)$, converges to the potential at equilibrium given by (6.5.1) $\phi^{Eq} = \phi^*$. For each value of ϕ_m, the transient time for the potential drop to reach the near-equilibrium state is the same as for $C_{Fe^{2+}}(x_d(t),t)$.

Physically, this can be described as convergence to a state of equilibrium after a large time of pit propagation ($C_{Fe^{2+}}(x_d(t),t) \approx$ constant as $t \to \infty$). A system leading to this specific situation, the quasi-stationary state, almost simultaneously is described in the next chapter (Chapter 7). We define a quasi-stationary system when the profile does not change any more after a large time.

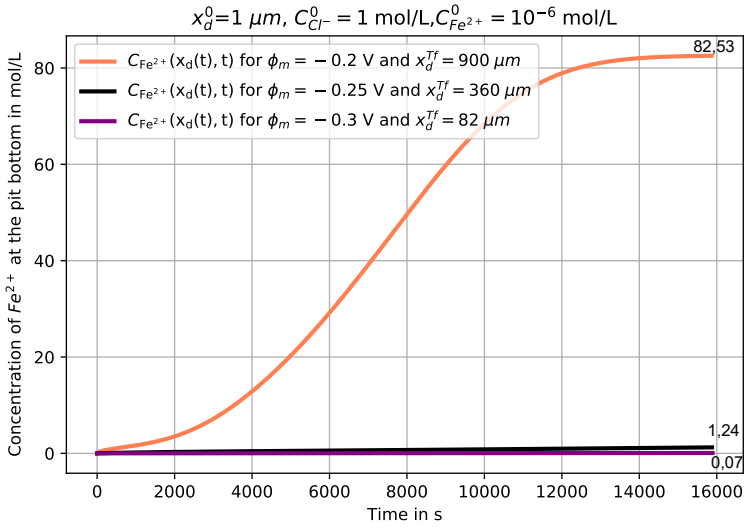

Figure 6.5.13: Evolution of the metallic cations concentration $C_{\mathrm{Fe}^{2+}}$ at the bottom of the pit as a function of time (after 4,45 hours of pit propagation which corresponds to the final pit depth x_d^{Tf}).

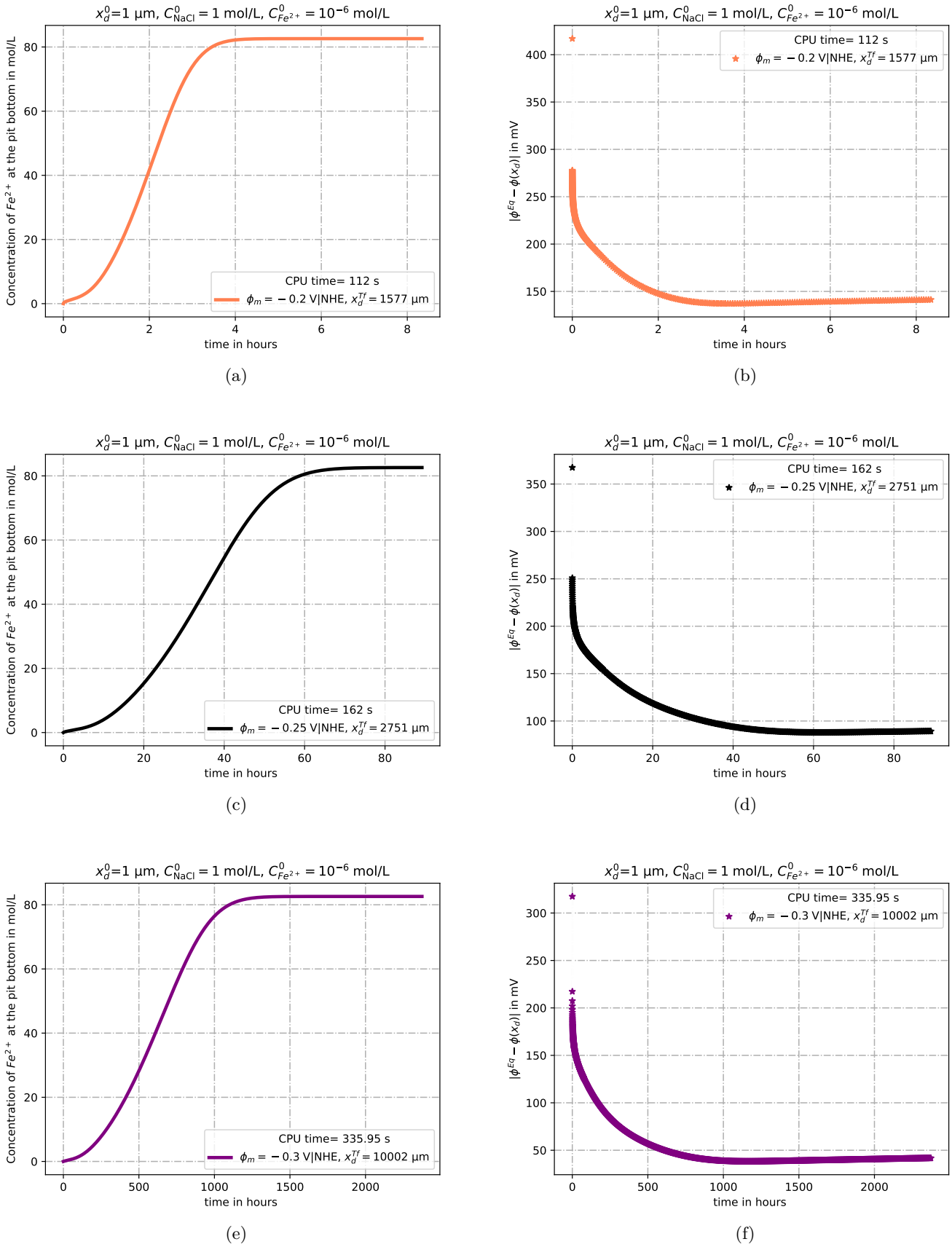

Figure 6.5.14: Large time behavior of the metallic cations concentration $C_{\mathrm{Fe}^{2+}}(x_d(t),t)$ as well as the difference between the potential at equilibrium $\phi^{\mathrm{Eq}}\left(C_{\mathrm{Fe}^{2+}}(x_d(t),t)\right)$ and the potential drop $\phi(x_d(t),t)$ at the pit bottom for several metallic potential values ϕ_m.

6.5.3.2.2 Influence of the initial chloride concentration $C^0_{Cl^-}$

In this paragraph, we will study the influence of the initial concentration of the bulk solution C^0_{NaCl} on

- the solution chemistry of the pit solution, in particular the concentration of the metallic cations $C_{Fe^{2+}}$,
- the potential drop in the pit solution (we recall that the potential drop is the difference in potential between the solution at the pit entrance and the potential in the solution at the pit bottom),
- the speed of the pit propagation (evolution of the pit depth in time).

Figure 6.5.15 shows the pit propagation kinetics for several initial chloride concentrations between 0,001 mol/L and 1 mol/L. It shows that the speed of the pit propagation increases with the initial chloride concentration. After one hour of propagation, the corrosion speed for the case $C^0_{NaCl} = 1$ mol/L is roughly 9 times faster than the case $C^0_{NaCl} = 0{,}001$ mol/L.

We recall that in our model the speed corrosion is given by the Butler-Volmer formula (6.2.15). This formula mainly depends on the potential drop and the metallic cations concentration at the pit bottom. Therefore, in order to understand the result of Figure 6.5.15, we need to study the influence of the initial chloride concentration on both the potential drop (Figure 6.5.16) and the metallic cation concentration (Figure 6.5.18) at the bottom of the pit.

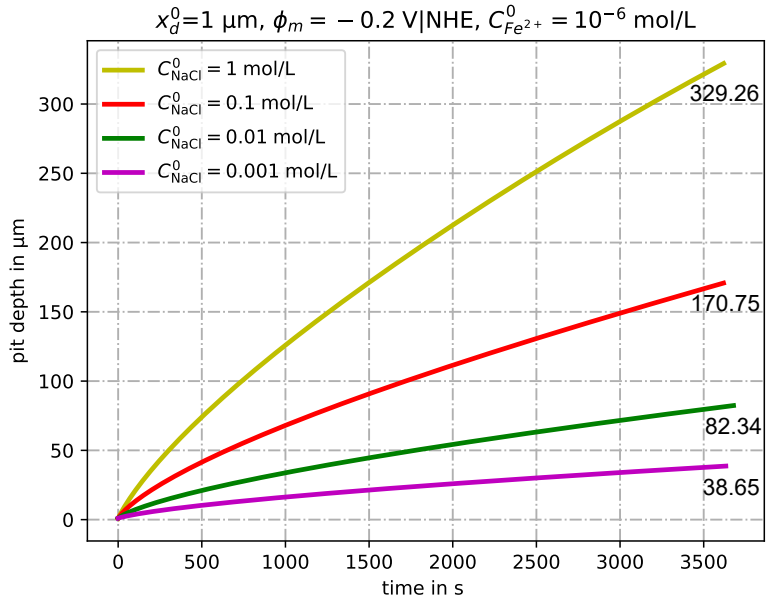

Figure 6.5.15: Influence of the initial concentration of chloride ions Cl^- on the evolution of the pit depth in time.

Figure 6.5.16 shows the influence of the initial chloride concentration on the evolution of both the potential in the pit solution and the potential drop in time.

Figure 6.5.16a shows the distribution of **the initial potential** in the pit solution for several initial concentrations of NaCl while Figure 6.5.16b shows the distribution of **the potential** in the pit solution after 1 hour of propagation. Similarly, Figures 6.5.16a and 6.5.16b show that high (resp.

low) initial concentrations of NaCl reduce (resp. increase) the potential drop in the pit solution. In other words, the potential drop is low for conductive solutions.

Figure 6.5.16c shows the evolution of the potential drop with time for several initial concentrations of NaCl. We conclude that the potential drop decreases with high initial concentrations of NaCl. Next, by Ohm's law, we have that

$$\begin{aligned} \text{potential drop} &= \text{ resistance } * \text{ density of current} \\ &= \frac{1}{\text{conductivity}} * \text{ density of current.} \end{aligned} \tag{6.5.6}$$

In view of (6.5.6), we deduce from Figure 6.5.16c that the potential drop and the resistance have the same behavior. In other words, in this case, the density of current had less influence on the potential drop than the resistance of the pit solution.
In addition, we deduce from 6.5.16c that throughout the first hour of pit propagation, the potential drop increases in time. Thus, it increases with depth as shown in Figure 6.5.17b.

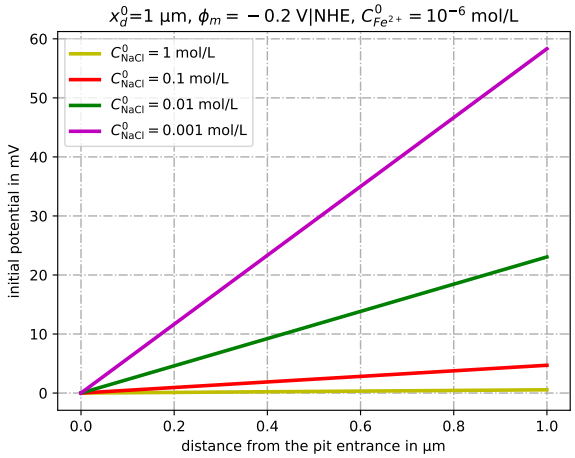

(a) Distribution of the initial potential in the pit solution for several initial concentrations of NaCl.

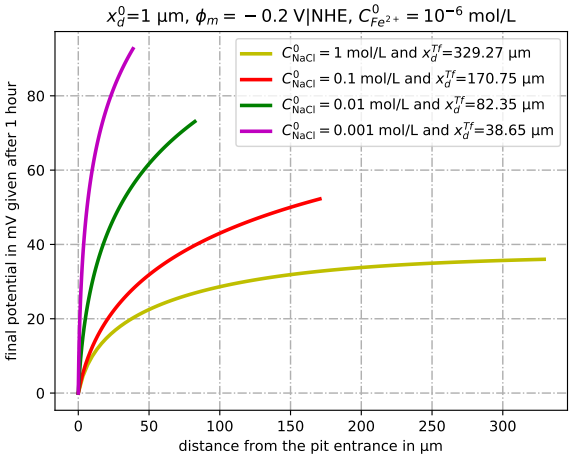

(b) Distribution of the potential in the pit solution after 1 hour of propagation for several initial concentrations of NaCl.

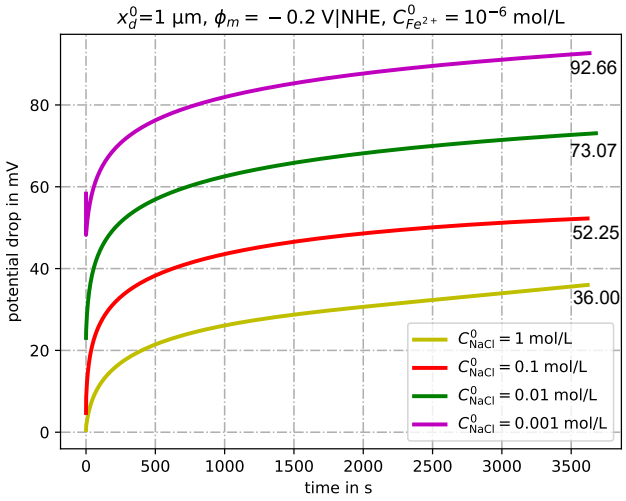

(c) Influence of the initial concentration of NaCl on the time evolution of the potential drop in the pit solution with time.

Figure 6.5.16: Influence of the initial concentration of NaCl on the time evolution of the potential and the potential drop at the pit solution.

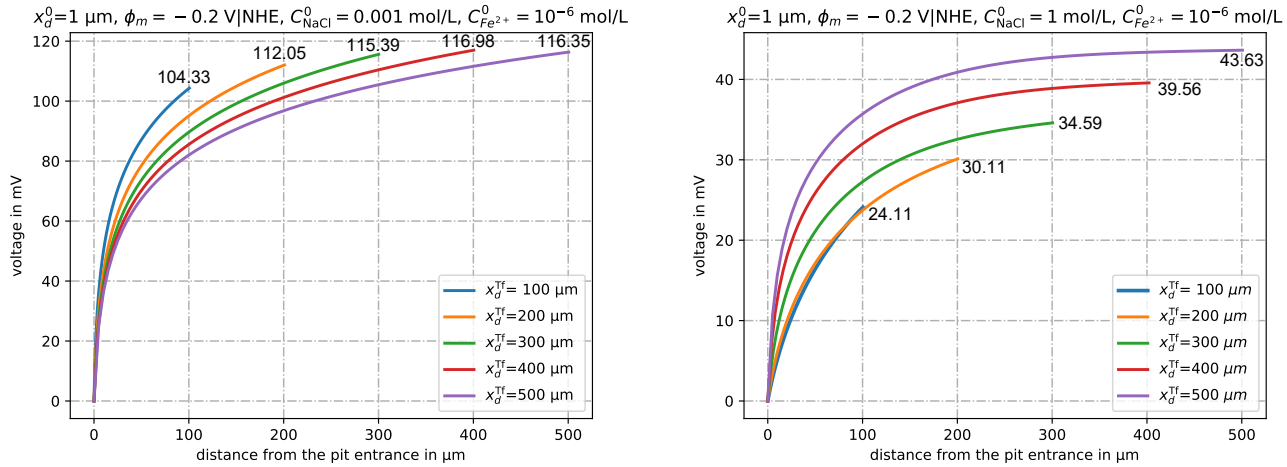

(a) Evolution of the potential drop for $C^0_{\mathrm{NaCl}} = 0.001$ mol/L. (b) Evolution of the potential drop for $C^0_{\mathrm{NaCl}} = 1$ mol/L.

Figure 6.5.17: Influence of the initial concentration of NaCl on the time evolution of the potential drop at the pit solution; the final pit depth varies from 100 µm to 500 µm.

Next, for several initial chloride concentrations $C^0_{\mathrm{Cl}^-}$, Figure 6.5.18 shows the evolution of the metallic cations concentrations $C_{\mathrm{Fe}^{2+}}(x_d(t),t)$ at the pit bottom. $C_{\mathrm{Fe}^{2+}}(x_d(t),t)$ increases slightly for initial low concentration of Cl^-. However, it reaches a significant value for initial high concentration of Cl^-. A similar behavior has been noted in Figure 6.5.13.

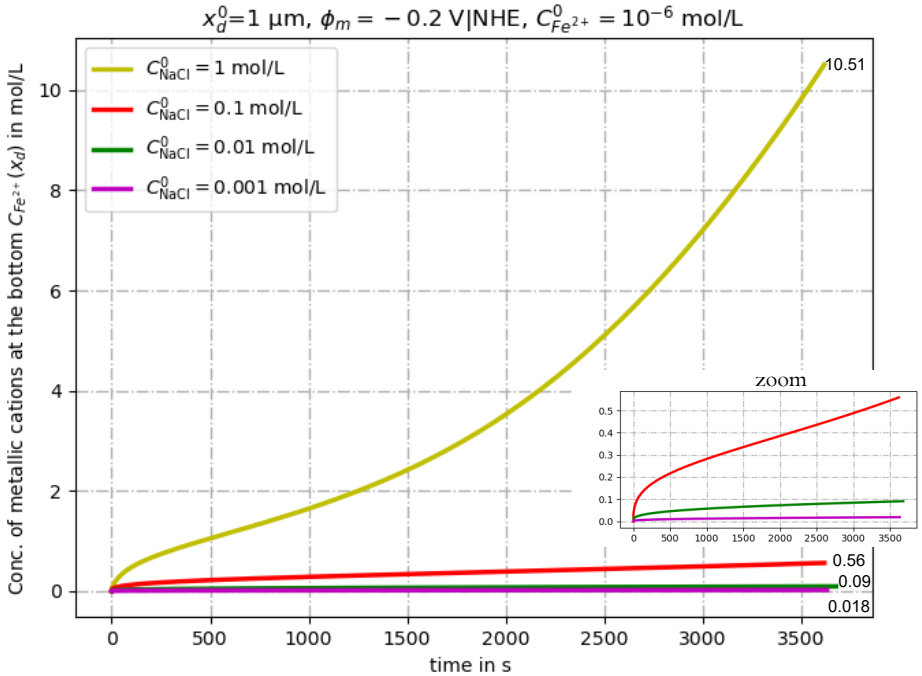

Figure 6.5.18: Influence of the initial concentration of NaCl on the time evolution of the metallic cation concentration $C_{\mathrm{Fe}^{2+}}$ at the pit bottom.

Estimate of the corrosion speed :

For simplicity, we note the Butler-Volmer flux $f_{Fe^{2+}}\Big(\phi(x_d(t),t),C_{Fe^{2+}}(x_d(t),t)\Big)$ as

$$f_{Fe^{2+}}\left(\phi(x_d),C_{Fe^{2+}}(x_d)\right).$$

By (6.3.4), we recall that the corrosion speed is proportional to the Butler-Volmer flux which is given, in its dimensional form, by

$$\begin{aligned} f_{Fe^{2+}}\left(\phi(x_d),C_{Fe^{2+}}(x_d)\right) &= k_a \exp\Big(-\frac{F}{RT}(\phi(x_d)-\phi_m)\Big) - k_c\,\frac{C_{Fe^{2+}}(x_d)}{C_{\text{ref}}}\exp\Big(\frac{F}{RT}(\phi(x_d)-\phi_m)\Big) \\ &= f^{a}_{Fe^{2+}}\left(\phi(x_d),C_{Fe^{2+}}(x_d)\right) - f^{c}_{Fe^{2+}}\left(\phi(x_d),C_{Fe^{2+}}(x_d)\right), \end{aligned} \tag{6.5.7}$$

where the anodic reaction (dissolution) is given by

$$f^{a}_{Fe^{2+}}\left(\phi(x_d),C_{Fe^{2+}}(x_d)\right) = k_a \exp\Big(-\frac{F}{RT}(\phi(x_d)-\phi_m)\Big) \tag{6.5.8}$$

and the cathodic reaction (absorption) is given by

$$f^{c}_{Fe^{2+}}\left(\phi(x_d),C_{Fe^{2+}}(x_d)\right) = k_c\,\frac{C_{Fe^{2+}}(x_d)}{C_{\text{ref}}}\exp\Big(\frac{F}{RT}(\phi(x_d)-\phi_m)\Big). \tag{6.5.9}$$

In view of Figure 6.5.16 and Figure 6.5.18, for the cases $C^0_{NaCl} = 10^{-3}$ mol/L and $C^0_{NaCl} = 1$ mol/L, we have the following estimates after 1 hour of propagation for $\phi_m = -0.2$ V|ENH.

C^0_{NaCl} (mol/L)	10^{-3}	1
$\phi(x_d)$ (V)	0,0926	0,036
$C_{Fe^{2+}}(x_d)$ (mol/L)	0,018	10,51
$f^{a}_{Fe^{2+}}\left(\phi(x_d),C_{Fe^{2+}}(x_d)\right)$ $(\text{mol.m}^{-2}.\text{s}^{-1})$	1,005 $. 10^{-3}$	9,125 $. 10^{-3}$
$f^{c}_{Fe^{2+}}\left(\phi(x_d),C_{Fe^{2+}}(x_d)\right)$ $(\text{mol.m}^{-2}.\text{s}^{-1})$	1,889 $. 10^{-10}$	1,215 $. 10^{-8}$

We conclude that $f^{a}_{Fe^{2+}}\left(\phi(x_d),C_{Fe^{2+}}(x_d)\right) \gg f^{c}_{Fe^{2+}}\left(\phi(x_d),C_{Fe^{2+}}(x_d)\right)$. It follows that the speed of corrosion is proportional to $f^{a}_{Fe^{2+}}\left(\phi(x_d),C_{Fe^{2+}}(x_d)\right)$. Next, from (6.5.8), since

$$f^{a}_{Fe^{2+}}\left(\phi(x_d),C_{Fe^{2+}}(x_d)\right) = k_a \exp\Big(\frac{F}{RT}(\phi_m-\phi(x_d))\Big) \text{ at } x = x_d(t),$$

it follows that the corrosion speed and $-\phi(x_d)$ have the same monotony. In other words, the corrosion speed increases (resp. decreases) with increasing (resp. decreasing) $-\phi(x_d)$.
Therefore, since the potential drop and the resistance of the pit solution have the same behavior as we have seen previously, it follows that the corrosion speed and the conductivity of the pit solution also have the same behavior which is consistent with the results in Figure 6.5.15.

Conclusions:

In the case of a constant initial data, simulations of the pit propagation for several values of metal potentials and initial NaCl concentrations show that:

1. The pit propagation speed increases with increasing ϕ_m even if the potential drop increases as well.
2. The pit propagation speed increases with increasing C^0_{NaCl} as a result of the increase of the solution conductivity which decreases the potential drop in the pit.
3. At an early stage of the pit propagation, the evolution of the corrosion speed is constant in time. However, the evolution of the corrosion speed decreases at large time (convergence to a quasi-stationary system). The transient time required to reach such a near equilibrium state strongly depends on the input parameters such as the value of ϕ_m and C^0_{NaCl}.

6.5.3.3 Quantification of the proportion of transport by migration versus total transport for the case of a constant initial data

It is of interest to quantify the proportion of transport by migration and by diffusion. This result could justify the simplification of the governing transport equation by neglecting the migration term which complexify strongly the equation resolution. We have mentioned that the concentrations of aqueous species in the dilute solution filling the pit (or crevice) are governed by the following mass-conservation equation (in its dimensionless form)(6.3.3a)

$$\frac{\partial C_i}{\partial t} = \frac{\partial}{\partial x}\left(D_i\left(\frac{\partial C_i}{\partial x} + z_i C_i \frac{\partial \phi}{\partial x}\right)\right), \quad t>0,\ 0<x<x_d(t), \quad (i=1,2,3). \tag{6.5.10}$$

The first term on the right hand side of (6.5.10) describes the rate of transport of ions by diffusion under concentration gradients. The second term represents the migration of charged species under electrostatic potential gradients.

Therefore, the ionic flux carried by the $i-$th ion species, is given in its dimensionless form by

$$\boldsymbol{J}_i := \boldsymbol{J}_i^{\text{diff}} + \boldsymbol{J}_i^{mig} := -D_i \frac{\partial C_i}{\partial x} - D_i\ z_i\ C_i \frac{\partial \phi}{\partial x}, \tag{6.5.11}$$

where

$$\boldsymbol{J}_i^{\text{diff}} = -D_i \frac{\partial C_i}{\partial x} \quad \text{is the diffusion flux which is associated with Fick's law} \tag{6.5.12}$$

and

$$\boldsymbol{J}_i^{mig} = -D_i\ z_i\ C_i \frac{\partial \phi}{\partial x} \quad \text{is the migration flux caused by the electric field } E = -\frac{\partial \phi}{\partial x}. \tag{6.5.13}$$

We compute the proportion of transport by migration of the species i versus total transport (by diffusion and migration) as follows

$$\%\ \text{migration\_transport\_i} = 100\ .\ \frac{|\boldsymbol{J}_i^{mig}|}{|\boldsymbol{J}_i^{\text{diff}}| + |\boldsymbol{J}_i^{mig}|}. \tag{6.5.14}$$

Figure 6.5.19, Figure 6.5.20 and Figure 6.5.21 show the evolution of the potential, the concentration profiles as well as the proportion of transport by migration for the three chemical aqueous species Fe^{2+}, Cl^- and Na^+ at each point of the pit solution and over a depth of 10 µm and 100 µm, respectively. These results are given by our model (6.3.1)–(6.3.3)–(6.3.4) using the initial data

$$x_d^0 = 1\ \mu\text{m}, \mathrm{C}_{\mathrm{Fe}^{2+}}^0 = 10^{-6}\ \text{mol/L},$$

and for several values of metal potentials and initial concentrations of NaCl.

For the metallic cations Fe^{2+} in dilute chloride solution with initial concentrations of NaCl varying between 0,001 mol/L and 1 mol/L, the rate of transport by migration increases when increasing the value of metal potential ϕ_m. For a fixed value of ϕ_m, it becomes more significant for lower initial concentrations of NaCl. Only in the case of a low metal potential with high initial concentration of NaCl, transport by migration is considered to be negligible.

Setting ϕ_m to -0.2 V, it follows from Figures 6.5.19c – 6.5.19d and 6.5.19e – 6.5.19f that transport by migration strongly depends on the potential drop in the pit solution. **Thus, transport by migration of the metallic cations is more important for higher potential drop induced by a low conductivity in the pit solution.**

On the other hand, Figure 6.5.20 and Figure 6.5.21 show that the transport of Cl^- and Na^+ ions occur 50 % by diffusion and 50 % by migration along the pit solution independently of the metal potential value and the initial concentration of NaCl.

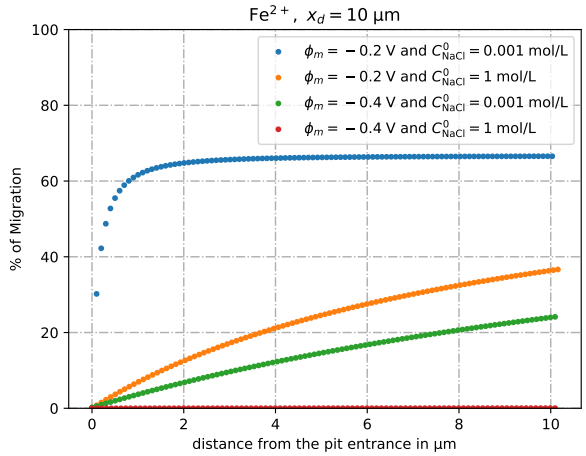

(a) Percentage of transport by migration of Fe^{2+} ions over a pit depth of 10 µm.

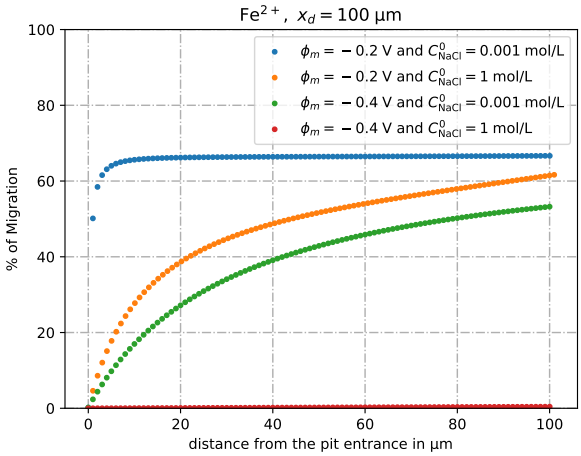

(b) Percentage of transport by migration of Fe^{2+} ions over a pit depth of 100 µm.

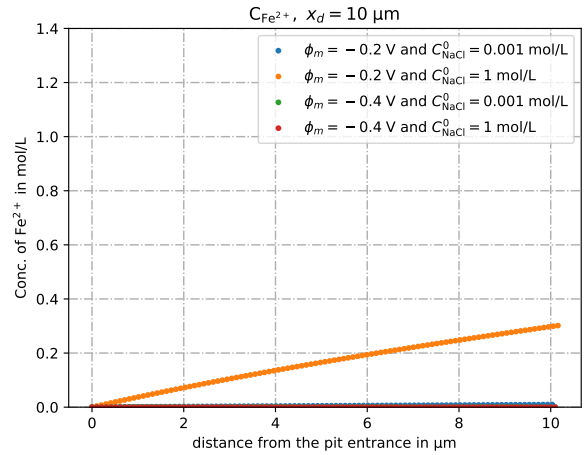

(c) Concentration profiles of Fe^{2+} ions over a pit depth of 10 µm.

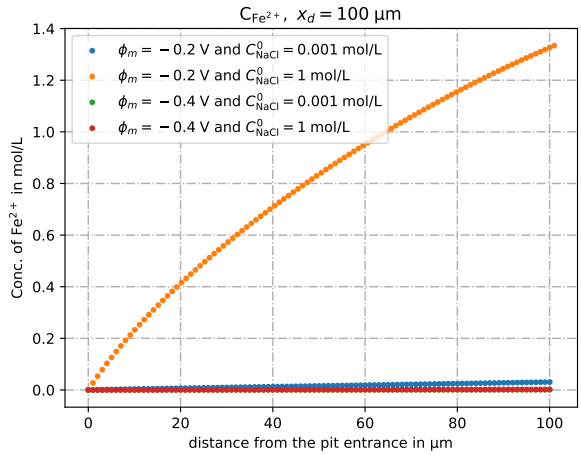

(d) Concentration profiles of Fe^{2+} ions over a pit depth of 100 µm.

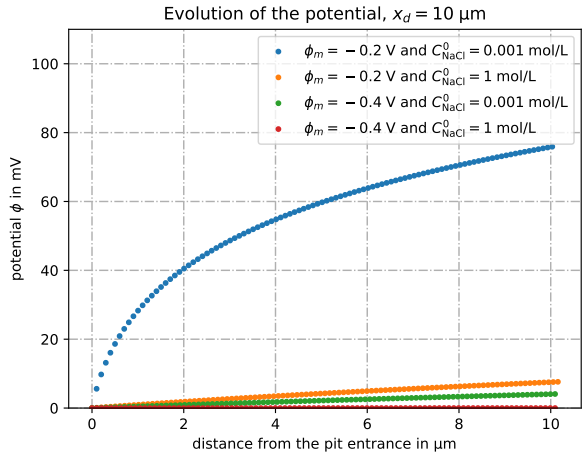

(e) Evolution of the potential over a pit depth of 10 µm.

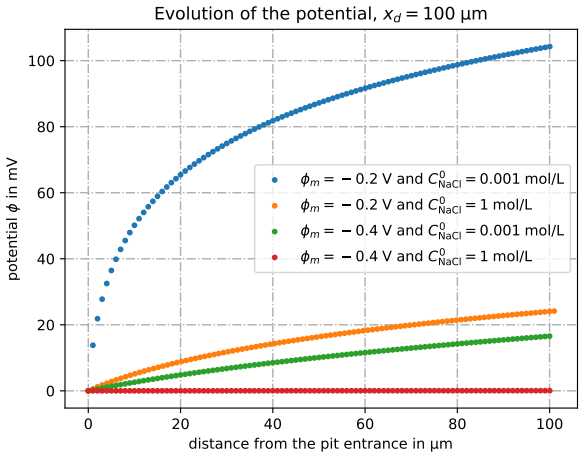

(f) Evolution of the potential over a pit depth of 100 µm.

Figure 6.5.19: Evolution of the proportion of transport by migration versus total transport of Fe^{2+} ions at each point of the pit solution, the profile of concentration of Fe^{2+} and the potential for several metal potentials and initial concentrations of NaCl.
(For pit depths: $x_d = 10$ µm and $x_d = 100$ µm.)

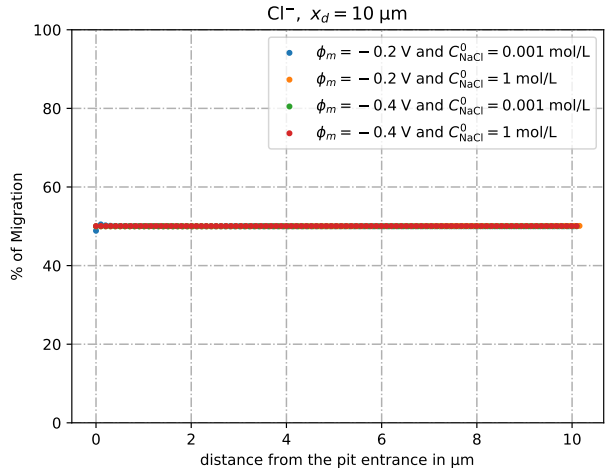

(a) Percentage of transport by migration of Cl^- ions over a pit depth of 10 µm.

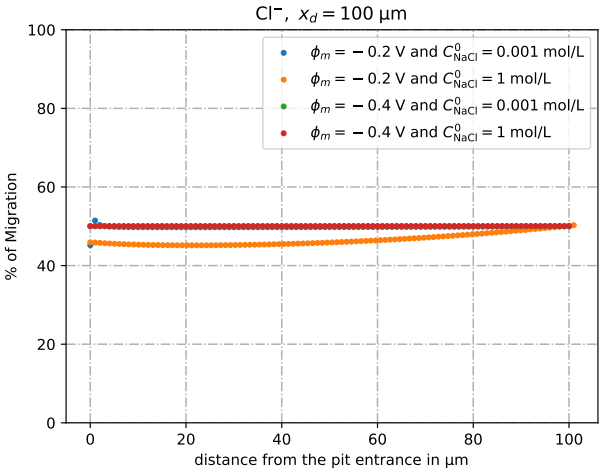

(b) Percentage of transport by migration of Cl^- ions over a pit depth of 100 µm.

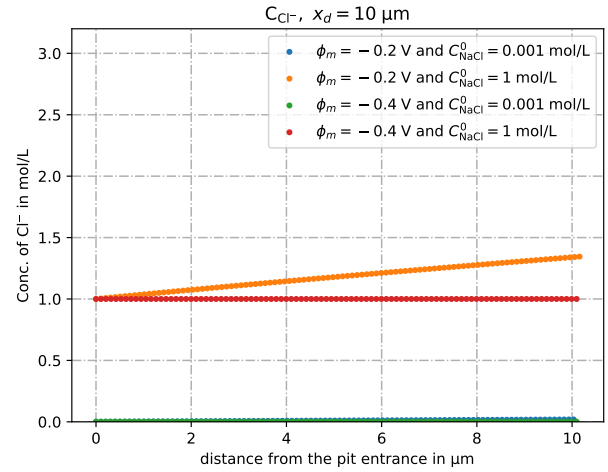

(c) concentration profiles of Cl^- ions over a pit depth of 10 µm.

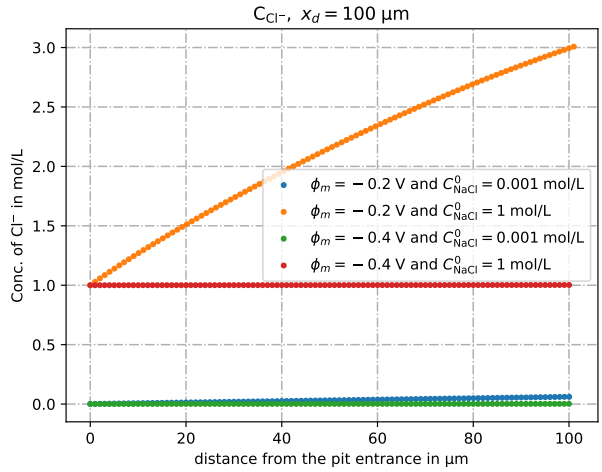

(d) concentration profiles of Cl^- ions over a pit depth of 100 µm.

Figure 6.5.20: Evolution of the proportion of transport by migration versus total transport of Cl^- ions at each point of the pit solution and their concentration profiles for several metal potentials and initial concentrations of NaCl. (For pit depths: $x_d = 10$ µm and $x_d = 100$ µm.)

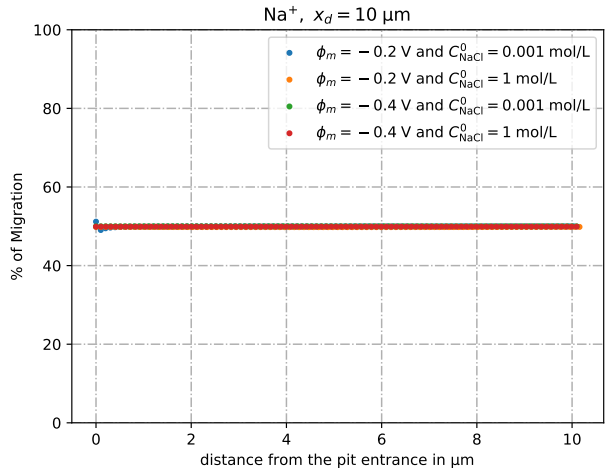

(a) Percentage of transport by migration of Na^+ ions over a pit depth of 10 µm.

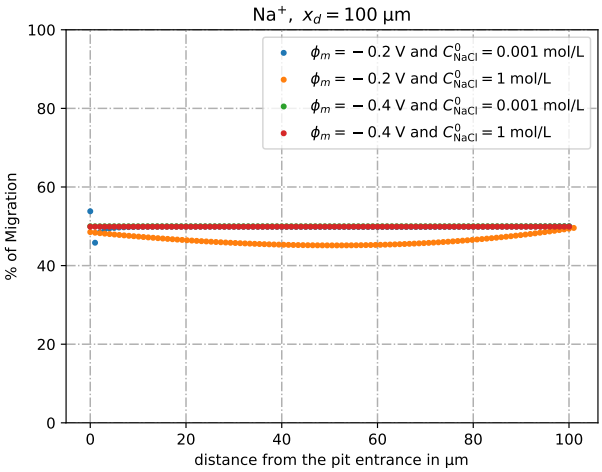

(b) Percentage of transport by migration of Na^+ ions over a pit depth of 100 µm.

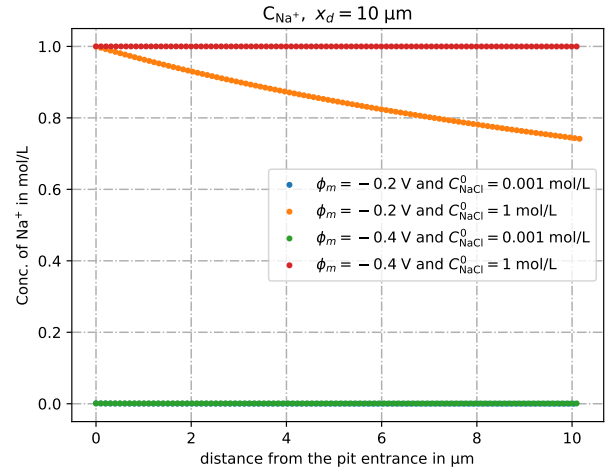

(c) concentration profiles of Na^+ ions over a pit depth of 10 µm.

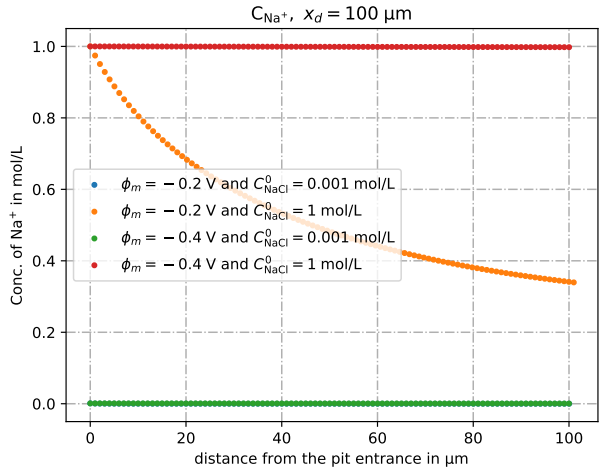

(d) concentration profiles of Na^+ ions over a pit depth of 100 µm.

Figure 6.5.21: Evolution of the proportion of transport by migration versus total transport of Na^+ ions at each point of the pit solution and their concentration profiles for several metal potentials and initial concentrations of NaCl. (For pit depths: $x_d = 10$ µm and $x_d = 100$ µm.)

Conclusions:
Transport of ionic species in the pit solution occurs both by diffusion and migration. In a dilute chloride solution with initially NaCl concentrations varying between 0.001 mol/L and 1 mol/L and Fe^{2+} concentrations around 10^{-6} mol/L, we have shown that:

1. The proportion of transport by migration is significant for high metal potential with low initial concentrations of NaCl (low conductive solution). This is due to the increase of the potential drop in the pit solution.

2. The proportion of transport by migration increases with depth. This is due to the increase of the potential drop in the pit solution as depth increases.

3. Transport by migration is negligible for low metal potential with high initial NaCl concentrations because the potential drop is negligible in this case.

4. Accurate kinetic models for pit dissolution cannot neglect the effect of migration in the transport of the charges species. Ignoring migration is only justified in the specific case where the potential drop is very low.

6.5.4 Simulations of the pit propagation with initial data close to the observed physical reality

We recall that the main objective of our study is to develop a time evolution model that aims to describe the pit propagation. Therefore, it seems important at this level to identify critical factors using our model (6.3.1)–(6.3.3) with moving interface (6.3.4) to describe the pit stability.

Criteria of pit stability

Like Laycock and White [44], to ensure the pit propagation, we consider the well-known requirement of a near-saturated local chemistry in the pit solution. Next, in order to ensure its stability, we adopt a critical factor in our model for which the minimum aggressive chemistry required to sustain pitting is described. This critical factor is defined in our model as **a critical concentration of metal cation at the bottom of the pit** and is denoted by C_{crit}. Its value is assumed to be about **60 % of the saturation in the metallic cation** C_{sat}. In fact, measurements with various techniques consistently produce C_{crit} values between about 50 and 80% of C_{sat} at ambient temperature [44], so that it seems to be consistent to consider the value of 60% of the saturation.

Therefore, to ensure the stability of the pit, the metallic cation concentration at the pit bottom $C_{Fe^{2+}}(x_d(t),t)$ should be greater than $C_{\text{crit}} = 60\%\ C_{\text{sat}}$ at all times.

Now, let us defined an approximate value of the saturation in metallic cations. Laycock [44] assumed that for his model 300 series alloy model, the saturated concentration C_{sat} is equal to 5 mol/L. Moreover, Srinivasan [75] had used a saturated concentration of the 316L cation[1] equal to 5.02 mol/L. Therefore, in our case of pure iron, we can assume that C_{sat}=5 mol/L. It follows that $C_{\text{crit}} = 3$ mol/L.

Next, from literature [44], we recall that the first step of pitting is nucleation. These pit nuclei are covered by a lacy cover that helps them to maintain a concentrated local chemistry [44] as shown in Figure 6.5.22.

[1]The 316L cation is designed to represent a metal cation whose characteristics represent the weighted average of the primary allowing elements (Fe, Cr, Ni).

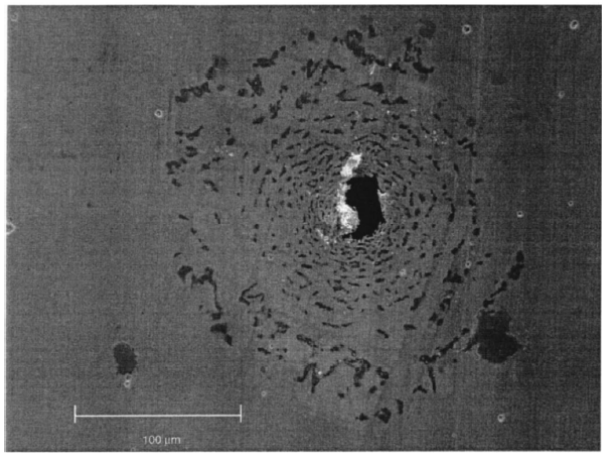

Figure 6.5.22: Plane view of a typical covered pit in 316 stainless steel, grown at 1500 mV in 1 M NaCl solution [44].

In fact, many pits are entirely dependent on the existence of these covers for their continued propagation. Thus, the objective of this paragraph is to identify the required conditions on ϕ_m to maintain the stability of the pit without the protection of these lacy covers. In other words, we need to identify the minimal value of the metal potential ϕ_m^{stable} (relative to the NHE reference) required to ensure the pit stability as a function of the initial pit depth $x_d^0 := x_d(0)$.

In our case of a one-dimensional pit, we can examine mathematically the disappearance of these lacy covers by imposing a Dirichlet boundary condition at the entrance of the pit. Here, the concentration of each aqueous species is equal to its values in the bulk solution. At the bottom of the pit, we consider a saturated concentration of metallic cations $C_{Fe^{2+}}(x_d(0),0) = 5$ mol/L. Therefore, using our model (6.3.1)–(6.3.3)–(6.3.4), we can consider in our simulations the following choice of initial data (a non constant distribution of concentrations in the pit solution for Fe^{2+} and Cl^-) (see Figure 6.5.23):

At the pit entrance ($x = 0$):

$$C_{Fe^{2+}}(0,0) = 10^{-6} \text{ mol/L} \quad \text{and} \quad C_{Na^+}(0,0) = C_{Cl^-}(0,0) = 1 \text{ mol/L}. \tag{6.5.15}$$

At the pit bottom ($x = x_d(0)$):

$$C_{Fe^{2+}}(x_d(0),0) = 5 \text{ mol/L}, \; C_{Na^+}(x_d(0),0) = 1 \text{ mol/L} \quad \text{and} \tag{6.5.16}$$

$$C_{Cl^-}(x_d(0),0) = 11 \text{ mol/L (by local electroneutrality of the solution)}.$$

At the pit solution ($0 < x < x_d(0)$):

$$C_{Fe^{2+}}(x,0) = \text{linear profile from } 10^{-6} \text{ mol/L at } x = 0 \text{ to } 5 \text{ mol/L at } x = x_d(0), \tag{6.5.17}$$

$$C_{Cl^-}(x,0) = \text{linear profile from } 1 \text{ mol/L at } x = 0 \text{ to } 11 \text{ mol/L at } x = x_d(0),$$

$$\text{and } C_{Na^+}(x,0) = 1 \text{ mol/L for all } 0 < x < x_d(0).$$

Figure 6.5.23 illustrates the initial data given by (6.5.15) – (6.5.17).

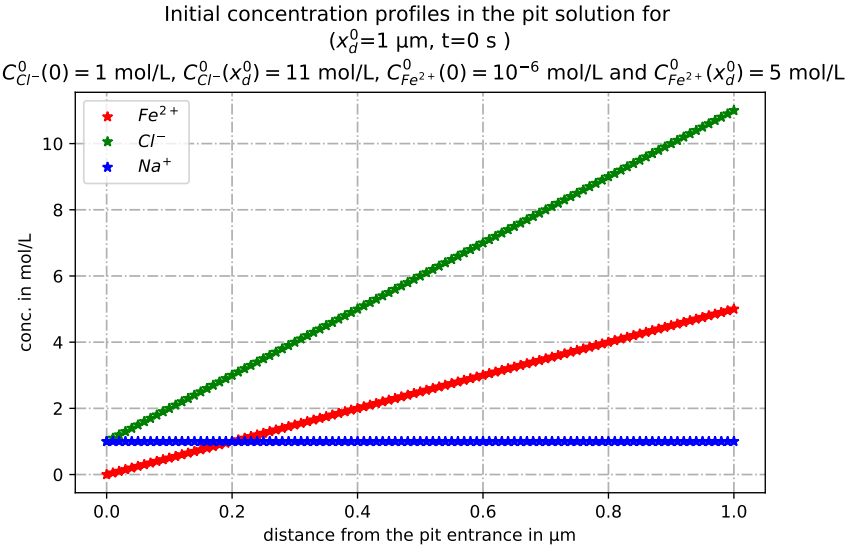

Figure 6.5.23: Initial concentration profiles (at t = 0) in the pit solution; case of a non constant initial data.

Next, using our model(6.3.1)–(6.3.3)–(6.3.4) under the initial data given above and for a given initial depth, we search for the lowest metal potential at which dissolution cannot be sustained. We define it as the critical potential ϕ_m^{stable}. It can be also named the repassivation potential [75]. For such a value, it follows that $C_{\text{Fe}^{2+}}(x_d(t),t) \geqslant C_{\text{crit}} = 3$ mol/L for all $t \geqslant 0$.

Figure 6.5.24 shows that for an initial pit depth of 1 µm and for the initial data (6.5.15) – (6.5.17), the repassivation potential is equal to −26 mV. For such a value and at the first instant of launching the simulation, the metallic cation concentration at the bottom of the pit $C_{\text{Fe}^{2+}}(x_d(t),t)$ decreases during 0,0022 s to reach its minimum value of 3,029 mol/L. Then, it becomes an increasing function in time as shown in Figure 6.5.25. It follows that $C_{\text{Fe}^{2+}}(x_d(t),t) \geqslant C_{\text{crit}} = 3$ mol/L for all $t \geqslant 0$, so that, the criterium of pit stability is respected. As a result, the pit reaches a very high concentration at the early time 0,5 s. This evolution of high concentration does not occur in reality because, in this case, a precipitation of a salt film occurs at the deepest part of the pit. In Figure 6.5.25, the precipitation zone starts above the dashed line.

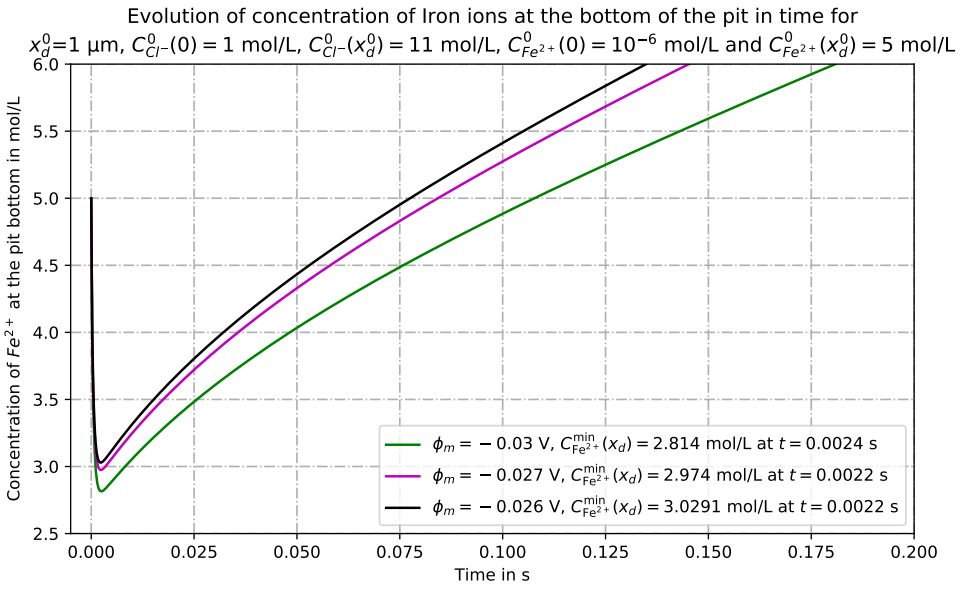

Figure 6.5.24: Search for the critical potential for the initial data (6.5.15) – (6.5.17) and an initial pit depth x_d^0= 1 µm.

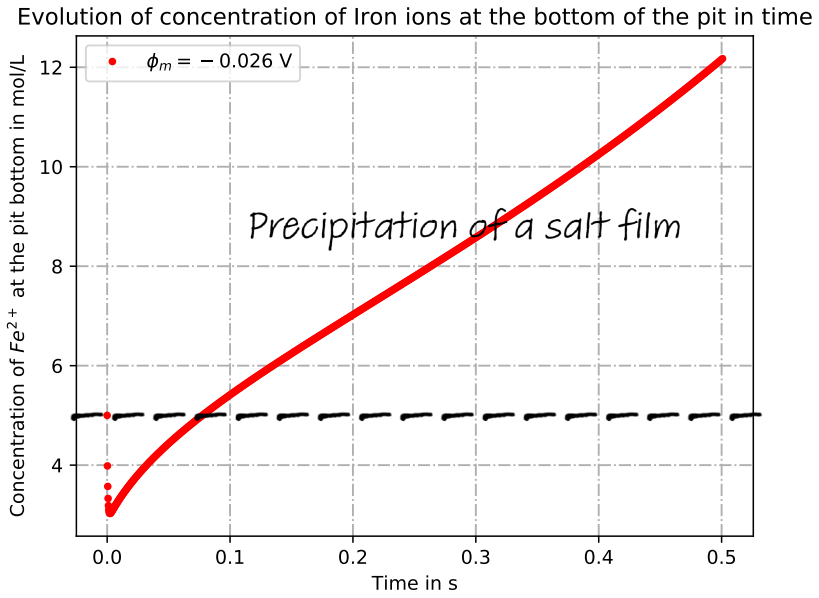

Figure 6.5.25: Evolution of the metallic cation concentration $C_{\mathrm{Fe}^{2+}}(x_d(t),t)$ at the bottom of the pit in time.

Next, we proceed in the same way as in Figure 6.5.24 to obtain Figure 6.5.26. It shows the repassivation potential ϕ_m^{stable} relative to the NHE reference for several initial pit depths $x_d^0 := x_d(0)$. We conclude that the repassivation potential ϕ_m^{stable} is a decreasing function of the initial pit depth.

The comparison of the results of Figure 6.5.26 with related studies [75, 76, 88] gives a good agreement between them, at least qualitatively. In fact, from [75], Figure 6.5.27 shows the behavior of the repassivation potential as a function of the pit depth from artificial pit experiments on stainless steels in chloride media.

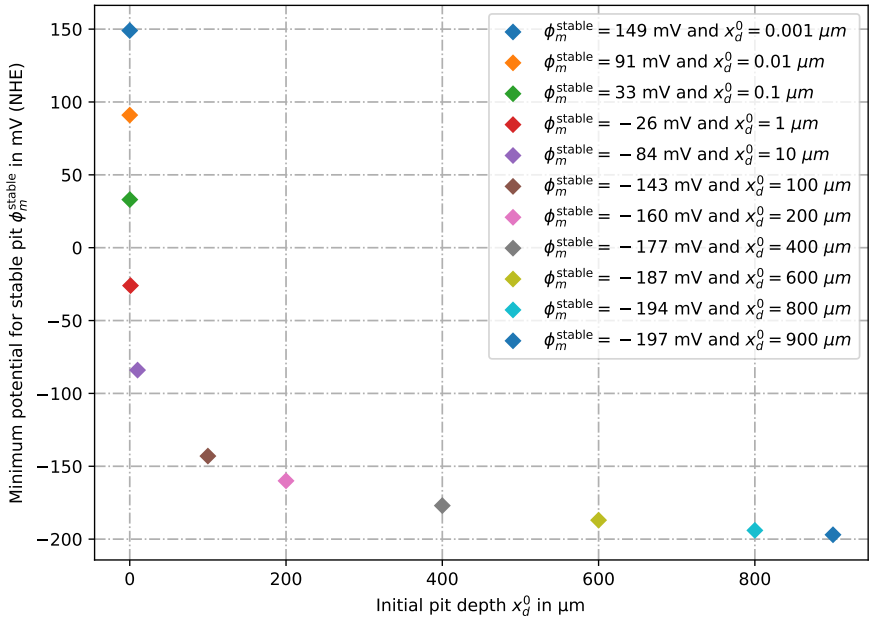

Figure 6.5.26: Identification of the minimal applied potential to ensure the stability of the pit as a function of its initial depth

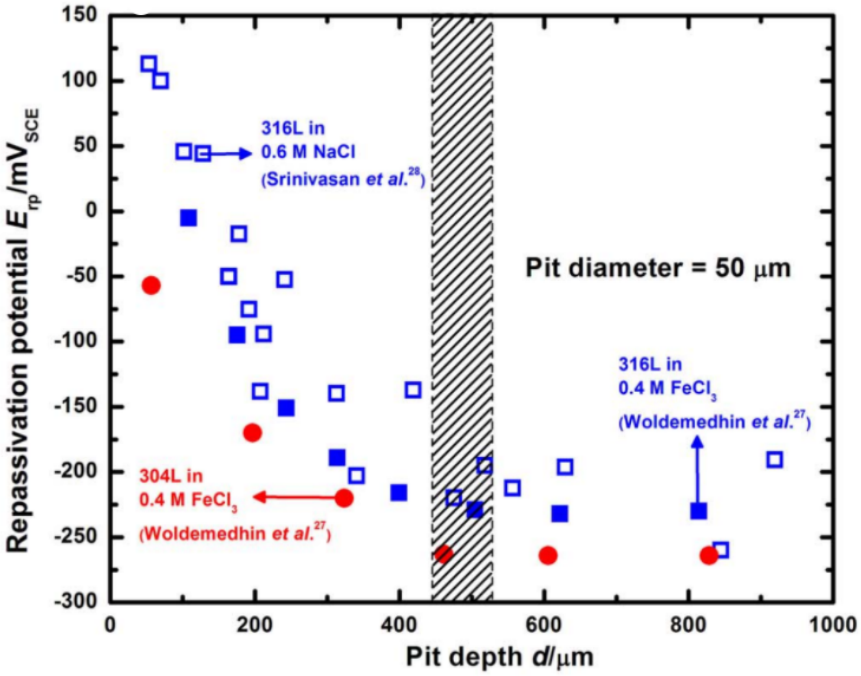

Figure 6.5.27: Observed behavior of the repassivation potential as a function of the pit depth from artificial pit experiments on stainless steels in chloride media [75].

We conclude from the comparison between the of Figure 6.5.26 and the Figure 6.5.27 that there is a similar behavior between them. This validates the hypothesis that the repassivation potential decreases as the initial pit depth increases. In order to obtain quantitatively the same results,

we should perform simulations that are more representative of the experiment or conversely an experiment that is representative of our simulation, thus an experiment that restores the same initial geometry, the same boundary conditions and the same kinetic law of dissolution.

6.5.5 Discussion

We have developed the time dependent model (6.3.1)–(6.3.3) with the moving boundary condition (6.3.4) to describe the potential in the cavity as well as the evolution of the pit or crevice chemistry. At this stage, only diffusion and ion migration were considered. Simulations show that:

1. for each initial depth $x_d^0 \in \{1\text{ nm}, 10\text{ nm}, 100\text{ nm}, 1\ \mu\text{m}, 10\ \mu\text{m}, 100\ \mu\text{m} - 900\ \mu\text{m}\}$, it is possible to identify the minimum applied potential for which the pit can propagate without repassivating during the time scale of our simulations (the criterium for stability is always respected).

   By comparing with literature, we deduce that the phenomena that we have integrated in the development of our model are sufficient at least qualitatively to explain such evolution of the repassivation potential as a function of the initial pit depth.

2. For a pit at a comparatively high potential, needed to ensure its stability, a high metallic cation concentration is reached. This leads to the formation of a salt film.

   In view of literature, Frankel and his colleagues [20, 21] suggest that the transition from metastable to stable pit growth can only be made by pits that are able to precipitate a salt film on long term [44]. This leads to the necessity to integrate the following reactions into the system for the simulation of long term propagation:

$$\mathrm{Fe}^{2+} + \mathrm{Cl}^- \rightleftharpoons \mathrm{FeCl}^+, \tag{6.5.18}$$

   and

$$\mathrm{FeCl}^+ + \mathrm{Cl}^- \rightleftharpoons \mathrm{FeCl}_2. \tag{6.5.19}$$

As we have shown in Chapter 2, many numerical models focus on the stable growth stage of pitting corrosion and on the critical factors influencing its stability. It follows from these studies that the two main criteria to be considered are **the critical concentration of metal cation** and **the critical pH**. Thus, to take into account the notion of pH, it will be necessary to integrate the reaction into the system (6.3.1)–(6.3.3)–(6.3.4). This is the subject of the next section.

6.6 Diffusion-Migration-Reaction model for five ions with moving interface

6.6.1 Motivation

At this level, we have shown that the phenomena that we have integrated in the development of our model (6.3.1)–(6.3.3)–(6.3.4) are sufficient at least qualitatively to describe the stability of the pit and to identify the main factors that influence the corrosion speed.

On the other hand, we have realized that other phenomena which are involved during pitting need to be described. Among these phenomena, we must integrate the chemical reactions in the system to deal with the formation of complex ions and precipitation.

One objective is to integrate, first, the hydrolysis reactions of iron cations in the system. Indeed,

this reaction induces the formation of H^+ cations which changes the acidity of the solution, a criterium often proposed in literature for the pit stability.

6.6.2 Derivation of the equations

In this section, we consider reactions among ions; the dimensional *Nernst-Planck* equation introduced in (6.2.2a) becomes:

$$\frac{\partial C_i}{\partial t} = \nabla \cdot \left(D_i \Big(\nabla C_i + \frac{z_i F}{RT} C_i \nabla \phi \Big) \right) + \mathcal{R}_i \left(\{C\} \right), \quad i = 1, \dots, M, \tag{6.6.1}$$

where $\mathcal{R}_i(\{C\}) := \mathcal{R}_i(C_1, \dots, C_M)$.

We start by giving the dimensional 1D model with five ions including diffusion, migration and reaction terms. For simplicity, we set

$$C_1 := C_{Fe^{2+}}, \quad C_2 := C_{Na^+}, \quad C_3 := C_{Cl^-}, \quad C_4 := C_{H^+}, \quad C_5 := C_{Fe(OH)^+}.$$

We assume that the following reaction takes place in the system:

$$\mathrm{Fe}^{2+} + \mathrm{H_2O} \underset{\mathrm{k}_{1b}}{\overset{\mathrm{k}_{1f}}{\rightleftharpoons}} \mathrm{Fe\,(OH)}^{+} + \mathrm{H}^{+}. \tag{6.6.2}$$

This reaction proceeds in both directions: forwards and backwards. When equilibrium is reached, the forward and the backward rates become equal, and the amount of reactants and products obeys the fundamental law of mass action:

$$K_1 = \frac{k_{1f}}{k_{1b}} = \frac{\frac{C_4}{C_{\text{ref}}} \frac{C_5}{C_{\text{ref}}}}{\frac{C_1}{C_{\text{ref}}} \frac{C_{H_2O}}{C_{\text{ref}}}} \simeq 10^{-9.316} \qquad \text{(Law of Mass Action)}, \tag{6.6.3}$$

where $C_{\mathrm{H_2O}} = C_{\text{ref}} = 1$ mol/L. K_1 is called the equilibrium constant of the chemical reaction (6.6.2).

This leads to consider the following diffusion-migration-reaction model with moving interface

For $t > 0$ and $0 < x < x_d(t)$, we have

$$\begin{cases}
\dfrac{\partial C_1}{\partial t} = \dfrac{\partial}{\partial x}\left(D_1 \left(\dfrac{\partial C_1}{\partial x} + z_1 \dfrac{F}{RT} C_1 \dfrac{\partial \phi}{\partial x} \right) \right) - k_{1f} \dfrac{C_1}{C_{\text{ref}}} + k_{1b} \dfrac{C_4}{C_{\text{ref}}} \dfrac{C_5}{C_{\text{ref}}}, & \text{(6.6.4a)} \\
\dfrac{\partial C_2}{\partial t} = \dfrac{\partial}{\partial x}\left(D_2 \left(\dfrac{\partial C_2}{\partial x} + z_2 \dfrac{F}{RT} C_2 \dfrac{\partial \phi}{\partial x} \right) \right), & \text{(6.6.4b)} \\
\dfrac{\partial C_3}{\partial t} = \dfrac{\partial}{\partial x}\left(D_3 \left(\dfrac{\partial C_3}{\partial x} + z_3 \dfrac{F}{RT} C_3 \dfrac{\partial \phi}{\partial x} \right) \right), & \text{(6.6.4c)} \\
\dfrac{\partial C_4}{\partial t} = \dfrac{\partial}{\partial x}\left(D_4 \left(\dfrac{\partial C_4}{\partial x} + z_4 \dfrac{F}{RT} C_4 \dfrac{\partial \phi}{\partial x} \right) \right) + k_{1f} \dfrac{C_1}{C_{\text{ref}}} - k_{1b} \dfrac{C_4}{C_{\text{ref}}} \dfrac{C_5}{C_{\text{ref}}}, & \text{(6.6.4d)} \\
\dfrac{\partial C_5}{\partial t} = \dfrac{\partial}{\partial x}\left(D_5 \left(\dfrac{\partial C_5}{\partial x} + z_5 \dfrac{F}{RT} C_5 \dfrac{\partial \phi}{\partial x} \right) \right) + k_{1f} \dfrac{C_1}{C_{\text{ref}}} - k_{1b} \dfrac{C_4}{C_{\text{ref}}} \dfrac{C_5}{C_{\text{ref}}}, & \text{(6.6.4e)}
\end{cases}$$

Next to have a good understanding of the behavior of the above system, we look for its non-dimensional form. This latter non-dimensional system is of the same type as (6.6.4), but with differently defined parameters. These parameters are given by (6.2.3) and we recall their expression below

$$x = L\widehat{x}, \quad t = \frac{L^2}{D_0}\widehat{t}, \quad C_i = C_0 \widehat{C}_i, \quad D_i = D_0 \widehat{D}_i, \quad \phi = \frac{RT}{F}\widehat{\phi}. \tag{6.6.5}$$

Then, we can deduce that the rate constants k_{1f} and k_{1b} for the forward and backward reaction are normalized by $\dfrac{D_0 C_{\text{ref}}}{L^2}$ and $\dfrac{D_0 C_{\text{ref}}^2}{L^2 C_0}$, respectively. Indeed, we have that

$$\frac{\partial C_1}{\partial t} = \frac{\partial}{\partial x}\left(D_1\left(\frac{\partial C_1}{\partial x} + z_1\frac{F}{RT}C_1\frac{\partial \phi}{\partial x}\right)\right) - k_{1f}\frac{C_1}{C_{\text{ref}}} + k_{1b}\frac{C_4}{C_{\text{ref}}}\frac{C_5}{C_{\text{ref}}};$$

from (6.6.5), we obtain

$$C_0\frac{D_0}{L^2}\frac{\partial \widehat{C_1}}{\partial \hat{t}} = \frac{1}{L}\frac{\partial}{\partial \hat{x}}\left(\frac{D_0 C_0}{L}\widehat{D_1}\left(\frac{\partial \widehat{C_1}}{\partial \hat{x}} + z_1\frac{F}{RT}\widehat{C_1}\frac{RT}{F}\frac{\partial \hat{\phi}}{\partial \hat{x}}\right)\right) - k_{1f}\frac{C_1}{C_{\text{ref}}} + k_{1b}\frac{C_4}{C_{\text{ref}}}\frac{C_5}{C_{\text{ref}}},$$

so that

$$\frac{\partial \widehat{C_1}}{\partial \hat{t}} = \frac{\partial}{\partial \hat{x}}\left(\widehat{D_1}\left(\frac{\partial \widehat{C_1}}{\partial \hat{x}} + z_1\widehat{C_1}\frac{\partial \hat{\phi}}{\partial \hat{x}}\right)\right) - \frac{L^2}{D_0 C_0}\left(k_{1f}\frac{C_0\widehat{C_1}}{C_{\text{ref}}} - k_{1b}\frac{C_0\widehat{C_4}}{C_{\text{ref}}}\frac{C_0\widehat{C_5}}{C_{\text{ref}}}\right).$$

Then, we deduce that

$$\widehat{k_{1f}} = \frac{L^2}{D_0 C_{\text{ref}}}k_{1f}, \quad \widehat{k_{1b}} = \frac{L^2 C_0}{D_0 C_{\text{ref}}^2}k_{1b}.$$

Thus, the system (6.6.4) becomes

For $\hat{t} > 0$ and $0 < \hat{x} < \widehat{x_d(t)}$, we have

$$\begin{cases}
\dfrac{\partial \widehat{C_1}}{\partial \hat{t}} = \dfrac{\partial}{\partial \hat{x}}\left(\widehat{D_1}\left(\dfrac{\partial \widehat{C_1}}{\partial \hat{x}} + z_1\widehat{C_1}\dfrac{\partial \hat{\phi}}{\partial \hat{x}}\right)\right) - \widehat{k_{1f}}\widehat{C_1} + \widehat{k_{1b}}\widehat{C_4}\widehat{C_5}, & \text{(6.6.6a)}\\
\dfrac{\partial \widehat{C_2}}{\partial \hat{t}} = \dfrac{\partial}{\partial \hat{x}}\left(\widehat{D_2}\left(\dfrac{\partial \widehat{C_2}}{\partial \hat{x}} + z_2\widehat{C_2}\dfrac{\partial \hat{\phi}}{\partial \hat{x}}\right)\right), & \text{(6.6.6b)}\\
\dfrac{\partial \widehat{C_3}}{\partial \hat{t}} = \dfrac{\partial}{\partial \hat{x}}\left(\widehat{D_3}\left(\dfrac{\partial \widehat{C_3}}{\partial \hat{x}} + z_3\widehat{C_3}\dfrac{\partial \hat{\phi}}{\partial \hat{x}}\right)\right), & \text{(6.6.6c)}\\
\dfrac{\partial \widehat{C_4}}{\partial \hat{t}} = \dfrac{\partial}{\partial \hat{x}}\left(\widehat{D_4}\left(\dfrac{\partial \widehat{C_4}}{\partial \hat{x}} + z_4\widehat{C_4}\dfrac{\partial \hat{\phi}}{\partial \hat{x}}\right)\right) + \widehat{k_{1f}}\widehat{C_1} - \widehat{k_{1b}}\widehat{C_4}\widehat{C_5}, & \text{(6.6.6d)}\\
\dfrac{\partial \widehat{C_5}}{\partial \hat{t}} = \dfrac{\partial}{\partial \hat{x}}\left(\widehat{D_5}\left(\dfrac{\partial \widehat{C_5}}{\partial \hat{x}} + z_5\widehat{C_5}\dfrac{\partial \hat{\phi}}{\partial \hat{x}}\right)\right) + \widehat{k_{1f}}\widehat{C_1} - \widehat{k_{1b}}\widehat{C_4}\widehat{C_5}, & \text{(6.6.6e)}
\end{cases}$$

where

$$\widehat{k_{1f}} = \frac{L^2}{D_0 C_{\text{ref}}}k_{1f}, \quad \widehat{k_{1b}} = \frac{L^2 C_0}{D_0 C_{\text{ref}}^2}k_{1b}. \qquad \text{(6.6.7)}$$

Next, from (6.6.3) we have that $K_1 = \dfrac{k_{1f}}{k_{1b}}$. It follows from (6.6.7) that

$$K_1 = \frac{k_{1f}}{k_{1b}} = \frac{C_0}{C_{\text{ref}}}\frac{\widehat{k_{1f}}}{\widehat{k_{1b}}} = \frac{C_0}{C_{\text{ref}}}\widehat{K_1}, \quad \text{where } \widehat{K_1} = \frac{\widehat{k_{1f}}}{\widehat{k_{1b}}} = \frac{\widehat{C_4}\,\widehat{C_5}}{\widehat{C_1}}. \qquad \text{(6.6.8)}$$

In view of the equality $\widehat{K_1} = \dfrac{\widehat{k_{1f}}}{\widehat{k_{1b}}}$, the full non-dimensional model is given by

$$\begin{cases} \dfrac{\partial}{\partial x}\left(\sigma\dfrac{\partial\phi}{\partial x}\right)+\displaystyle\sum_{i=1}^{5}\frac{\partial}{\partial x}\left(z_iD_i\frac{\partial C_i}{\partial x}\right)=0, \quad 0<x<x_d(t),\, t>0, & \text{(6.6.9a)}\\ \sigma\dfrac{\partial\phi}{\partial x}+\displaystyle\sum_{i=1}^{5}z_iD_i\frac{\partial C_i}{\partial x}=2\widehat{f}(\phi,C_1) \quad \text{at} \quad x=x_d(t), & \text{(6.6.9b)}\\ \phi(0,t)=0, \quad t>0, & \text{(6.6.9c)} \end{cases}$$

where $\sigma := \displaystyle\sum_{i=1}^{5} z_i^2 D_i\, C_i$

and

$$\widehat{f}\,(\phi,C_1)=\widehat{k}_a\exp\big(-(\phi-\widehat{\phi}_m)\big)-\widehat{k}_c\,\frac{C_0}{C_{\text{ref}}}\,C_1\exp\big(\phi-\widehat{\phi}_m\big), \qquad \text{(6.6.10)}$$

For $t>0$ and $0<x<x_d(t)$, we have

$$\begin{cases} \dfrac{\partial C_1}{\partial t}=\dfrac{\partial}{\partial x}\left(D_1\left(\dfrac{\partial C_1}{\partial x}+z_1C_1\dfrac{\partial\phi}{\partial x}\right)\right)-\widehat{k_{1f}}\left(C_1-\dfrac{1}{\widehat{K_1}}C_4C_5\right), & \text{(6.6.11a)}\\ \dfrac{\partial C_2}{\partial t}=\dfrac{\partial}{\partial x}\left(D_2\left(\dfrac{\partial C_2}{\partial x}+z_2C_2\dfrac{\partial\phi}{\partial x}\right)\right), & \text{(6.6.11b)}\\ \dfrac{\partial C_3}{\partial t}=\dfrac{\partial}{\partial x}\left(D_3\left(\dfrac{\partial C_3}{\partial x}+z_3C_3\dfrac{\partial\phi}{\partial x}\right)\right), & \text{(6.6.11c)}\\ \dfrac{\partial C_4}{\partial t}=\dfrac{\partial}{\partial x}\left(D_4\left(\dfrac{\partial C_4}{\partial x}+z_4C_4\dfrac{\partial\phi}{\partial x}\right)\right)+\widehat{k_{1f}}\left(C_1-\dfrac{1}{\widehat{K_1}}C_4C_5\right), & \text{(6.6.11d)}\\ \dfrac{\partial C_5}{\partial t}=\dfrac{\partial}{\partial x}\left(D_5\left(\dfrac{\partial C_5}{\partial x}+z_5C_5\dfrac{\partial\phi}{\partial x}\right)\right)+\widehat{k_{1f}}\left(C_1-\dfrac{1}{\widehat{K_1}}C_4C_5\right), & \text{(6.6.11e)}\\ D_1\dfrac{\partial C_1}{\partial x}+2D_1C_1\dfrac{\partial\phi}{\partial x}=-\dot{x}_d(t)C_1+\widehat{f}(\phi,C_1), \quad t>0 \text{ and } x=x_d(t) & \text{(6.6.11f)}\\ D_i\dfrac{\partial C_i}{\partial x}+z_iD_iC_i\dfrac{\partial\phi}{\partial x}=-\dot{x}_d(t)C_i \quad (i=2,\ldots,5), \quad t>0 \text{ and } x=x_d(t) & \text{(6.6.11g)}\\ C_i(0,t)=a_i, \quad (i=1,2,\ldots,5), \quad t>0 \text{ and } x=0 & \text{(6.6.11h)} \end{cases}$$

along with the free boundary condition (6.3.4)

$$\dot{x}_d(t)=b\,\widehat{f}(\phi,C_1) \quad \text{on} \quad x_d(t), \qquad \text{(6.6.12)}$$

where

$$\widehat{K_1}=\frac{\widehat{k_{1f}}}{\widehat{k_{1b}}}=\frac{C_4\,C_5}{C_1} \qquad \text{(6.6.13)}$$

and

$$\widehat{k_{1f}}=\frac{L^2}{D_0C_{\text{ref}}}k_{1f}. \qquad \text{(6.6.14)}$$

Here, we have dropped the symbol $\widehat{\cdot}$ for notational simplicity except for the reaction rate constants $\widehat{k_{1f}}$ and $\widehat{k_{1b}}$ satisfying (6.6.7), the equilibruim constant $\widehat{K_1}$ satisfying (6.6.8), $\widehat{f}$, $\widehat{\phi}_m$, $\widehat{k}_a$ and $\widehat{k}_c$ satisfying (6.6.10).

Chemical equilibrium at every position x and at every time t

In the pit solution, the hydrolysis reaction (6.6.2) $\mathrm{Fe^{2+}} + \mathrm{H_2O} \underset{\widehat{k_{1b}}}{\overset{\widehat{k_{1f}}}{\rightleftharpoons}} \mathrm{Fe\,(OH)^{+}} + \mathrm{H^{+}}$ occurs. It does not stop but comes to equilibrium (which then lasts forever when undisturbed).

In general, it is considered that the reaction takes place much faster than the diffusion and migration except probably at the first moments of the pit propagation where a high current explosion takes place. Only in this case, the transport can be probably faster than the reaction.

After these first moments of pit propagation, one can expect that the reaction is much faster than the transport of ions. This means that in (6.6.2) the rate of the forward reaction $\widehat{k_{1f}}$ tends to infinity ($\widehat{k_{1f}} \to \infty$). It follows that the term $(C_1 - \dfrac{1}{\widehat{K_1}} C_4 C_5)$ must be set to 0 in each of the equations (6.6.11a), (6.6.11d) and (6.6.11e). Therefore, the following relation holds, at least approximately

$$C_4(x,t)\, C_5(x,t) = \widehat{K_1} C_1(x,t) \quad \text{for any } x, t. \tag{6.6.15}$$

This implies that the equilibrium state of the reaction (6.6.2) is achieved at every position x and at every time t.

Remark 6.6.1. *The initial data for the concentrations*

$$C_1(x,0) = C_1^0(x), \quad C_4(x,0) = C_4^0(x), C_3(x,0) = C_3^0(x) \quad \textit{for all } 0 \leqslant x \leqslant x_d(0)$$

must satisfy the condition (6.6.15).

6.6.3 Numerical simulations of the diffusion-migration-reaction model in the case of constant initial data

In this subsection, the dimensional parameters are used.

6.6.3.1 Identification of the initial data to use in our simulations

We consider a one-dimensional pit grown in 1 mol/L NaCl which initially contains 10^{-6} mol/L of Fe^{2+}. Next, according to Remark 6.6.1, the initial data must be at the equilibrium state, so that it satisfies (6.6.15) which is equivalent in its dimensional form to (6.6.3).

At equilibrium, we assume that

$$C^{0,\mathrm{eq}}_{\mathrm{Fe}^{2+}} = (10^{-6} - y)\ \mathrm{mol/L} \quad \text{and} \quad C^{0,\mathrm{eq}}_{\mathrm{H}^{+}} = C^{0,\mathrm{eq}}_{\mathrm{Fe(OH)}^{+}} = y\ \mathrm{mol/L},$$

where y is the concentration of each reactant and product in the chemical reaction (6.6.2) at equilibrium.

Next in order to find the value of y, we need to solve the following quadratic equation

$$y^2 + K_1\, y - 10^{-6} K_1 = 0. \tag{6.6.16}$$

This quadratic equation (6.6.16) is derived from (6.6.3). Indeed, it follows from (6.6.3) that

$$K_1 = \frac{k_{1f}}{k_{1b}} = \frac{\dfrac{C^{0,\mathrm{eq}}_{\mathrm{H}^{+}}}{C_{\mathrm{ref}}} \dfrac{C^{0,\mathrm{eq}}_{\mathrm{Fe(OH)}^{+}}}{C_{\mathrm{ref}}}}{\dfrac{C^{0,\mathrm{eq}}_{\mathrm{Fe}^{2+}}}{C_{\mathrm{ref}}} \dfrac{C_{H_2O}}{C_{\mathrm{ref}}}} \quad \text{where} \quad C_{\mathrm{H_2O}} = C_{\mathrm{ref}} = 1\ \mathrm{mol/L},$$

so that, $K_1 = \dfrac{y^2}{10^{-6} - y}$. Then, (6.6.16) follows.

Setting $K_1 = 10^{-9.316}$, we compute (6.6.16) to obtain the following initial data

$$C^0_{\mathrm{Fe}^{2+}}(x) = 9{,}782\ .\ 10^{-7}\ \mathrm{mol/L}, C^0_{\mathrm{H}^{+}}(x) = C^0_{\mathrm{Fe(OH)}^{+}}(x) = 2{,}173\ .\ 10^{-8}\ \mathrm{mol/L},$$

$$C^0_{Na^+}(x) = 1 \text{ mol/L and } C^0_{Cl^-}(x) = 1.0000019565232072 \text{ mol/L},$$

where $C_{Cl^-}(x)$ is given by supporting the local-electroneutrality of the solution.

We consider an initial pit depth x_d^0 of 1 μm and we set ϕ_m to -0.3 V|NHE.

Computations are performed with the following choice of the reference parameters:

$$D_0 = 1 \times 10^{-9}\ m^2.s^{-1}, \quad L = 1\ \mu m, \quad C_0 = 1000 \text{ mol/m}^3 = 1 \text{ mol/}L.$$

As for the diffusion coefficients [5], we set

$$D_{Fe^{2+}} = 7{,}19\ .\ 10^{-10}\ m^2.s^{-1}, \quad D_{Cl^-} = 2{,}032\ .\ 10^{-9}\ m^2.s^{-1}, \quad D_{Na^+} = 1{,}334\ .\ 10^{-9}\ m^2.s^{-1},$$
$$D_{H^+} = 9{,}31\ .\ 10^{-9}\ m^2.s^{-1} \text{ and } D_{Fe(OH)^+} = 0{,}75\ .\ 10^{-9}\ m^2.s^{-1}$$

6.6.3.2 Numerical simulations

1) Verification of the chemical equilibrium

To start the simulations, the first step is to give a value for the forward reaction rate constant k_{1f}. As mentioned above, the constant k_{1f} will tend to ∞. Numerically, it comes to search the magnitude of this constant for which the relation (6.6.15) holds at every position x of the pit solution and at every time t. In other words, from (6.6.3), it comes to show that the following ratio is approximately equal to 1

$$\frac{K_1\ C_{Fe^{2+}}}{C_{H^+}\ C_{Fe(OH)^+}} \approx 1 \qquad \text{for all } t > 0,\ 0 \leqslant x \leqslant x_d(t). \tag{6.6.17}$$

Numerically, to avoid divergence of the Newton method in the numerical simulations, we have tried several choices for the forward reaction rate constant k_{1f}. If we choose a value of $k_{1f} > 10^5$ mol.m^{-3}.s^{-1}, it is necessary to take an extremely small time step which makes the computing time (CPU time) very large (see Figure 6.6.1). Indeed, Figure 6.6.1 shows that for $k_{1f} = 10^9$ mol.m^{-3}.s^{-1}, the equilibrium state of the reaction (6.6.2) is respected very early. However, the CPU time is large (226 s) for simulating only a final depth of 1,1 µm which corresponds to 18 s of pit propagation.

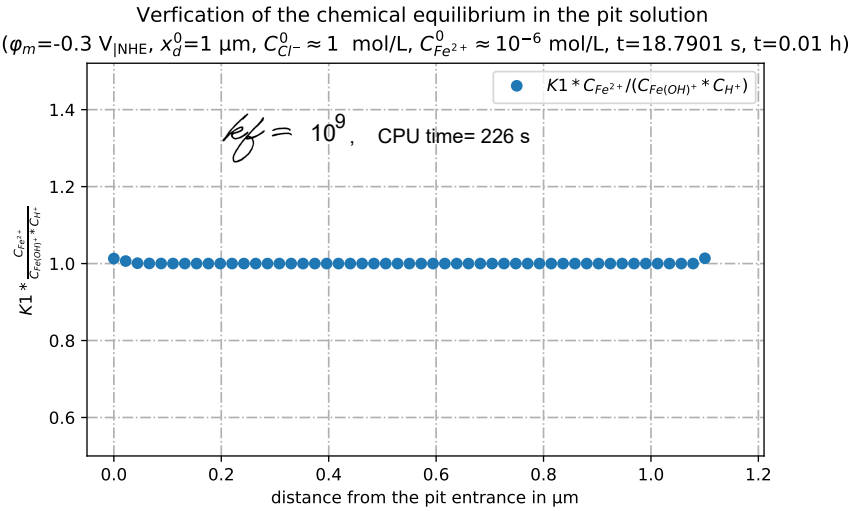

Figure 6.6.1: Illustration of the code sensibility to the choice of the value of the reaction rate constant k_{1f}.

[5] Reference: https://www.aqion.de/site/194: PhreeqC (Version 3) – A Computer Program for Speciation, Batch-Reaction, One-Dimensional Transport, and Inverse Geochemical Calculations; [The diffusion coefficients are taken from the thermodynamic database "phreeqc.dat"].

Therefore, since we aim to simulate on long periods of time, we choose to avoid such a situation.

Remark 6.6.2. *The code is very sensitive to the choice of the input data k_{1f}.*

Setting k_{1f} to 10^5 mol.m^{-3}.s^{-1} seems to be the optimal choice to run long simulation periods. Then, since $K_1 = \dfrac{k_{1f}}{k_{1b}} = 10^{-9.316}$, it follows that $k_{1b} = 2{,}07 \,.\, 10^{14}$ mol.m^{-3}.s^{-1}.

In this simulation, we adopt three time steps:

- $\Delta t_1 = 10^{-6}$ s for the first 60 iterations in time ($n < 60$; n is the number of iterations in time). We can describe the first times of the simulation as an explosion stage,
- $\Delta t_2 = 10^{-1}$ for $60 \leqslant n < 150$,
- $\Delta t_3 = 10^{2}$ for $n \geqslant 150$; the system is more stable.

In Figure 6.6.2, for two distinct times, we compute the ratio given by (6.6.17) at every position x of the pit solution to verify the chemical equilibrium along the pit solution. As we have shown previously, to satisfy the chemical equilibrium, it comes to verify that the ratio (6.6.17) is approximately equal to 1.

Figure 6.6.2a shows approximately the first time ($t_1 = 3309$ s) from which the chemical equilibrium is respected almost everywhere along the pit solution. In fact, the reaction takes place quickly to adjust the values of concentrations at early time. Once the chemical equilibrium is reached, it will be respected forever (when undisturbed) as we have shown, after $t_2 = 33{,}53$ hours of pit propagation, in Figure 6.6.2b. We conclude that the chemical equilibrium is respected at any time $t > t_1$.

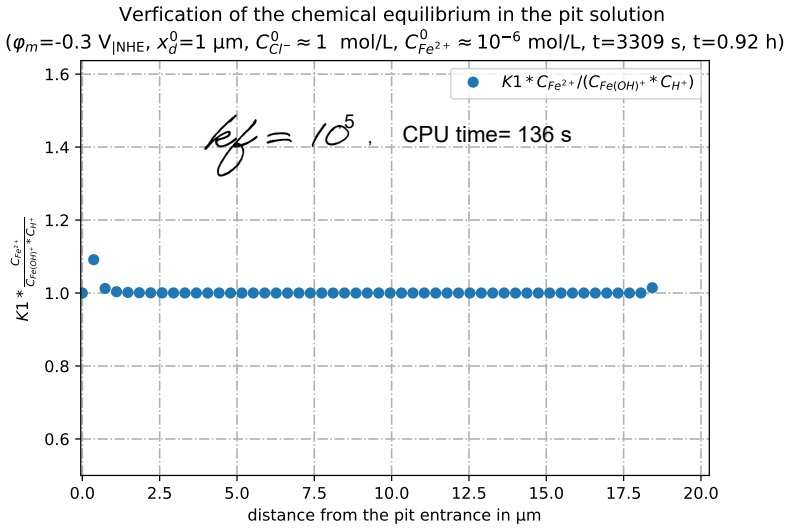

(a) Verification of the chemical equilibrium at each position of the pit solution at $t_1 = 3309$ s.

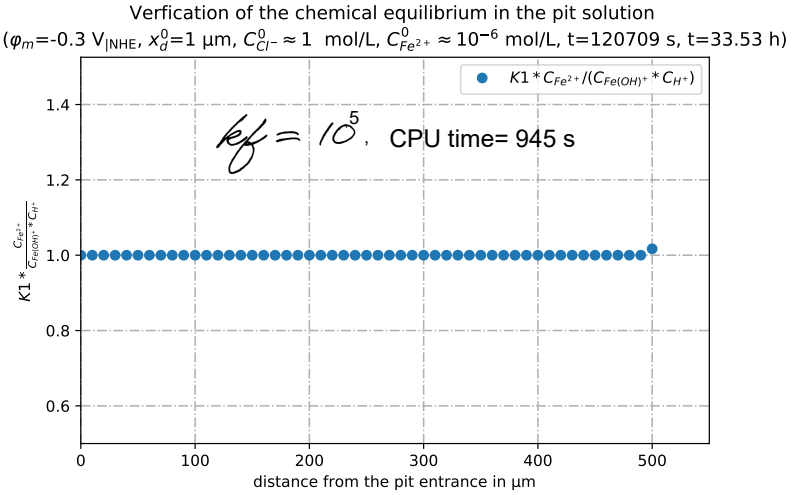

(b) Verification of the chemical equilibrium at each position of the pit solution at $t_2 = 33{,}53$ hours (which corresponds to a pit depth of 500 µm).

Figure 6.6.2: Verification of the chemical equilibrium in the pit solution at two distinct times.

Remark 6.6.3 (About the CPU time)**.** *In our code we use an adaptive time step to control the propagation speed of the pit. Indeed, the first moments of the pit propagation (system startup) can be described as an explosion state. Here we need to consider a small time step to capture this huge evolution. Then, the system becomes more stable. In this case a larger time step can be used.*

Therefore, the different possible choices of these time steps have an impact on the CPU time. So, the given value of the CPU time is only an approximate value that allows us to have an idea about the order of magnitude of the time needed to run the code.

2) Evolution of the concentrations of each chemical species and the acidity of the pit solution

Figure 6.6.3 shows the evolution of the chemical aqueous species concentrations in the pit solution over a depth of 500 µm. Figure 6.6.3b shows that there is less accumulation of H^+ ions than $Fe(OH)^+$ ions in the pit solution. This is due to the faster diffusion in the pit solution of the H^+

ions than the $Fe(OH)^+$ ions [79, p.86] :

$$D_{H^+} = 9{,}31 \,.\, 10^{-9}\ m^2.s^{-1} \quad \text{and} \quad D_{Fe(OH)^+} = 0{,}75 \,.\, 10^{-9}\ m^2.s^{-1}\ .$$

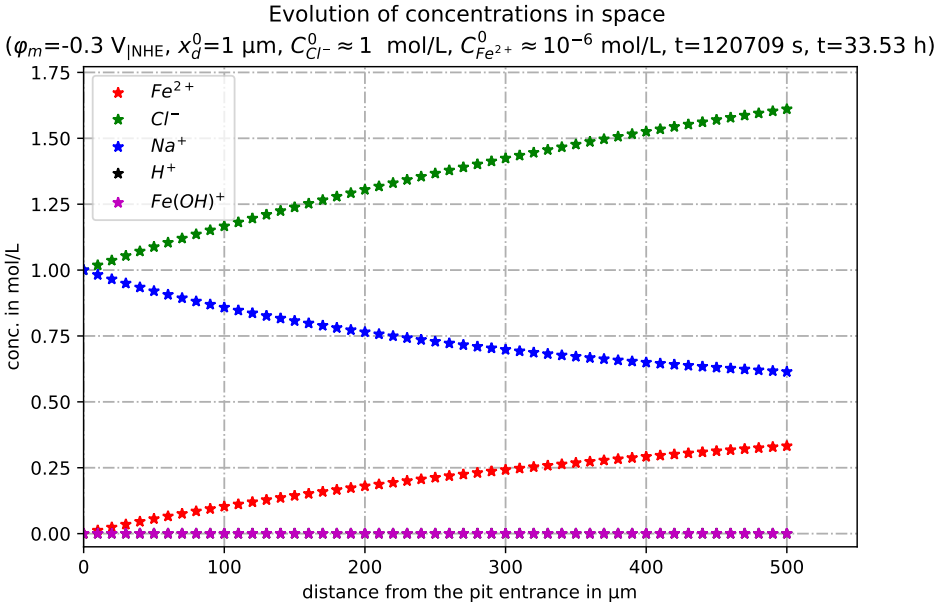

(a) Evolution of all the species concentrations in the pit solution.

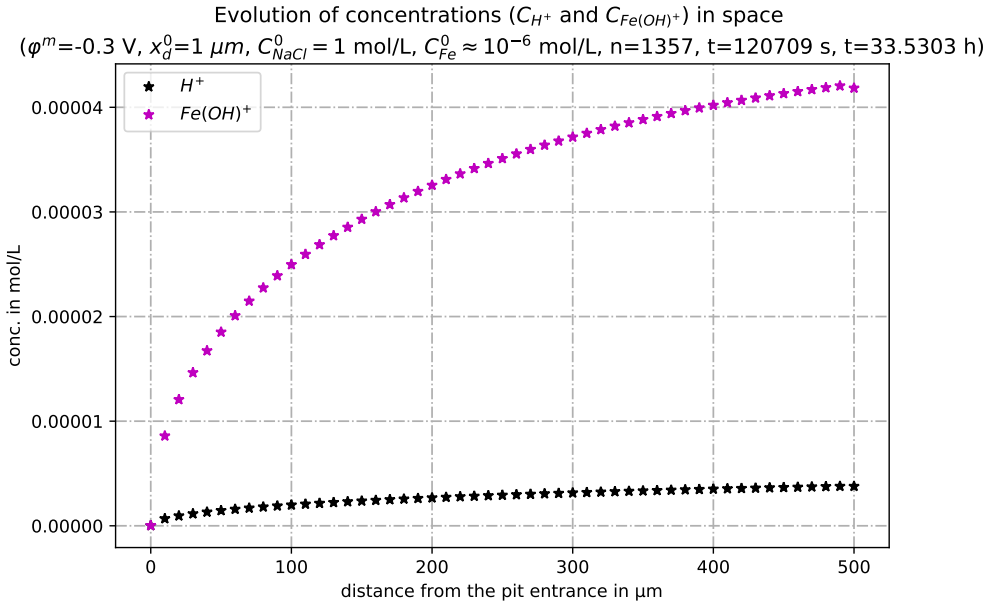

(b) Zoom on the H^+ and $Fe(OH)^+$ concentrations in the pit solution.

Figure 6.6.3: Evolution of the concentrations in the pit solution.

Next, we recall that the acidity of the pit solution is given by the value of pH. The pH (Potential Hydrogen) is defined as the negative decimal logarithm of the hydrogen ion activity. In the aqueous solution, we have that $0 < \text{pH} < 14$. It can be determined by

$$\text{pH} = -\log_{10} C_{H^+}. \tag{6.6.18}$$

Figure 6.6.5 shows the evolution of the acidity along the pit solution over a depth of 500 μm. The acidity of the solution increases in space and reaches its maximum at the pit bottom. It increases

also in time due to increasing the H^+ concentration. In fact, initially, the pH of the solution is equal to 7.58 as shown in Figure 6.6.4. Then, after 33,5 hours of pit propagation, it reaches the value 5,3.

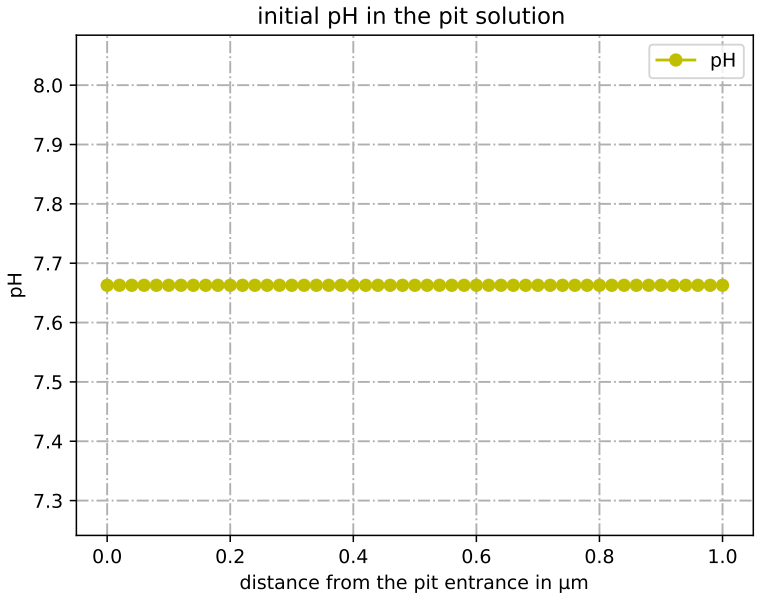

Figure 6.6.4: The initial pH of the pit solution over a depth of 1 μm.

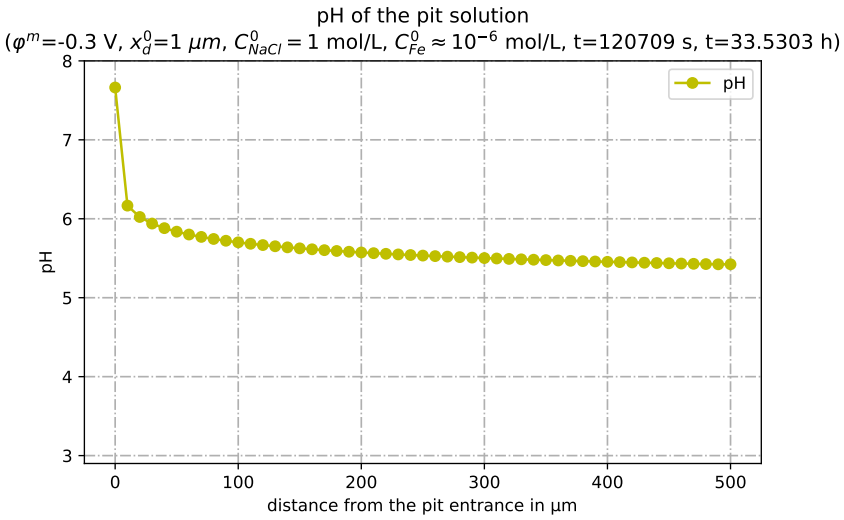

Figure 6.6.5: Evolution of the acidity along the pit solution over a depth of 500 μm.

As we have shown, **the acidity of the pit solution reaches its maximum at the pit bottom**. In the other side, similarly, the metallic cation concentration $C_{\mathrm{Fe}^{2+}}$, as shown in Figure 6.6.3a, reaches its maximum at the pit bottom. **Therefore, we deduce that the acidity and the metallic cations concentrations have a similar behavior. This reflects the strong link between the two critical factors influencing the pit stability.**

6.6.4 The various parameters that influence the acidity of the pit solution

In this subsection, we present the various parameters that influence the acidity of the pit solution.

1) Evolution of the pH in time

Figure 6.6.6 shows that the pH in the pit solution decreases in time. It can be explained as we have shown previously by an increase of the metallic cation concentration in the pit solution which results in the production of more H^+ ions by reaction (6.6.2). Figure 6.6.6b shows that the pH decreases very slowly in time.

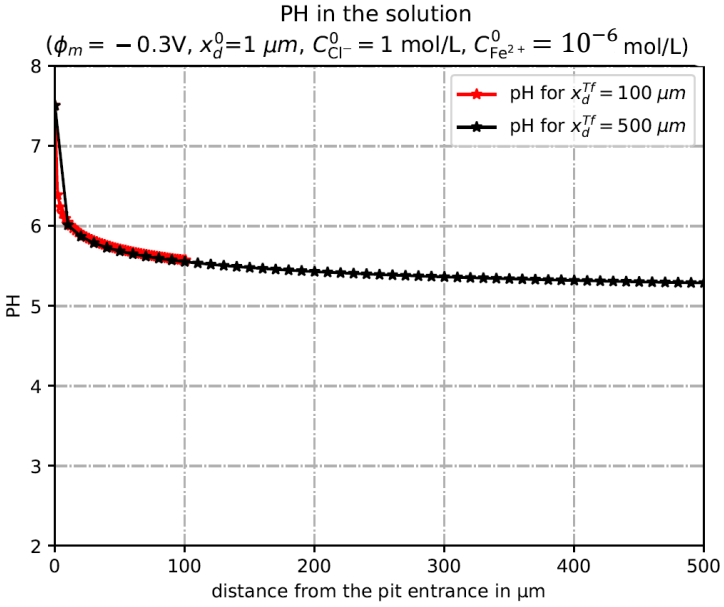

(a) pH on the pit solution over a depth of 100 μm and 500 μm.

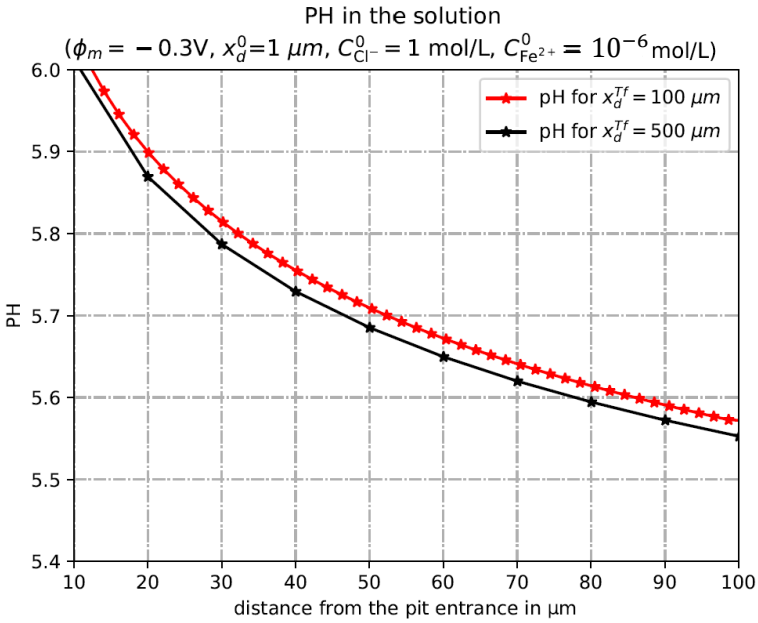

(b) Zoom on the pH of the pit solution over a depth of 100 μm.

Figure 6.6.6: Evolution of the acidity of the pit solution in time.

Figure 6.6.7 shows the evolution of the pH in the pit solution at early time. Initially, the pH is equal to 7,663. When the pit depth evolves by 102 nm, the pH decreases by a value of 1,025 to become 6,637. Next, when the pit depth reaches 5 µm, the pH only decreases by a value of 1,35 to become 6,307. We deduce that that the evolution of the pH is progressively slower in time.

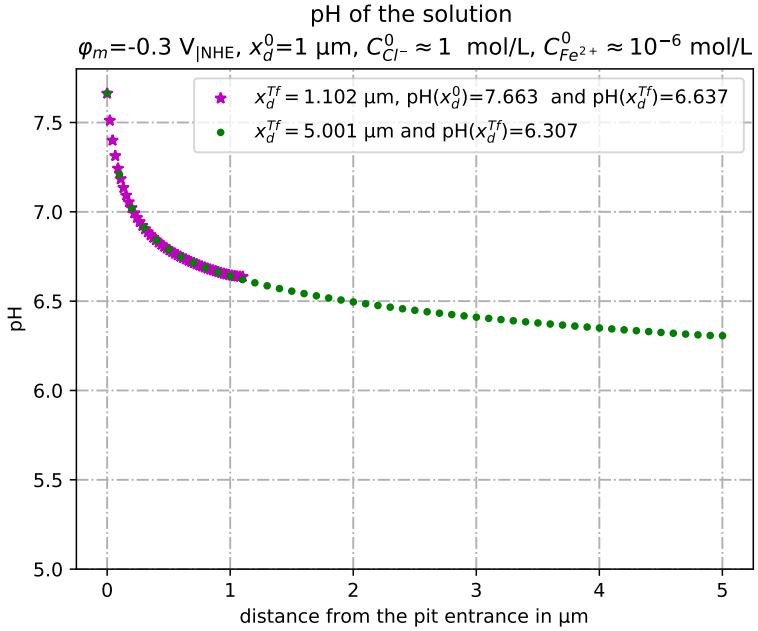

Figure 6.6.7: Evolution of the pH in the pit solution at early time.

2) Evolution of pH in function of the metal potential ϕ_m

Figure 6.6.8 shows that the acidity of the pit solution increases with metal potential. This is in agreement with the much higher metallic cation concentration in the pit at high potential.

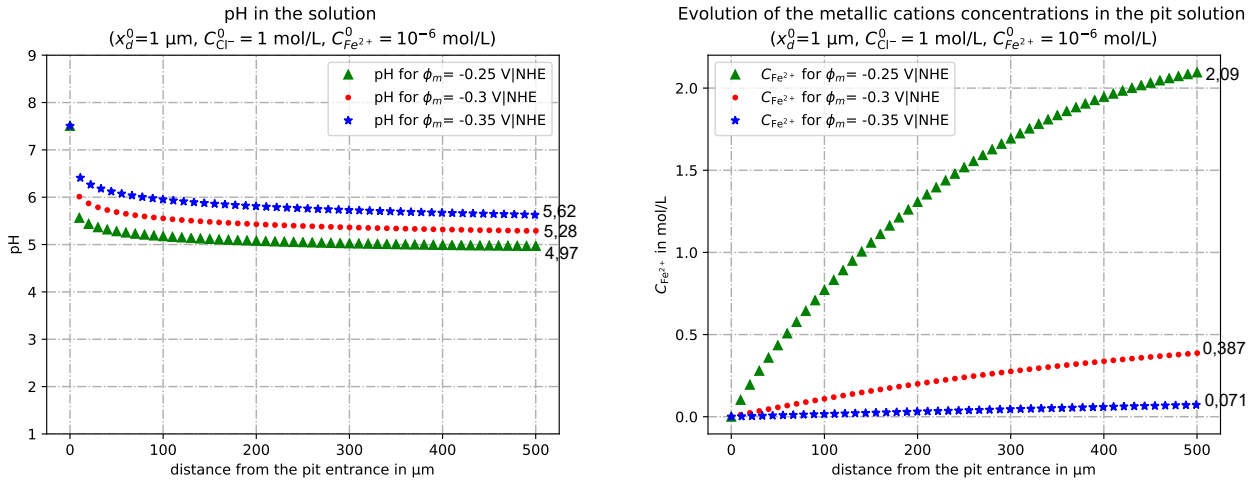

(a) Evolution of the pH on the pit solution for several metal potentials ϕ_m.

(b) Evolution of the metallic cations concentrations in the pit solution for several metal potentials ϕ_m.

Figure 6.6.8: Link between the critical factors of the pit stability.

3) Evolution of the pH in function of the equilibrium constant K_1

Now, we assume that the following reaction takes place in the system:

$$\mathrm{Cr^{3+}} + \mathrm{H_2O} \underset{\mathrm{k_{1b}}}{\overset{\mathrm{k_{1f}}}{\rightleftharpoons}} \mathrm{Cr\,(OH)^{2+}} + \mathrm{H^+}. \tag{6.6.19}$$

Let K_1 be the equilibrium constant of the chemical reaction (6.6.19). It is given by

$$K_1 = \frac{k_{1f}}{k_{1b}} = \frac{\frac{C_{Cr(OH)^{2+}}}{C_{\text{ref}}}\frac{C_{H^+}}{C_{\text{ref}}}}{\frac{C_{Cr^{3+}}}{C_{\text{ref}}}\frac{C_{H_2O}}{C_{\text{ref}}}} \simeq 10^{-4.022} \tag{6.6.20}$$

where $C_{H_2O} = C_{\text{ref}} = 1$ mol/L.

For the computations, we precede in the same way to determine the initial data. Next, for the diffusion coefficients [6], we set

$$D_{\text{Cr}^{3+}} = 5{,}95 \,.\, 10^{-10}\ m^2.s^{-1}, \quad D_{\text{Cl}^-} = 2{,}032 \,.\, 10^{-9}\ m^2.s^{-1}, \quad D_{\text{Na}^+} = 1{,}334 \,.\, 10^{-9}\ m^2.s^{-1},$$

$$D_{\text{H}^+} = 9{,}31 \,.\, 10^{-9}\ m^2.s^{-1} \text{ and } D_{\text{Cr(OH)}^{2+}} = 7{,}3 \,.\, 10^{-10}\ m^2.s^{-1}.$$

Numerically, we set $k_{1f} = 10^5$ mol.m^{-3}.s^{-1}. Then, since $K_1 = \frac{k_{1f}}{k_{1b}} = 10^{-4.022}$, it follows that $k_{1b} = 1{,}0519 \,.\, 10^9$ mol.m^{-3}.s^{-1}.

Figure 6.6.9 shows that the acidity of the pit solution increases sharply with increasing the value of the equilibrium constant. There is a great influence of the chromium in the acidity of the solution. It follows that in a stainless steel (Fe-Cr-Ni), the chromium is the dominant element which controls the acidity of the pit solution.

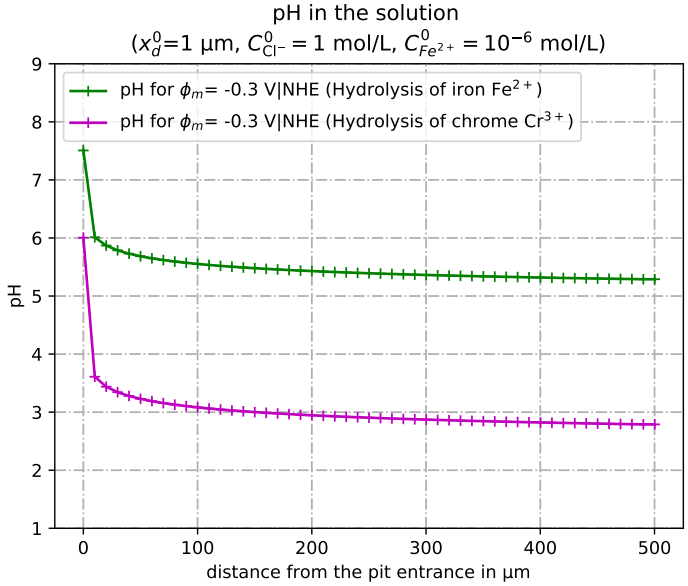

Figure 6.6.9: Evolution of the pH in the pit solution for two equilibrium constants.

6.6.5 Conclusions

In order to take into account the criteria of pH to study the stability of the pit, we have considered a diffusion-migration-reaction model with a moving boundary given by (6.6.9)–(6.6.11)–(6.6.12). It is a five-species model which includes the H^+ ion. The solution acidity is given through the H^+ concentration.

The numerical observations that can be drawn are as follows:

[6] Reference: https://www.aqion.de/site/194.

1. Since the reaction is much faster than the diffusion and migration, some difficulties were encountered in choosing a suitable value of k_{1f} (the rate of the forward reaction). These difficulties are either problems of convergence when $k_{1f} \to \infty$ (greater than 10^5) or, as we have shown in subsection 6.6.3.2, the chemical equilibrium is not obtained immediately.

2. We note that the solution acidity increases in time. It reaches its maximum at the pit bottom. Therefore, it is an increasing function of space and time.

3. There is a strong link between the two criteria of pit stability: the critical pH and the metallic cation concentration.

4. The solution acidity increases with increasing the metal potential.

5. The solution acidity increases with increasing the constant of equilibrium.

In this chapter, in paragraph 6.5.3.2, we have shown the influence of different parameters on the system without taking into account any passivation criteria. We have shown that for different values of ϕ_m, the system converges to a state of equilibrium after a large time of pit propagation and that the transient time required to reach this near-equilibrium state decreases strongly with increasing ϕ_m. Therefore, we can assume that our model (6.3.1)–(6.3.3)–(6.3.4) converges at large time to a quasi-stationary system. We define a quasi-stationary system as a system where the profile does not change at large time.

A system leading to this specific situation **almost simultaneously** can also be derived using a special case of coefficient values (the oxidation rate constant k_a and the reduction rate constant k_c) in the Butler-Volmer formula given by (6.2.15).

On the other hand, mathematically, using these new specific coefficient values of k_a and k_c in the Butler-Volmer formula allow us to derive a reduced model for our strongly coupled diffusion-migration model (6.3.1)–(6.3.3)–(6.3.4). We will show that this reduced model possesses a nearly exact solution (an approximate solution). The major advantage of developing such a nearly exact solution is to allow the validation of our numerical scheme developed to describe this complex phenomenon.

These constitute the different points discussed in the next chapter.

Chapter 7

Quasi-stationary approximation

Finding an explicit solution to model (6.3.1)-(6.3.3) and (6.3.4) seems to be unreachable. Therefore, the aim of this Chapter is to derive a certain singular limit of this model which possesses an approximate solution. We then compare this approximate solution with numerical simulations of our full system. It turns out that the numerical solution agrees extremely well with the approximate solution of the singular limit under certain conditions which will be specified later.

7.1 Derivation of the limit system

Now we discuss the low-concentration reduction system of model (6.3.1)-(6.3.3). First, we derive a reduced system which has a simple form. Therefore one can find an exact solution easily. The idea is roughly as follows. We have so far set the representative concentration C_0 at $C_0 = 1\,\mathrm{mol/L} = 1000\,\mathrm{mol/m^3}$. Now we vary C_0 and consider the limit as C_0 tends to zero (For example, C_0 tends to $1\,\mathrm{mol/m^3}$.)

To make the situation clear we choose C_0 to be the value of C_{NaCl} at the pit entrance :

$$C_{\mathrm{Fe^{2+}}} = 0, \quad C_{\mathrm{Na^+}} = C_{\mathrm{Cl^-}} = C_0 \quad \mathrm{mol/m^3},$$

thus, in the non-dimensional expression, the boundary conditions in (6.3.3d) becomes

$$C_1(0,t) = 0, \quad C_2(0,t) = C_3(0,t) = 1. \tag{7.1.1}$$

Recall that the constant b in (6.3.4) is given by

$$b = \frac{C_0}{N_{\mathrm{Fe}}} \quad \text{(non-dimensional molar volume of solid iron)}, \tag{7.1.2}$$

where N_{Fe} is the concentration of atoms in solid iron. Therefore, letting $C_0 \to 0$ and letting $b \to 0$ are equivalent. **We shall henceforth use b as a varying small parameter.**

7.1.0.1 Derivation of the reduced system

In what follows, for simplicity, we write

$$u = C_1, \quad v = C_2, \quad w = C_3$$

The dimensionless concentrations for $\mathrm{Fe^{2+}}, \mathrm{Na^+}$ and $\mathrm{Cl^-}$, respectively, and introduce a new time variable

$$\tau = bt.$$

Next, we use the following symbols:

$$\square_x := \frac{\partial \square}{\partial x}, \quad \square_\tau := \frac{\partial \square}{\partial \tau}.$$

In view of the new time variable, the equations (6.3.3) are rewritten as:

$$\begin{cases} bu_\tau = D_1 \left(u_x + 2u\phi_x\right)_x & (0 < x < x_d(\tau),\, \tau > 0), \\ bv_\tau = D_2 \left(v_x + v\phi_x\right)_x & (0 < x < x_d(\tau),\, \tau > 0), \\ bw_\tau = D_3 \left(w_x - w\phi_x\right)_x & (0 < x < x_d(\tau),\, \tau > 0). \end{cases} \tag{7.1.3}$$

The boundary conditions (6.3.3b), (6.3.3c) become:

$$\begin{cases} D_1 \left(u_x + 2u\phi_x\right) = -bu\dot{x}_d(\tau) + \widehat{f}(\phi,u) & \text{at} \quad x = x_d(\tau), \\ D_2 \left(v_x + v\phi_x\right) = -bv\dot{x}_d(\tau) & \text{at} \quad x = x_d(\tau), \\ D_3 \left(w_x - w\phi_x\right) = -bw\dot{x}_d(\tau) & \text{at} \quad x = x_d(\tau). \end{cases} \tag{7.1.4}$$

The free boundary condition (6.3.4) is written as

$$\dot{x}_d(\tau) = \widehat{f}(\phi,u) \quad \text{at} \quad x = x_d(\tau), \tag{7.1.5}$$

where, by (6.2.21),

$$\begin{aligned} \widehat{f}(\phi,u) &= \widehat{k}_a \exp(-(\phi - \widehat{\phi}_m)) - \widehat{k}_c \frac{C_0}{C_{\text{ref}}}\, u \exp(\phi - \widehat{\phi}_m) \\ &= \frac{L}{D_0 C_0} \left(k_a \exp(-(\phi - \widehat{\phi}_m)) - k_c \frac{C_0}{C_{\text{ref}}}\, u \exp(\phi - \widehat{\phi}_m) \right). \end{aligned} \tag{7.1.6}$$

Now we assume that b is very small. Then (7.1.3) implies

$$\begin{cases} 0 \approx D_1 \left(u_x + 2u\phi_x\right)_x & (0 < x < x_d(\tau),\, \tau > 0), \\ 0 \approx D_2 \left(v_x + v\phi_x\right)_x & (0 < x < x_d(\tau),\, \tau > 0), \\ 0 \approx D_3 \left(w_x - w\phi_x\right)_x & (0 < x < x_d(\tau),\, \tau > 0). \end{cases} \tag{7.1.7}$$

We **approximate** the above system by the following limit system in which b **is set to** 0**.**

$$\begin{cases} 0 = D_1 \left(u_x + 2u\phi_x\right)_x & (0 < x < x_d(\tau),\, \tau > 0), \\ 0 = D_2 \left(v_x + v\phi_x\right)_x & (0 < x < x_d(\tau),\, \tau > 0), \\ 0 = D_3 \left(w_x - w\phi_x\right)_x & (0 < x < x_d(\tau),\, \tau > 0). \end{cases} \tag{7.1.8}$$

Similarly, (7.1.4) can be approximated by the following set of boundary conditions:

$$\begin{cases} D_1 \left(u_x + 2u\phi_x\right) = \dot{x}_d(\tau) & \text{at} \quad x = x_d(\tau), \\ D_2 \left(v_x + v\phi_x\right) = 0 & \text{at} \quad x = x_d(\tau), \\ D_3 \left(w_x - w\phi_x\right) = 0 & \text{at} \quad x = x_d(\tau). \end{cases} \tag{7.1.9}$$

Combining (7.1.8) and (7.1.9), we obtain

$$\begin{cases} D_1 \left(u_x + 2u\phi_x\right) = \dot{x}_d(\tau) & (0 \le x \le x_d(\tau),\, \tau > 0), \\ v_x + v\phi_x = 0 & (0 \le x \le x_d(\tau),\, \tau > 0), \\ w_x - w\phi_x = 0 & (0 \le x \le x_d(\tau),\, \tau > 0). \end{cases} \tag{7.1.10}$$

Indeed, integrating each equation of (7.1.8) by x shows that they are independent of x, hence, by (7.1.9), the system (7.1.10) holds for all $\tau > 0$ and $0 \le x \le x_d(\tau)$.

Remark 7.1.1. In obtaining (7.1.8)–(7.1.9) from (7.1.3)–(7.1.4), we used the approximation $b \to 0$ (or equivalently $C_0 \to 0$). However, we do not let $C_0 \to 0$ in (7.1.6), as otherwise the term $\widehat{f}$ for the Butler-Volmer formula would become meaningless. We keep (7.1.6) as it is.
□

The last two equations of (7.1.10) and the boundary conditions (6.3.1c), (7.1.1) imply

$$v = \exp(-\phi), \quad w = \exp(\phi). \tag{7.1.11}$$

Using the electro-neutrality condition $2u + v - w = 0$, we then get

$$u = \frac{1}{2}\left(\exp(\phi) - \exp(-\phi)\right). \tag{7.1.12}$$

Substituting this into the first equation of (7.1.10) yields

$$D_1\left(3\exp(\phi) - \exp(-\phi)\right)\phi_x = 2\dot{x}_d(\tau).$$

Integrating this equality by x and using the boundary condition (6.3.1c), we find that

$$3\exp(\phi) + \exp(-\phi) = \frac{2\dot{x}_d(\tau)}{D_1}x + 4 \quad (0 \le x \le x_d(\tau)). \tag{7.1.13}$$

Setting $x = x_d(\tau)$, we obtain

$$\dot{x}_d(\tau) = \frac{D_1\left(3\exp(P) + \exp(-P) - 4\right)}{2x_d(\tau)}, \tag{7.1.14}$$

where $P(\tau) := \phi(x_d(\tau),\tau)$ denotes the potential at the pit bottom. Thus, if we know the potential at the pit bottom, then the speed of corrosion is given by (7.1.14).

The next step is to estimate the value of $P(\tau)$.

First, we recall that $\widehat{\phi}^*$ is the unique value $\widehat{\phi^*} = \widehat{\phi^*}(u)$ at which $\widehat{f}$ vanishes as shown in Figure 6.5.7 (see Appendix A). Its dimensional value ϕ^* is called ϕ^{eq} in the literature. It turns that

$$\widehat{f}(\widehat{\phi^*},u) = \widehat{k}_a \exp(-(\widehat{\phi^*} - \widehat{\phi}_m)) - \widehat{k}_c \frac{C_0}{C_{\rm ref}} u \exp(\widehat{\phi^*} - \widehat{\phi}_m) = 0.$$

Also, $\widehat{\phi^*}$ satisfies the following non-dimensional formula (See Appendix A):

$$\widehat{\phi}^*\left(\widehat{C}_{\mathrm{Fe}^{2+}}\right) = \widehat{\phi}_m + \frac{1}{2}\ln\left(\frac{\widehat{k}_a C_{\rm ref}}{\widehat{k}_c C_0 \widehat{C}_{\mathrm{Fe}^{2+}}}\right), \tag{7.1.15}$$

where the constants $\widehat{\phi}_m, \widehat{k}_a$ and $\widehat{\mathrm{k}}_{\mathrm{c}}$ in (6.2.25) are given in (6.2.21). Here, we recall that $\widehat{C}_{\mathrm{Fe}^{2+}} = u$.

More details about the estimation of the $\widehat{\phi}^*\left(\widehat{C}_{\mathrm{Fe}^{2+}}\right)$ value and the derivation of the above formula (7.1.15) are set out in the Appendix A.

Next we show the following result which plays **a key role in obtaining a good approximate solution of the limit system** (7.1.8)–(7.1.9) and (7.1.5).

Proposition 7.1.2. *We have that*

$$\widehat{\phi}^* - P(\tau) \to 0 \quad \textit{as} \quad C_0 \to 0. \tag{7.1.16}$$

Proof of (7.1.16). By (7.1.5) and (7.1.14), we have

$$\frac{D_1(3Q+Q^{-1}-4)}{2x_d(\tau)} = \dot{x}_d(\tau) = \widehat{f}(P,u), \tag{7.1.17}$$

where

$$P(\tau) := \phi(x_d(\tau),\tau) \ \text{ and } \ Q = \exp(P).$$

Note also that, by (7.1.12),

$$u(x_d(\tau),\tau) = \frac{1}{2}(Q-Q^{-1}). \tag{7.1.18}$$

Since $u(x_d(\tau),\tau) \geq 0$, we have $Q \geq 1$, hence, by (7.1.17),

$$\widehat{f}(P,u) \geq 0, \qquad \text{therefore} \ \ P \leq \widehat{\phi}^*. \tag{7.1.19}$$

Next, (7.1.17) and (7.1.6) yield

$$\frac{C_0 D_0 D_1(3Q+Q^{-1}-4)}{2Lx_d(\tau)} = k_a \exp(-(P-\widehat{\phi}_m)) - k_c \frac{C_0}{C_{\rm ref}}\, u \exp(P-\widehat{\phi}_m).$$

Thus, by (7.1.18),

$$\frac{C_0 D_0 D_1(3Q+Q^{-1}-4)}{2L\,x_d} = k_a \exp(\widehat{\phi}_m)\left(Q^{-1} - \frac{C_0}{\lambda}\left(Q^2-1\right)\right), \tag{7.1.20}$$

where λ is the constant given by

$$\lambda := 2\exp\left(\frac{2F}{RT}\phi_m\right)\frac{k_a C_{\rm ref}}{k_c}. \tag{7.1.21}$$

So far, we have regarded P, Q as functions of τ (that depend on the parameter C_0), but we can also regard P, Q as functions of the pit depth x_d, since $x_d(\tau)$ is monotonically growing.

In what follows, we regard P, Q as functions of x_d, and fix x_d at an arbitrary value. Then P, Q will depend only on C_0. Let us first show that

$$Q \to \infty \quad \text{ as } \ C_0 \to 0. \tag{7.1.22}$$

To prove (7.1.22), assume the contrary. Then there exists a sequence $C_0^{(j)} \to 0$ $(j \to \infty)$ and a constant $M > 0$ such that $Q \leq M$ for $C_0 = C_0^{(j)}$ $(j = 1,2,3,\ldots)$. Next we rewrite (7.1.20) as follows:

$$Q^{-1} = \frac{C_0 D_0 D_1(3Q+Q^{-1}-4)}{2k_a \exp(\widehat{\phi}_m) L\,x_d} + \frac{C_0}{\lambda}\left(Q^2-1\right).$$

Setting $C_0 = C_0^{(j)}$ and letting $j \to \infty$, we see that the right-hand side of the above formula tends to 0. On the other hand, the left-hand side is not less than M^{-1}. This is a contradiction, and (7.1.22) is proved.

Next, by (7.1.20) and $Q \geq 1$, we have

$$\lambda Q^{-1} \geq C_0(Q^2-1).$$

Letting $C_0 \to 0$ and using (7.1.22), we get

$$C_0 Q^2 \to 0 \quad \text{ as } \ C_0 \to 0. \tag{7.1.23}$$

Furthermore, the formula of Butler-Volmer flux $\widehat{f}(P,u)$ can be formulated as function of $\widehat{\phi}^*$ as follows (See Appendix A for more details)

$$\widehat{f}(P,u) = \left(\widehat{k}_a \widehat{k}_c \frac{C_0}{C_{\text{ref}}} u\right)^{1/2} \left(\exp\left(-(P-\widehat{\phi}^*)\right) - \exp\left(P-\widehat{\phi}^*\right)\right). \tag{7.1.24}$$

Now, by (7.1.24), the inequality $\widehat{\phi}^* \geq P$ in (7.1.19) and (6.2.21), we have

$$\begin{aligned}\widehat{f}(P,u) &= \left(\widehat{k}_a \widehat{k}_c \frac{C_0}{C_{\text{ref}}} u\right)^{1/2} \left(\exp\left(-(P-\widehat{\phi}^*)\right) - \exp\left(P-\widehat{\phi}^*\right)\right) \\ &\geq 2\left(\widehat{k}_a \widehat{k}_c \frac{C_0}{C_{\text{ref}}} u\right)^{1/2} (\widehat{\phi}^* - P) = \frac{2L}{D_0 C_0}\left(k_a k_c \frac{C_0}{C_{\text{ref}}} u\right)^{1/2} (\widehat{\phi}^* - P)\end{aligned}$$

Combining this with (7.1.17), we obtain

$$\frac{D_1(3Q + Q^{-1} - 4)}{2x_d(\tau)} \geq \frac{2L}{D_0 C_0}\left(k_a k_c \frac{C_0}{C_{\text{ref}}} u\right)^{1/2} (\widehat{\phi}^* - P),$$

which, in view of (7.1.18), implies that

$$\frac{D_0 D_1 (3Q + Q^{-1} - 4) C_0^{1/2}}{2\sqrt{2}\sqrt{Q - Q^{-1}}} \frac{1}{L x_d(\tau)} \geq \left(\frac{k_a k_c}{C_{\text{ref}}}\right)^{1/2} (\widehat{\phi}^* - P) \geq 0.$$

The left-hand side of the above inequality tends to 0 if we let $C_0 \to 0$ by virtue of (7.1.22) and (7.1.23). Hence $\widehat{\phi}^* - P \to 0$ as $C_0 \to 0$. The proof of (7.1.16) is complete. □

Then, in view of Proposition 7.1.2, it is reasonable to expect that

$$P(\tau) := \phi\left(x_d(\tau),\tau\right) \approx \widehat{\phi}^* \quad \text{if } C_0 \text{ is very small.} \tag{7.1.25}$$

Thus, it follows from (6.2.21) and (7.1.15) that

$$\begin{aligned}P(\tau) := \phi(x_d(\tau),\tau) \approx \widehat{\phi}^*(\widehat{C}_{\text{Fe}^{2+}}) = \widehat{\phi}^*(u) &= \widehat{\phi}_m + \frac{1}{2}\ln\left(\frac{\widehat{k}_a C_{\text{ref}}}{\widehat{k}_c C_0 u}\right) \\ &= \frac{F}{RT}\phi_m + \frac{1}{2}\ln\left(\frac{k_a C_{\text{ref}}}{k_c C_0 u}\right).\end{aligned}$$

Hence

$$\exp(2P) \approx \exp\left(\frac{2F}{RT}\phi_m\right)\frac{k_a C_{\text{ref}}}{k_c C_0 u} \quad \text{at} \quad x = x_d(\tau). \tag{7.1.26}$$

Substituting (7.1.12) into (7.1.26) and writing $Q := \exp(P)$, we obtain

$$Q^3 - Q \approx \lambda C_0^{-1}, \tag{7.1.27}$$

where λ is given by (7.1.21)

$$\lambda := 2\exp\left(\frac{2F}{RT}\phi_m\right)\frac{k_a C_{\text{ref}}}{k_c}.$$

Thus $Q = \exp(P)$ is well approximated by a positive root of the following cubic equation:

$$Q^3 - Q = \frac{\lambda}{C_0}. \tag{7.1.28}$$

The positive root of (7.1.28) is unique since $\lambda > 0$. We denote this root by $Q^* = Q^*(C_0)$ and henceforth identify the potential P at the pit bottom with $P^* := \ln Q^*$.

Remark 7.1.3. *From (7.1.28) we see that Q^* is roughly proportional to $C_0^{-1/3}$ if C_0 is very small, while $Q^* \approx 1$ if C_0 is large.*

7.1.0.2 Profiles of approximate solutions of the reduced model

Now, by solving the cubic equation (7.1.28), we can obtain **an explicit approximate solution**. First, we start by determining the profile of the non-dimensional free boundary x_d. To do so, using Q^*, we can rewrite (7.1.14) as

$$\dot{x}_d(\tau) = \frac{D_1\big(3Q^* + (Q^*)^{-1} - 4\big)}{2x_d(\tau)}, \tag{7.1.29}$$

In the normal (dimensionless) time scale $t = b^{-1}\tau$ where b is given by (7.1.2), the above formula becomes

$$\dot{x}_d(t) = \frac{D_1C_0\big(3Q^* + (Q^*)^{-1} - 4\big)}{2N_{\mathrm{Fe}}\, x_d(t)}. \tag{7.1.30}$$

Thus the speed of corrosion is proportional to $(x_d)^{-1}$. Solving (7.1.30), we obtain

$$\boxed{x_d(t) = \Big(\gamma t + \big(x_d(0)\big)^2\Big)^{1/2} \quad \text{where} \quad \gamma = \frac{D_1C_0\big(3Q^* + (Q^*)^{-1} - 4\big)}{N_{\mathrm{Fe}}}.} \tag{7.1.31}$$

This is a non-dimensional expression, but the dimensional expression of (7.1.31) takes precisely the same form if one replaces $x_d, t.\, D_1$ by their dimensional counterparts.

Next, in order to find the profile of ϕ, u, v, w, we substitute (7.1.29) into (7.1.13), to get

$$3\exp(\phi) + \exp(-\phi) = \rho(C_0)\,\frac{x}{x_d(\tau)} + 4 \qquad (0 \le x \le x_d(\tau)), \tag{7.1.32}$$

where

$$\rho(C_0) = 3Q^* + (Q^*)^{-1} - 4. \tag{7.1.33}$$

This is a quadratic equation for $Z := \exp(\phi)$ of the form

$$3Z^2 - \big(\rho(C_0)y + 4\big)\,Z + 1 = 0 \quad \text{where} \quad y = x/x_d(\tau). \tag{7.1.34}$$

Solving this quadratic equation, we obtain

$$\exp\big(\phi(x,\tau)\big) = \frac{\rho(C_0)y + 4 + \sqrt{\big(\rho(C_0)y + 4\big)^2 - 12}}{6}, \quad \text{where} \quad y = x/x_d(\tau).$$

Here we used $\phi(0,\tau) = 0$ to determine the sign in front of $\sqrt{\ }$. Thus we can express ϕ as

$$\phi(x,\tau) = \Phi\left(\frac{x}{x_d(\tau)}\right) \qquad (0 \le x \le x_d(\tau),\ \tau > 0), \tag{7.1.35}$$

where $\Phi(y)$, $0 \le y \le 1$, is a function given by

$$\exp\big(\Phi(y)\big) = \frac{\rho(C_0)y + 4 + \sqrt{\big(\rho(C_0)y + 4\big)^2 - 12}}{6}. \tag{7.1.36}$$

Then, by (7.1.12) and (7.1.11), we can express u,v,w as

$$u(x,\tau) = U\left(\frac{x}{x_d(\tau)}\right), \quad v(x,\tau) = V\left(\frac{x}{x_d(\tau)}\right), \quad w(x,\tau) = W\left(\frac{x}{x_d(\tau)}\right), \tag{7.1.37}$$

where

$$U = (\exp(\Phi) - \exp(-\Phi))/2, \quad V = \exp(-\Phi), \quad W = \exp(\Phi).$$

Remark 7.1.4. *Note that the functions $\Phi(y), U(y), V(y), W(y)$ depend on Q^* (hence on C_0) but are independent of τ. Thus the profiles of ϕ, u, v, w are* **stationary** *in the sense that they are given by simply stretching the profiles of Φ,U,V,W horizontally as the pit grows. In particular, the values of ϕ, u, v, w at the pit bottom remain the same for all time (same conclusion as in the end of paragraph 6.5.3.2.1 when the system converges to an equilibrium state).*

Remark 7.1.5. *We remark that (7.1.35)–(7.1.37) is* **not** *an exact solution of the reduced system (7.1.8)–(7.1.9)–(7.1.5)* **but simply an approximation**, *since, in deriving (7.1.35), (7.1.37), we replaced (7.1.27) by (7.1.28) (which means that we replaced $P(\tau) \approx \widehat{\phi}^*$ by $P(\tau) = \widehat{\phi}^*$), but actually there is a tiny gap between $P(\tau)$ and $\widehat{\phi}^*$. One can expect that (7.1.35)-(7.1.37) is* ***a good approximation of the solution of the reduced system****.*

7.2 Numerical simulations for the three species model

In this section we present numerical simulations of solutions of system (6.3.1)–(6.3.3)–(6.3.4) under the boundary conditions (7.1.1) and $\phi = 0$ at the pit entrance. The initial values are:

$$C_{Fe^{2+}}(x,0) = 10^{-6}, \quad C_{Na^+}(x,0) = C_{Cl^-}(x,0) = C_0 \text{ mol/m}^3, \quad x_d(0) = 1\,\mu\text{m}. \tag{7.2.1}$$

The computations are done for different values of C_0 in the following range:

$$C_0 = 1\,\text{mol/m}^3 = 10^{-3}\,\text{mol/L} \quad \sim \quad 1000\,\text{mol/m}^3 = 1\,\text{mol/L}. \tag{7.2.2}$$

The details of the scheme are described in Section 6.4 of Chapter 6.

Choice of the values of rate constants k_a and k_c:

In this chapter, the values of rate constants k_a and k_c are not realistic for iron dissolution kinetics but they are acceptable values to compare numerically the solutions of our full system (6.3.1)–(6.3.3)–(6.3.4) with the approximate solutions of the reduced model.

In view of (B.0.14) (see Appendix B), k_a and k_c must satisfy the equation

$$k_{c_{|NHE}} = k_{a_{|NHE}} \exp\left(\frac{2F}{RT} \times -0.44\right) \quad (\text{mol.m}^{-2}.\text{s}^{-1}). \tag{7.2.3}$$

We set

$$k_{a_{|NHE}} = 1{,}15 \,.\, 10^{10} \text{ mol.m}^{-2}.\text{s}^{-1}. \tag{7.2.4}$$

Physically, this choice of $k_{a_{|NHE}}$ makes it possible to reach the equilibrium almost instantly. Again, it differs strongly from the k_a value proposed in literature for iron dissolution which is about $k_{a_{|NHE}}^{\text{literature}} = 89{,}0636$ (mol.m^{-2}.s^{-1}) (see Appendix B).

In view of (7.2.3) and (7.2.4), it follows that

$$k_{c_{|NHE}} = 1{,}54 \,.\, 10^{-5} \text{ mol.m}^{-2}.\text{s}^{-1}. \tag{7.2.5}$$

Numerically, we use these values of k_a (7.2.4) and k_c (7.2.5) to compare the numerical simulations of the original system (6.3.1)–(6.3.3)–(6.3.4)–(7.1.1) with the approximate solution (7.1.35)–(7.1.37) of the reduced system (7.1.8)–(7.1.9)–(7.1.5).

With k_a, k_c as in (7.2.4) and (7.2.5), and with the following choice of parameters

$$C_{\text{ref}} = 1000\,\text{mol/m}^3, \qquad \phi_m = -0{,}45\,\text{V},$$

we have

$$\lambda \approx 8{,}598 \tag{7.2.6}$$

where λ is given by (7.1.21). Thus by (7.1.28),

$$Q^*(1) \approx 2{,}211 \quad \text{and} \quad Q^*(1000) \approx 1{,}0042. \tag{7.2.7}$$

Using the values of Q^* in (7.2.7), we can calculate $\rho(C_0)$ (given by (7.1.33)) as

$$\rho(C_0) \approx \begin{cases} 3{,}085 & \text{if } C_0 = 1\,\text{mol/m}^3 = 10^{-3}\,\text{mol/L}, \\ 0{,}008 & \text{if } C_0 = 1000\,\text{mol/m}^3 = 1\,\text{mol/L}. \end{cases} \tag{7.2.8}$$

For each value of C_0 in the above range (7.2.2), we see a good agreement between the computed solution of the full system (6.3.1)–(6.3.3)–(7.2.1) and the explicit approximate solution (7.1.35)–(7.1.37). More precisely, the solution starting from a spatially homogeneous initial data (7.2.1) quickly approaches the profile of (7.1.35)–(7.1.37) within a short time and remains close to it thereafter.

We recall that the approximate solutions found analytically are given by (7.1.35)–(7.1.37).

The case $C_0 = 10^{-3}$ mol/L

Figure 7.2.1a (left) shows the spatially homogeneous initial data (7.2.1) and the profiles of the approximate solution (7.1.37) at t= 0 s.

Figure 7.2.1b (right) shows the graphs of $C_{Fe^{2+}}(x,t), C_{Na^+}(x,t), C_{Cl^-}(x,t)$ $(0 \le x \le x_d(t))$ at an early time (around $t = 774\,\text{s}$). It describes the concentration distribution of each ion in the pit solution given by the numerical scheme of the original system (6.3.1)–(6.3.3)–(6.3.4)–(7.1.1): $C_{Fe^{2+}}$ (red), C_{Na^+} (blue), C_{Cl^-} (green). It shows the numerical solutions and the approximate solution (7.1.37) (continuous lines) which turn out to be very close.

The CPU time given in Figure 7.2.1b presents the time needed to run the code. It reflects the speed of execution of our simulation.

The graph of the potential ϕ is given in Figure 7.2.2.

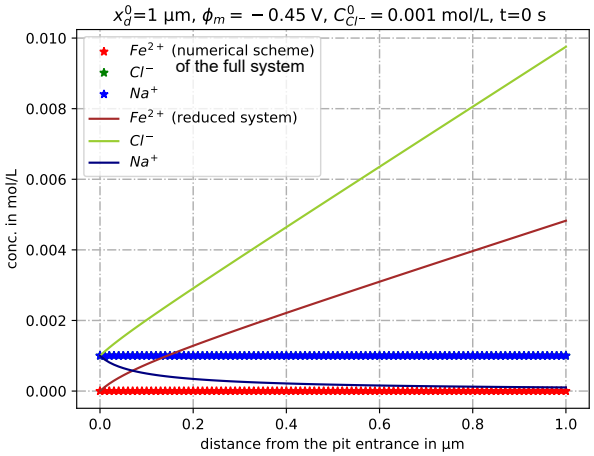

(a) The spatially homogeneous initial data (7.2.1) and the special solution (7.1.37) at initial time: (t= 0 s, $x_d(0) = 1$ µm).

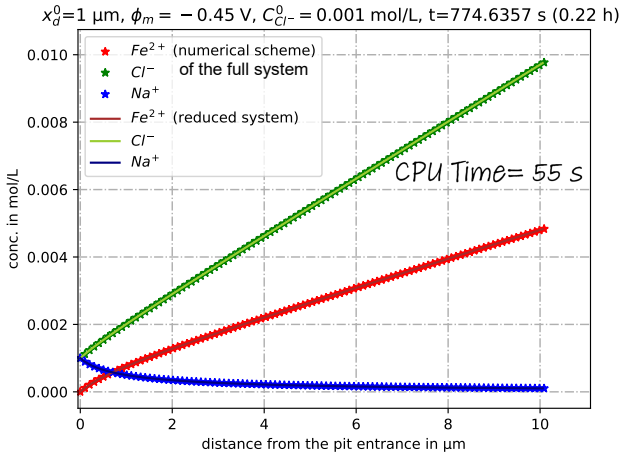

(b) Concentration profiles in the pit solution given by the numerical scheme and the approximate solution (7.1.37) at t = 774,6357 s and for $x_d(774{,}6357) = 10$ µm.

Figure 7.2.1: Concentrations in the pit solution (early time) for $C_0 = 0.001$ mol/L and $C^0_{\mathrm{Fe}^{2+}} = 10^{-6}$ mol/L.

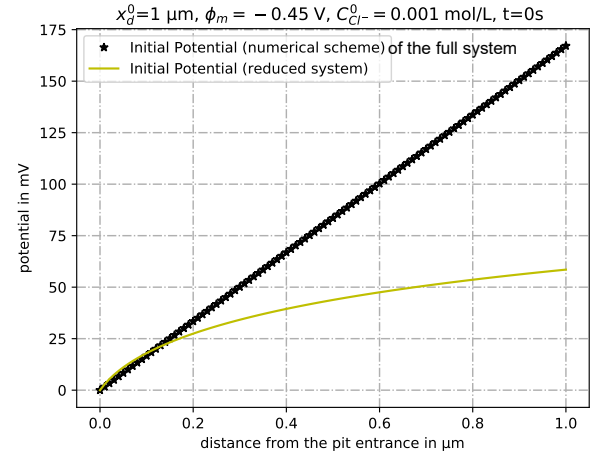

(a) Initial potential profiles in the pit solution given by solving the system (6.3.1) numerically and the approximate solution (7.1.36) at initial time: (t= 0 s, $x_d(0) = 1$ µm).

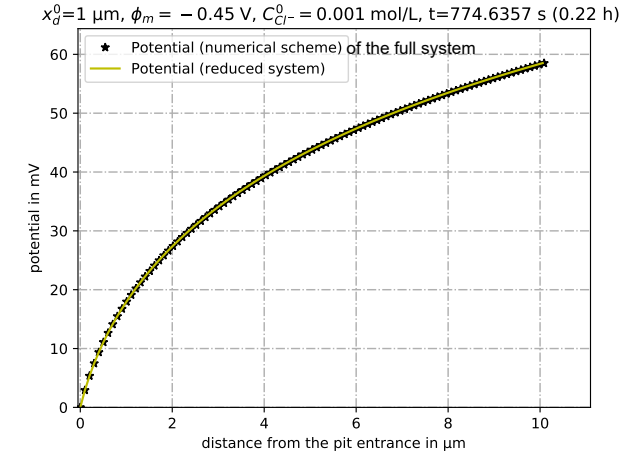

(b) Potential profiles given by the numerical scheme and the approximate solution (7.1.36) at t = 774,6357 s and for $x_d(774{,}6357) = 10$ µm.

Figure 7.2.2: Potential in the pit solution (early time) for $C_0 = 0.001$ mol/L and $C^0_{\mathrm{Fe}^{2+}} = 10^{-6}$ mol/L.

The next figures show the profiles at a much later dissolution time (around $t = 77183$ s). The profiles remain the same as those at the earlier time except that the horizontal spatial scale is different. As mentioned earlier, this is the characteristic feature of the functions (7.1.35)–(7.1.37).

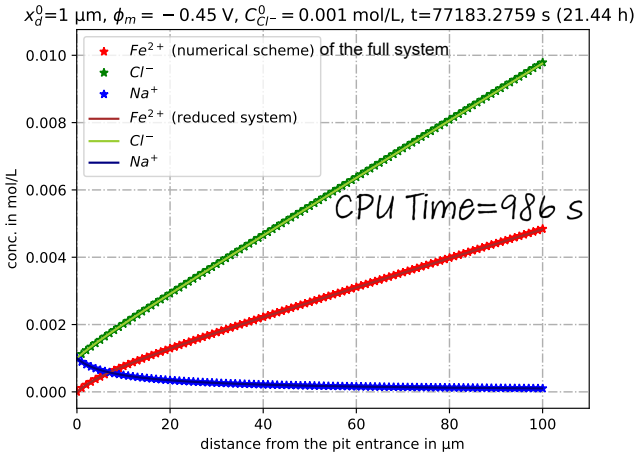

(a) Concentration profiles in the pit solution given by the numerical scheme and the approximate solution (7.1.37) at t = 77183,27 s and for $x_d(77183{,}27) = 100$ µm.

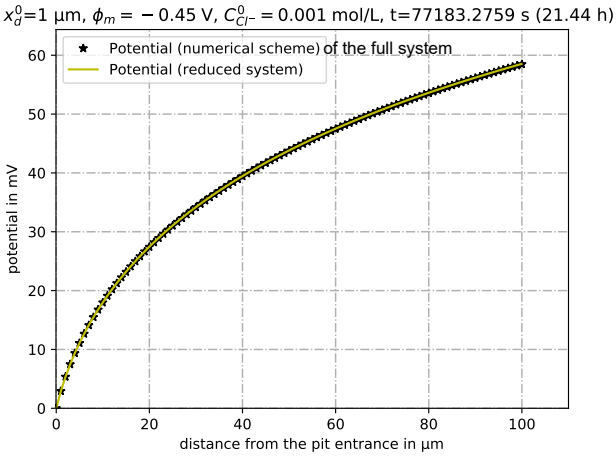

(b) Potential profiles given by the numerical scheme and the approximate solution (7.1.36) at t = 77183,27 s and for $x_d(77183{,}27) = 100$ µm.

Figure 7.2.3: Concentrations and potential (later time) for $C_0 = 0.001$ mol/L and $C^0_{\mathrm{Fe}^{2+}} = 10^{-6}$ mol/L.

Finally, the following figure shows the graph of the pit depth $x_d(t)$ as a function of time. The continuous line indicates the growth predicted by the formula (7.1.31), that is,

$$x_d(t) = \left(\gamma t + (x_d(0))^2\right)^{1/2}.$$

Again, the two curves show remarkable agreement. Thus the pit grows at the rate of $\sqrt{t}$.

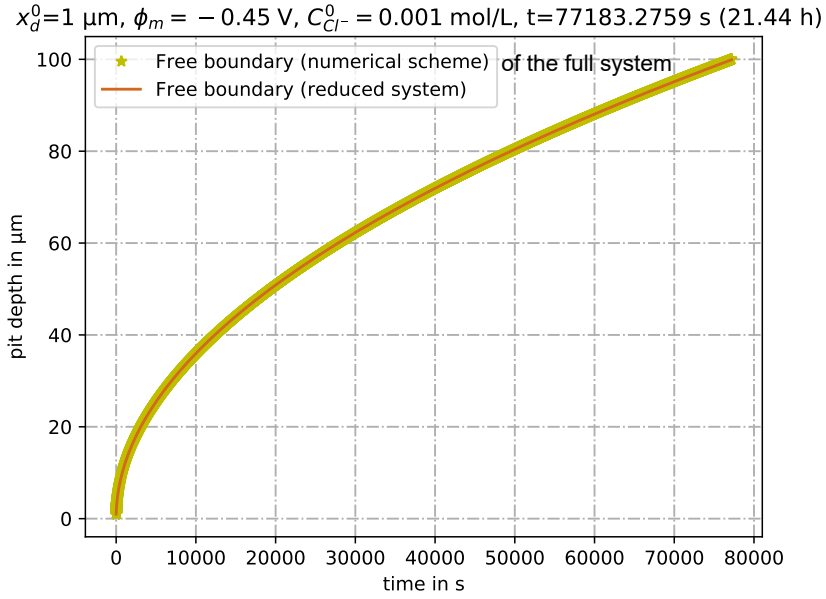

Figure 7.2.4: Evolution of the pit depth in time given by the numerical scheme and the approximate solution (7.1.31) for $C_0 = 0{,}001$ mol/L and $C^0_{\mathrm{Fe}^{2+}} = 10^{-6}$ mol/L.

The case $C_0 = 1\,\mathrm{mol/L}$

Finally we consider the case where the concentrations are higher, $\boldsymbol{C_0 = 1\,\mathrm{mol/L}}$. We note that the graph of the concentrations (Figure (7.2.5b)) and the potential ϕ (Figure (7.2.5d)) become more and more like straight lines. This is explained as follows. The function $\Phi(y)$ in (7.1.35) is obtained by solving the quadratic equation (7.1.32). More precisely, $Z := \exp(\Phi(y))$ is a solution of

$$3Z^2 - (\rho(C_0)y + 4)\, Z + 1 = 0.$$

This and $\Phi(0) = 0$ imply

$$\exp\left(\Phi(y)\right) = \frac{\rho(C_0)y + 4 + \sqrt{(\rho(C_0)y + 4)^2 - 12}}{6}. \tag{7.2.9}$$

As shown in (7.2.8), $\rho(C_0)$ becomes very small as C_0 gets larger, therefore $\exp(\Phi(y))$ (hence also $\Phi(y)$) becomes closer and closer to a constant function. Indeed, in this case, $\rho(C_0) = 0.008$ as shown in (7.2.8). Therefore, it follows from (7.2.9) that

$$\exp\left(\Phi(y)\right) \approx 1 + \frac{\rho(C_0)y}{6}, \quad \Phi(y) \approx \frac{\rho(C_0)y}{6}.$$

Thus the functions in (7.1.37) are estimated as follows:

$$U(y) = \frac{\exp(\Phi) - \exp(-\Phi)}{2} \approx \frac{\rho(C_0)y}{6}, \quad V(y) \approx 1 - \frac{\rho(C_0)y}{6}, \quad W(y) \approx 1 + \frac{\rho(C_0)y}{6}.$$

Therefore, Φ and U are small, while V and W are very close to 1 for $0 \le y \le 1$. This observation well agrees with the numerical simulations shown below.

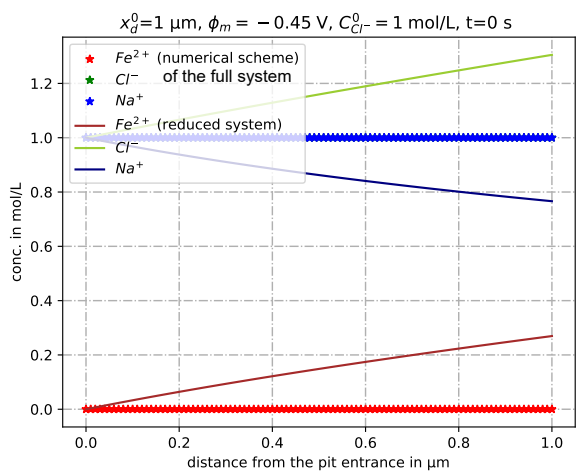

(a) The spatially homogeneous initial data (7.2.1) and the approximation solution given by (7.1.37) at initial time : (t= 0 s, $x_d(0) = 1$ µm).

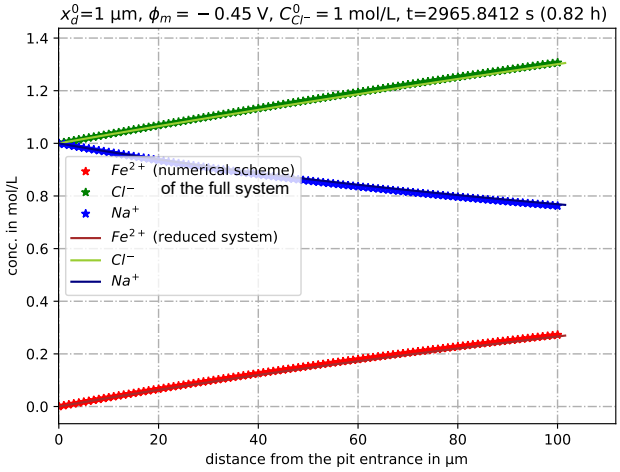

(b) Concentration profiles in the pit solution given by the numerical scheme and the approximate solution (7.1.37) at t = 2965,84 s and for $x_d(2965{,}84) = 100$ µm.

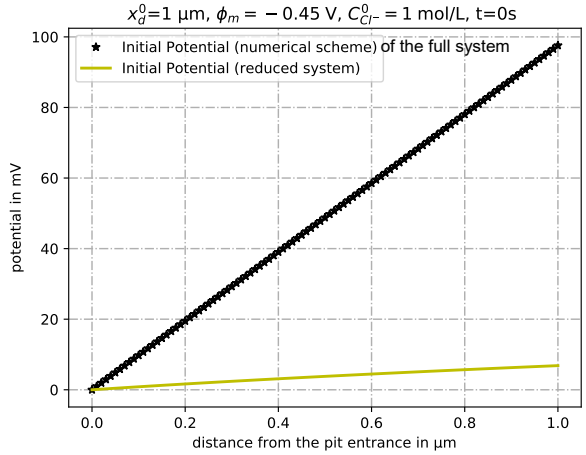

(c) Initial potential profiles in the pit solution given by solving the system (6.3.1) numerically and the approximate solution (7.1.36) at initial time : (t= 0 s, $x_d(0) = 1$ µm).

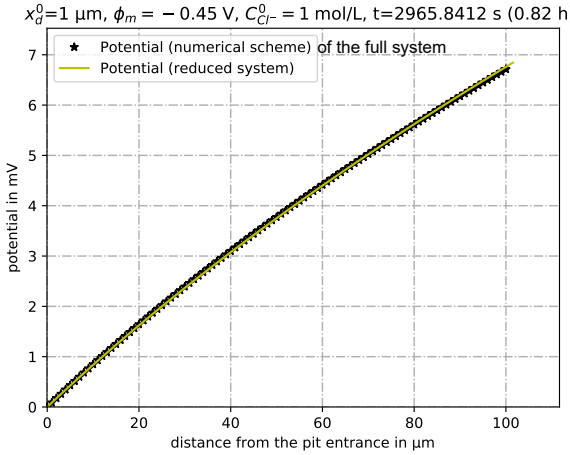

(d) Potential profiles given by the numerical scheme and the approximate solution (7.1.36) at t = 2965,84 s and for $x_d(2965{,}84) = 100$ µm.

Figure 7.2.5: Concentrations and potential (later time) for $C_0 = 1$ mol/L and $C^0_{\mathrm{Fe}^{2+}} = 10^{-6}$ mol/L.

Figure 7.2.6 shows the evolution of the pit depth in time (until t = 2965,84 s). It shows that for $C_0 = 1$ mol/L, the quasi-analytical interface given by the reduced model and the numerical interface are, again, quite in good agreement. Only a small difference appears between both solution at larger depth. It was not visible in the case $C_0 = 0.001$ mol/L. In the case $C_0 = 0.001$ mol/L, the agreement between those interfaces is perfect even at larger time (t= 77183,275 s).

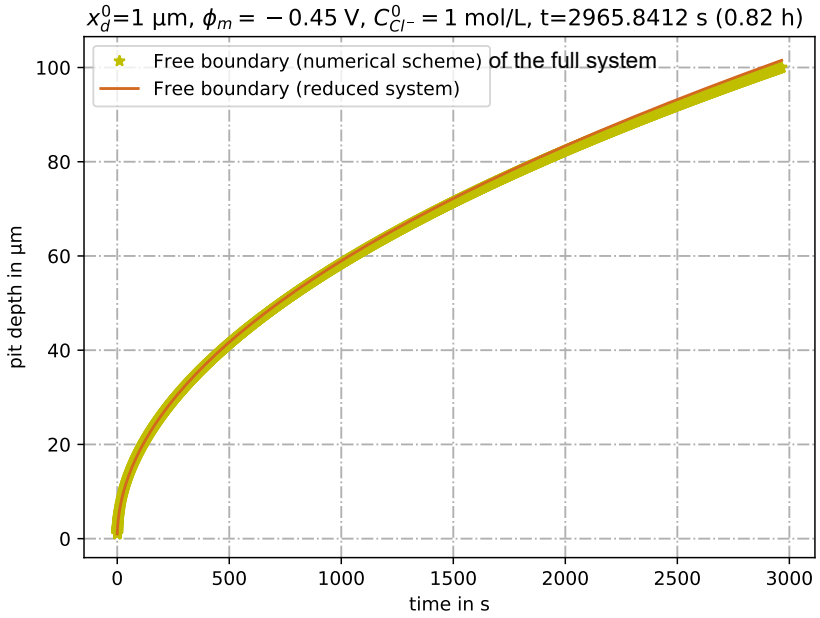

Figure 7.2.6: Evolution of the pit depth in time given by the numerical scheme and the approximate solution (7.1.31) for $C_0 = 1\,\text{mol/L}$ and $C^0_{\text{Fe}^{2+}} = 10^{-6}\,\text{mol/L}$.

Here are summarized all the steps used for deriving the approximate solution (7.1.35)-(7.1.37) of the reduced system (7.1.8)–(7.1.9)–(7.1.5):

Summary for the low concentration reduction system

1. We considered the system (6.3.1)–(6.3.4) and (7.1.1) for Fe^{2+},Na^{+},Cl^{-} without reaction. The corrosion speed is governed by the Butler-Volmer formula at the pit bottom. At the pit entrance, we impose the Dirichlet boundary conditions (7.1.1) and $\phi = 0$. Thus the constant C_0 represents C_{NaCl} at the pit entrance.

2. Using the new time variable $\tau = bt$, the equations for concentrations (6.3.3) and (7.1.1) are rewritten as (7.1.3)–(7.1.4)–(7.1.5), where $b = \dfrac{C_0}{N_{\mathrm{Fe}}}$ is the constant in (7.1.2). The equations (6.3.1) for ϕ remains the same.

3. First approximation: we set b to 0 to obtain the limit system (7.1.8)–(7.1.9)–(7.1.5) where we keep the free boundary (7.1.5) unchanged (see Remark 7.1.1).

4. We deduce that the unknowns of the system are given as follows (7.1.11)–(7.1.12)

$$u = \frac{1}{2}\left(\exp(\phi) - \exp(-\phi)\right), v = \exp(-\phi), w = \exp(\phi) \quad \text{for } \tau > 0,\ 0 \le x \le x_d(\tau)$$

and from (7.1.14) that

$$\dot{x}_d(\tau) = \frac{D_1\left(3\exp(P) + \exp(-P) - 4\right)}{2x_d(\tau)} \quad \text{where } P(\tau) := \phi(x_d(\tau),\tau).$$

5. We estimate the value of $P(\tau)$; we deduce from Proposition 7.1.2 that (7.1.25) holds. It is given by

$$P(\tau) := \phi\left(x_d(\tau),\tau\right) \approx \widehat{\phi}^* \quad \text{if } C_0 \text{ is very small.}$$

6. Setting $Q = \exp(P)$, it follows from (7.1.25) and (7.1.12) that

$$Q^3 - Q \approx \lambda C_0^{-1}$$

where λ is given by (7.1.21) $\lambda := 2\exp\left(\dfrac{2F}{RT}\phi_m\right)\dfrac{k_a C_{\mathrm{ref}}}{k_c}$. (Here, ϕ_m, k_a and k_c are in their dimensional form).

7. Second approximation: Q is well approximated by the positive root of the cubic equation (7.1.28): $Q^3 - Q = \dfrac{\lambda}{C_0}$, and we denote the root of this equation by $Q^* = Q^*(C_0)$.

8. We deduce the profiles of the approximate solution of the reduced model from solving the cubic equation (7.1.28) and the quadratic equation (7.1.34). We obtain

the profile of the approximate free boundary x_d (non-dimensional form) (7.1.31): $x_d(t) = \left(\gamma t + (x_d(0))^2\right)^{1/2}$ where $\gamma = \dfrac{D_1 C_0(3Q^* + (Q^*)^{-1} - 4)}{N_{\mathrm{Fe}}}$, where t is the normal (dimensionless) time scale such that $t = b^{-1}\tau$ and $b = \dfrac{C_0}{N_{Fe}}$,

the profile of the approximate potential ϕ in the pit solution (non-dimensional form) (7.1.36)

$$\phi(x,\tau) = \Phi(y) = \ln\left(\frac{\rho(C_0)y + 4 + \sqrt{(\rho(C_0)y+4)^2 - 12}}{6}\right) \quad \text{for all } 0 \le y \le 1, \quad \text{where}$$

$$y = \frac{x}{x_d(\tau)} \quad \text{and} \quad \rho(C_0) = 3Q^* + (Q^*)^{-1} - 4,$$

the profiles of the approximate concentrations $\{C_i\}_{i\in 1,2,3}$ in the pit solution (non-dimensional form) (7.1.37)

$$\widehat{C}_{Fe^{2+}}(x,t) = C_1(x,t) = u(x,\tau) = U(y) = \frac{\exp(\Phi(y)) - \exp(-\Phi(y))}{2},$$

$$\widehat{C}_{Na^{+}}(x,t) = C_2(x,t) = v(x,\tau) = V(y) = \exp(-\Phi(y)),$$

$$\widehat{C}_{Cl^{-}}(x,t) = C_3(x,t) = w(x,\tau) = W(y) = \exp(\Phi(y)).$$

9. The numerical simulations show that (7.1.35)–(7.1.37) is a very good approximation of the solution of the original system (6.3.1)–(6.3.3)–(7.1.1) for $C_0 = 1\,\text{mol/L}$ or lower.

10. Since the approximate solution (7.1.35)–(7.1.37) is given explicitly, we can study its properties in full detail. This presents one of our perspectives. Among other things, we see the following:

    - The pit depth $x_d(t)$ grows with the order $\sqrt{t}$.
    - $C_{\text{Fe}^{2+}}, C_{\text{Na}^{+}}, C_{\text{Cl}^{-}}, \phi$ at the pit bottom remain constant as time passes.

Chapter 8

Conclusions and Perspectives

The objective of this thesis was to develop a predictive model to describe the propagation of the pit and crevice corrosion in pure iron, as an aid to improve the understanding of the physical mechanisms underlying these phenomena.

Due to the complexity of the problem, we have chosen to start **in one-space dimension** to create a pertinent and efficient numerical scheme which will allow us to simulate the time evolution of pit propagation. The model has been developed step by step to gradually integrate the complexity of the chemical system.

8.1 Conclusions

The main conclusions from each chapter are summarized below.

1. In Chapter 2, we have described the mechanisms of pitting corrosion which can be divided into three distinct stages: initiation, propagation and repassivation stages.

   We were interested in the propagation stage. We reviewed the main critical factors to ensure the long-term pit propagation. In view of literature, these criteria are described in terms of critical concentration of metal cations and in terms of pit solution pH.

   Then, we reviewed some deterministic anodic-dissolution models to describe the pit and crevice propagation in a diluted solution. We discussed the fundamentals needed to describe localized corrosion kinetics for two corrosion regimes: the diffusion-controlled regime and the activation-controlled regime.

   Finally, we compared different computational models for pit/crevice corrosion introduced in literature according to the physical phenomenon described (diluted/concentrated solution, transport phenomena, chemical species, precipitation,..) and the mathematical methods used for its resolution (time evolution/steady state problem, numerical method, fixed/moving boundary,..), as well as the advantages and disadvantages of these models.

   In this context, we have defined the objectives of this doctoral thesis:

   a) to derive a relevant anodic-dissolution model to describe pit/crevice propagation,

   b) to propose an efficient numerical method for the strongly coupled nonlinear mathematical system which is implemented in an open source software (Python). We recall the advantages of our software :

- a complete mastering of all the input variables which allows us to examine the behavior of the mathematical system with respect to the variation of certain physical/ chemical parameters,
- the possible modification of the numerical scheme and the described physics to provide a more accurate description of the physical reality,
- the control of the numerical scheme in order to optimize the computation time/ accuracy of results.

2. In Chapter 3, we studied a first simplified model of pure iron dissolution with uncharged iron cations (see Problem (3.2.6)). We adopt the model introduced by S. Scheiner and C. Hellmich [62] to describe a pit growing in a stable corrosion mode. Here, we describe a pure diffusion-controlled corrosion regime.

   The main objective of this first study was **to deal with a free boundary problem** in order to describe the kinetics of the pit propagation.

   From a mathematical point of view, the given system could be identified as a Stefan problem. This model involves the Fick's law of diffusion, governing the behavior of the dissolved metal ion (uncharged ion) in the pit. The system was solved for a moving boundary condition with Dirichlet boundary conditions at the pit entrance and at the pit bottom (saturated concentration at the bottom).

   We defined a self-similar solution (a special solution) for this physical free boundary problem (3.3.10)–(3.3.13)) by using a self-similar variable (3.3.1).

   Then, by means of several simulations, we have shown the influence of two parameters: the diffusion coefficient D and the saturated concentration C_{sat} on the time evolution of the pit depth. We conclude that

   - if the diffusion coefficient D **increases** by factor λ, the pit depth **increases** $\approx \sqrt{\lambda}$ times,
   - if the diffusion coefficient D **is decreased** by a factor λ, the time needed to reach a given final pit depth is **increased** λ times,
   - we compared the two extreme cases where C_{sat}= 5,1 mol/L (value close to the reality) and C_{sat}= 140,2 mol/L (not real value). We show that the pit depth increases only 12 times from the case C_{sat}= 5,1 mol/L to the case C_{sat}= 140,2 mol/L,
   - the pit depth grows with the order of $\sqrt{t}$.

   On the other hand, we have presented some numerical results which illustrate the convergence for large times of the solution of the physical problem (3.2.6) **for an arbitrary non monotone initial data** to the self-similar solution (3.3.10)–(3.3.13).

   Finally, we performed a new change of variables to obtain a classical one-phase Stefan problem which was studied in Chapter 4.

3. In Chapter 4, we revisited the one-dimensional one-phase Stefan problem with a Dirichlet boundary condition at x = 0 as stated in the book of Avner Friedman about parabolic equations [24]. It was given by Problem (4.2.1). We proved that under rather general hypotheses on the initial data, the solution converges to a self-similar profile as t $\to \infty$. The results are valid for non negative initial data which are bounded from above by some upper solution.

4. In Chapter 5, we described the numerical method used to solve the one-dimensional one-phase Stefan problem introduced in Chapter 4. To do so, we considered an Arbitrary Lagrangian

Eulerian (ALE) formulation of this problem given by ($\mathcal{S}$) (Problem (4.2.1) cf. Chapter 4). This method is usually referred to as the Variable Space Grid (VSG) method. It is based on a decoupling of the displacement of the free boundary from the numerical solution of the diffusion equation. It provides rather accurate numerical results. This method, which is used as an adaptive technique to handle the displacement of the free boundary, permits to avoid numerical interpolations.

Finally, we presented numerical results which illustrate the convergence of the solution of ($\mathcal{S}$) to the self-similar solution given by (5.3.1).

5. In Chapter 6, we gradually derived a more complicated anodic-dissolution model in one-space dimension. It was intended to describe an activation-controlled corrosion regime. This situation of corrosion does not completely correspond to reality, but it indicates the most severe conditions under which the pit/crevice are susceptible to propagate.

   This model is a mathematical model of partial differential equations (6.3.1)–(6.3.3)–(6.3.4) which simulates the propagation of a pit in pure iron steel exposed to aqueous NaCl solution.

   It is a time dependent deterministic model based on many known physical phenomena. It involves an anodic reaction of dissolution, the transport of aqueous chemical species by diffusion and migration and the moving of the iron interface.

   Then, we proposed an **efficient numerical** solution method for the strongly coupled nonlinear system of partial differential equations. In that purpose, we have developed an implicit in time numerical scheme based on **the ALE method together with a Newton procedure**.

   In order to validate our mathematical model, we compared several numerical simulations with similar previous studies discussed in literature. Theses comparisons show a **good qualitative agreement** of our results with similar studies.

   Through many simulations, we have examined the behavior of our system with respect to the variations of certain physical parameters. We showed the impact of the potential ϕ_m applied to the surface of the pure iron steel and the influence of the initial chloride concentration $C^0_{\mathrm{Cl}^-}$ on the time evolution of the concentrations of the ionic species in the pit, the potential drop and the corrosion speed. We conclude that the corrosion rate increases with increasing the applied potential ϕ_m and with C^0_{NaCl}. On the other hand, the evolution of the corrosion speed decreases at large time (convergence to a quasi-stationary system). The transient time required to reach such a near equilibrium state strongly depends on the input parameters such as the values of ϕ_m and C^0_{NaCl}. Then, we have shown that, in general case, the transport of ionic species in the pit occurs by diffusion and migration. Thus, for accurate results, we cannot neglect the effect of migration in the transport of ionic species.

   Then, we have worked on the minimum applied potential to stabilize the pit propagation as a function of pit depth. Our model was able to reproduce the experimental data qualitatively.

   In the last step, we have integrated the hydrolysis reactions of iron cations in the system. This reaction induces the formation of H^+ cations which changes the acidity of the solution, a criterium often proposed in literature for pit stability.

   This final model developed in this thesis is a diffusion-migration-reaction model with moving interface for five-species including H^+ ion. By means of several simulations, we have shown

that the solution acidity increases in time and reaches its maximum at the bottom of the pit. Similarly, it increases with the applied potential ϕ_m and the equilibrium constant of the hydrolysis reaction (depending on the composition of the steel).

In this chapter, we have shown the influence of different parameters on the system without taking into account any passivation criteria. We have noted that for different values of ϕ_m, the system converges to a state of equilibrium after a large time of pit propagation and that the transient time required to reach this near-equilibrium state decreases strongly with increasing ϕ_m. Therefore, we can conclude that our model (6.3.1)–(6.3.3)–(6.3.4) converges at large time to a quasi-stationary system (the profile does not change any more at large time). A system leading to this specific situation **almost simultaneously** can be derived also using a special case of coefficient values (the oxidation rate constant k_a and the reduction rate constant k_c) in the Butler-Volmer formula given by (6.2.15).

6. In Chapter 7, we derived a reduced system for our diffusion-migration model (6.3.1)–(6.3.3)–(6.3.4). This limit system is obtained by using a new time variable and by letting the representative concentration C_0 tends to zero. Then, by means of two approximations, we have found analytically an approximation solutions for this reduced system.

   Numerically, for $C_0 = 1\,\mathrm{mol/L}$ or lower, we showed that the approximate solutions (7.1.35)–(7.1.37) of the reduced system (7.1.8)–(7.1.9)–(7.1.5) are a very good approximation of the solution of our strongly coupled diffusion-migration model (6.3.1)–(6.3.3)–(6.3.4) using a special choice of rate constants k_a and k_c in the Butler-Volmer formula.

   The major advantage of developing such a nearly exact solution is to allow the validation of our numerical scheme developed to describe this complex phenomenon.

8.2 Perspectives

We now present some possibilities for further developments in each chapter.

1. As a follow up of Chapter 4, it could be interesting to prove the convergence to self-similar profile for more general initial data, which can possibly take values above the constant h ;
2. As a follow up of Chapter 5, we propose to prove the convergence of the numerical method ; a first step will be to try to prove the convergence of the semi discretized scheme in time ;
3. As a follow up of Chapter 6,
   - in view of Frankel and his colleagues studies [20, 21] where they suggest that the transition from metastable to stable pit growth can only be made by pits that are able to precipitate a salt film on long term, we propose to integrate the following reactions into the system for the simulation of long term propagation:

     $$\mathrm{Fe}^{2+} + \mathrm{Cl}^- \rightleftharpoons \mathrm{Fe\,Cl}^+, \tag{8.2.1}$$

     and

     $$\mathrm{Fe\,Cl}^+ + \mathrm{Cl}^- \rightleftharpoons \mathrm{Fe\,Cl_2}. \tag{8.2.2}$$

   - It is known that pits in stainless steel tend to form *lacy metallic covers* at the pit entrance, which help the interior of the pits to maintain concentrated local chemistry [43, 44]. Thus, we suggest to take into account the presence of the **lacy metallic cover**, which slows down the exchange of ions between the inside and the outside of the pit. This effect can be represented by a Robin type boundary conditions of a special type at the entrance of the pit $x = 0$.

- We suggest to implement a numerical scheme for a three dimensional axi-symmetric configuration taking into account a moving interface to describe the morphology of the pit as time evolves.

Appendix A

Extension of the Butler-Volmer formula for the corrosive ion flux to electric current density

A.1 The Butler-Volmer formula and the electrical current density

We recall that in our model, we study the pit corrosion of pure iron. So that to describe the corrosion rate, we are limited only at one electrochemical reaction in the bottom of the pit which is the anodic reaction. It is given by

$$\mathrm{Fe} \quad \underset{k_c}{\overset{k_a}{\rightleftharpoons}} \quad \mathrm{Fe}^{2+} \; + \; 2\,\mathrm{e}^{-}.$$

We adopt the Butler-Volmer equation to describe the rate of oxidation and reduction of this electrochemical reaction. We recall that its **dimensional expression** is given by

$$f_{\mathrm{Fe}^{2+}}(\phi,C_{\mathrm{Fe}^{2+}}) = k_a \exp\Big(-\frac{F}{RT}(\phi-\phi_m)\Big) - k_c\,\frac{C_{\mathrm{Fe}^{2+}}}{C_{\mathrm{ref}}}\exp\Big(\frac{F}{RT}(\phi-\phi_m)\Big), \tag{A.1.1}$$

where k_a and k_c are positive constants that represent the speed of oxidation of iron and that of reduction, respectively ($\mathrm{mol/m^2 s}$). F, R, T are defined in Table 6.1, C_{ref} is a reference concentration which is usually set at $C_{\mathrm{ref}} = 1000\,\mathrm{mol/m^3} = 1\mathrm{mol/L}$ in ideal system, while ϕ_m denotes the electric potential applied on the iron steel surface (which is assumed to be constant in relative to some standard electrode in the bulk solution) and ϕ is defined as the electric potential of the aqueous solution in contact with the steel surface. **In this case, the pit corrosion phenomenon is considered to be under potentiostatic condition.**

Remark A.1.1. *In general, in (A.1.1), the variable ϕ is defined as the potential drop in the solution in the cavity; i.e. the difference of potential at the pit entrance and potential at the pit bottom, just outside the electrical double layer* [1] *on the metal surface [67]. So that, since in our model the potential at the pit entrance is fixed at 0, ϕ in (A.1.1) is reduced only to the potential at the pit bottom.*

Next, since $f_{\mathrm{Fe}^{2+}}(\phi,C_{\mathrm{Fe}^{2+}})$ is strictly decreasing in ϕ, for any fixed value of $C_{\mathrm{Fe}^{2+}} > 0$ there exists a unique value $\phi^* = \phi^*(C_{\mathrm{Fe}^{2+}})$ such that $f_{\mathrm{Fe}^{2+}}(\phi^*,C_{\mathrm{Fe}^{2+}}) = 0$ as shown in Figure 6.5.7. This value ϕ^* is called ϕ^{eq} in literature (the potential at equilibrium). If ϕ is at this value, the rate of iron dissolution and that of absorption are equal. Therefore, the system is at equilibrium. It follows that

$$k_a \exp\Big(-\frac{F}{RT}(\phi^*-\phi_m)\Big) = k_c\,\frac{C_{\mathrm{Fe}^{2+}}}{C_{\mathrm{ref}}}\exp\Big(\frac{F}{RT}(\phi^*-\phi_m)\Big). \tag{A.1.2}$$

[1] A double layer is a structure that appears on the surface of a solid when it is exposed to a fluid. The characteristic thickness of this double layer is given by the **Debye length** as we have introduced in (6.2.6).

Denote by $i^{eq} = i^{eq}(C_{\mathrm{Fe}^{2+}})$ the electric current density corresponding to the above ion flux:

$$i^{eq}(C_{\mathrm{Fe}^{2+}}) = z_{Fe^{2+}} F k_a \exp\Big(-\frac{F}{RT}(\phi^* - \phi_m)\Big) = z_{Fe^{2+}} F k_c \frac{C_{\mathrm{Fe}^{2+}}}{C_{\mathrm{ref}}} \exp\Big(\frac{F}{RT}(\phi^* - \phi_m)\Big). \quad \text{(A.1.3)}$$

Then the electric current density generated by the ion flux $f_{\mathrm{Fe}^{2+}}(\phi, C_{\mathrm{Fe}^{2+}})$ for arbitrary values of ϕ is written in the following simpler form

$$i_{\mathrm{Fe}^{2+}} = z_{Fe^{2+}} F f_{\mathrm{Fe}^{2+}}(\phi, C_{\mathrm{Fe}^{2+}}) = i^{eq}(C_{\mathrm{Fe}^{2+}}) \left(\exp\Big(-\frac{F}{RT}(\phi - \phi^*)\Big) - \exp\Big(\frac{F}{RT}(\phi - \phi^*)\Big)\right), \quad \text{(A.1.4)}$$

where $\phi^* = \phi^*(C_{\mathrm{Fe}^{2+}}) := \phi^{eq}(C_{\mathrm{Fe}^{2+}})$.

A.2 Derivation of the Nernst equation

Now, in order to estimate the values of ϕ^* and i^{eq}, let us return to (A.1.2). Let A^{eq} denote the value of (A.1.2) (thus $i^{eq} = z_{Fe^{2+}} F A^{eq}$). By making a product of the left-hand side and the right-hand side of this equality, we get

$$(A^{eq})^2 = k_a k_c \frac{C_{\mathrm{Fe}^{2+}}}{C_{\mathrm{ref}}}. \qquad \left(C_{\mathrm{ref}} = 1000\,\mathrm{mol/m^3}\right)$$

Hence

$$A^{eq} = A^{eq}(C_{\mathrm{Fe}^{2+}}) = \left(k_a k_c \frac{C_{\mathrm{Fe}^{2+}}}{C_{\mathrm{ref}}}\right)^{1/2}. \quad \text{(A.2.1)}$$

Thus, as in (A.1.4),

$$\begin{aligned} f_{\mathrm{Fe}^{2+}}(\phi, C_{\mathrm{Fe}^{2+}}) &= A^{eq}(C_{\mathrm{Fe}^{2+}}) \left(\exp\Big(-\frac{F}{RT}(\phi - \phi^*)\Big) - \exp\Big(\frac{F}{RT}(\phi - \phi^*)\Big)\right) \\ &= \left(k_a k_c \frac{C_{\mathrm{Fe}^{2+}}}{C_{\mathrm{ref}}}\right)^{1/2} \left(\exp\Big(-\frac{F}{RT}(\phi - \phi^*)\Big) - \exp\Big(\frac{F}{RT}(\phi - \phi^*)\Big)\right). \end{aligned} \quad \text{(A.2.2)}$$

Note also that

$$i^{eq}(C_{\mathrm{Fe}^{2+}}) = z_{Fe^{2+}} F A^{eq}(C_{\mathrm{Fe}^{2+}}) = z_{Fe^{2+}} F \left(k_a k_c \frac{C_{\mathrm{Fe}^{2+}}}{C_{\mathrm{ref}}}\right)^{1/2}. \quad \text{(A.2.3)}$$

Let us also estimate the value of ϕ^*. From (A.1.2), we have

$$\frac{2F}{RT}(\phi^* - \phi_m) = \ln\left(\frac{k_a C_{\mathrm{ref}}}{k_c C_{\mathrm{Fe}^{2+}}}\right).$$

Thus

$$\phi^*\left(C_{\mathrm{Fe}^{2+}}\right) = \phi_m + \frac{RT}{2F} \ln\left(\frac{k_a C_{\mathrm{ref}}}{k_c C_{\mathrm{Fe}^{2+}}}\right), \quad \text{(A.2.4)}$$

so that

$$\phi^*\left(C_{\mathrm{Fe}^{2+}}\right) - \phi_m = \frac{RT}{2F} \ln\left(\frac{k_a}{k_c}\right) + \frac{RT}{2F} \ln\left(\frac{C_{\mathrm{ref}}}{C_{\mathrm{Fe}^{2+}}}\right). \quad \text{(A.2.5)}$$

This formula (A.2.5) is equivalent to what is known as **Nernst equation**, which is given in the form

$$\varepsilon^{eq} \quad \left(:= \phi_m - \phi^*\right) = E^0_{\mathrm{Fe}^{2+}/\mathrm{Fe}} + \frac{RT}{z_{\mathrm{Fe}^{2+}} F} \ln\left(\frac{C_{\mathrm{Fe}^{2+}}}{C_{\mathrm{ref}}}\right), \quad \text{(A.2.6)}$$

where ε^{eq} is the electrode potential of iron in contact with the pit solution at equilibrium, $E^0_{\mathrm{Fe}^{2+}/\mathrm{Fe}}$ denotes the standard potential for $\mathrm{Fe}^{2+} \leftrightarrow \mathrm{Fe}$, which is known to be -0.44 V relative to the standard hydrogen electrode at room temperature.
By analogy with (A.2.5), we deduce that

$$E^0_{\mathrm{Fe}^{2+}/\mathrm{Fe}} = \frac{RT}{z_{Fe^{2+}} F} \ln\left(\frac{k_c}{k_a}\right). \quad \text{(A.2.7)}$$

A.3 Tafel equation

The Tafel equation is an equation in electrochemical kinetics relating the rate of an electrochemical reaction to the overpotential η. It is an approximation of the Butler-Volmer equation in the case of $|\eta| > 0.1\text{V}$ [7].

Next, we try to derive the Tafel equation from the Butler-Volmer equation. To do so, let define the overpotential η as follows

$$\eta := \varepsilon - \varepsilon^{eq} = \phi^* - \phi \tag{A.3.1}$$

where ε is the potential driving the corrosion reaction defined by

$$\varepsilon := \phi_m - \phi \tag{A.3.2}$$

and

$$\varepsilon^{eq} := \phi_m - \phi^*. \tag{A.3.3}$$

The expression of ε^{eq} is given by (A.2.6). Next, we rewrite (A.1.4) as a function of η to obtain

$$i_{\text{Fe}^{2+}} = i^{\,eq}(C_{\text{Fe}^{2+}}) \left(\exp\left(\frac{F}{RT}\,\eta\right) - \exp\left(\frac{-F}{RT}\,\eta\right)\right), \tag{A.3.4}$$

where $i^{\,eq}(C_{\text{Fe}^{2+}})$ is given by (A.1.3).

More precisely, (A.3.4) is given in the following general form

$$i_{\text{Fe}^{2+}} = i^{\,eq}(C_{\text{Fe}^{2+}}) \left(\exp\left(\frac{z_{Fe^{2+}}\ \alpha\ F}{RT}\,\eta\right) - \exp\left(\frac{-z_{Fe^{2+}}\ (1-\alpha)\ F}{RT}\,\eta\right)\right), \tag{A.3.5}$$

where α is the charge transfer coefficient which is equal to $\alpha = \dfrac{1}{2}$, $z_{Fe^{2+}} = +2$ and

$$i^{\,eq}(C_{\text{Fe}^{2+}}) = z_{Fe^{2+}}\ F\ k_a \exp\left(\frac{z_{Fe^{2+}}\ \alpha\ F}{RT}\,\varepsilon^{eq}\right)$$

and also

$$i^{\,eq}(C_{\text{Fe}^{2+}}) = z_{Fe^{2+}}\ F\ k_c\, \frac{C_{\text{Fe}^{2+}}}{C_{\text{ref}}} \exp\left(\frac{-z_{Fe^{2+}}\ (1-\alpha)\ F}{RT}\,\varepsilon^{eq}\right).$$

Next, from (A.3.5), we derive the following three cases which depend on the value of η:

Case1: if $\eta \gg \dfrac{RT}{z_{Fe^{2+}}F} \approx 12{,}8$ mV; it follows that

$$i_{\text{Fe}^{2+}} = i^{\,eq}(C_{\text{Fe}^{2+}}) \exp\left(\frac{z_{Fe^{2+}}\ \alpha\ F}{RT}\,\eta\right), \tag{A.3.6}$$

so that

$$\eta = \frac{-R\,T}{z_{Fe^{2+}}\ \alpha\ F}\ \ln\left(i^{eq}(C_{Fe^{2+}})\right) + \frac{R\,T}{z_{Fe^{2+}}\ \alpha\ F}\ \ln(i_{Fe^{2+}}). \tag{A.3.7}$$

Case2: if $|\eta| \gg \dfrac{RT}{z_{Fe^{2+}}F}$ and $\eta < 0$; we obtain

$$i_{\text{Fe}^{2+}} = -i^{\,eq}(C_{\text{Fe}^{2+}}) \exp\left(\frac{-z_{Fe^{2+}}\ (1-\alpha)\ F}{RT}\,\eta\right), \tag{A.3.8}$$

so that

$$\eta = \frac{RT}{z_{Fe^{2+}}\ (1-\alpha)\ F}\ \ln\left(i^{eq}(C_{Fe^{2+}})\right) - \frac{RT}{z_{Fe^{2+}}\ (1-\alpha)\ F}\ \ln(|i_{Fe^{2+}}|). \tag{A.3.9}$$

[7] Reference: https://en.wikipedia.org/wiki/Tafel_equation

Case3: if $|\eta| \to 0$; it follows that

$$i_{\mathrm{Fe}^{2+}} = i^{\,eq}(C_{\mathrm{Fe}^{2+}})\frac{z_{Fe^{2+}}\ F}{RT}\ \eta, \tag{A.3.10}$$

where $i^{\,eq}(C_{\mathrm{Fe}^{2+}})$ is given by (A.1.3).

In the case 3, since the overpotential is very low, the system will be close to equilibrium and the Butler-Volmer equation will be linearly approximated by (A.3.10).

However, the Tafel equation is a special case of the general Butler-Volmer equation **limited to the case where $\eta \gg 0$. Thus, it is given by** (A.3.6)**.** It is a relationship between the overpotential η and the natural logarithm of the density of current $\ln\left(|i_{Fe^{2+}}|\right)$.

Tafel equation

$$i_{\mathrm{Fe}^{2+}} = i^{\,eq}(C_{\mathrm{Fe}^{2+}})\exp\Big(\frac{z_{Fe^{2+}}\ \alpha\ F}{RT}\ \eta\Big) \text{ if } \eta \gg \frac{RT}{z_{Fe^{2+}}F} \approx 12{,}8 \text{ mV}, \tag{A.3.11}$$

where

$$i^{\,eq}(C_{\mathrm{Fe}^{2+}}) = z_{Fe^{2+}}Fk_a\exp\Big(\frac{F}{RT}\varepsilon^{eq}\Big).$$

Illustration:

An example of the evolution of the electric current density i as a function of the overpotential η is presented in Figure A.3.1. Here, we consider a general electrochemical reaction for the couple $Ox^{n+} \leftrightarrow Red$ given by

$$Red \quad \underset{k_c}{\overset{k_a}{\rightleftharpoons}} \quad Ox^{n+} + \mathrm{ne}^-,$$

where Red denotes the reductant which loses electrons, while Ox denotes the oxidant which gains electrons and n is the valence of the ion species. Moreover, we present the anodic current density i_a and the cathodic current density i_c. We have that

$$i = i_a + i_c \tag{A.3.12}$$

such that

$$i_a = n\ F\ k_a\ a_{Red}\ \exp\Big(\frac{n\ \alpha\ F}{RT}\ \varepsilon\Big) \text{ where } a_{Red} \text{ denotes the reductant activity,} \tag{A.3.13}$$

and

$$i_c = -n\ F\ k_c\ a_{Ox}\ \exp\Big(\frac{-n\ (1-\alpha)\ F}{RT}\ \varepsilon\Big) \text{ where } a_{Ox} \text{ denotes the oxydant activity.} \tag{A.3.14}$$

Also, they are given in the form

$$i_a = i_a^{eq}\ \exp\Big(\frac{n\ \alpha\ F}{RT}\ \eta\Big) \tag{A.3.15}$$

where

$$i_a^{eq} = n\ F\ k_a\ a_{Red}\ \exp\Big(\frac{n\ \alpha\ F}{RT}\ \varepsilon^{eq}\Big), \qquad a_{Red} = 1 \tag{A.3.16}$$

and

$$i_c = i_c^{eq}\ \exp\Big(\frac{-n\ (1-\alpha)\ F}{RT}\ \eta\Big) \tag{A.3.17}$$

where

$$i_c^{eq} = -n\ F\ k_c\ a_{Ox}\ \exp\Big(\frac{-n\ (1-\alpha)\ F}{RT}\ \varepsilon^{eq}\Big). \tag{A.3.18}$$

We have that

$$i^{eq} = i_a^{eq} = |i_c^{eq}|. \tag{A.3.19}$$

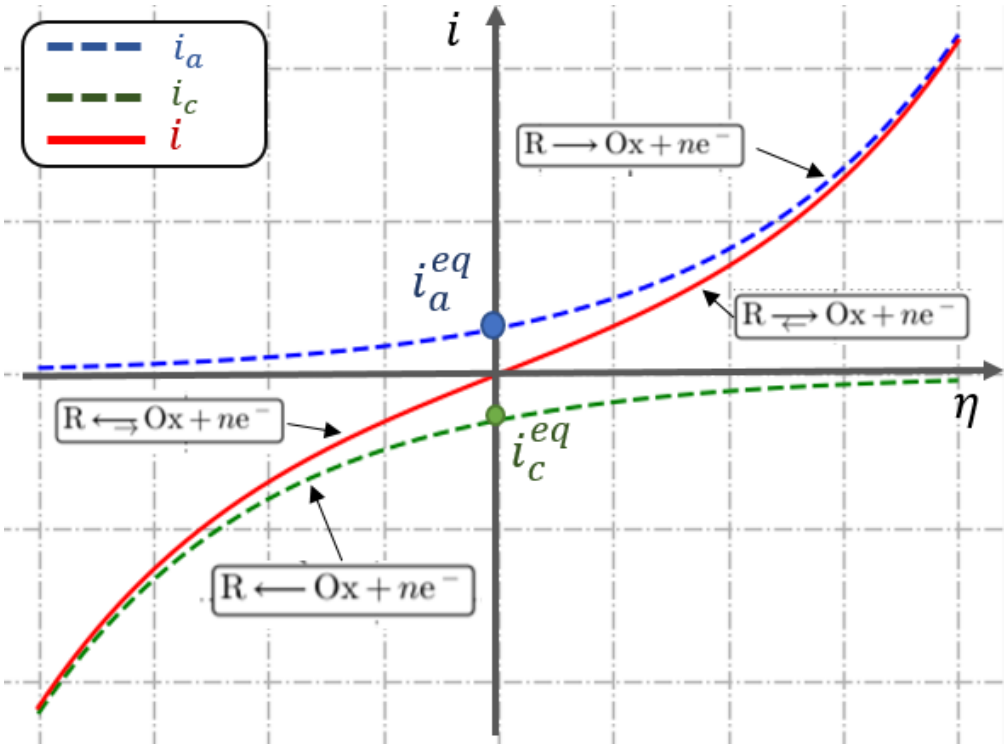

Figure A.3.1: Polarisation curve $i = f(\eta)$ from Butler-Volmer formula.

Appendix B

Determination of the rate constant values of oxidation k_a and reduction k_c in the Butler-Volmer formula

It is extremely important to give correctly the values of the oxidation rate constant k_a and the reduction rate constant k_c corresponding to the electrochemical reaction of the couple $Fe^{2+} \leftrightarrow Fe$. These constants appear in the Butler-Volmer formula which is given by

$$f_{\mathrm{Fe}^{2+}}(\phi, C_{\mathrm{Fe}^{2+}}) = k_a \exp\Big(-\frac{F}{RT}(\phi-\phi_m)\Big) - k_c \frac{C_{\mathrm{Fe}^{2+}}}{C_{\mathrm{ref}}} \exp\Big(\frac{F}{RT}(\phi-\phi_m)\Big). \tag{B.0.1}$$

The values of the constants k_a and k_c can be determined from Tafel law given in literature by (A.3.6):

$$i_{\mathrm{Fe}^{2+}} = i_a = i^{eq}(C_{\mathrm{Fe}^{2+}}) \exp\Big(\frac{z_{Fe^{2+}}\ \alpha\ F}{RT}\ \eta\Big) \tag{B.0.2}$$

where

$$\eta = \varepsilon - \varepsilon^{eq},\ \alpha = \frac{1}{2},\ z_{Fe^{2+}} = 2$$

and

$$i^{eq}(C_{\mathrm{Fe}^{2+}}) = z_{Fe^{2+}}\ F\ k_a \exp\Big(\frac{z_{Fe^{2+}}\ \alpha\ F}{RT}\ \varepsilon^{eq}\Big).$$

Then (B.0.2) becomes

$$i_{\mathrm{Fe}^{2+}} = i_a = 2\ F\ k_a\ \exp\Big(\frac{F}{RT}\ \varepsilon\Big) \tag{B.0.3}$$

where

$$\varepsilon = \phi_m - \phi.$$

As an example, for the anodic reaction of iron, Turnbull and Gardiner [67, 81] found that between pH 3 and 8.5, an expression of the form

$$i_a = i_0 \exp\big(\frac{F}{RT}\varepsilon\big) \tag{B.0.4}$$

with $i_0 = 1{,}96 \times 10^{11}$ A.m^{-2} describes the iron dissolution current i_a and ε is the electrode potential, with respect to the saturated calomel electrode (SCE), controlling the rate of the electrochemical reaction.

The choice of the reference electrode is very important. The saturated calomel reference electrode (SCE) is the world's most commonly used reference electrode. Therefore, we deduce the value of k_a with respect to this reference. It follows from (B.0.3) and (B.0.4) that

$$k_{a|SCE} = \frac{i_0}{2F} = \frac{1{,}96 \times 10^{11}}{2\ \times\ 96485{,}3321} = 1{,}01569842\ \times\ 10^6\ \ \mathrm{mol.m^{-2}.s^{-1}}. \tag{B.0.5}$$

Next, we deduce the value of the reduction rate constant k_c from equation (A.2.7) given by

$$E^0_{\mathrm{Fe}^{2+}/\mathrm{Fe}} = \frac{RT}{z_{Fe^{2+}}F}\ln\left(\frac{k_c}{k_a}\right) \tag{B.0.6}$$

where $E^0_{\mathrm{Fe}^{2+}/\mathrm{Fe}} = -0{,}44\ \mathrm{V}_{|\mathrm{NHE}} = -0{,}68\ \mathrm{V}_{|\mathrm{SCE}}$.

We recall that to convert a given potential "p" from SCE reference to NHE reference (Normal hydrogen electrode), we use the following relation

$$p\ \mathrm{V}_{|\mathrm{SCE}} = (p + 0{,}24)\ \mathrm{V}_{|\mathrm{NHE}}. \tag{B.0.7}$$

From (B.0.6), we deduce that

$$k_{c|SCE} = k_{a|SCE}\ \exp\left(\frac{z_{Fe^{2+}}\ F}{RT}E^0_{\mathrm{Fe}^{2+}/\mathrm{Fe}}\right), \tag{B.0.8}$$

where F, R, T are given in Table 6.1, so that

$$k_{c|SCE} = 1{,}039\ \times\ 10^{-17}\ \mathrm{mol.m^{-2}.s^{-1}}. \tag{B.0.9}$$

Now, we denote k_a and k_c values with respect to NHE reference. To do so, we recall that the anodic dissolution is given by (B.0.4)

$$i_a = i_0 \exp\left(\frac{F}{RT}\ \varepsilon_{|SCE}\right) = i_0 \exp\left(\frac{F}{RT}\ \varepsilon_{|NHE}\right)\exp\left(\frac{F}{RT}(-0{,}24)\right). \tag{B.0.10}$$

From (B.0.3), we have

$$i_{a|SCE} = i_{a|NHE} = 2\ F\ k_{a|SCE}\ \exp\left(\frac{F}{RT}\ \varepsilon_{|SCE}\right) = 2\ F\ k_{a|NHE}\ \exp\left(\frac{F}{RT}\ \varepsilon_{|NHE}\right). \tag{B.0.11}$$

It follows from (B.0.10) and (B.0.11) that

$$2\ F\ k_{a|NHE}\ \exp\left(\frac{F}{RT}\ \varepsilon_{|NHE}\right) = i_0 \exp\left(\frac{F}{RT}\ \varepsilon_{|NHE}\right)\exp\left(\frac{F}{RT}(-0{,}24)\right), \tag{B.0.12}$$

so that

$$k_{a_{|NHE}} = \frac{i_0}{2\ F}\ \exp\left(\frac{F}{RT}(-0.24)\right) = k_{a_{|SCE}}\ \exp\left(\frac{F}{RT}(-0.24)\right) \tag{B.0.13}$$

$$= 1{,}01569842\ .\ 10^6\ .\ \exp\left(\frac{F}{RT}(-0.24)\right) = 89{,}0636\ (\mathrm{mol.m^{-2}.s^{-1}})$$

Next, using (B.0.6), it follows that

$$k_{c_{|NHE}} = k_{a_{|NHE}}\ \exp\left(\frac{2F}{RT} \times -0.44\right) = 1{,}1852\ .10^{-13}\ (\mathrm{mol.m^{-2}.s^{-1}}). \tag{B.0.14}$$

Conclusion:

In relative to SCE reference, we obtain

$$k_{a_{|SCE}} = 1{,}01569842\ .\ 10^6\ (\mathrm{mol.m^{-2}.s^{-1}}) \text{ and } k_{c_{|SCE}} = 1{,}0392\ .10^{-17}\ (\mathrm{mol.m^{-2}.s^{-1}}).$$

In relative to NHE reference, we obtain

$$k_{a_{|NHE}} = 89{,}0636\ (\mathrm{mol.m^{-2}.s^{-1}}) \quad \text{and} \quad k_{c_{|NHE}} = 1{,}1852\ .10^{-13}\ (\mathrm{mol.m^{-2}.s^{-1}}).$$

Remark B.0.1. *Since the machine error is of order* 10^{-16}*, it is better to consider the values in relative to* ***NHE reference*** *to avoid any numerical problem with the value* $k_{c_{|ECS}} = 1{,}0392\ .10^{-17}(\mathrm{mol.m^{-2}.s^{-1}})$

Bibliography

[1] T. Aiki and A. Muntean. A free-boundary problem for concrete carbonation: Front nucleation and rigorous justification of the $\sqrt{t}$-law of propagation. *Interfaces and Free Boundaries*, 15, 01 2013.

[2] T. Aiki and A. Muntean. Large-time asymptotics of moving-reaction interfaces involving nonlinear henry's law and time-dependent dirichlet data. *Nonlinear Analysis: Theory, Methods & Applications*, 93:3–14, 2013.

[3] F. A. Almuaili. *Characterisation of 3D pitting corrosion kinetics of stainless steel in chloride containing environments*. PhD thesis, The University of Manchester (United Kingdom), 2017.

[4] O. Axelsson, Iterative solution methods, Cambridge University Press, 1994.

[5] N. Bensalah. *Pitting corrosion*. BoD–Books on Demand, 2012.

[6] M. Bertsch, J. Goncerzewicz, and D. Hilhorst. Large time behaviour of solutions of scalar viscous and nonviscous conservation laws. *Applied mathematics letters*, 12(3):83–87, 1999.

[7] H. Böhni. Breakdown of passivity and localized corrosion processes. *Langmuir*, 3(6):924–930, 1987.

[8] D. Brochet, D. Hilhorst, and X. Chen. Finite dimensional exponential attractor for the phase field model. *Applicable Analysis*, 49(3-4):197–212, 1993.

[9] J. Caldwell and Y-Y. Kwan. A brief review of several numerical methods for one-dimensional stefan problems. *Thermal Science*, 13(2):61–72, 2009.

[10] A. F. Chadwick, J. A. Stewart, R. A. Enrique, S. Du, and K. Thornton. Numerical modeling of localized corrosion using phase-field and smoothed boundary methods. *Journal of The Electrochemical Society*, 165(10):C633, 2018.

[11] F. Dabosi. *Corrosion localisée*. EDP Sciences, 2012.

[12] F. Dabosi, G. Beranger, B. Baroux. *Localized corrosion*. 1994.

[13] J. Donea, A. Huerta, J-Ph. Ponthot, and A. Rodriguez-Ferran. Arbitrary lagrangian-eulerian methods, volume 1 of encyclopedia of computational mechanics, chapter 14. *John Wiley & Sons Ltd*, 3:1–25, 2004.

[14] I. Ekeland and R. Temam. *Analyse Convexe et Problemes Variationnels (Dunod, 1974)*. 1999.

[15] G. Engelhardt, M. Urquidi-Macdonald, and D. D. Macdonald. Unification of the deterministic and statistical approaches for predicting localized corrosion damage. I. Theoretical foundation. *Corrosion Science*, 46(11):2755–2780, 2004.

[16] G. Engelhardt, M. Urquidi-Macdonald, and D. D. Macdonald. A simplified method for estimating corrosion cavity growth rates. *Corrosion Science*, 39(3):419–441, 1997.

[17] P. Ernst, and R.C. Newman. Pit growth studies in stainless steel foils. I. Introduction and pit growth kinetics. *Corrosion Science*, 44(5): 927–941, 2002.

[18] P. Ernst, and R.C. Newman. Pit growth studies in stainless steel foils. II. Effect of temperature, chloride concentration and sulphate addition. *Corrosion Science*, 44(5): 943–954, 2002.

[19] L. C. Evans. Partial differential equations. *Graduate studies in mathematics*, 19(2): 943–954, 1998.

[20] G. S. Frankel. Pitting corrosion of metals a review of the critical factors. *Journal of the Electrochemical society*, 145(6):2186–2198, 1998.

[21] G. S. Frankel, L. Stockert, F. Hunkeler, and H. Boehni. Metastable pitting of stainless steel. *Corrosion*, 43(7):429–436, 1987.

[22] A. Friedman. Analyticity of the free boundary for the stefan problem. *Archive for Rational Mechanics and Analysis*, 61(2):97–125, 1976.

[23] A. Friedman. Free boundary problems for parabolic equations I. melting of solids. *Journal of Mathematics and Mechanics*, 8:499–517, 1959.

[24] A. Friedman. *Partial differential equations of parabolic type.* Prentice-Hall, Inc., Englewood Cliffs, N.J. 1964.

[25] R. M. Furzeland. A comparative study of numerical methods for moving boundary problems. *IMA Journal of Applied Mathematics*, 26 (4):411–429, 1980.

[26] J. Galvele. Tafel's law in pitting corrosion and crevice corrosion susceptibility. *Corrosion Science - CORROS SCI*, 47:3053–3067, 12 2005.

[27] G. T. Gaudet, W.T. Mo, T.A. Hatton, J.W. Tester, J. Tilly, H.S. Isaacs, S. Hugh and R.C. Newman. Mass transfer and electrochemical kinetic interactions in localized pitting corrosion. *AIChE journal*, 32(6):949–958, 1986.

[28] D. Gilbarg, N.S. Trudinger, Elliptic Partial Differential Equations of Second Order, Springer, 1983.

[29] M. C. Gonçalves and F. Margarido. *Materials for construction and civil engineering.* Springer, 2015.

[30] S. Heurtault. *Propagation d'une piqûre unique de corrosion sur acier inoxydable austénitique.* PhD thesis, Paris 6, 2016.

[31] D. Hilhorst, J. Hulshof. A free boundary focusing problem. *Proceedings of the American Mathematical Society*, 121(4):1193–1202, 1994.

[32] T. J. R. Hughes, W. Liu and T. K. Zimmerman. Lagrangian–Eulerian finite element formulation for incompressible viscous flows, Comput. Methods Appl. Mech. Engrg. 29:329–349, 1981.

[33] H. S. Isaacs. The behavior of resistive layers in the localized corrosion of stainless steel. *Journal of the Electrochemical Society*, 120(11):1456–1462, 1973.

[34] H. S. Isaacs, J. H. Cho, M. L. Rivers, and S. R. Sutton. In situ x-ray microprobe study of salt layers during anodic dissolution of stainless steel in chloride solution. *Journal of the Electrochemical Society*, 142(4):1111, 1995.

[35] S. Jafarzadeh, Z. Chen, and F. Bobaru. Computational modeling of pitting corrosion. *Corrosion Reviews*, 37(5):419–439, 2019.

[36] S. Jafarzadeh, Z. Chen, and F. Bobaru. Peridynamic modeling of repassivation in pitting corrosion of stainless steel. *Corrosion*, 74(4):393, 2018.

[37] E. Javierre, C. Vuik, F.J. Vermolen, and S. Van der Zwaag. A comparison of numerical models for one-dimensional stefan problems. *Journal of Computational and Applied Mathematics*, 192(2):445–459, 2006.

[38] D. A. Jones. *Principles and prevention of corrosion*. Macmillan, 1992.

[39] B. J. Kirby. *Micro-and nanoscale fluid mechanics: transport in microfluidic devices*. Cambridge university press, 2010.

[40] D. Krouse, N. Laycock, and C. Padovani. Modelling pitting corrosion of stainless steel in atmospheric exposures to chloride containing environments. *Corrosion Engineering, Science and Technology*, 49(6):521–528, 2014.

[41] S. Kutluay, A.R. Bahadir, A. Özdeş. The numerical solution of one-phase classical Stefan problem, J. Comput. Appl. Math., 81(1):135–144, 1997.

[42] D. Landolt. *Corrosion et chimie de surfaces des métaux*, volume 12. PPUR presses polytechniques, 2003.

[43] N. J. Laycock and R. C. Newman. Localised dissolution kinetics, salt films and pitting potentials. *Corrosion science*, 39(10-11):1771–1790, 1997.

[44] N. J. Laycock and S. P. White. Computer simulation of single pit propagation in stainless steel under potentiostatic control. *Journal of the Electrochemical Society*, 148(7):B264–B275, 2001.

[45] N. J. Laycock, S. P. White, J.S. Noh, P.T. Wilson and R.C. Newman. Perforated covers for propagating pits. *Journal of the Electrochemical Society*, 145(4):1101, 1998.

[46] C. Liu and G.R. Kelly. A Review of the Application of Finite Element Method (FEM) to Localized Corrosion Modeling. *Corrosion*, 75(11):1285–1299, 2019.

[47] B. Malki and B. Baroux. Computer simulation of the corrosion pit growth. *Corrosion Science*, 47(1):171–182, 2005.

[48] W. Mai, S. Soghrati and R. G. Buchheit. A phase field model for simulating the pitting corrosion. *Corrosion Science*, 110:157–166, 2016.

[49] W. Mai, S. Soghrati and R. G. Buchheit. New phase field model for simulating galvanic and pitting corrosion processes. *Electrochimica Acta*, 260:290–304, 2018.

[50] A. M. Meirmanov. *The Stefan Problem*, volume 3. Walter de Gruyter, 2011.

[51] M. H. Moayed and R.C. Newman. Using pit solution chemistry for evaluation of metastable pitting stability of austenitic stainless steel. *Materials and Corrosion*, 56(3):166–173, 2005.

[52] J. L. Mousson, B. Vuillemin, R. Oltra, D. Crusset, G. Santarini, and P. Combrade. Modeling of the propagation of crevice corrosion. 2004.

[53] W. D. Murray and F. Landis. Numerical and machine solutions of transient heat-conduction problems involving melting or freezing: part i—method of analysis and sample solutions. *Journal of Heat Transfer*, 81(2):106–112, 1959.

[54] J. Newman and K. E. Thomas-Alyea. Electrochemical systems. *John Wiley & Sons*, 2012.

[55] F. Nobile and L. Formaggia. A stability analysis for the arbitrary Lagrangian Eulerian formulation with finite elements. East-West Journal of Numerical Mathematics, 7:105–132, 1999.

[56] P. Pedeferri. *Corrosion science and engineering*. Springer, 2018.

[57] M.H. Protter and H.F. Weinberger. *Maximum principles in differential equations*. Springer Science & Business Media, 2012.

[58] R. Ricci and W. Xie. On the stability of some solutions of the stefan problem. *European Journal of Applied Mathematics*, 2(1):1–15, 1991.

[59] D. G. Schaeffer. A new proof of the infinite differentiability of the free boundary in the stefan problem. *Journal of Differential Equations*, 20(1):266–269, 1976.

[60] J-F. Scheid. Méthodes numériques pour la dynamique des fluides. *Institut E. Cartan UMR*, 7502:2011–2012, 2007.

[61] S. Scheiner and C. Hellmich. Finite volume model for diffusion-and activation-controlled pitting corrosion of stainless steel. *Computer Methods in Applied Mechanics and Engineering*, 198(37-40):2898–2910, 2009.

[62] S. Scheiner and C. Hellmich. Stable pitting corrosion of stainless steel as diffusion-controlled dissolution process with a sharp moving electrode boundary. *Corrosion science*, 49(2):319–346, 2007.

[63] G. Segal, K. Vuik, and F. Vermolen. A conserving discretization for the free boundary in a two-dimensional stefan problem. *Journal of Computational Physics*, 141(1):1–21, 1998.

[64] S. M. Sharland. A mathematical model of crevice and pitting corrosion—ii. the mathematical solution. *Corrosion Science*, 28(6):621–630, 1988.

[65] S. M. Sharland. A review of the theoretical modelling of crevice and pitting corrosion. *Corrosion Science*, 27(3):289–323, 1987.

[66] S. M. Sharland. *A Theoretical Study of Crevice and Pitting Corrosion in Steels*. PhD thesis, University of London, 1988.

[67] S. M. Sharland, C. P. Jackson, and A. J. Diver. A finite-element model of the propagation of corrosion crevices and pits. *Corrosion Science*, 29(9):1149–1166, 1989.

[68] S. M. Sharland and P. W. Tasker. A mathematical model of crevice and pitting corrosion—i. the physical model. *Corrosion Science*, 28(6):603–620, 1988.

[69] T. Shibata and T Takeyama. Stochastic theory of pitting corrosion. *Corrosion*, 33(7):243–251, 1977.

[70] J. Soltis. Passivity breakdown, pit initiation and propagation of pits in metallic materials–review. *Corrosion Science*, 90:5–22, 2015.

[71] N. Sridhar. Local corrosion chemistry—a review. *Corrosion*, 73(1):18–30, 2017.

[72] J. Srinivasan and R. G. Kelly. Evaluating the critical chemistry for repassivation at the corroding surface using mass transport model-based artificial pit experiments. *Journal of The Electrochemical Society*, 163(13):C768–C777, 2016.

[73] J. Srinivasan and R. G. Kelly. On a recent quantitative framework examining the critical factors for localized corrosion and its impact on the galvele pit stability criterion. *Corrosion*, 73(6):613–633, 2017.

[74] J. Srinivasan and R. G. Kelly. One-dimensional pit experiments and modeling to determine critical factors for pit stability and repassivation. *Journal of The Electrochemical Society*, 163(13):C759, 2016.

[75] J. Srinivasan, C. Liu, and R. G. Kelly. Geometric evolution of flux from a corroding one-dimensional pit and its implications on the evaluation of kinetic parameters for pit stability. *Journal of The Electrochemical Society*, 163(10):C694, 2016.

[76] J. Srinivasan, M. J. McGrath, and R. G. Kelly. A high-throughput artificial pit technique to measure kinetic parameters for pitting stability. *Journal of The Electrochemical Society*, 162(14):C725, 2015.

[77] H. H. Strehblow and P. Marcus. Mechanisms of pitting corrosion. *Corrosion mechanisms in theory and practice*, pages 201–238, 1995.

[78] R. Temam. Infinite-dimensional dynamical systems in mechanics and physics, volume 68. *Springer Science & Business Media*, 2012.

[79] S. Tricoit. *Modélisation et simulation numérique de la propagation de la corrosion par piqûres du fer en milieu chloruré: contribution à l'évaluation de la durabilité des aciers au carbone en conditions de stockage géologique*. PhD thesis, Université de Bourgogne, 2012.

[80] A. Turnbull. Review of modelling of pit propagation kinetics. *British Corrosion Journal*, 28(4):297–308, 1993.

[81] A. Turnbull and M. K. Gardner. Electrochemical polarization studies of BS 4360 50D steel in 3.5% NaCl. *Corrosion Science*, 22(7):661–673, 1982.

[82] A. Turnbull and J. G. N. Thomas. A model of crack electrochemistry for steels in the active state based on mass transport by diffusion and ion migration. *Journal of the Electrochemical Society*, 129(7):1412–1422, 1982.

[83] B. Wallen. Critical pitting temperatures of UNS S31600 in different sea waters. *Book institute of materials*, 762:19–25, 2001.

[84] J. C. Walton. Mathematical modeling of mass transport and chemical reaction in crevice and pitting corrosion. *Corrosion Science*, 30(8-9):915–928, 1990.

[85] J. C. Walton, G. Cragnolino, and S. K. Kalandros. A numerical model of crevice corrosion for passive and active metals. *Corrosion Science*, 38(1):1–18, 1996.

[86] J. A. Weil, J.P. Marco, P. Thieullen. *Mathématiques L2 Cours complet avec 700 tests et exercices corrigés*. Pearson, 2007.

[87] B. E. Wilde and E. J. E. A. Williams. The use of current/voltage curves for the study of localized corrosion and passivity breakdown on stainless steels in chloride media. *Electrochimica Acta*, 16(11), 1971.

[88] M. T. Woldemedhin, J. Srinivasan, and R. G. Kelly. Effects of environmental factors on key kinetic parameters relevant to pitting corrosion. *Journal of Solid State Electrochemistry*, 19(12):3449–3461, 2015.

[89] J. Xiao and S. Chaudhuri. Predictive modeling of localized corrosion: an application to aluminum alloys. *Electrochimica Acta*, 56(16):5630–5641, 2011.

[90] A. Zurek. Numerical approximation of a concrete carbonation model: study of the $\sqrt{t}$-law of propagation, Numerical Method of Partial Differential Equations 35 (2019), 1801–1820.

Titre : Modélisation et simulation numérique de la vitesse de propagation d'une piqûre de corrosion
Mots clés : Modélisation, Simulation numérique, Analyse mathématique, Equations aux dérivées partielles non linéaires fortement couplées, Corrosion par piqûre, Interface mobile, Problème de Stefan, Méthode ALE
Résumé :

La corrosion des aciers joue un rôle central dans divers domaines technologiques. Ainsi, l'évaluation des dommages que les aciers sont susceptibles de subir dans le temps sous l'action de la corrosion représente un défi important pour s'assurer qu'ils ne seront pas affectés pendant leur durée de vie prévue. Cette étude est centrée sur un phénomène de corrosion particulier qui est la corrosion par piqûre des aciers en contact avec une solution de chlorure de soduim (NaCl). Les objectifs scientifiques de cette thèse sont relatifs à la modélisation physico-chimique de la corrosion par piqûre, l'analyse mathématique et les simulations numériques. Dans ce contexte, dans un premier temps, on a étudié un cas simple de ce phénomène de corrosion qui décrit la dissolution de fer pur. Ce modèle est transformé à l'aide d'un changement de variable approprié en un problème unidimensionnel à frontière libre, connu dans la littérature sous le nom de problème de Stefan à une phase. On a étudié en particulier la stabilisation en temps long de la solution de ce problème vers un profil auto-similaire. Pour prouver le resultat de convergence, on a appliqué un principe de comparaison ainsi que des notions de sur- et sous- solutions appropriées. Ensuite, au regard de la complexité physique du phénomène de corrosion par piqûre, le travail a été découpé en différentes étapes basées sur la construction d'un modèle à complexité physique croissante permettant d'identifier l'influence des différentes hypothèses physiques du modèle. On a ainsi développé un modèle mathématique sous la forme d'un système d'équations aux dérivées partielles fortement couplées pour d'écrire la vitesse de propagation d'une piqûre dans un fer pur. Il s'agit d'un modèle unidimensionnel de diffusion-migration-réaction avec une interface mobile pour cinq espèces chimques. Pour la résolution numérique de ces modèles, on a introduit la méthode ALE qui est une méthode robuste particulièrement adaptée à la résolution des problèmes évolutifs ainsi que la méthode de Newton. Finalement, comme il n'est généralement pas possible de trouver une solution explicite à un modèle complexe de diffusion-migration avec une interface mobile, un modèle réduit du modèle complet a été dérivé. On a montré que ce modèle réduit admet une solution approchée qui représente une approximation du modèle complet sous certaines conditions. Ce modèle réduit permet également de valider le schéma numérique développé pour le modèle complet.

Title : Modeling and computer simulation of the propagation rate of pit corrosion
Keywords : Modeling, Numerical simulation, Mathematical analysis, Coupled nonlinear partial differential equations, Pit corrosion, Moving interface, Stefan problem, ALE method
Abstract :

Steel corrosion plays a central role in different technological fields. The prediction of long term corrosion behavior of stainless steel is needed to ensure that its physical integrity will not be affected during its expected life time. In this study, we focus on pitting corrosion of steels in contact with a solution of sodium chloride (NaCl). The scientific objectives of this thesis are related to the physico-chemical modeling of pitting corrosion, by means of mathematical analysis and numerical simulations. First, we studied a simple case of a corrosion phenomenon which describes a pure iron dissolution in sodium chloride. We proved that under rather general hypotheses on the initial data, the solution of this iron dissolution model converges to a self-similar profile as $t \to +\infty$. This result is proved for an equivalent one-dimensional formulation of the physical model known as a one-phase Stefan problem. In order to prove the convergence result, we applied a comparison principle together with suitable upper and lower solutions. Then, we gradually derived a more complicated anodic-dissolution model in one-space dimension. It is a strongly coupled mathematical model of partial differential equations which represents the propagation of a pit in pure iron steel. It involves an anodic reaction of dissolution, the transport of aqueous chemical species by diffusion and migration and the moving of the iron interface. Then, we proposed an efficient numerical solution method for this system. To that purpose, we have developed an implicit in time numerical scheme based on the ALE method together with a Newton procedure. Through many simulations, we have examined the behavior of our system with respect to the variations of certain physical parameters. In the last step, we have integrated the hydrolysis reactions of iron cations in the system. This final model developed in this thesis is a diffusion-migration-reaction model with a moving interface for five-species. Finally, we derived a reduced system for our diffusion-migration model. Then, by means of two approximations, we analytically found an approximating solution for this reduced system, which turns out to be a very good approximation of the solution of our strongly coupled diffusion-migration model. The major advantage of developing such a nearly exact solution is to allow the validation of our numerical scheme.

Université Paris-Saclay
Espace Technologique / Immeuble Discovery
Route de l'Orme aux Merisiers RD 128 / 91190 Saint-Aubin, France